THE PHYSICAL REVIEW

VOLUME 93 Second Series NUMBER 2

JANUARY 15, 1954

Published for the
AMERICAN PHYSICAL SOCIETY
by the
AMERICAN INSTITUTE OF PHYSICS
Lancaster, Pa. and New York, N. Y.

THE
PHYSICAL REVIEW
A Journal of ...
Established by E. L. Nichols in 1893
Published by the American Institute of Physics
for the
AMERICAN PHYSICAL SOCIETY
Officers
President
Harrison Brown
Institute for Nuclear Studies
University of Chicago
Chicago 37, Illinois
Vice-President
H. A. Barton
Cornell University
Ithaca, New York
Secretary
K. K. Darrow
Bell Telephone Laboratories
(On leave)
Columbia University
New York 27, New York
Treasurer
G. B. Pegram
Columbia University
New York 27, New York
Associate Secretary
for the Pacific Coast
J. Kaplan
University of California at Los Angeles
Los Angeles, California
Associate Editor
A. Goldhaber
Brookhaven National Laboratory
Upton, Long Island
New York
BOARD OF EDITORS
Assistant Editor
S. Pasternack
Associate Editors
Atomic and Molecular
W. P. Allis
F. G. Brickwedde
W. B. Fretter
Conyers Herring
H. W. Lewis
Arnold Nordsieck
Nuclear
W. A. Fowler
Kenneth Greisen
Charles Kacser
R. E. Marshak
W. K. H. Panofsky
V. F. Weisskopf
... for publication should be submitted to S. A. Goldhaber, ... National Laboratory, Upton, Long Island, New York. The ... authors are requested to pay a publication charge of $10 per ... however, provides them to 100 free reprints. Instructions will ... galley proofs.
... correspondence concerning papers in the process of publication ... addressed to the Publication Manager, American Institute of ... 55 Street, New York 22, New York.
Subscription Price
... and Canada: ... $15.00
... $30.00
Back Numbers
... number of this volume complete ... is available
Price, ... $10.00
Thereafter ... $15.00
... until July, 1939:
... July, 1939–December, 1941:
... January, 1942–December, 1944:
... January, 1945–
... 1893–1913: $4.00
... and orders for back numbers should be addressed to ... Institute of Physics, 57 East 55 Street, New York 22, New York.
... In the case of members of the American Physical Society ... in the case of other subscribers to the ... Physical Review, Cornell University, Ithaca, New York.
... Pennsylvania.
... at Lancaster, Pennsylvania, under the Act of March 3, 1879.
... Section 34.64, P. L. & R. of 1948, authorized ...
The Physical Review is ...
Entered as second-class matter March ...
Acceptance for mailing at special rate of postage ...

THE
PHYSICAL REVIEW

A journal of experimental and theoretical physics established by E. L. Nichols in 1893

SECOND SERIES, VOL. 93, NO. 2 JANUARY 15, 1954

Light Scattering in Liquid Helium

A. W. LAWSON AND LOTHAR MEYER
Institute for the Study of Metals, University of Chicago, Chicago, Illinois
(Received October 5, 1953)

Classical formulas appear to describe adequately the data reported here on the relative scattering of light by liquid and gaseous helium. Anomalous scattering at the λ point, if present, is less than the relatively large experimental error of about 20 percent.

THE light scattering of liquid helium has been discussed theoretically by Goldstein,[1] Schiff,[2] Galanin,[3] and Ginsburg.[4] The lowest predicted value for the scattering is given by Rayleigh's classical theory of density fluctuations.[5]

According to this approach, the fraction of light scattered per unit volume, per unit solid angle, is given by

$$\frac{i}{I}=\frac{\pi^2}{18\mu_0^4\lambda_0^4}(\mu_0^2-1)(\mu_0^2+2)^2kT\chi, \qquad (1)$$

where μ_0 is the index of refraction corresponding to the wavelength λ_0 of the scattered light, k is the Boltzmann constant, T the absolute temperature, and χ is the isothermal compressibility. Despite the fact that the temperature of liquid helium is considerably less than its Debye temperature, Brillouin[6] has demonstrated that Eq. (1) is still valid in this temperature range for optical wavelengths. If, however, the λ-point phenomena are related to the condensation of an *ideal* Bose-Einstein gas, the scattering below the λ point should be by orders of magnitude higher and critical opalescence should be expected at the λ point itself.

Two experimental observations of the light scattering in liquid helium are recorded in the literature, one by McLennan, Smith, and Wilhelm,[7] and the other by Jakovlev.[8]

McLennan, Smith, and Wilhelm found that the intensity of the light scattered by liquid helium could not be distinguished from the background in their experiment, which indicates that the scattering is of the order of magnitude given by Eq. (1). Jakovlev, comparing visually the scattering of air with that of liquid helium, came to the same conclusion.

We have measured the light scattering of liquid helium in a more quantitative manner. The apparatus is shown schematically in Fig. 1. The scattering chamber consisted of the lower end of a thin-walled stainless steel tube of 1-in. o.d., with a quartz window on top and another at the side. These windows were mounted on the metal with Araldyte plastic.[9] A concave surface mirror on the bottom of the scattering chamber reflected the light beam back out of the cryostat. A high-pressure H-4 mercury arc lamp mounted outside the cryostat at the top of the stainless steel tube served as light source. A metal stopcock was used as light switch. No effort was made to use monochromatic light, as the available intensity at all wavelengths was needed to achieve adequate sensitivity. The scattered light was measured with a photomultiplier tube No. P-28 mounted immediately in front of the side window of the scattering chamber. It was separated by a quartz

[1] L. Goldstein, Phys. Rev. **57**, 241 (1940).
[2] L. I. Schiff, Phys. Rev. **57**, 844 (1940).
[3] A. Galanin, J. Exptl. Theoret. Phys. **10**, 1267 (1940).
[4] V. L. Ginsburg, J. Phys. (U.S.S.R.) **7**, 305 (1943).
[5] See, for instance, R. H. Fowler, *Statistical Mechanics* (Macmillan Company, New York, 1936), second edition, p. 768.
[6] Brillouin's theory [L. Brillouin, Ann. Phys. **17**, 88 (1922)] does not include zero-point energy as it is based on classical quantum theory. Introduction of the zero-point correction into his theory affects the values computed by Eq. (1) by less than 5 percent.
[7] McLennan, Smith, and Wilhelm, Phil. Mag. **14**, 161 (1932).
[8] I. A. Jakovlev, J. Phys. (U.S.S.R.) **7**, 307 (1948).
[9] Araldyte is the trade name of Ciba Company for ethoxyline resins.

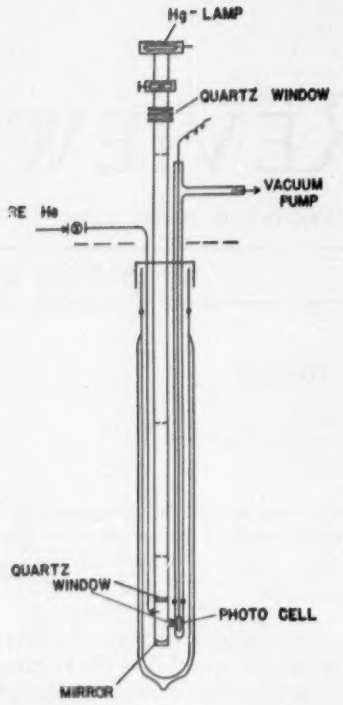

FIG. 1. Apparatus for measuring the scattering of light by liquid helium.

bulb and by high vacuum from the helium bath.[10] The photocurrent was measured with a galvanometer arrangement with a sensitivity of 3×10^{-11} amp/mm deflection. The scattering chamber could be filled with helium via a stainless-steel capillary. The purification of the helium used for the scattering experiments required extreme care. The helium was first purified under 2000 lb/sq in. over charcoal at 80°K, and then once more led over well-degassed charcoal in a liquid nitrogen bath before entering the vacuum system connected with the scattering chamber. During filling, the gas flow rate had to be kept below 1 liter per minute. The liquid used for the scattering experiments was condensed from this highly purified gas.

[10] Originally the photocell was placed directly in the liquid helium surrounding the scattering chamber. Under these conditions the sensitivity of the cell became extremely low, and the results were erratic. This behavior is probably due to the fact that the Cs-Sb surfaces of these cells are semiconductors with an extremely small gap between the valence and conduction bands, and so become practically insulators at helium temperatures. Surrounding the photomultiplier tube with high vacuum was sufficient to keep it at a temperature around 50°K in spite of the fact that the quartz vacuum chamber was covered for more than 10 inches with He II. The latter temperature seemed to provide nearly optimum working conditions for this type of phototube, because then the sensitivity was unimpaired and the noise level low.

The standard equipment for transferring liquid helium into the cryostat, for pumping on the helium bath, etc., are not shown in Fig. 1, nor is the Dewar with liquid nitrogen surrounding the helium Dewar.

As the measurement of the absolute ratio of intensity of the primary beam to that of the light scattered under a 90° angle seemed rather complicated, we preferred to calibrate the system by determining the light scattered by helium gas under 1 atmosphere at its boiling point. By taking the ratio of the light scattered by the liquid at different temperatures, $S_L(T)$, to the light scattered by the gas at the boiling point under the same conditions, $S_g(\text{bp})$, we eliminate the necessity of knowing the intensity of the primary beam, the geometric factors, etc. Equation (1) then reduces to[11]

$$\frac{S_L(T)}{S_g(\text{bp})}=\frac{(\epsilon_L-1)^2}{(\epsilon_g-1)^2}\frac{T}{4.2}\chi_L P_g. \qquad (2)$$

The results of a typical run are given in Table I.

TABLE I. Comparison of observed and calculated values of $S_L(T)/S_g(\text{bp})$.

1	2	3	4	5	6	7	8
T°K	P atmos	Phase	Galv. deflect. in cm	Background deflection in cm	4 minus 5	$S_L(T)/S_g(\text{bp})$ obs	$S_L(T)/S_g(\text{bp})$ calc. Eq. (2)
4.2	1	gas	3.0_0	2.8_0	0.2_0	1.0	
4.2	1	liq.	3.6_0	2.8_0	0.8_0	4.0	3.8
2.1	1	liq.	3.0_0	2.8_0	0.2_0	1.0	1.0
1.5	1	liq.	2.9_5	2.8_0	0.1_5	0.7_5	0.7

Within our accuracy of about 20 percent, the light scattering of liquid helium is in experimental agreement with Eq. (2) if one uses the experimentally determined values for μ_0^2 or ϵ and χ.[12] No excess scattering larger than our experimental error is observed at the λ point. This conclusion was confirmed by several runs in which the temperature of the bath was allowed to warm up slowly from 2.1 to 2.2°K during an interval of from 10 to 20 minutes. The galvanometer readings remained constant within the experimental accuracy and did not

[11] Equation (2) is derived by using the ideal gas law. Actually, the deviation from the ideal gas law at the helium bp is about 25 percent. However, using the second virial coefficient B as measured by Keesom and Walstra [Physica **7**, 985 (1940)], not only χ_g, but also the value of ϵ changes, since it has to be calculated from the values given for −191° and 0°C by means of the gas density at 4.2°K. Both corrections cancel each other within 10 percent, which does not exceed the accuracy of our measurements and the accuracy to which the compressibility of the liquid is known.

[12] See W. H. Keesom, *Helium* (Elzevier, Amsterdam, 1942), pp. 136, 319, 134, 236.

deviate perceptibly from the normal value as the λ point was passed.[13]

It should be emphasized that the principal source of error in this experiment is impurities. Although it might be presumed that it would be relatively simple to purify helium, our experience indicates that extraordinary precautions must be taken to avoid the introduction of miniscule particles of dust. Any deviation from our strict routine in handling the helium gas inevitably led to a considerably enhanced background scattering.

The results reported here are consistent with those of Taconis[14] and Reekie,[15] who were unable to detect any change in the x-ray diffraction pattern of liquid helium at the λ point.

[13] The liquid in the scattering chamber was kept under 1-atmosphere pressure to avoid bubble formation during warming or cooling of the bath, so the λ point of the liquid helium in the chamber was a few thousandths of a degree lower than that in the bath. In some runs the temperature of the bath was kept as near as possible (±0.0003°) to the λ point of the liquid helium in the scattering chamber. Even then there was not the slightest indication of an increase in scattering.

[14] W. H. Keesom and K. W. Taconis, Physica **5**, 270 (1938).

[15] Reekie, Hutchison, and Beaumont, Proc. Phys. Soc. (London) **A66**, 409 (1953).

Iodide Impurity Absorption in Potassium and Sodium Bromides

C. J. DELBECQ, J. E. ROBINSON, AND P. H. YUSTER
Chemistry Division, Argonne National Laboratory, Lemont, Illinois
(Received September 16, 1953)

Optical absorption bands due to a dilute iodide ion impurity in potassium bromide and sodium bromide are reported. Experimental data show, and semiquantitative theoretical arguments are given, which indicate that the displacement of the iodide impurity absorption from the absorption of the bromide lattice is approximately equal to the difference in the electron affinities of iodine and bromine.

INTRODUCTION

THE first fundamental optical absorption in the alkali halides is attributed to an electronic transition associated with the halide ion.[1] It has been suggested that a dilute substitutional negative ion impurity in an alkali halide crystal will give rise to an optical absorption which is displaced from that of the pure crystal.[2] In the simplest picture the position of the impurity absorption band will depend only on the difference in electron affinities of the negative ion impurity and the negative ion of the base lattice.

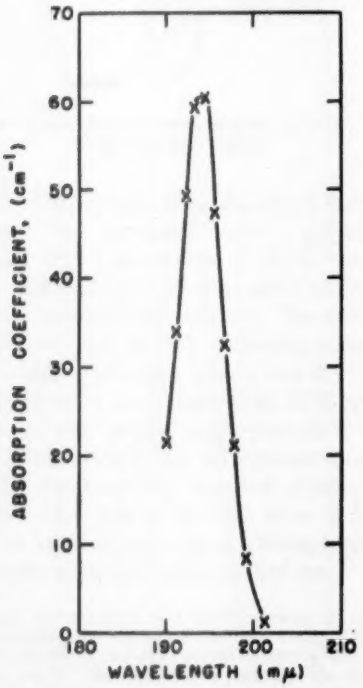

FIG. 1. Absorption, measured at liquid nitrogen temperature, of iodide impurity in potassium bromide.

In the present paper results will be reported on the absorption bands due to a dilute I^- impurity in potassium bromide and sodium bromide.

Semiquantitative arguments will be given which suggest that the difference in the energy of the absorption in the impurity I^- in potassium bromide and sodium bromide and the Br^- in KBr and NaBr arises principally from difference in the electron affinities of I and Br.

EXPERIMENTAL

Single crystals of potassium bromide and of sodium bromide, each containing of the order of 10^{-3} mole percent of I^- impurity, were grown by the Kyropoulos method. Figures 1 and 2 show the absorption bands, measured at liquid nitrogen temperature, due to the presence of I^- in potassium bromide and sodium bromide, respectively. These absorption spectra were obtained by subtracting the absorption spectrum of the pure alkali bromide from that of the alkali bromide containing the I^- impurity. Table I contains the positions of the first fundamental bands and the positions and half-widths of the iodide impurity bands for potassium bromide and sodium bromide at liquid nitrogen temperature. (The fundamental bands of sodium bromide and potassium bromide at liquid nitrogen temperature lie too far in the ultraviolet to be measured with our apparatus; therefore, an estimate was made from the positions determined by others[3] at room temperature.) Using the data in the table, it is seen that the iodide impurity band in potassium bromide is displaced from the fundamental band by an amount $\Delta E(I^-, KBr) = 0.40$ ev; in the case of NaBr, $\Delta E(I^-, NaBr) = 0.35$ ev. The difference between the electron affinities of bromine and iodine is about 0.34 ev and is approximately equal to the above ΔE values.

DISCUSSION

A theoretical discussion of the displacement of the iodide absorption peaks from the first fundamental bromide absorption band must consider, in addition to the difference between the vacuum electron affinities of Br and I, those energy differences, relative to the pure bromides, of the terminal states of the absorption act

[1] F. Seitz, *Modern Theory of Solids* (McGraw-Hill Book Company, Inc., New York, 1940), pp. 407–419; N. F. Mott and R. W. Gurney, *Electronic Processes in Ionic Crystals* (Oxford University Press, London, 1940), p. 98.

[2] N. F. Mott and R. W. Gurney, *Electronic Processes in Ionic Crystals* (Oxford University Press, London, 1940), p. 102.

[3] F. Seitz, *Modern Theory of Solids* (McGraw-Hill Book Company, Inc., New York, 1940), p. 410.

which result from the very appreciable difference in size of bromide and iodide ions. These energy changes, although small compared to the absorption frequency itself, are by no means individually negligible against the frequency shift in question.

Since the crystals reported on here are very dilute substitutional solid solutions, an appropriate model for discussion is an infinite NaBr or KBr matrix in which a single I^- ion is embedded substitutionally, at $T=0°K$. The principal terms by which the ground-state energy of such a system differs from that of a pure bromide (aside from the electron affinities) arise from: compression of the iodide wave function relative to its extent in a pure NaI or KI lattice, increased first neighbor overlap in the vicinity of the solute ion, and changes in Madelung energies due to displacements of the matrix ions. The configuration of lowest energy clearly corresponds to a compromise among these terms, and a valence electron on the iodide has because of them an energy higher than that of a valence electron on a bromide in pure NaBr or KBr by an amount

TABLE I. Energy difference between iodide impurity absorption and fundamental absorption in sodium bromide and potassium bromide.

	First fundamental band (1)	I^- Impurity band Peak (2)	Half-width (ev)	ΔE (ev) (1) − (2)
KBr	1820A (6.80 ev)	1935A (6.40 ev)	0.20	0.40
NaBr	1830A (6.76 ev)	1930A (6.41 ev)	0.25	0.35

greater than the difference in the vacuum electron affinities. The displacements of the matrix ions also influence the nonconducting state (or states) to which an iodide valence electron may be raised by optical absorption. According to the Franck-Condon principle, the displacements persist throughout the optical transition. In the excited state, therefore, the net potential due to polarization of the electron distributions on the matrix ions by the positive hole at the solute differs from that occurring in the case of a pure bromide lattice. It may readily be seen that this gives a positive contribution to the energy of the final state. It is to be noted that the final state is *not* an exciton state in the usual sense, since the iodide is not translationally equivalent to the rest of the halide lattice.

In assessing the influence of the several "size-effect" perturbing terms on the absorption frequency, we are reduced by lack of a sufficiently precise computational technique to order-of-magnitude estimates. A crude evaluation can be made in terms of the familiar model of the absorption process as the transfer of an electron from a halide to neighboring alkali ion. As mentioned

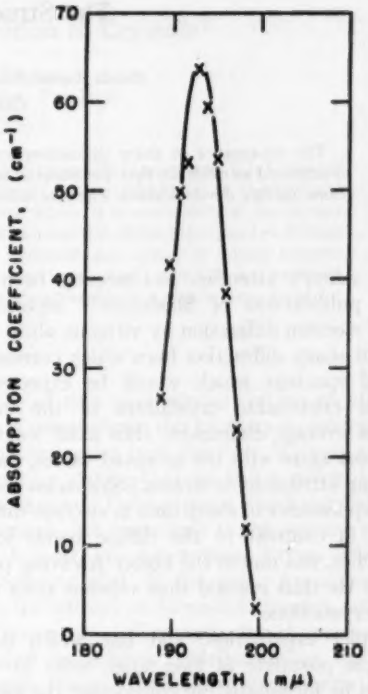

FIG. 2. Absorption, measured at liquid nitrogen temperature, of iodide impurity in sodium bromide.

above, the perturbation of the electrostatic lattice potential due to ionic displacements is common to both ground and excited states. We assume the remainder of the size-effect increase of the ground-state energy to be roughly equal to the cost in strain energy[4] of substituting an iodide ion for a bromide. Elasticity theory would then indicate an equilibrium relative displacement of first neighbors to the solute of about five percent and a strain energy of order 0.1 ev for both NaBr and KBr. To within an order of magnitude, the polarization energy of the excited state may be taken as that produced by a positively charged sphere, enclosing the solute, in a dielectric continuum. If we take the radius of this sphere to be the first neighbor distance, increasing the radius by five percent gives a positive change in the excited state energy of order 0.1 ev for both NaBr and KBr. The size-effect terms raise both the ground and excited levels of the system by approximately equal amounts and give to the absorption frequency a net contribution which is small compared to the difference in the electron affinities of Br and I. We should therefore expect the displacement of the iodide impurity absorption from the absorption of the bromide lattice to be approximately equal to the difference in electron affinities.

[4] N. F. Mott and F. R. N. Nabarro, Proc. Phys. Soc. (London) 52, 86 (1940).

The Structure of Vitreous Silica

JOSEPH S. LUKESH
Knolls Atomic Power Laboratory, Schenectady, New York*
(Received October 1, 1953)

The appearance of sharp diffraction lines in electron-diffraction patterns of vitreous silica has been interpreted as evidence that the material is crystalline. The method of sample preparation was such as to cause surface devitrification. The conclusions are, therefore, unwarranted.

THE writer's attention has recently been called[1] to publications of Shishacow[2,3] reporting the results of electron diffraction by vitreous silica. Shishacow found sharp diffraction lines which correspond to calculated spacings which would be expected from tetragonal cristobalite crystallites of the order of 15–20A in average dimension. (His axial lengths and ratio do not agree with the accepted values, the differences being attributed to strains.) Shishacow concluded that the appearance of sharp lines in electron-diffraction patterns, in contrast to the diffuse bands found in x-ray studies, was due to the higher resolving power of electrons. He thus implied that vitreous silica consists of small crystallites.

A simpler explanation, and one which does not require the postulate of long-range order in vitreous silica, can be formulated by considering the method of sample preparation followed by Shishacow. He prepared his material by careful grinding, followed by air flotation. The material thus collected consisted of particles of the order of less than a tenth of a micron in diameter. Significantly, the surface had been highly worked during the grinding process. The degree of working and, in addition, the local temperatures involved should have been enough to cause devitrification of the glass to cristobalite, at least on the surface. Since electron diffraction is essentially a surface phenomenon, the cristobalite pattern would have been predominant.

It would appear that the results reported by Shishacow do not support the thesis that vitreous silica consists of minute crystallites. Further, Maxwell and Mosley[4] obtained electron-diffraction patterns by transmission through very thin films of vitreous silica formed by blowing without abrasion. Their patterns consisted principally of diffuse bands. Some portions of sharp lines were present, but these might have been due to impurities or surface devitrification.

* Operated for the U. S. Atomic Energy Commission by the General Electric Company.

[1] R. Hillig (private communication).

[2] N. A. Shishacow, Nature **136**, 514 (1935).

[3] N. A. Shishacow, J. Tech. Phys. (U.S.S.R.) **5**, 1834 (1935).

[4] L. R. Maxwell and V. M. Mosley, Phys. Rev. **47**, 330 (1935).

The Theory of Defect Concentration in Crystals*

G. H. VINEYARD† AND G. J. DIENES
Brookhaven National Laboratory, Upton, New York

(Received October 2, 1953)

The theory of the formation of vacancy and interstitial defects in crystals is re-examined. It is suggested that a Born-von Karman type of lattice provides an adequate model for the calculation of the essential parameters giving the concentration of defects as a function of temperature. It is concluded that the entropy of formation depends only on the lattice frequencies before and after formation of the defect, and no further contribution to the entropy arises even though the enthalpy of formation may appear to remain temperature dependent at constant pressure. Data on vacancy concentration in NaCl and LiF are analyzed roughly in the light of present ideas. The results for NaCl are understandable in a simple way; those for LiF seem to require more complete calculations.

I. INTRODUCTION

THE concentration of lattice defects in a crystal, according to statistical mechanics, is given by[1]

$$c=n/N=Ae^{-E/kT}, \tag{1}$$

where n=number of defects; N=total number of atoms; E=energy of formation of a defect; and A=pre-exponential constant. If there are no entropy changes other than the entropy of mixing, then the constant A in (1) is equal to unity. Experimentally, A often differs from unity by orders of magnitude. Two main contributions to the value of A have been considered in the literature.[2,3] First, the vibrational frequencies around a defect are altered, which contributes to the entropy of formation. Second, the energy of formation depends on the interatomic distance and, hence, on the temperature via the volume expansion. Mott and Gurney[2] and Frenkel[3] assumed that E depends linearly on the temperature as

$$E=E_0-\alpha T, \tag{2}$$

giving a contribution to A of $e^{\alpha/k}$. However, Haven and van Santen[4] have pointed out recently that a temperature dependence alloted to the enthalpy of formation requires some entropy of formation because of the thermodynamic connection:

$$(\partial H/\partial T)_P=T(\partial S/\partial T)_P.$$

From this they find a further entropy term to be necessary because of Mott and Gurney's temperature-dependent enthalpy and arrive at a negative contribution to the entropy of formation rather than a positive one as would be derived from (2).

Because of this unsatisfactory state of affairs, we decided to reinvestigate this problem by taking account of thermal expansion from the start. We may anticipate the results by stating that we find a common error in previous analyses. Energy terms which depend only on the volume do not contribute to the entropy of formation, and these are the entropy terms which have often been included in the past. According to our analysis, the entropy of formation depends only on the lattice frequencies before and after formation of the defect, and no further contribution to the entropy arises even though the enthalpy of formation may appear to remain temperature dependent at constant pressure.

In Sec. II the detailed thermodynamic arguments are given, and in Sec. III we discuss briefly application to actual experimental data.

II. THERMODYNAMICS OF THE FORMATION OF LATTICE DEFECTS

The discussion will first be carried through for the case of a monatomic substance in which each atom occupies an equivalent position when in the perfect state. Generalization to more complicated substances is easily made. The discussion is limited to the case where hydrostatic pressure is the only stress. The crystal may exist in a perfect state, and this will be assumed to be a lattice of the Born-von Karman type, that is, one in which the thermal oscillations are of sufficiently small amplitude that the potential energy is a quadratic function of the atomic displacements. The energy of the crystal, relative to the state in which the atoms are all at rest at infinite separation, consists of a potential energy of equilibrium ϕ_p plus a dynamic part which, by normal mode analysis, is equal to the kinetic and potential energies of a set of independent simple harmonic oscillators. These oscillators are characterized by their frequencies which, together with ϕ_p (under the condition of hydrostatic pressure), depend on the volume of the crystal and on no other thermodynamic variables.

The internal partition function of the N-atom

* Work carried out under contract with the U. S. Atomic Energy Commission.

† On leave from the University of Missouri, Columbia, Missouri.

[1] See, for example, F. Seitz, *Modern Theory of Solids* (McGraw-Hill Book Company, Inc., New York, 1940), p. 458.

[2] N. F. Mott and R. W. Gurney, *Electronic Processes in Ionic Crystals* (University Press, Oxford, 1948), pp. 29–30.

[3] J. Frenkel, *Kinetic Theory of Liquids* (Clarendon Press, Oxford, 1946), Chapter I.

[4] Y. Haven and J. H. van Santen, Philips Research Repts. 7, 474 (1952).

perfect crystal is now

$$Z_p = e^{-\phi_p/T} \prod_{\nu_p} e^{-\nu_p/2T}(1-e^{-\nu_p/T})^{-1}, \quad (1)$$

where ν_p is the frequency of one of the $3N$-6 lattice oscillators, measured in energy units; T is the temperature in energy units; and the product is taken over the entire set of oscillator frequencies.

The Helmholtz free energy, pressure, entropy, and internal energy are given by

$$A_p = -T \ln Z_p = \phi_p + \sum_{\nu_p}\left[\frac{\nu_p}{2} + T\ln(1-e^{-\nu_p/T})\right], \quad (2)$$

$$P = -\left(\frac{\partial A_p}{\partial V}\right)_T = -\frac{d\phi_p}{dV} - \sum_{\nu_p}[\tfrac{1}{2} + (e^{\nu_p/T}-1)^{-1}]\frac{d\nu_p}{dV}, \quad (3)$$

$$S_p = -\left(\frac{\partial A_p}{\partial T}\right)_V = \sum_{\nu_p}\left[-\ln(1-e^{-\nu_p/T}) + \frac{\nu_p}{T}(e^{\nu_p/T}-1)^{-1}\right], \quad (4)$$

$$U_p = A_p + TS_p = \phi_p + \sum_{\nu_p}\nu_p[\tfrac{1}{2} + (e^{\nu_p/T}-1)^{-1}]. \quad (5)$$

Here the correction to the entropy because of the indistinguishability of the atoms has been omitted, which is permissible because all systems to be considered will have the same number of atoms.

At temperatures appreciably above the characteristic temperature of the crystal, the thermodynamic functions assume the following simplified forms:

$$A_p \cong \phi_p + \sum_{\nu_p} T\ln\frac{\nu_p}{T}. \quad (6)$$

$$P \cong -\frac{d\phi_p}{dV} - \sum_{\nu_p}\frac{T}{\nu_p}\frac{d\nu_p}{dV}. \quad (7)$$

$$S_p \cong \sum_{\nu_p}\left(1-\ln\frac{\nu_p}{T}\right). \quad (8)$$

$$U_p \cong \phi_p + \sum_{\nu_p} T = \phi_p + 3NT. \quad (9)$$

Consider next a crystal identical with the perfect crystal just treated, except that it possesses one defect, e.g., an atom has been moved from the interior to a site on the surface, or a surface atom has been moved to an interior interstitial position. This imperfect crystal now constitutes a second mechanical system describable by a volume-dependent potential energy of equilibrium ϕ_i and a set of independent simple harmonic lattice oscillators characterized by the volume dependent frequencies ν_i. All of the preceding formulas for thermodynamic quantities now apply to the imperfect lattice simply upon replacement of the subscript p by the subscript i throughout. The entropy and free energies so calculated do not include the entropy of mixing, which arises because of the different equivalent sites on which the defect may be formed.

At thermal equilibrium the concentration of defects c (atomic fraction) is given by the formula[1,5]

$$c = e^{-g/T}, \quad (10)$$

where g is the increase of Gibbs free energy of the system, exclusive of the entropy of mixing, attendant upon the formation of one defect at temperature T and pressure P.

Following the preceding discussion, g can be written

$$g = G_i - G_p, \quad (11)$$

where G_i and G_p are the Gibbs free energy of the imperfect and perfect crystals, respectively.

Experimentally one always determines defect concentrations over a restricted range of temperatures, and an equation of the type of (1) is employed to analyze the data in terms of an enthalpy (or energy) of formation and a pre-exponential factor. In most cases a plot of $\ln c$ *vs* $1/T$ proves to be very nearly linear over the entire experimental range. These circumstances suggest that the most useful form in which to elaborate (10) is the following:

Let T_1 be a temperature near the middle of the experimental range. Development of g in Taylor series about T_1 gives

$$g(T) = g(T_1) + (\partial g/\partial T_1)_P(T-T_1) + \tfrac{1}{2}(\partial^2 g/\partial T_1^2)_P(T-T_1)^2 + \cdots. \quad (12)$$

As long as the experimental data can be represented by a straight line in the usual plot, the first two terms of (12) must give an adequate approximation to g. Consequently, we shall discard the quadratic and higher terms. The present model allows one to estimate these terms and confirms the expectation that they are small in cases of interest.

If we employ (11) and the relation $(\partial G/\partial T)_P = -S$, (12) becomes

$$g(T) = g_1 + T_1 s_1 - Ts_1 = h_1 - Ts_1, \quad (13)$$

where $s = S_i - S_p$ (the entropy of formation of one defect, exclusive of the entropy of mixing), $h = H_i - H_p$, the enthalpy of formation of one defect, and the subscript 1 means that the quantity is to be evaluated at temperature T_1. Finally, the equilibrium concentration of defects in the temperature range of interest becomes

$$c = \exp\{s_1 - h_1/T\}. \quad (14)$$

The entropy and enthalpy (14) may be written down at once from the preceding formulas. For many cases of interest the lattice frequencies will all be smaller than

[5] The case of pairs or other complexes of defects requires a simple numerical factor in the exponent of (10). Equation (10) is the basic form, of which Eq. (1) is a common specialization.

T_1, and good approximations can be found in the early terms of expansions in ν/T. Subsequent developments will be confined to this case. From (8) one finds $s=\sum \ln(\nu_p/\nu_i)+O(\nu^2/T^2)$, so that, to first order,

$$s_1=\sum \ln(\nu_p/\nu_i), \tag{15}$$

the summation being over all vibrational modes. Equation (15) is essentially the same as a term already employed by Mott and Gurney[2] to take care of altered vibrational frequencies around a defect. It is now apparent that this vibrational entropy, if properly computed, should not be supplemented by any other entropy terms.[6] It should be added that thermal expansion and attendant subtle effects, on the basis of which the temperature dependence of the enthalpy of formation was first suggested, are provided for in the present model.

The calculation of h will be simplified here by setting $P=0$, an adequate approximation in most experiments. Then from the relation $H=A+TS+PV$, one finds

$$\begin{aligned} h&=\phi_i-\phi_p+\sum_{\nu_i}\nu_i[\tfrac{1}{2}+(e^{\nu_i/T}-1)^{-1}] \\ &\quad -\sum_{\nu_p}\nu_p[\tfrac{1}{2}+(e^{\nu_p/T}-1)^{-1}] \\ &=\phi_i-\phi_p+\frac{1}{12T}\sum(\nu_i^2-\nu_p^2)+O(\nu^2/T^2). \end{aligned} \tag{16}$$

Again a good approximation to h_1 will often be obtainable by omitting all terms in ν/T from (16). The ϕ terms should be computed at V_1, the equilibrium volume at T_1, rather than at V_0, the equilibrium volume at $T=0$. This generally involves a slight correction, probably smaller than the inaccuracy in the calculated value of $\phi(V_0)$ itself, which may be estimated as follows:

$$\begin{aligned} \phi(V)\cong\phi(V_0)&+\left(\frac{d\phi}{dV}\right)_{V_0}(V-V_0) \\ &+\frac{1}{2}\left(\frac{d^2\phi}{dV^2}\right)_{V_0}(V-V_0)^2. \end{aligned} \tag{17}$$

At $T=0$, with neglect of the zero-point vibrational energy, ϕ is just the internal energy of the system. Then $d\phi=-PdV$, $d\phi/dV=-P$, $d^2\phi/dV^2=-dP/dV=(1/V)B$, where B is the bulk modulus at absolute zero. Setting $P=0$ gives

$$\phi(V_1)\cong\phi(V_0)+\frac{1}{2}BV_0\left(\frac{V_1-V_0}{V_0}\right)^2. \tag{18}$$

As examples, for NaCl with $T_1=900°$K the second term in (18) equals 3 percent of the first term; for LiF with $T_1=1000°$K the second term is 8/10 percent of the first.

[6] Presumably this conclusion is also valid for the formation of a saddle point configuration during diffusion. Consequently, one of the entropy contributions ΔS_1, previously considered positive by one of us (G.J.D.) in an earlier analysis of entropies of activation [Phys. Rev. 89, 185 (1953)], should be zero.

The potentials ϕ can be calculated theoretically by well-known methods.[7,8] It should be pointed out that in ionic crystals, such as the alkali halides, the condition of electrical neutrality requires that vacancies be created in pairs of opposite sign. At elevated temperatures association of positive and negative vacancies will not be important,[9] and the concentration of separated pairs of vacancies (number of pairs divided by number of molecules in the crystal) is given by a simple modification of Eq. (10):

$$c=e^{-g/2T}, \tag{19}$$

where g is the Gibbs free energy increase, exclusive of the entropy of mixing, upon formation of a well-separated pair of positive- and negative-ion vacancies. All other formulas are then readily transcribed for this case.

III. COMPARISON WITH EXPERIMENT

Etzel and Maurer[10] have measured the electrical conductivity of NaCl and deduced a concentration of vacancy pairs

$$c=e^{(1.67-1.01/T)}$$

in the temperature range 825 to 1000°K. (T in the above is in units of electron volts.) The value 1.01 ev for half the enthalpy of pair formation is in good agreement with Mott and Littleton's[11] theoretical value.

To calculate the entropy term, one should make a normal mode analysis of the perfect and imperfect crystals, an especially difficult task for the latter case. An approximate value may be obtained much more simply, however, by using an Einstein model for the lattice, as has already been suggested by Mott and Gurney.[2] If one assumes, with these writers, that only the nearest neighbors of the vacancy will be affected, and then only in respect to vibrations along a line joining them with the defect, one has a total of 12 altered modes per defect pair. If one assumes that the ratio of the altered to original frequencies is the same for positive and negative vacancies, one obtains from Eq. (15) the entropy change per defect pair of $s_1=12\ln(\nu_p/\nu_i)$. A fit to Etzel and Maurer's data is now obtained if $s_{1/2}=1.67$, which requires $\nu_p/\nu_i=1.32$. In the absence of a complete calculation, it may be said that this value seems entirely reasonable. In the simplest possible situation, that of nearest-neighbor interaction only in a cubic lattice, one immediately computes that $\nu_p/\nu_i=\sqrt{2}$, since creation of the vacancy halves the force constant for vibration of the neighbor.

[7] See reference 2, Chapter II.

[8] See also the recent review: P. W. M. Jacobs and F. C. Tompkins, Quart. Revs. 6, 238 (1952).

[9] A theoretical treatment of association is given by J. R. Reitz and J. A. Gammel, J. Chem. Phys. 19, 894 (1951).

[10] H. W. Etzel and R. J. Maurer, J. Chem. Phys. 18, 1003 (1950).

[11] N. F. Mott and M. J. Littleton, Trans. Faraday Soc. 34, 485 (1938).

Similar measurements by Haven[12] on LiF gave

$$c = e^{(6.2-1.34/T)}.$$

The enthalpy of activation is similar to that for NaCl in the sense that it is increased essentially by the ratio of the cohesive energies (a ratio of 1.32) The entropy term of 6.2, analyzed as for NaCl, requires $\nu_p/\nu_i = 2.8$, a somewhat high value. A resolution of this difficulty would require more detailed calculations. For example, nearest-neighbor interactions could lower this value appreciably. Further, Haven analyzes his data in a somewhat different manner from Etzel and Maurer and the two sets of results are not strictly comparable.

Simple application of the theoretical analysis appears, therefore, to be in reasonable agreement with experiment. There are additional terms, of course, which contribute to changes of the vibrational frequencies which then should be included in calculating ν_p/ν_i of Eq. (15), such as over-all dilation due to strains around the defects and long-range elastic distortion of the crystal. These effects are being investigated by Huntington[13,14] both for the formation of defects and the formation of saddle point configuration during diffusion.

At the present state of analysis, from Eq. (15) the strong inference is that the entropy of formation for vacancies is positive while for interstitials it is negative. Extensive calculations will be necessary, however, before dependable theoretical values for this entropy can be found.

ACKNOWLEDGMENT

The writers are very much indebted to H. B. Huntington for discussions and some essential suggestions.

[12] Y. Haven, Rec. trav. chim. 69, 1259, 1471 (1950).

[13] H. B. Huntington, Phys. Rev. 91, 246 (1953).
[14] H. B. Huntington (to be published).

PHYSICAL REVIEW VOLUME 93, NUMBER 2 JANUARY 15, 1954

Temperature Variation of the Magnetic Inelastic Scattering of Slow Neutrons*

LÉON VAN HOVE
Institute for Advanced Study, Princeton, New Jersey
(Received October 2, 1953)

The main features of the temperature variation of the magnetic inelastic scattering of slow neutrons in iron, recently measured by Palevsky and Hughes, are accounted for, by use of a theoretical description of the scattering in terms of the correlation between pairs of spins at different positions and different times. Proofs will be given in a later paper devoted to a general discussion of space-time correlations and of their use in scattering theory.

THE temperature variation of the total scattering cross section of iron for very slow neutrons has been measured by Palevsky and Hughes[1] in the temperature range $100°K < T < 1300°K$ and for neutron incident wavelength λ varying from 5 to 13A. After subtracting the contribution of scattering by the iron nuclei, one obtains a considerable residual cross section σ_{magn} to be attributed to the magnetic interaction of the neutron with the magnetic electrons of iron. Two striking properties of the residual scattering are revealed by the experiment:

(a) For temperatures above as well as below the Curie temperature $T_c = 1043°K$ of iron, σ_{magn} is proportional to λ, indicating that the scattering is inelastic.

(b) As a function of temperature σ_{magn}, which vanishes at $T=0$ on theoretical grounds, exhibits a maximum at the Curie point, with an abrupt change of slope. Its decrease on the left of the maximum is much faster than on the right. The ratio σ_{magn}/σ_l of σ_{magn} to its largest observed value σ_l is independent of λ and is plotted against T/T_c in Fig. 1 (solid line), with indication of the experimental points. One has $\sigma_l = 3.5$ barns for $\lambda = 8A$.

Our object is to interpret briefly these properties, restricting ourselves to temperatures below 1179°K, the α–γ transition point of iron.

The inelastic nature of the magnetic scattering (property *a*) for wavelengths λ larger than the Bragg cutoff is a direct consequence of the strong exchange interaction between the magnetic spins of iron: when the Bragg condition is not satisfied the energy transfer ΔE between neutrons and system of interacting spins is continuously distributed, without singular peak at $\Delta E = 0$. This fact is independent of the presence or absence of long-range order and holds thus for paramagnetic as well as ferromagnetic iron. It was recognized by Van Vleck,[2] who discussed a few features of the distribution of ΔE in the limit of infinite temperature.

For the magnitude and temperature dependence of

* Part of this work was carried out at Brookhaven National Laboratory and supported by the U. S. Atomic Energy Commission.
[1] H. Palevsky and D. J. Hughes, Phys. Rev. 92, 202 (1953).

[2] J. H. Van Vleck, Phys. Rev. 55, 924 (1939).

σ_{magn}, as shown by Moorhouse,[3] spin-wave theory can be used when $T \ll T_c$. Adopting the atomic (Heisenberg) model of ferromagnetism, with the value $s_0 = 1$ for the atomic spin and the low-temperature determination of the exchange interaction,[4] one obtains the lower curve of Fig. 1 for the calculated value of σ_{magn} divided by the largest experimental value σ_l. Both in absolute magnitude and in temperature dependence, the agreement is quite bad outside the low-temperature region, in fact for all temperatures at which σ_{magn} can be separated from nuclear effects with any accuracy. Higher-order corrections are found too small to modify this conclusion.

Despite the absence of a reliable theory of ferromagnetism at temperatures of the order of the Curie temperature, the main features of the observed temperature dependence of σ_{magn} for $T \gtrsim T_c/2$ can be understood by describing the magnetic scattering in terms of the correlation $\mathcal{G}_T(\mathbf{r},t) = \langle \mathbf{S}_0(0) \cdot \mathbf{S}_r(t) \rangle_T$ between the atomic spin $\mathbf{S}_0$ at lattice position 0, considered at time 0, and the atomic spin $\mathbf{S}_r$ at lattice position $\mathbf{r}$, considered at time t. We have

$$\mathbf{S}_r(t) = \exp(itH/\hbar)\mathbf{S}_r \exp(-itH/\hbar),$$

where H is the Hamiltonian. $\langle \cdots \rangle_T$ denotes the average over the thermal distribution. For scattering of long-wavelength neutrons by a polycrystal at temperature T, one finds, neglecting lattice vibrations,

$$\sigma_{magn} = \frac{\hbar\lambda}{6\pi M}\left(\frac{2\gamma e^2}{m_0 c^2}\right)^2 \sum_r \int_{-\infty}^{\infty} dt \cdot f(r,t) \cdot [g_T(\mathbf{r},t) - g_0(\mathbf{r},t)], \quad (1)$$

where

$$g_T(\mathbf{r},t) = \mathcal{G}_T(\mathbf{r},t) - \lim_{t' \to \infty} \mathcal{G}_T(\mathbf{r},t'), \quad g_0 = g_T \text{ with } T = 0,$$

$$f(r,t) = r^{-1} \int_0^{\infty} |F(\kappa)|^2 \cdot \cos(\hbar\kappa^2 t/2M) \cdot \sin(\kappa r)\kappa d\kappa,$$

M and m_0 denote the neutron and electron masses, γ is the neutron magnetic moment in nuclear magnetons, and $F(\kappa)$ is the form factor of the magnetic electrons. Assuming the Hamiltonian invariant under simultaneous rotations of all spins, and thus neglecting dipole-dipole interactions, one can establish that

$$g_T(\mathbf{r},t) - g_0(\mathbf{r},t) = s_0^2\{1 - (I_T/I_0)^2\} \cdot g_T'(\mathbf{r},t), \quad (2)$$

[3] R. G. Moorhouse, Proc. Phys. Soc. (London) **A64**, 1097 (1951).
[4] C. Kittel, Revs. Modern Phys. **21**, 541 (1949), esp. Eq. (2.1.17).

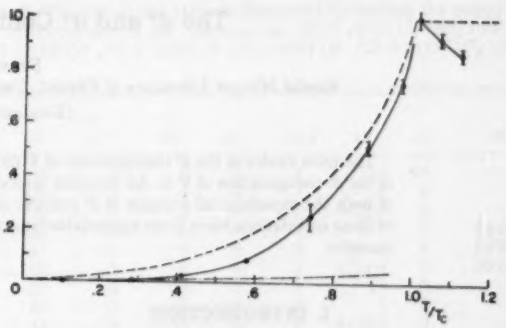

FIG. 1. Observed magnetic cross section σ_{magn}, in units of σ_l (———); σ_{magn} calculated from spin-wave theory, in units of σ_l (–·–·–); factor $\{1-(I_T/I_0)^2\}$ (– – – –).

where I_T is the saturation intensity of magnetization of the crystal at temperature T and $g_T'(\mathbf{r},t)$ is a function so normalized that for all temperatures it takes the value 1 at $\mathbf{r} = t = 0$ and tends to zero for r or $t \to \infty$.

If (2) is inserted into (1), σ_{magn} is seen to contain the factor $1-(I_T/I_0)^2$, known from the experimental values of I_T and plotted in Fig. 1 (upper curve). This factor accounts for a considerable part of the temperature variation of σ_{magn}. The rest of the variation comes from the temperature dependence of g_T', expected to be rather weak except when T approaches 0 or T_c. When $T \to T_c$, the asymptotic form of g_T' for r or $t \to \infty$ depends strongly on $T - T_c$, corresponding to an increase in range of the correlation. This predicts an increase of

$$\{1-(I_T/I_0)^2\}^{-1} \cdot \sigma_{magn}$$

when the Curie point is approached on either side, in full agreement with the observations. The essential features of the temperature variation of σ_{magn} in the region $T \gtrsim \frac{1}{2}T_c$ are thus qualitatively accounted for. A more quantitative treatment, as well as a theoretical estimate of the absolute magnitude of σ_{magn}, must be based on an approximate evaluation of the space-time correlation function $\mathcal{G}_T(\mathbf{r},t)$. This problem, as well as the general use of space-time correlation functions in scattering theory, will be discussed in detail elsewhere.

The author's thanks are due to D. J. Hughes and H. Palevsky for making their results available before publication and for several discussions, and to G. Placzek for valuable remarks.

The d^3 and d^4 Configurations of Vanadium*

SYDNEY MESHKOV
Randal Morgan Laboratory of Physics, University of Pennsylvania, Philadelphia, Pennsylvania
(Received October 5, 1953)

The term values of the d^3 configuration of V III are calculated using the experimentally observed energies of the d^4 configuration of V II. An iterative type calculation is then made for the term values of d^4 in terms of both the experimental energies of d^3 and the calculated values of the still unidentified terms of d^3. Each of these calculations leads to an appreciable improvement of the agreement between calculated and observed energies.

I. INTRODUCTION

IN this paper we shall first calculate the term values of the d^3 configuration of V III in terms of the experimentally observed energies of the d^4 configuration of V II. The formalism used for the calculation was developed in a previous paper.[1] It allows us to express the energies of any ion or atom in terms of the experimentally observed energies of ions of higher ionization, or, as we pointed out, in terms of the energies of lower ionization. It is possible to write the terms of d^4 as a function of the experimentally observed energies of d^3 plus a linear combination of parameters which represents the change in value of the Slater[2] integrals as we go from the d^3 configuration to the d^4 configuration.

Conversely, we can write the terms of d^3 as a function of d^4 energies and the various changes in parameters. In Sec. II, we shall discuss in detail the derivation and application of the appropriate equations which will allow us to do the calculation. Use is made of Many's[3] extensive calculations on the same two configurations; of particular value are his calculated values of the various radial parameters for both the d^3 and d^4 configurations. The results of the calculation of the term values of d^3 are compared with experiment, and we find that the root-mean-square deviation is reduced from Many's value of ± 625 cm^{-1} to ± 244 cm^{-1}.

In Sec. III, using Eqs. (84) of Racah,[4] we calculate new values of the radial integrals A, B, C, for the d^3 configuration. These parameters together with Many's parameters for d^4 give us new values of ΔA, ΔB, and ΔC. From the experimental values of d^3, from our newly calculated values of the still unidentified terms of d^3, and from the new ΔA, ΔB, and ΔC, we compute the term values of d^4. The root-mean-square deviation is reduced from Many's value of ± 986 cm^{-1} to ± 663 cm^{-1}.

This iterative method could be repeated once again by calculating the radial integrals associated with d^4, subtracting them from the new radial integrals of d^3, thus obtaining a new set of parameters ΔA, ΔB, and ΔC. The terms of d^3 could then be recalculated from this new set ΔA, ΔB, and ΔC, from the experimental energies of d^4, and from the newly calculated values of the still unidentified terms of d^4.

Our calculation seems to confirm Many's objection to White's[5] classification of $d^3\,{}^2P$ as being at 11 327 cm^{-1}.[6] However, we do not find that both the $d^3\,{}^2P$ and the $d^3\,{}^2H$ terms lie at the same level. We find that they should be separated by 1560 cm^{-1}.

We also agree with Many's objection to the classification of $d^4\,{}^1D^+$ at 44 658 cm^{-1}. Our calculated value of $d^4\,{}^1D^+$ is 47 785 cm^{-1}; Many's is 48 093 cm^{-1}.

II. CALCULATION OF d^3 TERMS

In order to derive the equations which relate the terms of d^4 to those of d^3, we use the method developed in Sec. II of M. We also require the use of the coefficients of fractional parentage given in Table III of Racah.[7] The equations are listed in Table I.

Our problem is that of trying to solve these equations for the various matrix elements of d^3 in terms of the experimentally observed energies of d^4 and in terms of the ΔA, ΔB, and ΔC. However, the above equations (Table I) are not all given in terms of the observed energies but in terms of the various matrix elements of the energies. Our first task is to build a scheme which lets us express both the diagonal and off-diagonal elements in terms of the observed energies. Consider a 2×2 matrix whose diagonal elements are a and b, and whose off-diagonal elements are c. Let there also be given the matrix

$$S=\begin{vmatrix} \alpha & \beta \\ -\beta & \alpha \end{vmatrix}$$

* Part of a dissertation in Physics presented to the Faculty of the Graduate School of the University of Pennsylvania in partial fulfillment of the requirements for the degree of Doctor of Philosophy.

[1] S. Meshkov, Phys. Rev. 91, 871 (1953), referred to as M.

Errata to Reference 1

Text: Two lines after Eq. (15): for equal to 0 read odd.

TABLE I.

Entry: $d^3\rho(^3P[^3P])-d\rho(^3P)$: for $-54\frac{1}{2}$ read $-27\frac{1}{2}$.

TABLE III.

Entry: $p^3s(^3S)-p^3s(^1P)$: for $3\frac{1}{2}$ read 1.
$p^3s(^3S)-N$: for $2^{-\frac{1}{2}}$ read 2^{-1}.
$p^3s(^1S)-p^3s(^1P)$: for 1 read $3\frac{1}{2}$.
$p^3s(^3D)-p^3s(^3D)$: for $-3\frac{1}{2}$ read -3.

[2] J. C. Slater, Phys. Rev. 34, 1293 (1929).
[3] A. Many, Phys. Rev. 70, 511 (1946).
[4] G. Racah, Phys. Rev. 62, 438 (1942), referred to as R II.
[5] H. E. White, Phys. Rev. 33, 672 (1929).
[6] 11 327 cm^{-1} is the center of gravity of the doublet 11 207 cm^{-1} and 11 387 cm^{-1}.
[7] G. Racah, Phys. Rev. 63, 367 (1943).

TABLE I. The elements of the energy matrices of the configuration d^4. The use of this table is illustrated by writing the energy of the $_2{}^3F$ term of d^4. Note that the multiplier, N, does not operate on the coefficients of ΔA, ΔB, and ΔC. $W(d^4\ {}_2{}^3F) = (1/420)[16W(d^3\ {}_2{}^3P)+56W(d^3\ {}_2{}^4P)+315W(d^3\ {}_1{}^3D)+15W(d^3\ {}_2{}^3D)+30(21)^{\frac{1}{2}}W(d^3\ {}_{1,2}{}^3D)+14W(d^3\ {}_2{}^3F)+224W(d^3\ {}_2{}^4F)+90W(d^3\ {}_2{}^3G)+110W(d^3\ {}_2{}^2H)]+6\Delta A-2\Delta B+7\Delta C$.

d^4	N	d^3 $_2{}^3P$	$_2{}^4P$	$_1{}^3D$	$_2{}^3D$	$_{1,2}{}^3D$	$_2{}^3F$	$_2{}^4F$	$_2{}^3G$	$_2{}^3H$	$6\Delta A$	ΔB	ΔC	E[a]
$W(_0{}^1S)$	1	0	0	2	0	0	0	0	0	0	1	14	14	...
$W(_4{}^1S)$	1	0	0	0	2	0	0	0	0	0	1	6	6	...
$W(_{0,4}{}^1S)$	1	0	0	0	0	2	0	0	0	0	0	$6(21)^{\frac{1}{2}}$	0	...
$W(_2{}^3P)$	1/180	14	64	135	35	$-30(21)^{\frac{1}{2}}$	56	56	0	0	1	−7	7	24 024
$W(_4{}^3P)$	1/45	25	14	0	10	0	25	16	0	0	1	−3	4	19 854
$W(_{2,4}{}^3P)$	$(14)^{\frac{1}{2}}/90$	−5	8	0	−5	$15(3)^{\frac{1}{2}}/(7)^{\frac{1}{2}}$	10	−8	0	0	0	$4(14)^{\frac{1}{2}}$	0	10 015
$W(_2{}^1D)$	(1/140)	42	0	105	45	$30(21)^{\frac{1}{2}}$	28	0	60	0	1	15	9	...
$W(_4{}^1D)$	1/70	42	0	0	20	0	63	0	15	0	1	3	6	...
$W(_{2,4}{}^1D)$	$\sqrt{2}/140$	−42	0	0	30	$10(21)^{\frac{1}{2}}$	42	0	−30	0	0	$12(2)^{\frac{1}{2}}$	0	...
$W(_2{}^3D)$	1/105	14	49	0	60	0	21	21	45	0	1	−5	4	18 317
$W(_4{}^5D)$	1/5	0	3	0	0	0	0	7	0	0	1	−21	0	206
$W(_4{}^1F)$	1/280	120	0	0	200	0	105	0	3	132	1	0	6	26 840
$W(_2{}^3F)$	1/420	16	56	315	15	$30(21)^{\frac{1}{2}}$	14	224	90	110	1	−2	7	26 724
$W(_4{}^3F)$	1/840	200	448	0	120	0	175	112	405	220	1	−8	4	17 136
$W(_{2,4}{}^3F)$	1/420	−40	112	0	30	$30(21)^{\frac{1}{2}}$	35	−112	−135	110	0	12	0	6863
$W(_2{}^1G)$	1/252	0	0	189	25	$-30(21)^{\frac{1}{2}}$	70	0	66	154	1	−6	9	29 912
$W(_4{}^1G)$	1/504	0	0	0	88	0	385	0	507	28	1	−4	6	24 424
$W(_{2,4}{}^1G)$	$(11)^{\frac{1}{2}}/252$	0	0	0	−10	$6(21)^{\frac{1}{2}}$	35	0	−39	14	0	$4(11)^{\frac{1}{2}}$	0	8841
$W(_4{}^3G)$	1/840	0	0	0	200	0	315	560	297	308	1	−12	4	14 572
$W(_4{}^3H)$	1/30	0	0	0	0	0	5	20	9	26	1	−17	4	12 634
$W(_4{}^1I)$	1/5	0	0	0	0	0	0	0	3	7	1	−15	6	19 192

[a] E is the numerical value of the matrix elements of the d^4 configuration when $C/B=3.41$. E is expressed in units of cm^{-1}.

which diagonalizes the 2×2 matrix to give λ^+ and λ^-, the experimentally observed energies. From matrix transformation theory, we can write

$$\begin{aligned} a&=\alpha^2\lambda^+ + \beta^2\lambda^-,\\ b&=\beta^2\lambda^+ + \alpha^2\lambda^-,\\ c&=\alpha\beta(\lambda^+ - \lambda^-), \end{aligned} \tag{1}$$

where

$$\begin{aligned} \alpha^2&=\tfrac{1}{2}\{1+[1+4c'^2/(a'-b')^2]^{-\frac{1}{2}}\},\\ \beta^2&=\tfrac{1}{2}\{1-[1+4c'^2/(a'-b')^2]^{-\frac{1}{2}}\}. \end{aligned} \tag{2}$$

Let a', b', and c' represent the theoretical forms of a, b, and c expressed in terms of the radial parameters A, B, and C.

In order to evaluate α and β, it is necessary to know the C/B ratio for the particular configuration we are dealing with. At first, we shall use Many's values of the parameters B and C for the d^4 configuration: $B=628$ cm^{-1}, $C=2142$ cm^{-1}. This yields $C/B=3.41$. Different values of α and β must be calculated for each 2×2 matrix which we consider. Once the values of α and β are known, the various matrix elements a, b, and c can be computed. The numerical values of the matrix elements of the d^4 configuration are listed in Table I.

It is also necessary to know the values of ΔA, ΔB, and ΔC. Many has calculated

$$\begin{aligned} A(d^3)&=3958\ cm^{-1};\quad B(d^3)=766\ cm^{-1};\\ C(d^3)&=2855\ cm^{-1},\\ A(d^4)&=2271\ cm^{-1};\quad B(d^4)=628\ cm^{-1};\\ C(d^4)&=2142\ cm^{-1}. \end{aligned}$$

Therefore,

$$\begin{aligned} \Delta A&=A(d^4)-A(d^3)=-1687\ cm^{-1},\\ \Delta B&=B(d^4)-B(d^3)=-138\ cm^{-1},\\ \Delta C&=C(d^4)-C(d^3)=-714\ cm^{-1}. \end{aligned} \tag{3}$$

In our calculation, all of the equations of Table I except those involving the ^1S and ^1D terms of d^4 will be used. The ^1S and ^1D states are not used inasmuch as $^1S^+$ is not known and there is some doubt as to the proper classification of $^1D^+$. From Table I we formulate a set of normal equations for a least squares calculation which is to yield the various matrix elements for the d^3 configuration. From these matrix elements we can calculate the energies. The results of this calculation are listed in Table II, together with Many's results. The root-mean-square deviation of our calculated values from the experimental energies is reduced from ±625 cm^{-1} to ±244 cm^{-1}.

TABLE II. Energies of the d^3 configuration of V III. All numbers are in units of cm^{-1}.

Term	Experiment	Many	Δ_1[a]	Calculated	Δ_2[b]
$_2{}^3P$	...	15 844	...	15 655	...
$_2{}^4P$	11 668	11 873	205	11 506	−162
$^3D^-$	16 317	17 197	880	16 702	385
$^3D^+$	...	42 756	...	41 257	...
$_2{}^3F$	...	27 329	...	27 994	...
$_2{}^4F$	336	387	51	174	−162
$_2{}^3G$	12 089	12 015	−74	12 126	37
$_2{}^3H$	16 907	15 844	−1063	17 215	308
rms deviation			±625		±244

[a] Δ_1 is the deviation of Many's calculated value from experiment.
[b] Δ_2 is the deviation of the value calculated in this paper from experiment.

TABLE III. Energies of the d^4 configuration of V II. All numbers are in units of cm^{-1}.

Term	Experiment	Many	Δ_1[a]	Calculated	Δ_2[b]
$^3P^+$	32 169	31 870	−299	32 303	134
$^3P^-$	11 709	12 656	947	11 979	270
^3_4D	18 317	19 050	733	18 464	147
^5_4D	206	427	221	−71	−277
^1_4F	26 840	26 476	−364	26 506	−334
$^3F^+$	30 302	31 366	1064	31 468	1166
$^3F^-$	13 558	13 160	−398	13 029	−529
$^1G^+$	36 425	35 276	−1149	36 568	143
$^1G^-$	17 911	17 819	−92	17 780	−131
^3_4G	14 572	14 651	79	14 983	411
^3_4H	12 634	11 509	−1125	12 459	−175
^1_4I	19 191	17 050	−2141	18 629	−562
$^1S^+$	...	61 853	...	60 604	...
$^1S^-$	19 902	20 806	904	19 182	−720
$^1D^+$	...	48 093	...	47 785	...
$^1D^-$	20 981	22 597	1616	22 754	1773
rms deviation			±986		±663

[a] Δ_1 is the deviation of Many's calculated value from experiment.
[b] Δ_2 is the deviation of the value calculated in this paper from experiment.

III. CALCULATION OF d^4 TERMS

We now calculate the various matrix elements of d^4 using all of Table I. We use the known energies of d^3 together with the values which we have just calculated of the still experimentally unidentified terms of d^3. In order to use the one experimentally known ^2D energy of d^3, we calculate the value of the off-diagonal element $W(d^3\,_{1,3}{}^2D)$ using the experimental value of $^2D^-$ and the diagonal elements, $W(d^3\,_1{}^2D)$ and $W(d^3\,_3{}^2D)$, the values of which have been calculated in Sec. II. Using Eq. (4),

$$^2D^- = \tfrac{1}{2}[W(d^3\,_1{}^2D)+W(d^3\,_3{}^2D)] - \{\tfrac{1}{4}[W(d^3\,_1{}^2D)-W(d^3\,_3{}^2D)]^2 + [W(d^3\,_{1,3}{}^2D)]^2\}^{\frac{1}{2}}, \quad (4)$$

with $^2D^- = 16\,317$ cm^{-1}, $W(d^3\,_1{}^2D) = 36\,465$ cm^{-1}, and $W(d^3\,_3{}^2D) = 21\,494$ cm^{-1}, we obtain $W(d^3\,_{1,3}{}^2D) = 10\,214$ cm^{-1}. This value is the one used in the calculation of the d^4 energies.

In addition, we need values of ΔA, ΔB, and ΔC. We can improve on our previous values of these parameters by finding new values of A, B, and C for the d^3 configuration. These new values are called A_1, B_1, and C_1. To calculate these parameters, we use Eqs. (84) of R II except for those equations involving the ^2D terms. To account for the ^2D terms, we use Eqs. (5) which express the diagonal elements $W(d^3\,_1{}^2D)$ and $W(d^3\,_3{}^2D)$ as functions of A, B, C,

$$W(d^3\,_1{}^2D) = 3A+7B+7C,$$
$$W(d^3\,_3{}^2D) = 3A+3B+3C. \quad (5)$$

We use the experimental values for $W(d^3\,_3{}^4P)$, $W(d^3\,_3{}^4F)$, $W(d^3\,_3{}^2G)$, and $W(d^3\,_3{}^2H)$, the calculated values for $W(d^3\,_3{}^2P)$, $W(d^3\,_3{}^2F)$, $W(d^3\,_1{}^2D)$, and $W(d^3\,_3{}^2D)$. We do not include the equation for the off-diagonal element $W(d^3\,_{1,3}{}^2D)$, inasmuch as its use might lead to greater errors than would the use of the diagonal elements only. We find that a least-squares calculation yields

$$A_1(d^3) = 3962\ cm^{-1}; \quad B_1(d^3) = 752\ cm^{-1};$$
$$C_1(d^3) = 2810\ cm^{-1}.$$

Using these new values of d^3 parameters together with the A, B, and C calculated by Many for d^4, our new parameters ΔA_1, ΔB_1, ΔC_1 become

$$\Delta A_1 = 2271\ cm^{-1} - 3962\ cm^{-1} = -1691\ cm^{-1},$$
$$\Delta B_1 = 628\ cm^{-1} - 752\ cm^{-1} = -124\ cm^{-1},$$
$$\Delta C_1 = 2142\ cm^{-1} - 2810\ cm^{-1} = -668\ cm^{-1}.$$

We compute the term values of d^4 and list them in Table III together with the experimental values. The root-mean-square deviation is reduced from Many's value of ± 986 cm^{-1} to ± 663 cm^{-1}.

The writer is grateful to Dr. C. W. Ufford for his sincere interest and guidance.

Correlation Energies and Angular Components of the Wave Functions of the Ground States of H^-, He I, and Li II*

LOUIS C. GREEN, MARGARET N. LEWIS, MARJORIE M. MULDER, CYNTHIA W. WYETH, AND JOHN W. WOLL, JR.
Strawbridge Observatory, Haverford College, Haverford, Pennsylvania

(Received September 10, 1953)

With a view to examining the effects of configuration interaction in the ground state of the three simple atomic systems, H^-, He I, and Li II, a three-parameter variational function involving a symmetrized exponential in the nuclear distances and a linear factor in the interelectron distance has been obtained for He I and Li II. These functions together with the one of the same type already in existence for H^- have been expanded in series of Legendre functions of the cosine of the angle between the two radius vectors. The coefficients in these expansions are functions of the nuclear distances of the two electrons. The various component functions are presented, together with the coefficients with which they enter the expansions, and their contributions to the total energies. A discussion is given of the method of estimating the magnitude of the total correlation, or configuration interaction, energy and its radial, angular, and mixed parts. A table is given of the values of the correlation energy and its various parts for H^-, He I, and Li II.

THE great body of theoretical atomic spectroscopy is based on central-field wave functions. The fact that this method of approach gives results in good agreement with the classification of atomic energy states, as worked out more or less independently by the experimental spectroscopists, indicates that the central-field approximation is a good one. Furthermore, it is clear how the simple theory should be extended in a higher approximation to include the effects of exchange and configuration interaction. On the other hand, in those cases in which the theory has been most completely worked out, something is left to be desired. Hartree, Hartree, and Sirles[1] have superposed the $1s^22p^{q+2}$ and the $1s^22s^22p^q$ configurations for O III, O II, and O I, using wave functions with exchange. Jucys[2] has superposed the $1s^22s^22p^2$, $1s^22p^4$, $1s^22s^22p3p$, and the $1s^22s2p^23s$ for C I using self-consistent field wave functions without exchange. In both cases some slight improvement in the energies was found. The cause of this disappointing outcome is suggested by work on the ground state of He I,[3] which indicates that to obtain good results it would be necessary to superpose a large number of configurations.

In contrast to the wave functions derived on the central-field approximation are those which contain terms or functions in the interelectron distances r_{ij}. The Hylleraas[4] and the Baber and Hassé[5] wave functions for He I are of this type. With only a few exceptions[6] very little has been done on the more complex spectra with wave functions involving the r_{ij}'s. However, in two electron spectra, which are almost the only ones which have been worked out in detail, the inclusion in the wave function of fairly simple terms in r_{12} has yielded good values of the energy. On the other hand, there are certain disadvantages to using the r_{ij}'s. No simple combination of elementary functions of r_{ij} is an eigenfunction of any large part of the energy operator. In addition the r_i's and r_{ij}'s do not form an orthogonal coordinate system. The energy operator is therefore rather involved. This is true also of many of the integrals which arise when the minimum principle is applied.

Fortunately one may take advantage of the accuracy offered by the solutions involving the r_{ij}'s to learn something of the form which solutions in central-field wave functions would have to possess if they were to be of equal accuracy. To do so, one expands the r_{ij} solutions in series of central-field solutions. The latter should form complete orthogonal sets. The individual members of a set may be constructed from one-electron wave functions in such a way as to have the desired symmetry and exchange properties. That is, the individual members of the set may be chosen to represent particular levels arising from particular electron configurations. The coefficients in the expansion then show just what configurations must be superposed, and with what weight, to obtain a solution in the central-field approximation equivalent to the r_{ij} solution.[7]

The present paper takes the first step in the direction of such an expansion in the case of a relatively simple type of expression for the ground-state wave functions of H^-, He, and Li^+. This first step consists in expanding the solution involving r_{12} in terms of a series of normalized Legendre functions of the cosine of the angle between the two radius vectors. It is wise to begin the expansions in this way because some interesting results with regard to the relative importance of the various

* This research was supported in part by The United States Air Force under a contract monitored by the Office of Scientific Research, Air Research and Development Command, and in part by a U. S. Office of Naval Research contract. Both contracts were administered by the University of Pennsylvania.

[1] Hartree, Hartree, and Swirles, Trans. Roy. Soc. (London) A238, 229 (1939).

[2] A. Jucys (sometimes transliterated A. Yutsis), J. Exptl. Theoret. Phys. (U.S.S.R.) 19, 565 (1949).

[3] Green, Mulder, Ufford, Slaymaker, Krawitz, and Mertz, Phys. Rev. 85, 65 (1952).

[4] E. A. Hylleraas, Z. Physik 54, 347 (1929).

[5] T. D. H. Baber and H. R. Hassé, Proc. Cambridge Phil. Soc. 33, 253 (1937).

[6] H. M. James and A. S. Coolidge, Phys. Rev. 49, 688 (1936); E. Conwell, Phys. Rev. 74, 268 (1948); R. M. Thaler, Phys. Rev. 83, 131 (1951).

[7] The possibility of investigating configuration interaction in He I in this manner was suggested to one of us (L.C.G.) by Dr. G. Breit.

angular components of the wave functions appear at once. Besides the results of the more detailed expansions into configurations which might follow will depend on the particular type of function chosen for the radial components of the central-field wave functions.[8] The coefficients of the Legendre functions in the expansion are themselves functions of r_1 and r_2, the distances of the two electrons from the nucleus. We then have

$$\Psi^N(r_1,r_2,r_{12})=\sum_i c_i\Phi_i^N(r_1,r_2)P_i^N(\cos\theta), \qquad (1)$$

where Ψ^N is the normalized function involving r_{12} which is to be expanded, P_i^N is the normalized Legendre polynomial of order i, and the Φ_i^N's are normalized functions of r_1 and r_2 whose form is to be determined from Eq. (1). Ψ^N is normalized with respect to integration over r_1, θ_1, and φ_1, the coordinates of the first electron, r_2 for the second electron, r_{12}, and φ, the Euler angle which together with r_{12} specifies the direction of r_2 with respect to r_1. The Φ_i^N's are normalized with respect to integration over r_1, θ_1, φ_1, r_2, and φ. From Eq. (1) it then follows that Φ_i^N is given by the expression

$$\Phi_i^N=\frac{1}{c_i}\int\Psi^N P_i^N\sin\theta d\theta, \qquad (2)$$

and c_i by the expression

$$c_i=\left\{\int\left[\int\Psi^N P_i^N\sin\theta d\theta\right]^2 d\tau'\right\}^{\frac{1}{2}}, \qquad (3)$$

where $d\tau'$ indicates the volume element with respect to r_1, θ_1, φ_1, r_2, and φ.

Expansions of the type described in the above paragraph have already been carried through[9] using for Ψ^N the three and the six constant expressions for the ground state of He I given by Hylleraas.[4] However, these two Ψ^N's are of quite similar form so that, although the c_i's did not vary much between the two expansions, there was still some possibility of doubt as to the validity of the conclusions with regard to the relative importance of the various angular components of the ground-state wave function and to the size of the components of the correlation energy. It therefore seemed wise to repeat the foregoing work using a ground-state wave function containing terms in r_{12} but of a somewhat different functional form from those of Hylleraas. At the same time it was felt that it would be distinctly interesting to examine the variation in the importance of the correlation energy, together with its various parts, and of the different angular components of the ground-state wave function as one passes from the negative ion H^-, to the neutral atom He I, and on to the positive ion Li II. For such a comparison to be of the most interest it seemed that the same type of ground-state wave function should be used for the expansion in all three cases.

TABLE I. Values of the constants in Eq. (4) and of the computed energies (in units of $R_Z hc$).

	H^-	He I	Li II
N	0.0312241	0.675135	2.88811
Z_1	0.478[a]	1.436	2.362
Z_2	1.075[a]	2.208	3.299
α	0.3121[a]	0.2924	0.2770
E(cal)	−1.05184[a]	−5.80284	−14.55435
E(exp)	−1.05512[b]	−5.80752	−14.56079

[a] Taken from Chandrasekhar; see reference 10.
[b] Best calculated value, due to Henrich; see reference 11.

[8] The value of an expansion in terms of Legendre functions was pointed out to two of us (L.C.G. and M.M.M.) by Dr. E. U. Condon.

[9] Green, Mulder, and Milner, Phys. Rev. **91**, 35 (1953).

The best available three-parameter wave function for H^- is that due to Chandrasekhar.[10] It is of the form

$$\Psi^N=N(e^{-Z_1r_1-Z_2r_2}+e^{-Z_2r_1-Z_1r_2})(1+\alpha r_{12}), \qquad (4)$$

where r_1, r_2, and r_{12} are measured in atomic units and Z_1, Z_2, and α are chosen to give the lowest energy. This simple function gives an energy only 0.31 percent above that given by the best function now known, Henrich's eleven-parameter function.[11] The expression for Ψ^N in Eq. (4) is of a distinctly different form from the three- and six-parameter functions of Hylleraas for He I,[4] which were used in the earlier expansions.[9] The functions given by Hylleraas use the same effective nuclear charge for both electrons and the symmetrized exponential therefore does not appear. Furthermore, Hylleraas includes quadratic terms in r_1, r_2, and r_{12} in the final factor. It seemed therefore that if a function of the form given by Eq. (4) should prove to give good values of the energy for He I and Li II as well as for H^-, it would be plausible to take this as the type of function to be expanded.

The first task was, therefore, to obtain the values of the parameters in Eq. (4) which would give the lowest energies for the ground states of He I and Li II. The values found for these parameters as well as the energies which they yield are given in Table I together with the results of Chandrasekhar for H^-. In the first line is given the ion; in the second, the normalization constant; in the third, fourth, and fifth, the values of the parameters in Eq. (4); in the sixth the energy calculated from the energy integral using these values of the parameters and units of $R_H hc$, $R_{He}hc$, and $R_{Li}hc$ for H^-, He, and Li^+, respectively; in the first column of the seventh line the value of the H^- energy found by Henrich,[11] and in the second and third columns the experimental values of the energies for He I and Li II.[12] As already indicated Chandrasekhar's wave function gives an energy only 0.31 percent above Henrich's

[10] S. Chandrasekhar, Astrophys. J. **100**, 176 (1944).

[11] L. R. Henrich, Astrophys. J. **99**, 59 (1944).

[12] The values of the ionization energies and Rydberg constants were taken from Charlotte E. Moore, *Atomic Energy Levels*, National Bureau of Standards Circular 467 (U. S. Government Printing Office, Washington, D. C., 1949).

value. For He I the energy given by the wave function of Eq. (4) exceeds the experimental value by 0.081 percent and for Li II by 0.044 percent. All three wave functions are therefore quite good. It is interesting to note for comparison that with the Hylleraas three-parameter wave function,† the energy for H^- is 0.44 percent above Henrich's value and for He I it is 0.045 percent above the experimental value.

If one examines the values of the parameters in Table I, several points of interest emerge. As one passes from H^- to Li^+, the difference between the true nuclear charge and Z_1, the effective nuclear charge for the outer electron, shows the expected increase toward one. In other words, as the nuclear charge increases, the shielding of the outer electron by the inner becomes more complete. Chandrasekhar[10] has already pointed out that in H^- if α is set equal to zero, $Z_1=0.283$ and $Z_2=1.039$ so that dropping the r_{12} term increases the shielding of the outer electron by 0.195 unit. In He I for $\alpha=0$, one finds[12] $Z_1=1.19$ and $Z_2=2.18$ so that dropping the r_{12} term increases the shielding by 0.25 unit. In Li II setting $\alpha=0$ yields $Z_1=2.08$ and $Z_2=3.29$, so that in this case dropping the r_{12} term increases the shielding of the outer electron by 0.28 unit.

If the values of Z_2 in Table I are divided by the nuclear charges, one obtains a slowly varying number, which already in the case of Li^+ seems to be decreasing toward one, as was to be expected. A more interesting result is found in the values of α. One might at first expect that the relative importance of the r_{12} term would decrease sharply with increasing nuclear charge. However, Table I shows a rather slow decline for α, which we may attribute to the fact that the increasing nuclear charge pulls the electrons into a smaller volume and thereby increases their interaction.

When the values of the parameters in Eq. (4) had been found, the Ψ^N's were substituted into Eq. (3) and the values of the c_i's were obtained. Table II gives the values of the c_i's. The final line of the table gives the values of $\sum_i c_i^2$. If the expansions were complete and the normalization constants were exact, this sum should be one. Above all else Table II shows how far the ground-state wave functions for these atomic structures are from spherically symmetric. The coefficients of the P_1^N terms are 12 percent, 7 percent, and 5 percent of the coefficients of the P_0^N term for H^-, He I, and Li II, respectively. If the values of the c_i's for He I in Table II are compared with those found earlier[9] for the Hylleraas three- and six-parameter wave functions, one finds that the coefficients for the two three-parameter functions differ on the average, for the four coefficients given, by less than 0.6 percent. On the other hand, the coefficients of the two Hylleraas functions differ by almost 12 percent. These averages might vary markedly if a different number of coefficients were considered. However, in view of the difference in functional form of the three-parameter solutions and the similarity in form of the Hylleraas solutions, it is surprising that for not one of the coefficients computed does the difference between the three-parameter functions amount to as much as one-sixth of the difference of the two Hylleraas functions.

TABLE II. Values of c_i in the expansion $\Psi^N=\sum_i c_i\Phi_i^N P_i^N$.

	H^-	He I	Li II
c_0	0.993206	0.997467	0.998806
c_1	0.115067	0.070256	0.048251
c_2	0.016245	0.010387	0.007179
c_3	0.005375	0.003501	0.002426
$\sum_i c_i^2$	0.999991	0.999996	0.999998

With the values of the c_i's known, one can write from Eq. (2) explicit expressions for the Φ_i^N's. For $i=0$ these take the form

$$\Phi_0^N=\frac{\sqrt{2}N}{c_0}(e^{-Z_1r_1-Z_2r_2}+e^{-Z_2r_1-Z_1r_2})\left\{1+\frac{\alpha}{3}\left(\frac{r_<^2}{r_>}+3r_>\right)\right\},$$

and for $i=n>0$:

$$\Phi_n^N=\frac{\sqrt{2}N}{c_n}(e^{-Z_1r_1-Z_2r_2}+e^{-Z_2r_1-Z_1r_2})\times\left\{\frac{\alpha}{(2n+3)(2n+1)^{\frac{1}{2}}}\frac{r_<^n}{r_>^{n-1}}\left(\frac{r_<^2}{r_>^2}-\frac{2n+3}{2n-1}\right)\right\}.$$

When the Φ_i^N's are known, one may proceed to find the contribution to the total energies of the various components of the ground-state wave functions. For this purpose the terms in the integral

$$E=\int\sum_i(c_i\Phi_i^N P_i^N)^*H\sum_i(c_i\Phi_i^N P_i^N)d\tau,$$

where $d\tau$ indicates the volume element with respect to all six variables, have been computed separately and the results are presented in Table III. The first column of Table III gives the various terms in the integrand, where (i) is written for $c_i\Phi_i^N P_i^N$. The second, fourth and sixth columns give the contributions of these terms to the energy in units of R_Hhc, $R_{He}hc$, and $R_{Li}hc$ for H^-, He I, and Li II, respectively. The third, fifth, and seventh columns give the contributions of the various angular components to the energy if all of the angular components of lower order are also present. The next to the last line of Table III gives the sum of the contributions to the energy of the first four angular components, and the final lines gives the energy found for the complete wave function.

It is interesting to note from Table III that the spherically symmetric terms in the wave functions account for 96.0 percent, 98.7 percent, and 99.4 percent of the total energy given by the wave function in the

† H. Bethe, Z. Physik **57**, 815 (1929) and E. A. Hylleraas, Z. Physik **60**, 624 (1930).

[12] G. R. Taylor and R. G. Parr, Proc. Natl. Acad. Sci. U. S. **38**, 154 (1952).

TABLE III. Contributions to the total energy of the terms in $E=\int\Sigma_i(c_i\Phi_i{}^NP_i{}^N)^*H\,\Sigma_i(c_i\Phi_i{}^NP_i{}^N)d\tau$.

Terms	H^- Contributions of the terms	H^- Contributions of the angular components of the wave functions	He I Contributions of the terms	He I Contributions of the angular components of the wave functions	Li II Contributions of the terms	Li II Contributions of the angular components of the wave functions
$(0)^*H(0)$	−1.00925	−1.00925	−5.72603	−5.72603	−14.46774	−14.46774
$(1)^*H(1)$	+0.01003	−0.03968	+0.01700	−0.07014	+0.01731	−0.07855
$(1)^*H(0)+(0)^*H(1)$	−0.04971		−0.08714		−0.09586	
$(2)^*H(2)$	+0.00082		+0.00176		+0.00198	
$(2)^*H(0)+(0)^*H(2)$	−0.00428	−0.00215	−0.00787	−0.00480	−0.00872	−0.00576
$(2)^*H(1)+(1)^*H(2)$	+0.00131		+0.00131		+0.00098	
$(3)^*H(3)$	+0.00019		+0.00043		+0.00049	
$(3)^*H(0)+(0)^*H(3)$	−0.00102		−0.00190		−0.00212	
$(3)^*H(1)+(1)^*H(3)$	+0.00029	−0.00046	+0.00030	−0.00109	+0.00022	−0.00135
$(3)^*H(2)+(2)^*H(3)$	+0.00008		+0.00008		+0.00006	
Sum	−1.05154	−1.05154	−5.80206	−5.80206	−14.55340	−14.55340
$\int\Psi^{N*}H\Psi^Nd\tau$	−1.05184		−5.80284		−14.55435	

cases of H^-, He I, and Li II, respectively. Similarly the terms containing $\cos\theta$ account for 93.2 percent, 91.3 percent, and 90.7 percent of what remains of the total energy after the spherically symmetric terms have been removed. The terms containing the second-order Legendre polynomial account for 73.9 percent, 72.0 percent, and 71.5 percent of what is then left. Finally using all the figures available, one finds that the terms containing the third-order Legendre polynomial account for 59.2 percent, 58.6 percent, and 58.3 percent of what remains after the terms containing the Legendre polynomials of lower order have been removed.

From Tables II and III one can also see that the ratios of the contributions of the nonspherically symmetric components to those of the spherically symmetric ones are much larger for the wave function than for the energy. For H^- the ratios of the contributions to the wave function of the $P_1{}^N$, $P_2{}^N$, and $P_3{}^N$ components to that of the $P_0{}^N$ component are roughly 3, 8, and 12 times as large as the corresponding ratios of the contributions to the energy. For He I the similar set of numbers is 6, 12, and 18, and for Li II one finds 9, 18, and 26. These numbers give a clear illustration of the fact that a wave function chosen by minimizing the energy will in general yield an energy which is much closer to the true energy than the wave function itself is to the true wave function.

The figures in Tables II and III may also be used to obtain rough maximum and minimum estimates of the energies which purely radial wave functions may be expected to give for the ground state of H^-, He I, and Li II. Since such wave functions are often used in approximate calculations, it will be worthwhile to see how close a few of the better known purely radial functions come to yielding the estimated maximum energy. The energies given in Table III for the $P_0{}^N$ components are those which are found when all the other angular components are also present. However if the $P_0{}^N$ component is the only one present in the expansion given by Eq. (1), that is, if all the $\Phi_i{}^N$'s for $i>0$ are set equal to zero, then c_0 will be 1 and the energy is $1/c_0{}^2$ times the value given for the $P_0{}^N$ component in Table III. Such estimates of the values of the energies given by spherically symmetric functions may be regarded as rough maximum estimates because the functions used to compute the quantities in Table III do not, of course, give total energies as low as the experimental values. On the other hand if one attributes the entire difference between the experimental values and the computed total energies to the energies of the spherically symmetric components, one obtains rough minimum estimates of the energy. Quantities computed in these ways are listed in Table IV together with the energies given by three of the better known spherically symmetric functions and by one worked out by the present authors to use in connection with the computations of the correlation energies below. The energies for each element in Table IV are given in units of the Rydberg constant for that element times hc. The first line gives the energy as computed from the simple exponential. The second line gives the energy as computed from the three parameter function

$$\Psi^N=(c_1e^{-Z_1r_1}+c_2e^{-Z_2r_1})(c_1e^{-Z_1r_2}+c_2e^{-Z_2r_2}), \qquad (5)$$

where Z_1, Z_2, and the ratio of c_1 and c_2 have been chosen to yield the minimum energy.[14] The third line of Table IV gives the Hartree-Fock energy and the fourth the energy as found from the symmetrized exponential. The last two lines of Table IV give the maximum and minimum estimates of the energy to be expected from spherically symmetric wave functions computed as sug-

[14] A paper will appear in *The Physical Review* 93, February 15 (1954) dealing with this function and a two-parameter one, both of which are of the product type, and both of which compare favorably with the Hartree $1s^2$ function for He I-like ions.

TABLE IV. Energies given by spherically symmetric ground-state wave functions.

Functions	H^-	He I	Li II
$Ne^{-Z(r_1+r_2)}$	−0.9453	−5.6953	−14.4453
3-parameter [see Eq. (5)]	−0.9756	−5.7233	−14.4728
Hartree-Fock		−5.723[b]	−14.42[d]
$N\{e^{-Z_1r_1-Z_2r_2}+e^{-Z_2r_1-Z_1r_2}\}$	−1.0266[a]	−5.7513[c]	−14.4975
Estimated maximum	−1.0231	−5.7552	−14.5024
Estimated minimum	−1.0264	−5.7599	−14.5088

[a] From S. Chandrasekhar, see reference 10.
[b] From W. S. Wilson, see reference 15.
[c] From G. R. Taylor and R. G. Parr, see reference 13.
[d] From V. Fock and M. J. Petrashen, see reference 16 below. This value appears to be a misprint since it does not give energies even as low as the simple exponential in the first line of this table.

gested above. For He I it is possible to obtain similar maximum and minimum estimates from earlier work on the three- and six-parameter Hylleraas wave functions.[9] These values are $-5.7566\ R_{He}hc$ and $-5.7592\ R_{He}hc$ from the three parameter function and $-5.7574\ R_{He}hc$ and $-5.7584\ R_{He}hc$ from the six-parameter function, respectively. Examination of Table IV shows that only for the symmetrized exponential does the calculated energy approach the estimates of what is possible even with just spherically symmetric functions to closer than 0.02 unit. This result is, of course, a consequence of the fact that the first three wave functions are of the simple product type and therefore do not take into account any configuration interaction even among spherically symmetric terms, that is, they do not take into account any radial correlation in the positions of the electrons except in the average. For He I and Li II, even the symmetrized exponential is seen to leave something to be desired in the way of radial correlation. The fact that for H^- the symmetrized exponential gives a value a little lower than the estimated minimum energy would appear to mean that when angular components are added to the wave function the parameters in the spherically symmetric component must change considerably to yield the minimum total energy.

The data in Table III together with earlier work may be used to estimate the size of the correlation energy and its various component parts for the three atomic systems under consideration. It was suggested in an earlier paper[9] that for the purpose of examining the correlation energy one should write the wave function for the ground state of these simplest systems in the form

$$\Psi^N = c_{HF}\Phi_{HF}{}^N P_0{}^N + c_R\Phi_R{}^N P_0{}^N + c_A\chi_A{}^N. \tag{6}$$

In Eq. (6) $\Phi_{HF}{}^N$ is the Hartree-Fock wave function for the particular configuration and term, namely $1s^2\,{}^1S$, making the largest contribution to the energy of the ground state. $\Phi_R{}^N$ includes all the remaining terms in Ψ^N which are not angularly dependent. $\chi_A{}^N$ consists of all the angularly dependent terms in Ψ^N. The relation of the various quantities in Eq. (6) to those in Eq. (1) is given by the following set of equations:

$$c_{HF} = \int (c_0\Phi_0{}^N P_0{}^N)^*\Phi_{HF}{}^N P_0{}^N d\tau,$$

$$c_R = (1-c_{HF}{}^2)^{\frac{1}{2}},$$

$$\Phi_R{}^N = (c_0\Phi_0{}^N - c_{HF}\Phi_{HF}{}^N)/c_R,$$

$$\chi_A{}^N = \sum_{i=1} c_i\Phi_i{}^N P_i{}^N / \sum_{i=1} c_i{}^2,$$

$$c_A = \sum_{i=1} c_i{}^2.$$

The Hartree-Fock wave functions should be the best function which takes account of the electron interaction only in the average, that is, the best wave function which takes no account of the correlation in the position of the electrons except in the average. It includes no terms which depend on the instantaneous value of the interlectron distance. It is suggested that if $\Phi_R{}^N$ and $\chi_A{}^N$ are of sufficiently general form so that Ψ^N may be considered to be a good approximation to an exact solution of the Schrödinger equation, then the total correlation energy and its various parts may be found from the different terms obtained when Ψ^N as given in Eq. (6) is substituted into the energy integral,

$$\int \Psi^{N*} H \Psi^N d\tau =$$

$$+\left\{c_{HF}{}^2 \int (\Phi_{HF}{}^N P_0{}^N)^* H \Phi_{HF}{}^N P_0{}^N d\tau\right\}$$

$$+\left\{c_{HF}c_R \int (\Phi_{HF}{}^N P_0{}^N)^* H \Phi_R{}^N P_0{}^N d\tau + c_R c_{HF} \int (\Phi_R{}^N P_0{}^N)^* H \Phi_{HF}{}^N P_0{}^N d\tau + c_R{}^2 \int (\Phi_R{}^N P_0{}^N)^* H \Phi_R{}^N P_0{}^N d\tau\right\}$$

$$+\left\{c_{HF}c_A \int (\Phi_{HF}{}^N P_0{}^N)^* H \chi_A{}^N d\tau + c_A c_{HF} \int (\chi_A{}^N)^* H \Phi_{HF}{}^N P_0{}^N d\tau + c_A{}^2 \int (\chi_A{}^N)^* H \chi_A{}^N d\tau\right\}$$

$$+\left\{c_R c_A \int (\Phi_R{}^N P_0{}^N)^* H \chi_A{}^N d\tau + c_A c_R \int (\chi_A{}^N)^* H \Phi_R{}^N P_0{}^N d\tau\right\}. \tag{7}$$

The different terms in the energy integral fall into four types. These four types have been separately bracketed in Eq. (7). First, there is a term which involves only $\Psi_{HF}{}^{N}$. This term yields an energy which is equal to $c_{HF}{}^{2}$ times the energy of the Hartree-Fock solution and is the part of the total energy which does not depend on the correlation in the position of the electrons except in the average. Second, there is a group of three terms which yield that part of the energy which appears because terms arising from the radial correlation in the position of the electrons are included in the wave function. It is reasonable to refer to this part of the energy as the radial correlation energy. Third, there is a group of three terms which yield that part of the energy which appears because terms arising from the angular correlation in the position of the electrons are included in the wave function. This part of the energy is, therefore, referred to as the angular correlation energy. Fourth, there are two terms still remaining which yield that part of the energy which appears because terms arising from both the radial and the angular correlation in the position of the electrons are included in the wave function. This part of the energy may be called the mixed correlation energy.

TABLE V. Correlation energies in the ground states of H^-, He I, and Li II. The values are given in units of $R_H hc$, $R_{He} hc$, and $R_{Li} hc$ for H^-, He I, and Li II, respectively.

	H^-	He I	Li II
Radial	−0.0930	−0.0608	−0.0492
Angular	−0.0547	−0.0788	−0.0880
Mixed	+0.0121	+0.0020	+0.0014
Total corr.	−0.1356	−0.1376	−0.1358

The extension of the above discussion to other states and other atomic systems would seem to be clear.

If one adopts the definitions suggested above, one can estimate the value of the total correlation energy and its various parts for any of the three atomic systems considered here for which Hartree-Fock wave functions are known. Wilson[15] has given such a solution for He I and Fock and Petrashen[16] have given the solution for Li II, but unfortunately no solution for H^- seems to be available. In view of the lack of a Hartree-Fock solution for H^- it was decided to use the analytic product type wave function of Eq. (5) for all three atomic systems. This wave function has been compared with the available Hartree-Fock solutions for He I, Li II, Be III,[17] and C V.[18] It was found that it gave energies which were very close to the Hartree-Fock energies, and that with the exception of C V for which the Hartree-Fock function seems to be somewhat less accurate, the maximum difference between the normalized analytic and numerical wave functions was 1.2×10^{-3}.[14] Using this wave function, the values of c_{HF} were found to be 0.969074, 0.994907, and 0.998124 for H^-, He I, and Li II, respectively. With these values for c_{HF} and the values of the energy for this function as given in the second line of Table IV the correlation energies have been computed. The results are recorded in Table V. Table V gives the values of the total correlation energy and its component parts, the radial, angular, and mixed correlation energies. The values are given in units of $R_H hc$, $R_{He} hc$, and $R_{Li} hc$ for H^-, He I, and Li II, respectively. The radial correlation energy was computed by subtracting $c_{HF}{}^{2}$ times the Hartree-Fock energy, taken as suggested above from the second line of Table IV, from the energy given in the first line of Table III for the spherically symmetric component of the ground-state wave function. The mixed correlation energy was computed directly from the integrals listed in Eq. (7). The angular correlation energy was then computed by subtracting the energy of the spherically symmetric component and the mixed correlation energy from the total energy given by the ground-state wave function. Finally, the total correlation energy was computed by subtracting $c_{HF}{}^{2}$ times the Hartree-Fock energy, taken as above from the second line of Table IV, from the total energy given by the ground-state wave function for the particular atomic system.

The results given in Table V may be compared with those obtained earlier[9] for He I using the three- and six-parameter wave functions of Hylleraas. There the radial, angular, mixed, and total correlation energies were found to be −0.056, −0.079, +0.002, and −0.133 unit and −0.056, −0.075, +0.002, and −0.129 unit, respectively, for the three- and six-parameter functions. In making use of the results in Table V and in comparing them with the results of the earlier work, it must be remembered that all of the ground-state wave functions employed give energies above the experimental values. These differences amount to 0.0033, 0.0047, and 0.0064 unit for H^-, He I, and Li II, respectively, using a wave function of the form given in Eq. (4) and to 0.0026 and 0.0010 unit for the three- and six-parameter Hylleraas functions. These small differences represent corrections to the values of the energies given in Table V and in the earlier work, but just how these small quantities should be divided between the noncorrelation energy and the various parts of the correlation energy is not clear.

The most striking characteristic of the values in Table V is the remarkable similarity of the total correlation energies for the three atomic systems. Perhaps more significant is the fact that the total correlation energy accounts for 12.9 percent, 2.4 percent, and 0.9 percent of the energy of the ground-state wave function for H^-, He I, and Li II, respectively. Next one notices the downward trend of the magnitude of the radial and

[15] W. S. Wilson, Phys. Rev. 48, 536 (1935).
[16] V. Fock and M. J. Petrashen, Physik. Z. Sowjetunion 8, 547 (1935).
[17] D. R. Hartree and W. Hartree, Proc. Roy. Soc. (London) A149, 210 (1935).
[18] A. Jucys, Proc. Roy. Soc. (London) A173, 59 (1939).

the mixed correlation energies with increasing atomic number and the corresponding increasing importance of the angular correlation energy. A quantitative discussion of these results will be presented in a later paper.

In summary the present work gives the correlation energies in the ground states of H^-, He I, and Li II and the importance of the various angular components of the ground-state wave functions both in the total wave functions and in the energies computed from them. First the values of the three parameters in the ground-state wave function given by Eq. (4) were determined variationally for He I and Li II. These functions together with the one of the same type already in existence for H^- were then expanded in series of Legendre functions of the cosine of the angle between the two radius vectors. The size of the coefficients in these expansions indicate the importance of the nonspherically symmetric components of the ground-state wave functions. That is, the size of the coefficients indicate the importance of configuration interaction with configurations which are not spherically symmetric. This importance decreases as one passes from H^- to Li II. On a percentage basis the contribution of the various components to the ground-state energy is less important than their contribution to the wave function. This contribution to the energy becomes larger in absolute value but smaller relatively as one passes from H^- to Li II. On the basis of the size of the contribution of the spherically symmetric component to the total energy and to the wave function for the ground state, the accuracy of various spherically symmetric ground-state wave functions is considered. Definitions are given for the total correlation or configuration interaction energy and its radial, angular, and mixed parts. Making use of an excellent analytic approximation to the Hartree-Fock ground-state wave functions, the definitions of the configuration interaction energies are applied to the three atomic systems under consideration. The total configuration interaction energies are found to be remarkably similar in absolute value but of decreasing relative importance with increasing atomic number. The absolute value of the radial and mixed correlation energy decreases from H^- to Li II and the absolute value of the angular configuration interaction energy increases.

The authors wish to thank Mr. Paul P. Craig and Mr. Robert T. Seeley for help in the computations leading to Table I.

Cross Sections for Formation of Na^{22} from Aluminum and Magnesium Bombarded with Protons*

R. E. Batzel and G. H. Coleman
California Research and Development Company, Livermore, California
(Received May 28, 1953)

Cross sections for formation of Na^{22} from proton bombardment of aluminum and magnesium have been determined for the energy range from thresholds to 32 Mev. The $Al^{27}(p, pan)Na^{22}$ reaction has a threshold of 25 Mev and the cross section for the reaction rises to a value of 2.5 millibarn at 32 Mev. The cross section for the production of Na^{22} from magnesium has a value of 0.25 millibarn at 10 Mev, rises through a maximum of 9 millibarns at 17 Mev, drops to a minimum of 5 millibarns at 23 Mev and then rises to a value of 19 millibarns at 32 Mev.

INTRODUCTION

Cross sections for the formation of Na^{22} from natural aluminum and magnesium have been measured as a function of proton energy from the range 0-32 Mev. The excitation functions were measured by means of the stacked foil technique on the Berkeley linear accelerator. Sodium was separated from the foils by chemical means and counted on a Geiger counter. Corrections were made for radioactive decay, chemical yield, and counting yield of the counting arrangement.

Both these excitation functions have been run previously but have been redetermined because of inadequacies in the earlier work. Hintz and Ramsey[1] have studied the production of Na^{22} from aluminum from threshold to 100 Mev, but made no accurate determination of the cross section in the energy range near the threshold. Bartell and Softky[2] have determined the relative excitation function for the production of Na^{22} from natural magnesium, but no attempt was made to correct the counting samples for effects due to self-absorption and self-scattering. The shape of the curve of cross section *versus* energy is the same as that obtained by Bartell and Softky, but the absolute values for the cross section are about a factor of five lower.

PROCEDURE

A stack of pure aluminum foils was irradiated for approximately 1.2 microampere hours on the linear accelerator. The energy of the protons incident on the stack was 32 Mev and the variation in cross section was studied down to 25 Mev, the apparent threshold of the reaction. Magnesium foils were irradiated in a stack for approximately 1.5 microampere hours on the linear accelerator. The excitation function was studied in the energy range from 10 to 32 Mev. In both cases the beam was integrated by means of a standard Faraday cup assembly.

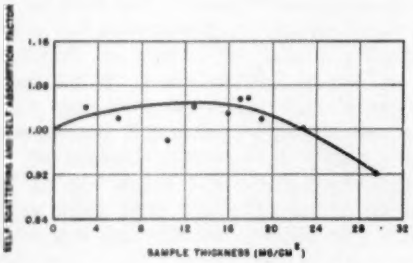

FIG. 1. Self-absorption—self-scattering Na^{22} in NaCl.

The sodium was separated chemically from the aluminum and magnesium. The foils were dissolved in dilute HCl and a known amount of sodium chloride added as a carrier so that a correction could be made for losses in the chemical separation procedure. The aluminum was precipitated as the hydroxide by the addition of ammonium hydroxide. The supernatant solution was evaporated to dryness and the ammonium chloride driven off by heating. The residue remaining after the ammonium chloride distillation was dissolved in water, cobalt carrier added, and cobaltous sulfide precipitated. The sodium was precipitated as sodium zinc uranyl acetate from a neutral solution. The sodium zinc uranyl acetate was dissolved in absolute alcohol saturated with HCl gas and the sodium chloride thus precipitated transferred to a plate to be weighed and counted.

In the case of magnesium, the sodium zinc uranyl acetate was precipitated directly after solution of the magnesium in dilute HCl and neutralization of the solution with ammonium hydroxide. An additional purification step was used in the magnesium samples and the low counting aluminum samples. This consisted of eluting the sodium chloride from a Dowex 50 cation column with 0.5 *M* HCl.

Absolute Beta Counting

The samples were counted with an argon-filled, chlorine-quenched Geiger counter used in conjunction with a scaling circuit. Na^{22} has a half-life of 2.60 years[3] and emits a 0.54-Mev positron[4] followed by a 1.28-Mev

* This work was done under the auspices of the U. S. Atomic Energy Commission.

[1] N. M. Hintz and N. F. Ramsey, Phys. Rev. **88**, 19 (1952).
[2] F. D. Bartell and S. Softky, Phys. Rev. **84**, 463 (1951).
[3] L. J. Laslett, Phys. Rev. **76**, 858 (1949).
[4] Marklin, Lidofsky, and Wu, Phys. Rev. **78**, 318 (1950).

gamma ray.[5] There is also a 1.8-Mev positron[6] transition in very low abundance. No K-capture branching was assumed,[7] although recent measurements indicate that the K-capture branching may be nine percent.[8] These decay characteristics made it imperative that the counting yield of the particular counting setup used be calibrated against an absolute standard. The standard used was a weightless Na^{22} sample mounted on a thin Tygon film and counted in a 4π geometry proportional counter to determine the absolute disintegration rate. This sample was then backed with aluminum and counted in the Geiger counter and the counting yield, including effects due to geometry, counting efficiency, backscattering, and window and air absorption determined directly. The effect due to the self-scattering and self-absorption of the counting samples was measured by placing equal aliquots of a standard Na^{22} solution into solutions containing varying amounts of sodium chloride carrier, precipitating the sodium chloride, and comparing the counting rates of these samples with a weightless standard sample placed directly on a counting plate. All counting was done with "infinite" aluminum backing. The "working curve" obtained by this method is shown in Fig. 1.

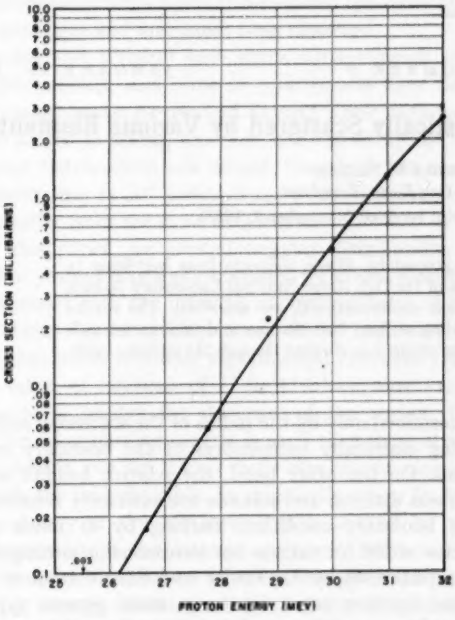

FIG. 2. Cross section for the production of Na^{22} from aluminum as a function of proton energy.

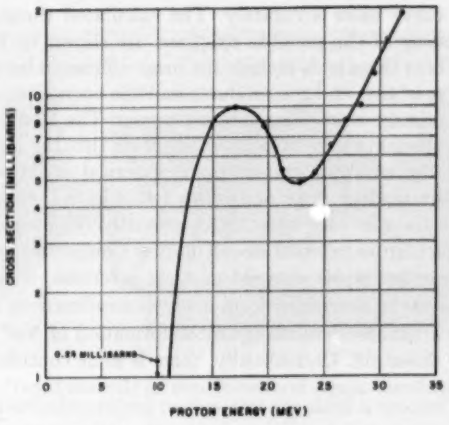

FIG. 3. Production of Na^{22} from magnesium as a function of proton energy.

RESULTS

The results are shown in Figs. 2 and 3. The cross section for production of Na^{22} from aluminum has a threshold of 25 Mev and rises steadily to a value of 2.5 millibarns at 32 Mev.

The cross section for formation of Na^{22} from magnesium has a value of 0.25 millibarn at 10 Mev, rises sharply through a maximum at 17 Mev, decreases to a minimum at 23 Mev, and then rises steadily to 32 Mev. This excitation function has the same shape as that obtained by Bartell and Softky,[2] but the observed cross sections are considerably lower than the reported values. However, Bartell and Softky indicated that only the shape of this particular excitation function was determined with any precision.

DISCUSSION

Na^{22} from Aluminum

The cross section for formation of Na^{22} from proton bombardment of aluminum has been determined previously[1] from threshold to 100 Mev. The present work defines the threshold and low-energy portion of

TABLE I. Threshold for possible reactions.

Reaction	Q(Mev)	Barrier (Mev)	Q + Barrier
$Al^{27}(p, pan)Na^{22}$	22.0	8.1	30.1
$Al^{27}(p, \alpha d)Na^{22}$	19.9	7.6	27.5
$Al^{27}(p, Li^6)Na^{22}$	18.4	7.0	25.4
$Al^{27}(p, 3p3n)Na^{22}$	50.2	9.6	59.8
$Al^{27}(p, THe^3)Na^{22}$	34.2	8.1	42.3
$Mg^{25}(p, \alpha n)Na^{22}$	15.0	5.3	20.3
$Mg^{25}(p, pdn)Na^{22}$	27.6	6.0	33.6
$Mg^{25}(p, \alpha)Na^{22}$	2.5	5.3	7.8
$Mg^{24}(p, 2pn)Na^{22}$	23.8	6.4	30.2
$Mg^{24}(p, pd)Na^{22}$	22.7	6.3	29.0
$Mg^{24}(p, He^3)Na^{22}$	16.1	5.2	21.3

The authors wish to thank the crew of the linear accelerator for the bombardments performed in the course of these studies.

[5] D. E. Alburger, Phys. Rev. **76**, 435 (1949).
[6] K. H. Morgenstern and K. P. W. Wolff, Phys. Rev. **76**, 1260 (1949).
[7] Good, Peaslee, and Deutsch, Phys. Rev. **69**, 313 (1946).
[8] R. H. Miller and R. Sherr, Bull. Am. Phys. Soc. **28**, No. 4, 12 (1953).

the curve more accurately. The calculated thresholds for some of the possible reactions are shown in Table I. These thresholds include the mass difference between the reactants and the products and the energy required for passage over the potential barrier. The Coulombic requirements were calculated assuming that the nucleus and the emitted fragments are spherical and tangent at the nuclear radii (taken as $1.48\times10^{-13}A^{\frac{1}{3}}$ cm) and that the particles come out consecutively. Because of uncertainties inherent in calculating Coulombic barrier requirements for charged particle reactions, it is not possible to determine from energy considerations what the actual mechanism is for the formation of Na^{22} near the threshold. Undoubtedly, there is some contribution from each of the following reactions: $Al^{27}(p, pan)Na^{22}$, $Al^{27}(p, \alpha d)Na^{22}$, and $Al^{27}(p, Li^6)Na^{22}$.

Na^{22} from Magnesium

Natural magnesium is an isotopic mixture of 78.6 percent Mg^{24}, 10.1 percent Mg^{25}, and 11.3 percent Mg^{26}. From the threshold considerations shown in Table I, the excitation function can be divided into two parts. The portion of the curve below 15 Mev represent the contribution to the excitation function due entirely to the $Mg^{25}(p, \alpha)Na^{22}$ reaction. Above this energy the mechanism of the reaction leading to the formation of Na^{22} is uncertain, and undoubtedly, is a combination of the possible reactions shown in Table I.

PHYSICAL REVIEW VOLUME 93, NUMBER 2 JANUARY 15, 1954

Angular Distributions of 22-Mev Protons Elastically Scattered by Various Elements

BERNARD L. COHEN AND RODGER V. NEIDIGH
Oak Ridge National Laboratory, Oak Ridge, Tennessee

(Received May 20, 1953; revised manuscript received November 2, 1953)

Angular distributions of 22-Mev protons elastically scattered by fifteen elements from beryllium to thorium were measured with the internal, circulating beam of the Oak Ridge National Laboratory 86-inch cyclotron. The experimental methods, which are somewhat unconventional, are described. The results show all the characteristics of diffraction scattering including at least two maxima and minima for each element. The angles at which these occur can be traced from element to element through the periodic table, following a λ/R dependence with fairly good accuracy.

I. INTRODUCTION

THE theory of the scattering or absorption of a wave by matter with which it interacts is a well-known differential equation-boundary value problem of classical physics. While the mathematical techniques are devious and varied, basically the solution is obtained by assuming the appropriate wave equation (in the case of particle scattering, the Schrödinger equation) valid throughout the region external to the scattering or absorbing material, and inserting the appropriate boundary conditions at its surface.[1] Computations of this type for the elastic scattering of neutrons have been made by Feld *et al.*,[2] assuming spherical nuclei and the Feshbach-Weisskopf[3] boundary condition. For incident neutrons with wavelength of the order of the dimensions of the scattering nucleus, they find angular distributions characterized by several maxima and minima, as is expected in analogy with the familiar diffraction patterns in optical and acoustical scattering. As is also expected from these analogies, the angles at which the maxima and minima occur are determined only by the radius of the scattering nucleus, being essentially independent of the boundary conditions. On the other hand, the relative heights of the various maxima and minima are extremely sensitive to the boundary condition, varying by as much as a factor of 100 for various not unreasonable assumptions. Computations by Le Levier and Saxon[4] confirm that these features are valid for a more general type of boundary condition, and for charged particles as well as neutrons. It is thus apparent that reasonably accurate measurements of elastic scattering angular distributions should provide:

(a) Accurate determinations of nuclear radii, since the positions at which maxima and minima occur can be determined with good precision.

(b) A very sensitive determination of the nuclear boundary condition. This boundary condition is also of great importance in nuclear reaction theory since the theoretical treatments of absorption and scattering are essentially two parts of the same problem.

(c) Some estimate of deviations from sphericity of the nuclear surface. This would provide a very important check on the determinations through quadrupole moments which do not have a completely satisfactory status.

[1] J. Blatt and V. F. Weisskopf, *Theoretical Nuclear Physics* (John Wiley and Sons, Inc., New York, 1952).
[2] Feld, Feshbach, Goldberger, Goldstein, and Weisskopf, NYO-636 (unpublished).
[3] H. Feshbach and V. F. Weisskopf, Phys. Rev. **76**, 1550 (1949).
[4] R. E. Le Levier and D. S. Saxon, Phys. Rev. **87**, 40 (1952).

Amaldi *et al.*[5] have made measurements for 14-Mev neutrons on lead, but only with sufficient accuracy to check the qualitative features of the theory. Two experiments[6,7] using 90-Mev neutrons and 340-Mev protons have been reported, but at these energies the nuclear radius loses meaning because of the high nuclear transparencies, and the boundary condition is less significant for the same reason and also because at these energies it is of little importance in connection with nuclear reaction theory. Neither of these experiments was able to provide accurate information on nuclear radii. A few measurements with low-energy protons have been reported,[8,9] but in these, the low energy severely reduces the diffraction region. In none of the measurements thus far mentioned has more than one minimum and maximum been observed.

Burkig and Wright[10] have made measurements with 18-Mev protons, and some of their results have been interpreted by Le Levier and Saxon.[4] Their data were taken at 10° intervals, however, and the details of the angular distributions are missed. Gugelot[11] has made measurements at 30° intervals for a few elements, but these suffer from the same deficiency.

In this paper, we present angular distributions of 22-Mev protons elastically scattered by fifteen elements as measured with the internal, circulating beam of the Oak Ridge National Laboratory 86-in. cyclotron by somewhat unconventional experimental methods. Data were taken at intervals of 2° to 4° which were found adequate to resolve the structure of the curves; the selection of scattering targets is such that these structural details can be traced from element to element through the periodic table. In practically every feature the accuracy of the measurements is limited by the characteristics of the internal cyclotron beam which include secular variations in mean energy of about 8 percent, energy inhomogeneity of about 10 percent, secular variations in angle of incidence on the target of about ½°, and inhomogeneity in this angle of a little less than 1°. It is believed that a suitable theoretical analysis of these data would provide items (a) and (b) above; it is doubtful whether, in its present form, it could provide information on nuclear eccentricities [item (c)]; however, if theoretical developments of the general theory can be extended to show exactly what type of data is necessary, it is believed that the techniques herein described might be used to provide such information.

[5] Amaldi, Bacciarelli, Cacciapuoti, and Trabacchi, Nuovo cimento **15**, 203 (1946).
[6] Bratenahl, Farnbach, Hildebrand, Leith and Moyer, Phys. Rev. **77**, 597 (1950).
[7] Richardson, Bali, Leith, and Moyer, Phys. Rev. **86**, 29 (1952).
[8] Baker, Dodd, and Simmons, Phys. Rev. **85**, 1051 (1952).
[9] L. M. Goldman, Phys. Rev. **89**, 349 (1953).
[10] J. W. Burkig and B. T. Wright, Phys. Rev. **82**, 451 (1951).
[11] P. C. Gugelot, Phys. Rev. **87**, 525 (1952).

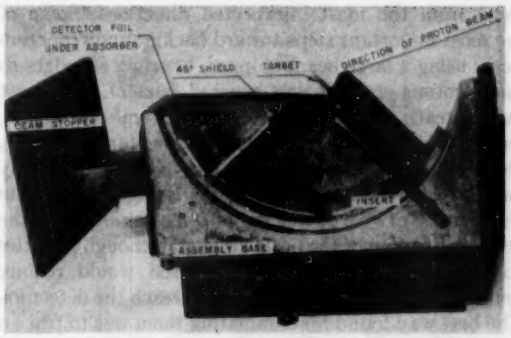

FIG. 1. Target assembly for measurements of angular distributions of elastically-scattered protons. One side shield is removed.

II. EXPERIMENTAL METHOD

A detailed account of the methods being used for measuring angular distributions of nuclear reaction products with the internal beam of the Oak Ridge National Laboratory 86-in. cyclotron is available elsewhere,[12] so that only the most pertinent details will be outlined here.

The target assembly, one variation of which is pictured in Fig. 1, consists essentially of a thin target at the center of a 3½-in. radius assembly base, an exchangeable insert fitting on the assembly base for mounting detectors and absorbers, a large plate to stop the beam after it has passed the assembly, and various pieces to shield against background.

The elastically-scattered protons are detected by the 38-minute beta activity they induce in copper foils by the (p,n) reaction. The copper must be covered with an absorber to eliminate activities induced by inelastically-scattered protons, deuterons, etc. The absorber thickness was chosen so as to slow the elastically-scattered protons to the energy at which the (p,n) cross section[13] is at its maximum. For example, for 21.5-Mev protons the detectors are covered with about 400 mg/cm² of aluminum which reduces 21.5-Mev protons to 13 Mev (the maximum of the cross section) and reduces protons of less than 18 Mev to below the 4.1-Mev threshold of the reaction. For light elements where the energy of the scattered protons varies with angle due to center-of-mass effects, the absorbers are stepped to equalize the energy and, therefore, the detection efficiency at each angle.

By far the most difficult experimental problem was the elimination of background. This was accomplished only after a long trial and error procedure in which a number of adjustments and changes were made to various parts of the assembly. The process was made especially difficult by the fact that the background was extremely variable from run to run, and seemed to

[12] B. L. Cohen and R. V. Neidigh, Rev. Sci. Instr. (to be published).
[13] S. N. Ghoshal, Phys. Rev. **80**, 939 (1950).

come from the most unexpected directions. Some of the most important steps toward background reduction were: using a large beam stopper, beveling all edges so that protons striking any exposed part of the target cannot reach the detectors without several scatterings, enlarging the carbon shield on the target holder, employing side shields, etc. The point was finally reached where the only important background was in the vicinity of 90°. It was found to be coming from the general direction of the beam stopper, although particles coming from the beam stopper itself would require several scatterings before they could reach the detectors. The best way found for eliminating them was to place a thick plate at about 45°, as shown in Fig. 1. This, of course, distorts the data in the vicinity of 45°, so that another run is needed with the 45° shield removed. A single measurement of an elastic proton angular distribution thus consists of three equal and consecutive bombardments: the first, with the 45° shield, the

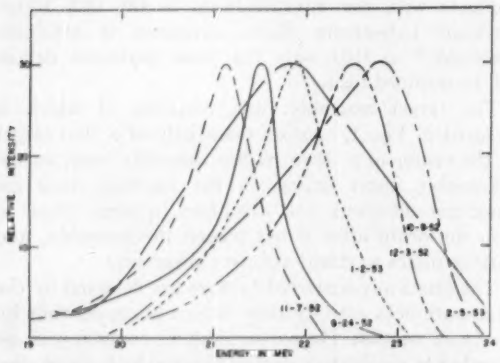

Fig. 2. Energy distribution of protons incident on the target for various dates. The great majority of the data was accumulated between 10-15-52 and 1-15-53. The method of making these measurements is described in reference 15.

second without it, and the third with the target removed to determine the background.

Up to about 90°, the background was seldom more than a few percent. At the largest angles, however, it occasionally was as high as 30 percent so that, even though it was corrected for by a separate run, its variability from run to run was sufficient to cause appreciable errors in a few cases (see caption for Fig. 7).

In order to find the absolute cross sections, it is necessary to measure the current on the target. This is done by removing and counting the target some time after the run, and calibrating the activity in the target with an auxiliary experiment in which the current is measured by using the published copper (p,n) cross section[13] near its maximum. Counting efficiencies and uncertainties in the absolute cross section of copper do not affect the result because the same activity is used in detecting the elastically-scattered protons. The largest source of error is probably in differences in energy and intensity between the angular distribution and calibration runs. In cases where the activity of the target is due to impurities, these were sometimes distilled off; and in some cases there was evidence that foreign materials were deposited on the target during the bombardment. Errors of ~30 percent were found to be common, and in some cases, they were much larger. In the final plotting of the data, a considerable weight was given to the facts that the Rutherford law must be valid at small angles

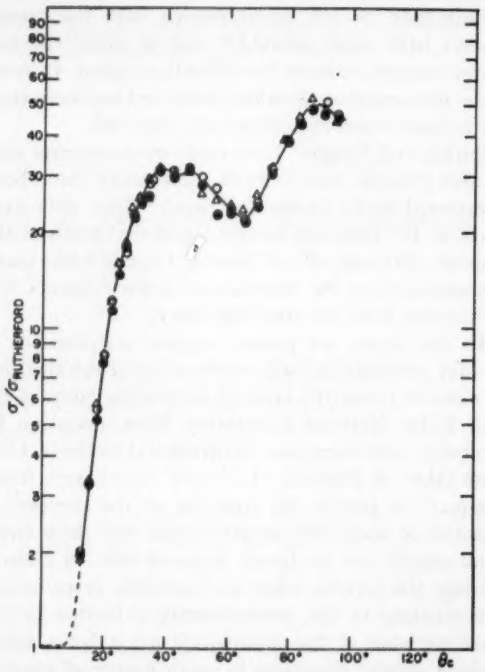

FIG. 3. Angular distribution of 22-Mev protons elastically scattered by beryllium. Data are plotted as the ratio of observed to Rutherford cross section to bring out the details. The curve at angles less than 12° is obtained from the absolute cross section with the inference that the Rutherford law is valid at small angles. Each experimental point represents a series of three runs as described in the text. Errors due to counting statistics are in all cases smaller than the size of the symbols representing the experimental points. Other sources of error are illustrated in Figs. 4 to 9; their magnitude may best be judged from the lack of agreement between the various runs. For beryllium, the energy in the center-of-mass system is 19.8 Mev.

for heavy elements, and that the ratio of the observed to the Rutherford cross section should vary slowly and continuously from element to element. For example, since the reproducibility of the absolute calibration for carbon was found to be poor, the Rutherford portion of the angular distribution was plotted by interpolating between beryllium and magnesium. The measured shapes of the angular distributions are not, of course, affected by these considerations.

The energy and energy distribution of the incident

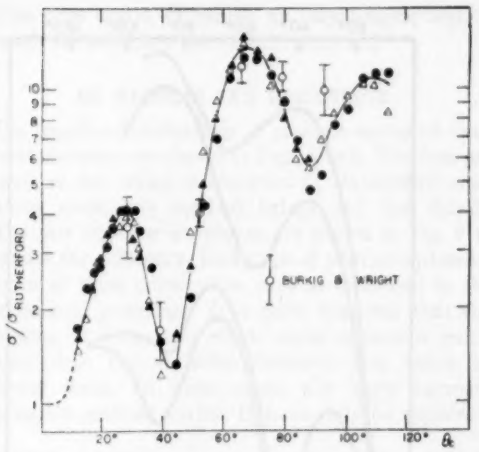

FIG. 4. Angular distribution of 22-Mev protons elastically scattered by aluminum. See caption under Fig. 3. Data of Burkig and Wright (see reference 10) was obtained with 18-Mev protons. For aluminum, the energy in the center-of-mass system is about 21.2 Mev. The run represented by the solid triangles was not considered valid at angles greater than 90° because the activity in the detector was not sufficiently greater than background.

beam were determined from time to time by measuring the copper excitation function in the vicinity of its threshold and comparing it with the very accurate published curve.[14] A method for rapid calculation of the energy spectrum from this data was developed.[15] Figure 2 shows the energy spectrum at various times while data were being taken.

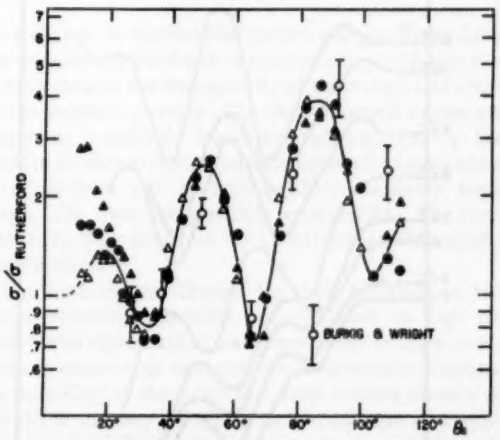

FIG. 5. Angular distribution of 22-Mev protons elastically scattered by nickel. See captions under Figs. 3 and 4. The poor data at small angles can be explained by a shift in the angle of incidence of the protons on the target, or in its homogeneity. Although this effect was found quite common, in no case were the discrepancies as large as in the case of nickel, which might also be partly the result of an error in target positioning.

[14] J. P. Blaser *et al.*, Helv. Phys. Acta **24**, 3 (1951).
[15] B. L. Cohen, Oak Ridge National Laboratory Report ORNL-1347 (unpublished).

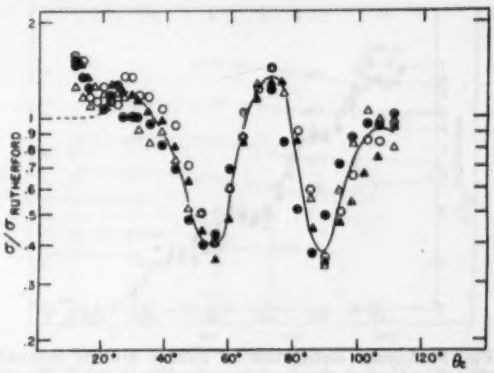

FIG. 6. Angular distribution of 22-Mev protons elastically scattered by niobium. See captions under Figs. 3 and 5. The general agreement between various runs was poorer for niobium than for any of the 14 other target elements used. The progressive shift of the open circles and solid triangles to the right of the solid circles indicates that the energy was higher for the latter run.

The average value of the angle of incidence, and its uniformity, are determined essentially by the distribution of orbit centers in the cyclotron and the radial width of the beam on the target. These were determined from time to time by auxiliary experiments which are described elsewhere.[12,16] A check is obtained by assuming the Rutherford law to be valid at small angles for heavy elements.

Radiation exposure of personnel incurred while changing detector inserts presented a very serious difficulty which was finally alleviated by arranging for the operation to be carried out very rapidly (~15 seconds), by the use of about 40 pounds of leaded protective clothing, and by waiting a short while after the end of bombardment.

Sparking from the dees melted parts of the target on several runs. This trouble was decreased (but never

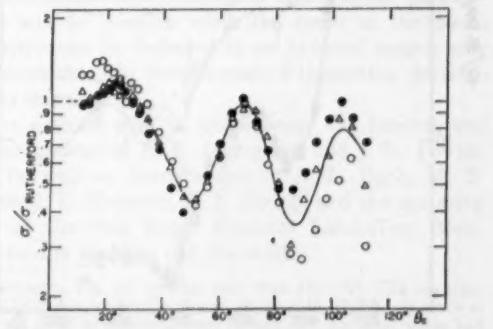

FIG. 7. Angular distribution of 22-Mev protons elastically scattered by palladium. See captions under Figs. 3 and 5. In several cases bad discrepancies between different runs were found at angles greater than 90°, but in no case were they as pronounced as in this; they may be due in part to background difficulties.

[16] B. L. Cohen, Oak Ridge National Laboratory Report ORNL-1348 (unpublished).

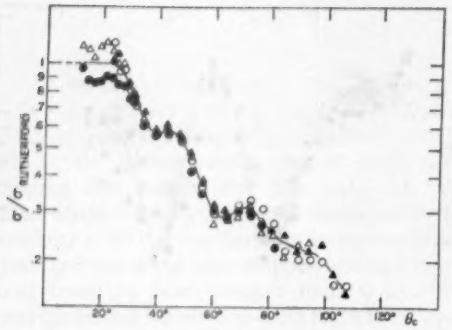

FIG. 8. Angular distribution of 22-Mev protons elastically scattered by thorium. See captions under Figs. 3 and 5. The runs represented by the solid triangles and open circles were not considered valid at angles less than 20° because of multiple scattering considerations. The other two runs were made with specially prepared thin targets.

eliminated) by setting the target at a larger than normal radius, by rounding all edges of the target assembly, and by canceling runs when the cyclotron vacuum was poor. The very considerable secular variation in the proton energy was greatly reduced, before data taking was initiated, by operating at a constant oscillator plate voltage. A complete enumeration of all the minor experimental difficulties encountered in an experiment

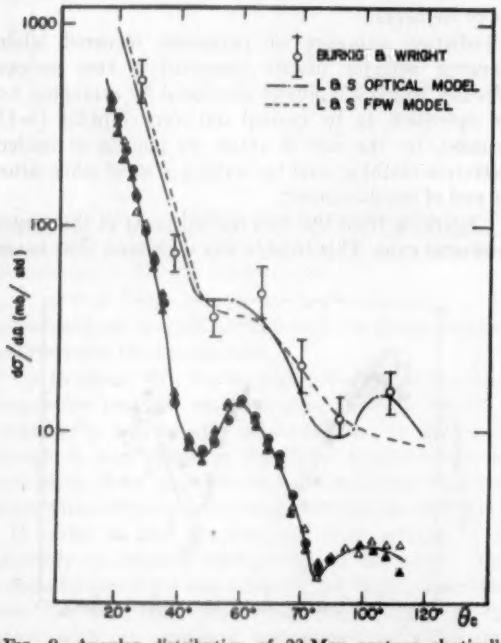

FIG. 9. Angular distribution of 22-Mev protons elastically scattered by aluminum. The data is the same as that shown in Fig. 4, except that it is plotted directly rather than as the ratio of observed to Rutherford cross section. The upper curves show the 18-Mev data of Burkig and Wright (see reference 10), and the calculations (for 18-Mev protons) of Le Levier and Saxon (see reference 4). The data from the experiment has been divided by five to avoid overlapping.

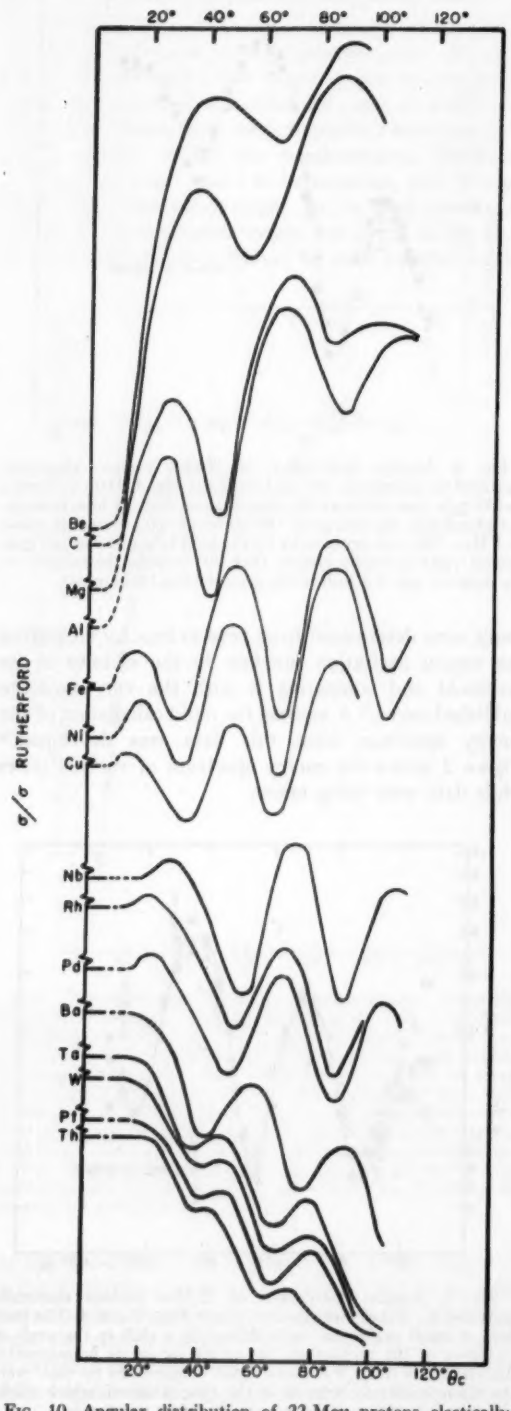

FIG. 10. Angular distribution of 22-Mev protons elastically scattered by various elements. The curves are based on the data given in Figs. 3–8 and on comparable data for nine other elements. There is no significance in the spacing between the various curves.

of this type would, of course, be very lengthy but, in general, the solutions were straightforward.

III. RESULTS AND DISCUSSION

The angular distributions of protons scattered from several elements are shown in Figs. 3 to 8. The data are plotted as the ratios of observed to Rutherford cross sections since this method brings out the details.

The raw data for aluminum are shown in Fig. 9 to illustrate the difference. Each type of pointer represents a series of three consecutive runs as described in the experimental procedure. It is quite apparent that the scattering of data on a single series of runs is much smaller than the variation between data taken at different times. In some cases, the angle between consecutive maxima varies; this can only be explained by a change in the incident proton energy. There are a few cases where the depth of minima vary, probably due to variations in the homogeneity of the energy and angle of the incident protons. The data at small angles are somewhat unreliable because small changes in the angle of incidence or its homogeneity, such as are known to occur from run to run, produce relatively large errors. The data are generally reproducible, however, and leave little doubt as to the pattern of the angular distributions.

TABLE I. Angles (in degrees) of maxima and minima in Fig. 10.

	Max	Min	Max	Min	Max	Min	Max
Be	42	65	90				
C	36	55	88				
Mg	28	45	70	85	102		
Al	27	42	67	90	111		
Fe	17	32	52	69	86	106	
Ni	19	33	51	68	87	105	
Cu	13	35	52	66	88		
Nb			~30	56	75	90	110
Rh			~21	53	71	88	~106
Pd			~23	51	70	89	105
Ba			~18	43	60	76	92
Ta				38	48	68	79
W				41	49	67	79
Pt				41	50	67	80
Th				40	44	63	72

The best curves through the data for each of the fifteen elements measured are combined in Fig. 10. Each curve represents at least three series of three runs; in many cases extra runs were made in order to increase the reliability of the data. The most striking feature of Fig. 10 is the way in which each maximum and minimum can be followed from element to element through the periodic table. From the usual theory for diffraction effects, one might expect the angle at which any particular feature occurs to be approximately proportional to λ/R, where λ is the wavelength of the incident protons and R is the nuclear radius. The angle at which each maximum and minimum occurs, multiplied by R/λ, (where R is taken to be $1.45A^{\frac{1}{3}}\times10^{-13}$ cm) is shown in Fig. 11. The $\theta\propto\lambda/R$ law[17] is borne out with an accuracy that would seem to be beyond expectation. It includes cases spanning almost the entire periodic table, as for example, the minimum which occurs at 85° for magnesium and 40° for thorium, following the λ/R law to within 10 percent for every element.

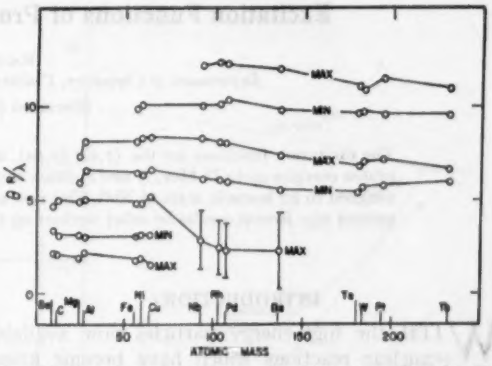

FIG. 11. Positions of maxima and minima from Fig. 10. The angle at which each maximum and minimum occurs is multiplied by R/λ, as is explained in the text. R was arbitrarily assumed to be $1.45\times10^{-13}A^{\frac{1}{3}}$.

Table I shows the angles at which the various maxima and minima occur.

Since detailed calculations would involve long phase-shift computations with Coulomb wave functions, they were considered beyond the scope of this work. The 18-Mev calculations of Le Levier and Saxon[4] for aluminum seem to agree qualitatively with these measurements, as shown in Fig. 9, but their minimum at 45° does not seem to be deep enough.

More precise measurements of these angular distributions will be possible when the beam of the 86-in. cyclotron can be deflected to an external target; new measurements will then be made if theoretical developments warrant.

The authors wish to acknowledge the interest and encouragement of R. S. Livingston and J. L. Fowler, and the various contributions of A. L. Boch, M. B. Marshall, E. Newman, B. L. Ferrell, and the operating staff of the Oak Ridge National Laboratory 86-in. cyclotron in carrying out this work.

[17] Actually, Fig. 11 verifies only that $\theta\propto1/A^{\frac{1}{3}}$. The constant 1.45×10^{-13} was arbitrarily chosen as the ratio of R to $A^{\frac{1}{3}}$ since at the time these calculations were carried out, no other value had been proposed.

Excitation Functions of Proton-Induced Reactions of Nb^{93} *

RALPH A. JAMES
Department of Chemistry, University of California, Los Angeles, California
(Received September 29, 1953)

The excitation functions for the (p,n), (p,pn), and $(p,\alpha n)$ reactions of Nb^{93} have been determined with proton energies up to 21 Mev. A new niobium activity with half-life of 13±2 hours was found and has been assigned to an isomeric state of Nb^{92}. This new activity decays by electron capture and emits a 2.35-Mev gamma ray. Recent results by other workers on the characteristics of the 10-day Nb^{92} were verified.

INTRODUCTION

WITH the high-energy particles now available, nuclear reactions which have become known under the general name of "spallation reactions" have become so numerous, and so many new radioactive species have been produced, that it seemed advisable to study some of the simpler types of such reactions in greater detail. Accordingly, a study of the excitation functions of reactions such as (p,pn), (p,α), $(p,\alpha n)$ has been undertaken and this work reports the results obtained with Nb^{93} as representative of elements of intermediate atomic number.

Stacks of niobium foils were bombarded in the deflected beam of the U.C.L.A. cyclotron, first, using the 12-Mev protons available prior to 1950 and again recently using the 20.8-Mev protons now available. The foils were then mounted on chip-board cards and counted in a Geiger-Müller counter of known geometry. The beam current was monitored by shielding the stacked foils with thin aluminum foil and measuring the current to the niobium foils by means of a galvanometer. The decay curves were plotted and resolved to give the yield of the 7-hour Mo^{93m}. Resolution of the other activities was so uncertain that their yield relative to Mo^{93} was determined in separate experiments as described below.

Weighed samples of 40 to 50 mg of spectroscopically pure Nb_2O_5 were bombarded in the circulating beam of the U.C.L.A. cyclotron, the desired energy being selected by position of the target probe. After measured quantities of molybdenum and zirconium carriers were added, the target was processed chemically, and fractions containing niobium, zirconium, and molybdenum, respectively, were separated and purified. Each fraction was finally converted to a chemical compound of known composition and weighed to determine the chemical yield. The samples were mounted on chip-board cards and various measurements made; decay curves and absorption curves were obtained with a thin window G-M tube; Gamma-ray spectra were measured with the use of the scintillation gamma-ray spectrometer described by Ticho;[1] in some cases, thin samples were prepared and the particles studied by means of the helical focusing β-ray spectrometer.[2] These measurements gave the yields of (p,pn) and $(p,\alpha n)$ reactions relative to the (p,n) reaction whose cross section at each energy was known from the stacked foil measurements described above.

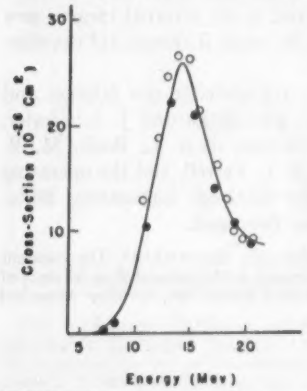

FIG. 1. Excitation function for the reaction $Nb^{93}(p,n)Mo^{93m}$.

RESULTS

Figure 1 shows the excitation function for the reaction $Nb^{93}(p,n)Mo^{93m}$ (7 hr) obtained by the stacked foil technique. The 0.262-Mev gamma ray[3] of Mo^{93} is largely converted[4,5] while the other two (0.69 and 1.51 Mev) are not converted to any appreciable extent. These conversion electrons are responsible for essentially all of the radiation detected in the Geiger-Müller tubes used here, as was shown by aluminum and lead absorption curves. These absorption curves were extrapolated to zero absorber thickness and the total number of disintegrations of Mo^{93} calculated. The total conversion coefficient, N_e-/N_γ was found to be 0.70.[5] The shape of the excitation function (Fig. 1) is essentially identical to that obtained by Forsthoff, Goeckermann, and Naumann[6] whereas the absolute values are somewhat lower, 0.26 barn at the maximum compared to 0.37 barn. Proton energy loss in the foils was calculated with the use of the rate of energy loss of protons in silver.

* This work was supported by the joint program of the U. S. Office of Naval Research and the U. S. Atomic Energy Commission.

[1] Harold K. Ticho, Phys. Rev. **84**, 847 (1951).
[2] B. T. Wright, Am. J. Phys. **20**, 130 (1952).
[3] L. Ruby and J. R. Richardson, Phys. Rev. **83**, 698 (1951).
[4] Kundu, Hult, and Pool, Phys. Rev. **77**, 71 (1950).
[5] Forsthoff, Goeckermann, and Naumann, Phys. Rev. **90**, 1004 (1953).

The decay curves of the chemically separated niobium fraction of targets bombarded at higher energies showed the well-known 10-day Nb^{92} and, in addition, an activity with a half-life of 13±2 hours. It was shown in agreement with Preiswerk and Stähelin,[6] by absorption curves and β-ray spectra measurements, that the 10-day activity decays primarily (or entirely) by electron capture and emits the 0.933-Mev gamma ray studied in detail by Ticho *et al.*[7] Recent results by these authors[8] show that the 1.84-Mev gamma ray is not due to a longer lived activity, as previously reported, but is actually due to the 10-day Nb^{92}. No beta particles were detected in the 10-day activity, but only the gamma ray and K x-ray. A niobium fraction was very carefully separated from all molybdenum and zirconium, and then absorption curves were determined on the sample at regular intervals until only 10-day activity remained. The decay curves through each of the absorbers were

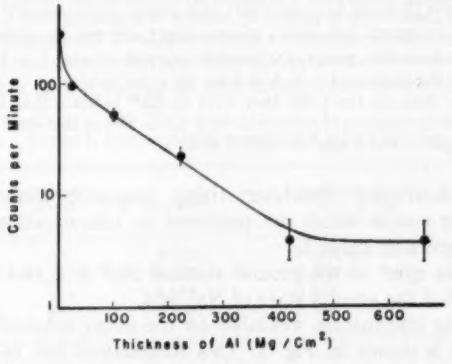

FIG. 2. Absorption curve of the 13-hour niobium activity.

then resolved, and the absorption curve of the 13-hour activity was determined. This absorption curve is shown in Fig. 2. If the radiation were particles, their energy would be approximately 1 Mev, and no such particles could be detected in the β-ray spectrometer. The assumption that they are electromagnetic radiation gives an energy of the order of 18 kev in satisfactory agreement with the energy of K x-rays in this region. A 2.35-Mev gamma-ray is also emitted by the 13-hour activity as determined with the scintillation gamma-ray spectrometer. It was shown that the 2.35-Mev gamma ray is not present in either the zirconium or molybdenum fraction of these targets and that the ratio of the zirconium or molybdenum fraction of these targets and that the ratio of the 2.35-Mev to the 0.92-Mev gamma ray is not changed by chemical separations very selective for niobium, this result making it certain that

[6] P. Preiswerk and P. Stähelin, Helv. Phys. Acta **24**, 300 (1951).
[7] Ticho, Green, and Richardson, Phys. Rev. **86**, 422 (1952).
[8] Ticho, Green, and Richardson (private communication, (1952).

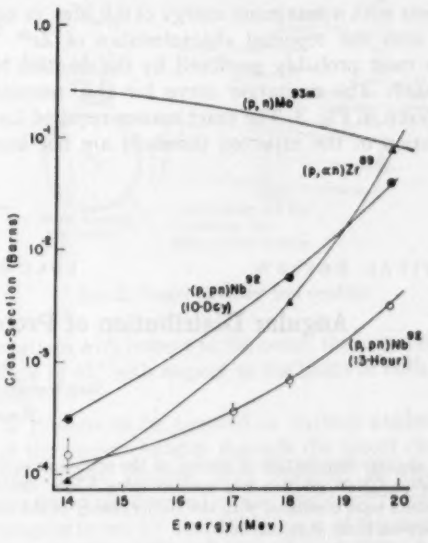

FIG. 3. Excitation functions of proton-induced reactions of Nb^{93}. (The curves for Zr^{89}, Nb^{93m}, and Nb^{92} should be considered only as relative yields rather than absolute cross sections since the counting efficiencies for x-rays were unknown.)

the 13-hour activity is a niobium isotope. The excitation curves (Fig. 3) for the 10-day and 13-hour activities show an almost constant ratio of the two, indicating that these species are formed by the same nuclear reaction, namely Nb$^{93}(p,pn)$Nb^{92}. Since the 10-day isomer does not grow from the 13-hour activity, the latter must decay by electron capture. The similarity of these excitation functions together with the fact that no positrons or annihilation radiation were observed would seem to rule out the possibility of this activity's being the 15-hour Nb^{90} formed by the reaction Nb$^{93}(p,p3n)$.

An isomer of Nb^{92} has been previously reported.[9] However, the half-life and radiation characteristics reported were so radically different from those found in this work that the two activities are probably not the same. The low cross section for formation of this 13-hour activity relative to the 10-day Nb^{92} makes resolution of the decay curves difficult, particularly if extreme care is not used in eliminating the last traces of the 7-hour Mo^{93}. It is these small amounts of Mo^{93} in the niobium fraction which are primarily responsible for the large probable error in the yield of the 13-hour activity at the lower energies (Fig. 3) where very little of the 13-hour activity is produced relative to the amount of Mo^{93}.

The zirconium fractions decayed with an 80±1 hour half-life for as long as the samples could be followed (about 6 half-lives), this fact indicating the presence of Zr^{89}. Measurements in the β-ray spectrometer showed

[9] M. L. Wiedenbeck, Phys. Rev. **70**, 435 (1946).

positrons with a maximum energy of 0.9 Mev in agreement with the reported characteristics of Zr^{89}. The Zr^{89} is most probably produced by the reaction $Nb^{93}(p,\alpha n)Zr^{89}$. The excitation curve for this reaction is also shown in Fig. 3. The exact masses required for the calculation of the expected threshold are not known.

The author is indebted to Professor J. R. Richardson for his interest and advice, to Mr. S. Plunkett and the operating crew of the cyclotron for their cooperation in obtaining the bombardments, and to Dr. Harold Ticho and Mr. David Green for performing the gamma-ray spectrometer measurements.

PHYSICAL REVIEW VOLUME 93, NUMBER 2 JANUARY 15, 1954

Angular Distribution of Protons from the Reaction $Na^{23}(d,p)Na^{24}$ †

PHILIP SHAPIRO*
State University of Iowa, Iowa City, Iowa
(Received July 31, 1953)

The angular distribution of several of the proton groups from the $Na^{23}(d,p)Na^{24}$ reaction was studied using 3-Mev deuterons. The results were compared with the Butler theory of the angular distributions from (d,p) reactions.

A value of $l_n=2$ is assigned to the orbital angular momentum of the neutron captured in the formation of the ground state of Na^{24} from Na^{23}. Since the available evidence indicates that the parity of the ground state of Na^{24} is even, a value of $l_n=2$ implies that the ground state of Na^{23} also has even parity.

The two proton groups resulting when Na^{24} is produced in the 0.472-Mev and 0.564-Mev excited states could not be resolved. The angular distribution of the sum of these two groups could not be uniquely interpreted. The author favors the interpretation that one of these levels is formed by capture of a neutron with $l_n=0$ and the other by capture of a neutron with $l_n=2$. Then both levels would have even parity, the possible spin values being 1 or 2 for one of the levels and 1, 2, 3, or 4 for the other level.

The data on the 1.341-Mev level in Na^{24} indicate that it is formed by capture of a neutron with $l_n=0$. Hence this level has even parity and a spin of either 1 or 2.

I. INTRODUCTION

THE study of the angular distribution of several of the proton groups from the $Na^{23}(d,p)Na^{24}$ reaction has been undertaken here. The results are compared with the theory of Butler[1] in order to obtain information on the spins and parities of several of the lower excited states of Na^{24} and on the parity of the ground state of Na^{23}. The results may also be used to check the accuracy of the shell model[2] in the assignment of orbital angular momentum states to individual nucleons in the nucleus.[3]

The energy of the proton groups resulting from the deuteron bombardment of Na^{23} has been studied by Sperduto and Beuchner[4] using magnetic analysis. Their results which are pertinent to this experiment are given in Table I.

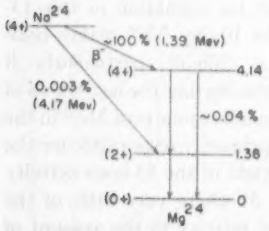

FIG. 1. Decay scheme of Na^{24}.

The spin[5] of the ground state of Na^{23} is $\frac{3}{2}$ and the spin[6] of the ground state of Na^{24} is 4.

The information available on the decay scheme[7] of Na^{24} is shown in Fig. 1. This information has to be analyzed so that the parity of the ground state of Na^{24} can be established. Mg^{24} is even-even so that the ground state has spin 0 and even parity. The angular correlation[8] of the cascade gamma rays from the 4.14-Mev level of Mg^{24} and the measurement of the internal pair conversion coefficients[9] of these gamma rays establish the spins and parities of the 1.38-Mev level and the 4.14-Mev level as shown in Fig. 1.

One can use this information on the energy levels of Mg^{24} and the data[10] available on the β decay of Na^{24} to determine the parity of the ground state of Na^{24}. The selection rules[11] for β decay indicate that if the parity of Na^{24} is odd, then both the 1.39-Mev and the 4.17-Mev β transitions are first forbidden. This is not in agreement with the ratio of the ft values for the two transitions; the ratio of the ft values for the 4.17-Mev

† This work was supported in part by the U. S. Atomic Energy Commission.
* Now at the U. S. Naval Research Laboratory, Washington, D. C.
[1] S. T. Butler, Proc. Roy. Soc. (London) **A208**, 559 (1951).
[2] See for instance, P. F. A. Klinkenberg, Revs. Modern Phys. **24**, 63 (1952).
[3] H. A. Bethe and S. T. Butler, Phys. Rev. **85**, 1045 (1952); S. T. Butler, Phys. Rev. **88**, 685 (1952).
[4] A. Sperduto and W. W. Buechner, Phys. Rev. **88**, 574 (1952).
[5] J. E. Mack, Revs. Modern Phys. **22**, 64 (1950).
[6] K. F. Smith, Nature **167**, 942 (1951).
[7] Hollander, Perlman, and Seaborg, Revs. Modern Phys. **25**, 469 (1953).
[8] E. L. Brady and M. Deutsch, Phys. Rev. **74**, 1541 (1948).
[9] S. D. Bloom, Phys. Rev. **88**, 312 (1952).
[10] J. F. Turner and P. E. Cavanagh, Phil. Mag. **42**, 636 (1951).
[11] E. J. Konopinski and L. M. Langer, Ann. Rev. Nuc. Sci. **2**, 261 (1953).

β transition to that of the 1.39-Mev transition is 4×10^6. If the parity of Na^{24} is even, then the 1.39-Mev transition is allowed and the 4.17-Mev transition is second forbidden, which is in reasonable agreement with the ratio of the *ft* values. Furthermore, the 4.17-Mev β spectrum has an allowed shape. If this β transition were first forbidden, it would have the unique forbidden shape[11] which deviates from the allowed shape. Hence the 4.17-Mev β transition cannot be first forbidden. From this one can conclude that the parity of the ground state of Na^{24} is even. Furthermore the 1.39-Mev β spectrum has an allowed shape[12] and the β-γ angular correlation[13] from Na^{24} is isotropic. This is in agreement with the conclusion that the 1.39-Mev transition is allowed.

II. APPARATUS

The statitron at the State University of Iowa was used as a source of 3-Mev deuterons. The energy spread of the deuteron beam was less than 0.5 percent and the energy of the deuteron beam could be repeated from day to day to better than 0.5 percent. The absolute value of the energy is only known to 5 percent. The above limits are conservative; actually spread in energy, reproducibility of energy setting and absolute value of energy are believed correct to a much higher accuracy.

TABLE I. Proton groups from $Na^{23}(d,p)Na^{24}$ reaction.

Proton group	*Q* (Mev)	Resultant energy level in Na^{24} (Mev)
1	4.731	0 (ground state)
2	4.259	0.472
3	4.167	0.564
4	3.390	1.341

Figure 2 shows a schematic diagram of the target chamber and counter. The target chamber is insulated from the statitron and can be used as a Faraday cage to collect the beam. The beam enters the target chamber through a slit (shown in Fig. 2) which is $\frac{1}{16}$ in. wide and $\frac{1}{4}$ in. high. This slit, which is insulated from the target chamber, determines the maximum size of the beam at the entrance to the target chamber.

A furnace was incorporated into the target chamber so that sodium targets could be evaporated in a vacuum to prevent oxidation of the sodium. The targets were evaporated onto a 1-mil silver foil,[14] which was used as a target backing. The silver target backing foils were checked for background by bombarding them with 3-Mev deuterons. Negligible background was found on all of the foils checked. The target was used at two

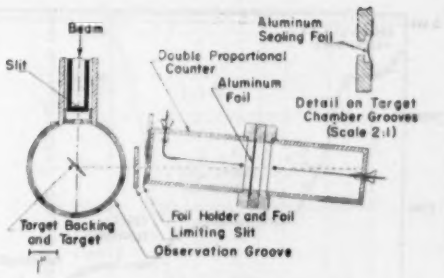

FIG. 2. Target chamber and counter.

orientations with respect to the beam, the target making an angle of 45° with respect to the beam in both orientations.

The protons to be counted at various angles come out of the target chamber through the target chamber grooves. These grooves were designed so that the protons could be observed at any angle with respect to the beam between 10° and 108° if part of the data were taken on one side of the beam and part of the data on the other side of the beam. For angles of 75° or less, the protons were observed going through the backing foil, and for angles greater than 85°, the protons were observed without going through the target backing. The shape of the target chamber grooves is shown in detail in Fig. 2. The grooves are $\frac{1}{4}$ in. high on the inside of the target chamber. The spread in azimuthal angle of the protons reaching the movable counter is limited to 3.5° by the limiting slit. With this arrangement protons within a solid angle of 1/2700 of a sphere are counted by the movable counter. The front half of a double proportional counter designed by Wm. E. Nickell was used as the movable counter. The movable counter has a large enough aperture so that all protons going through the observation grooves and limiting slit will be counted.

The central wire of the movable counter is a 5-mil tungsten wire maintained at a positive voltage of 1225 v. This counter and the monitor counter were filled with a mixture of 95-percent argon and 5-percent carbon dioxide at a pressure of 36 cm of mercury. Gas continually flowed through the counters in order to keep the counter gas as pure as possible. The pressure was kept at 36 cm by means of a Cartesian Manostat.[15]

The reaction was monitored by counting protons at a fixed angle with respect to the beam. The protons to be counted by the monitor counter come out through the window of one of two monitor tubes (not shown). These monitor tubes are on opposite sides of the beam. They make an azimuthal angle of 45° with respect to the beam and an angle of 30° with respect to the horizontal plane, thus making an angle of 52° with respect to the beam. The monitor counter could be placed over

[12] K. Seigbahn, Phys. Rev. **70**, 127 (1946).
[13] D. T. Stevenson and M. Deutsch, Phys. Rev. **83**, 1202 (1951).
[14] The silver foil was obtained from Baker and Company, Inc., 20 Church Street, New York 7, New York.
[15] Cartesian Manostat Model No. 5 was purchased from the Emil Greiner Company, 161 Sixth Avenue, New York 13, New York.

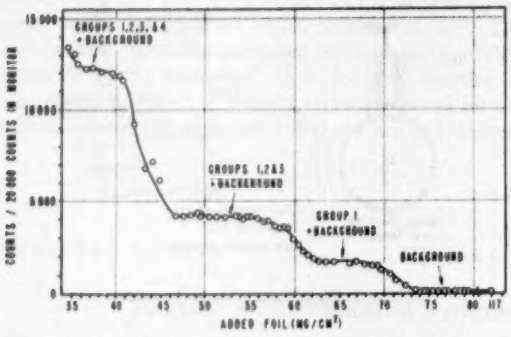
GROUPS 1,2,3, & 4 + BACKGROUND
GROUPS 1,2 & 3 + BACKGROUND
GROUP 1 + BACKGROUND
BACKGROUND
COUNTS / 20 000 COUNTS IN MONITOR
ADDED FOIL (MG/CM²)

FIG. 3. Counts in movable counter *vs* foil thickness (taken at 90°).

either of the monitor tubes and was always used so that it made an azimuthal angle of 90° with respect to the target. The monitor counter has sufficiently large aperture so that it counts all protons getting through the monitor tube. Protons within a solid angle of 1/1750 of a sphere were counted by the monitor counter. The central wire of 5-mil tungsten was maintained at a positive voltage of 1150 volts. The inside diameter of this counter was $\frac{1}{8}$ in., and it had an effective length of approximately 2 in.

The pulses from the proportional counters went to cathode followers which fed them to conventional linear amplifiers. The output of the amplifiers went to integral pulse-height discriminators and then to scaling circuits.

Aluminum foils of various thicknesses were used as absorbers in order to sort out the protons of different energies. These aluminum foils were carefully weighed and mounted on foil holders so that they could be placed in front of the movable counter. The thickness of these aluminum foils is known to ± 0.1 mg/cm^2.

III. PROCEDURE

A thin sodium target was evaporated onto the silver backing foil. No attempt was made to measure the target thickness. A target was considered to be of the right thickness if it was thin enough to permit resolution of the proton groups being studied and at the same time was thick enough to give a reasonable counting rate.

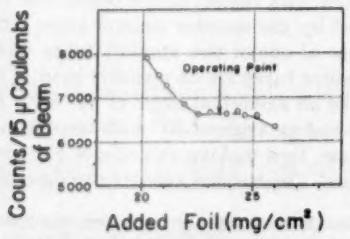

FIG. 4. Calibration of monitor counter.

The proton groups were separated by measurement of their range. The set of aluminum foils which could be placed in front of the movable counter was used as a variable absorber. The aluminum sealing foil on the target chamber and, in some cases, the target backing, were also between the target and the movable counter. Thus the movable counter could be used to count protons whose range is greater than a given value. The counts in the movable counter were all taken for a fixed number of counts in the monitor counter. A typical set of data is shown in Fig. 3.

The monitor counter counted all four groups of protons studied in this experiment. In order to determine the operating point of the monitor, the counting rate in the monitor was taken with various foils interposed between it and the monitor tube. These data and the operating point selected are shown in Fig. 4.

The counting rate in both the monitor counter and the movable counter are reasonably independent of discriminator setting. The monitor counting rate changes about $1\frac{1}{2}$ percent for a 5-v change in discriminator setting, and the counting rate in the movable counter does not change more than $1\frac{1}{2}$ percent for a 3-v change in the discriminator setting.

A set of data similar to that in Fig. 3 was taken at several angles. The abscissa in Fig. 3 only shows the aluminum foil added in front of the movable counter. It does not show any of the fixed absorbers that are between the target and the counter. The values obtained from these data for the range of the proton groups agrees reasonably well with the work of Sperduto and Buechner.[6] Groups 2 and 3 could not be resolved with this equipment. Therefore, the angular distribution of the sum of these two groups will be reported.

It was not necessary to run through a complete set of data, such as is shown in Fig. 3, at every angle. Since the energy of the protons varies slowly with angle, one can calculate the location of the flat regions of the curve and take counts only in these regions. This procedure does not introduce any error because data were taken over a sufficient range of oil thicknesses to insure that the right region was being covered.

In order to determine the intensity of any one of the proton groups, the background and the intensity of all proton groups of higher energy must be subtracted from the data. The background is due to neutrons counted in the movable counter and may be seen in Fig. 3. It is the small counting rate beyond the range of group 1.

As a check against systematic errors, the counting rate for the sum of all four proton groups was repeated on both sides of the beam for two angles. These counting rates taken on opposite sides of the beam did not agree. A thorough check made on the dimensions of all of the apparatus and on the alignment of the target chamber to the statitron showed that the beam spot was off-center with respect to the target chamber and that the limiting aperture of one of the monitor tubes was

farther away from the target than the other one. Corrections were made to the data to compensate for these errors. These corrections never exceeded 3 percent and could not introduce an error of more than 0.5 percent in the final results.

IV. RESULTS AND CONCLUSIONS

The experimental results, corrected and converted to the center-of-mass coordinate system, are shown as circles in Figs. 5, 6, and 7. The probable error in any point does not exceed the radius of the circle used in plotting the point. The curves are calculated from the Butler[1] theory of the angular distributions from (d,p) reactions using a value of $r_0=1.47\times(A^{\frac{1}{3}}+1)\times10^{-13}$ cm $=5.65\times10^{-13}$ cm. Although arbitrary units are used for the ordinates in the figures, the same units are used for all of the figures. Thus one can read the relative yields of the proton groups from the plotted results.

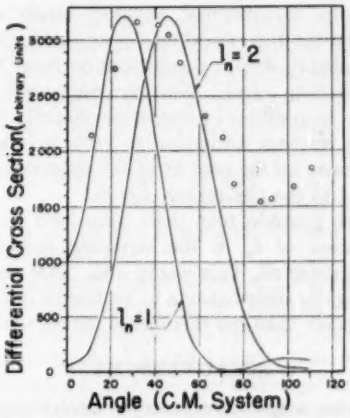

FIG. 5. Angular distribution of protons (ground state).

Angular Distribution of Protons (Ground State)

The theoretical curves for $l_n=1$ and $l_n=2$ are shown in Fig. 5 for comparison with the experimental results. If there were no further evidence available, one could not decide on this basis alone whether the experimental results are in agreement with the curve for $l_n=1$ or for $l_n=2$. The peak of the experimental curve lies between the peaks of the two theoretical curves and the width of the experimental curve is larger than that of the theoretical curves.

Values of l_n between 2 and 6 are the only values consistent with the known spins of the ground states of Na^{23} and Na^{24}. Hence a value of $l_n=2$ is assigned to the orbital angular momentum of the captured neutron in this reaction.

This result is in agreement with the shell model as one would expect that the ground state of Na^{24} is formed from Na^{23} by capture of a neutron into a d orbit. A value of $l_n=2$ implies no change of parity in the reaction.

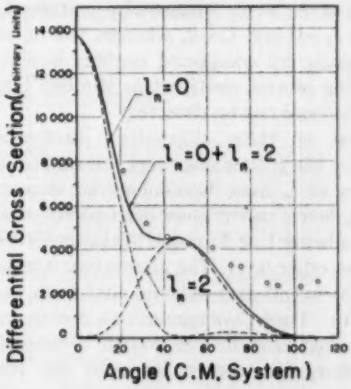

FIG. 6. Angular distribution of protons (0.472- and 0.564-Mev levels).

Since the parity of the ground state of Na^{24} is even, then the ground state of Na^{23} also must have even parity.

Angular Distribution of Protons (0.472-Mev and 0.564-Mev Levels)

Proton groups 2 and 3 could not be resolved with the apparatus used for this experiment. Figure 6 shows the angular distribution for the sum of these groups.

If one tries to fit the experimental results using a sum of theoretical curves involving only two values of l_n, then the only possible fit is for $l_n=0$ plus $l_n=2$. This is shown as a solid curve in the figure, the dashed curves being the individual curves for $l_n=0$ and for $l_n=2$. This result can be interpreted in four ways:

(1) One of the levels in Na^{24} is formed by capture of a neutron with $l_n=0$, and the other level is formed by capture of a neutron with $l_n=2$.

(2) Combinations of $l_n=0$ and $l_n=2$ may be involved in the formation of both of these levels.

(3) Both $l_n=0$ and $l_n=2$ are involved in the formation of one level while the other level is formed by capture of neutrons with either $l_n=0$ or $l_n=2$.

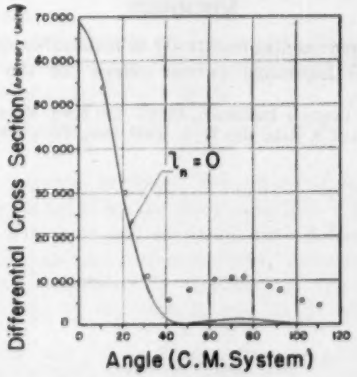

FIG. 7. Angular distribution of protons (1.341-Mev level).

(4) One of the levels is formed by capture of neutrons with both $l_n=0$ and $l_n=2$, whereas the other level is formed mostly by compound nucleus formation with the stripping process contributing through large values of l_n which could not be detected.

The first of these alternative interpretations is preferred by the author since very few cases of mixing of two values of l_n have been observed experimentally. Then both levels would have even parity, the possible spin values being 1 or 2 for one of the levels and 1, 2, 3, or 4 for the other level. The alternative interpretations (2) and (3) would also indicate that both levels have even parity. These interpretations are in agreement with the shell model. The fourth alternative seems quite unlikely but cannot be ruled out completely.

Other interpretations may be made if one uses mixtures of three or four values of l_n. Since the experimental results rise sharply in the forward direction, any mixture of various values of l_n must contain $l_n=0$. In addition to this, one could fit these results by adding to this two or three of the values $l_n=1, 2,$ or 3. Then there would be enough parameters available so that one could be sure to fit the experimental results. This would imply that the two levels in Na^{24} are of opposite paraty. The author does not favor these interpretations as they would be in complete disagreement with the shell model. Previous studies[16] of (d,p) and (d,n) angular distributions have in general shown agreement with the shell model. It is reasonable to assume that the shell model is correct unless positive evidence to the contrary is found.

It is hoped that future work on this reaction with better resolution will clarify the identification of these levels in Na^{24}.

Angular Distribution of Protons (1.341-Mev Level)

The experimental results for this group of protons, shown in Fig. 7, clearly fit the theoretical curve for $l_n=0$. Hence this level has even parity and a spin of either 1 or 2. This result is in agreement with the shell model.

Discussion

The experimental results are in reasonable agreement with the theoretical curves except for the angular distribution of group 1. These results suggest that although the Butler theory predicts the general shape of the angular distribution, some improvement in the theory is needed to account for all of the details of the angular distribution.

It may be necessary to take account of the Coulomb interaction of the incoming deuteron with the initial nucleus. The Coulomb barrier at a distance equal to r_0 from the center of the Na^{23} nucleus is 2.80 Mev as compared to the deuteron energy of 2.76 Mev in the center-of-mass system. On the other hand, Butler[17] has stated that for (d,p) reactions, the theory[3] should be quite good even for deuteron energies lower than the Coulomb barrier. He states that it is not so much the deuteron energy but the final proton energy which is of importance since the Coulomb field only enters in the way it affects the outgoing protons. In this experiment, the energy of the outgoing protons in the center-of-mass system was between 6.1 Mev and 7.5 Mev which was well above the Coulomb barrier.

All of the experimental angular distributions are higher than the theoretical curves at backward angles. This is probably due to a contribution from that part of the reaction which goes by compound nucleus formation. In addition to this, if the contribution from compound nucleus formation is very anisotropic, it might account for the poor fit of the experimental data for group 1 to the theoretical curves.

It is also possible that there may be a mixture of higher values of l_n in the stripping process which cannot be detected. This would also cause the experimental angular distributions to be higher in the backward direction than the theoretical curves shown.

V. ACKNOWLEDGMENT

The author wishes to express his sincere appreciation to Professor James A. Jacobs who directed this research and made many valuable suggestions during the course of the work. I am indebted to Professor F. Coester for several valuable discussions concerning the theory related to this experiment. Thanks are also due to Philip R. Malmberg and William E. Nickell for their help and suggestions and to Dr. W. W. Pratt who assisted in taking the data during long runs on the statitron. The cooperation of Mr. J. G. Sentinella and the members of the instrument shop who constructed the apparatus is very much appreciated.

[16] See for example Parkinson, Beach, and King, Phys. Rev. 87, 387 (1952); J. S. King and W. C. Parkinson, Phys. Rev. 88, 141 (1952).

[17] S. T. Butler (private letter dated March 28, 1952).

Some p- and d-Shell Nuclei in Intermediate Coupling

G. E. TAUBER* AND TA-YOU WU
National Research Council, Ottawa, Canada

(Received April 27, 1953; revised manuscript received July 27, 1953)

The theory of intermediate coupling has been applied to nuclei having either two particles or "holes" in the first p or d shell, such as He^6, Li^6, N^{14}, C^{14}, O^{18}, F^{18}, Ca^{38}, and A^{38}. A central nucleon-nucleon interaction of the form $(mP+nQ)V(r_{12})$, where P denotes the Majorana and Q the Bartlett operator, is assumed and calculations have been carried out for the exponential, Yukawa, and Gaussian types of potential $V(r_{12})$ with various "ranges." The coefficients m, n and the constants of the potential $V(r_{12})$ have been estimated from data for two free nucleons.

The secular equations have been solved and thus the degeneracy in the energy levels in the two extreme types of couplings has been removed. The energy levels of various spins for the various types of interactions and "ranges" have been plotted against the spin-orbit interaction parameter ζ. The range of ζ giving the correct spin for the ground state is found to depend on the type and "range" of $V(r_{12})$. The magnetic moments for these nuclei can also be obtained with the appropriate wave function for intermediate coupling. It is found that in the case of Li^6, a Yukawa potential having a "range" of about 1.0×10^{-13} cm accounts for both known excited states and gives a magnetic moment of $0.87\mu_N$. For N^{14}, the calculated magnetic moment is $0.36\mu_N$.

I. INTRODUCTION

THE empirical value found for the spin of the ground state of the Li^6 nucleus is one of the notable exceptions to the signal success of the nuclear shell model of Mayer *et al.*[1] According to it the nuclear configuration of Li^6 is $(1s)^2_P(1p)_P(1s)^2_N(1p)_N$,[2] which, in the extreme jj coupling has as the lowest state a group of degenerate levels with spin $I=3$, 2, 1, and 0. From symmetry considerations Feenberg[3] concludes that the spin of the lowest state for Li^6 is 3 while the observed value is 1.

To understand the observed spin of the ground states of Li^6, Inglis[4] has investigated the positions of the various levels of the configurations $(p)_P(p)_N$ for arbitrary couplings between the LS and jj limits. The purpose of the present paper is to extend the investigation of Inglis to see whether, by assuming nucleon-nucleon interactions of various forms and ranges and various spin-orbit interactions, it is possible to account for the two known excited states of Li^6,[5] as well as for $I=1$ of the ground state, and to calculate the magnetic moment of the ground state and also to apply the method to the configuration $(d)_P(d)_N$.

II. THE SECULAR EQUATION

The Hamiltonian of a many-nucleon nucleus may be assumed to be

$$H=\sum_i H(r_i)+\sum_{i\neq j} V_{ij}(r_{ij})+\sum_i H_i(\mathbf{l}_i\cdot\mathbf{s}_i), \quad (1)$$

where $H(r_i)$ is the one-particle Hamiltonian of a nucleus in a central field, V_{ij} the nucleon-nucleon interaction (between nucleons outside the complete shells) which is in addition to the part represented by the central field, and $H_i(\mathbf{l}_i\cdot\mathbf{s}_i)$ is the spin-orbit interaction. According as

$$V_{ij}\gg H_i \quad (2)$$

or

$$V_{ij}\ll H_i, \quad (3)$$

one has the limiting cases of LS coupling and jj coupling, respectively. Appropriate to these cases, one may conveniently use the LS representation and the JM representation. In an intermediate coupling scheme, one may express the wave function of the system in terms of either representation, and obtain the energy values from the corresponding secular equation.[6] If the coupling is known to be close to either limit, the eigenvalues and eigenfunctions may be calculated by the perturbation method. Thus if (2) is nearly satisfied, one may employ the LS representation in which the matrix of $\Sigma H(r_i)+\Sigma V_{ij}(r_{ij})$, where V_{ij} is central and does not contain tensor forces, is diagonal and $\Sigma H_i(\mathbf{l}_i\cdot\mathbf{s}_i)$ in general non-diagonal. Similarly, if the coupling is close to the jj extreme, i.e., (3) is nearly satisfied, the JM representation is used, where the matrix of $\Sigma H_i(\mathbf{l}_i\cdot\mathbf{s}_i)$ is diagonal and V_{ij} not.

For the configuration of a p proton and p neutron outside closed shells, the 36 states can be grouped in the (LS) limiting case into the levels

$$^{31}D_2,\ ^{33}P_{0,1,2},\ ^{31}S_0,\ ^{13}D_{1,2,3},\ ^{11}P_1,\ ^{13}S_1. \quad (4)$$

For two identical nucleons, the singlet isotopic spin states are excluded by the Pauli principle. The matrix elements of $\mathbf{l}_i\cdot\mathbf{s}_i$ in this representation are known[7] and the secular equations obtained. These, together with the other cases considered in this section, are given in Appendix I. In the (jj) limiting case, on the other hand,

* National Research Laboratories Postdoctorate Fellow.

[1] M. G. Mayer, Phys. Rev. **74**, 235 (1948); **75**, 1969 (1949); **78**, 16 (1950); Haxel, Jensen, and Suess, Phys. Rev. **75**, 1766 (1949).

[2] P. F. A. Klinkenberg, Revs. Modern Phys. **24**, 63 (1952).

[3] E. Feenberg, Phys. Rev. **76**, 1275 (1949).

[4] D. R. Inglis, Phys. Rev. **87**, 915 (1952); Revs. Modern Phys. **25**, 390 (1953).

[5] F. Ajzenberg and T. Lauritsen, Revs. Modern Phys. **24**, 321 (1952).

[6] E. U. Condon and G. H. Shortley, *Theory of Atomic Spectra* (Cambridge University Press, Cambridge, 1951), Chap. XI.

[7] See reference 6, Table I, p. 268.

one obtains the following levels in ascending order:

$$\begin{aligned}&(\tfrac{1}{2}\ \tfrac{1}{2})_{3,2,1,0}: && \zeta,\\ &(\tfrac{1}{2}\ \tfrac{1}{2})_{4,1},\quad (\tfrac{1}{2}\ \tfrac{1}{2})_{2,1}: && -\tfrac{1}{2}\zeta,\\ &(\tfrac{1}{2}\ \tfrac{1}{2})_{1,0}: && -2\zeta.\end{aligned} \tag{5}$$

Here the spin-orbit interaction parameter ζ is defined by[8]

$$\zeta=h^2\int_0^\infty R_n{}^2(r)\xi(r)dr$$

and assumed to be equal for neutrons and protons. (It is negative for a particle and positive for a "hole.") The appropriate matrix elements of the nucleon-nucleon interaction in this representation are conveniently obtained by transforming the diagonal levels (4) into the JM representation.[9]

For the configuration of a d proton and d neutron outside a closed shell one obtains similarly the following levels in the LS limiting case:

$$\begin{aligned}&{}^{31}G_4,\ {}^{31}D_2,\ {}^{31}S_0,\ {}^{33}F_{2,3,4},\ {}^{33}P_{0,1,2},\\ &{}^{13}G_{3,4,5},\ {}^{13}D_{1,2,3},\ {}^{13}S_1,\ {}^{11}F_3,\ {}^{11}P_1;\end{aligned} \tag{4a}$$

and in the jj limit again

$$\begin{aligned}&(5/2\quad 5/2)_{5,4,3,2,1,0}: && 2\zeta,\\ &(5/2\quad 3/2)_{4,3,2,1},\quad (3/2\quad 5/2)_{4,3,2,1}: && -\tfrac{1}{2}\zeta,\\ &(3/2\quad 3/2)_{3,2,1,0}: && -3\zeta.\end{aligned} \tag{5a}$$

III. CALCULATION OF ENERGY LEVELS IN THE LS LIMIT

A general nucleon-nucleon interaction of the form

$$V_{12}=(mP+nQ)V(|\mathbf{r}_1-\mathbf{r}_2|) \tag{6}$$

has been assumed, where P and Q are the Majorana and Bartlett operators, respectively, and V a central potential. For any two-particle problem the elements of the energy matrix can be readily calculated from trace invariance with the help of the wave functions of the individual two-particle states (Appendix III). Furthermore, as we are dealing only with central interaction, the potential can be expanded in a series of Legendre polynomials[10]

$$V(|\mathbf{r}_1-\mathbf{r}_2|)=\sum_{k=0}^{\infty} f_k(r_1,r_2)P_k(\cos\omega_{12}), \tag{7}$$

and the resulting interaction expressed in terms of Slater integrals defined by

$$F^k(n,n')=\int_0^\infty\int_0^\infty R_n{}^2(r_1)R_{n'}{}^2(r_2)f_k(r_1,r_2)dr_1dr_2. \tag{8}$$

The energies of the various states in the LS limit for the p-p and d-d configurations are given in Table I.

Talmi[11] has shown that it is possible to use harmonic-oscillator wave functions and carry out the integration for various types of potentials. In terms of his integrals I_l,

$$I_l=N_l{}^2\int_0^\infty \exp(-\nu r^2)r^{2l+2}V(r)dr, \tag{9}$$

the F's are given as follows:

p-p nucleon:[12]

$$\begin{aligned}&F_0=[5(I_0+I_2)+2I_1]/12, && F_0=F^0,\\ &F_2=[(I_0+I_2)-2I_1]/12, && F_2=F^2/25;\end{aligned} \tag{10}$$

d-d nucleon:

$$\begin{aligned}&15F_0=(63/16)(I_0+I_4)+(7/4)(I_1+I_3)+(29/8)I_2, && F_0=F^0;\\ &21F_2=(9/16)(I_0+I_4)-(1/2)(I_1+I_3)-(1/8)I_2, && F_2=F^2/49;\\ &35F_4=(3/16)(I_0+I_4)-(3/4)(I_1+I_3)+(9/8)I_2, && F_4=F^4/441.\end{aligned} \tag{11}$$

Here ν is the constant in the central, simple harmonic potential $V(r)=\nu^2\hbar^2r^2/2m$ and is related to the extension $1/(\nu)^{\frac{1}{2}}$ of the harmonic oscillator wave function which, from results of mirror nuclei, has been taken to be $1/(\nu)^{\frac{1}{2}}=2.4\times10^{-13}$ cm by Talmi.[11]

In order to make any explicit calculations it is necessary to specify the potential. We shall consider the

TABLE I.

State	Energy states for two p nucleons in the LS limit $mP+nQ$
${}^3D$	$(m+n)(F_0+F_2)$
${}^1D$	$(m-n)(F_0+F_2)$
${}^3P$	$(m-n)(-F_0+5F_2)$
${}^1P$	$(m+n)(-F_0+5F_2)$
${}^3S$	$(m+n)(F_0+10F_2)$
${}^1S$	$(m-n)(F_0+10F_2)$

State	Energy states for two d nucleons in the LS limit $mP+nQ$
${}^3G$	$(m+n)(F_0+4F_2+F_4)$
${}^1G$	$(m-n)(F_0+4F_2+F_4)$
${}^3F$	$(m-n)(-F_0+8F_2+9F_4)$
${}^1F$	$(m+n)(-F_0+8F_2+9F_4)$
${}^3D$	$(m+n)(F_0+3F_2+36F_4)$
${}^1D$	$(m-n)(F_0-3F_2+36F_4)$
${}^3P$	$(m-n)(-F_0-7F_2+84F_4)$
${}^1P$	$(m+n)(-F_0-7F_2+84F_4)$
${}^3S$	$(m+n)(F_0+14F_2+126F_4)$
${}^1S$	$(m-n)(F_0+14F_2+126F_4)$

[8] See reference 6, p. 122.
[9] See reference 6, Table I, p. 294.

[10] J. C. Slater, Phys. Rev. **34**, 1293 (1929).
[11] I. Talmi, Helv. Phys. Acta **25**, 185 (1952).
[12] The F_0 and F_2 are related to the K, L integrals of E. Feenberg and M. Phillips [Phys. Rev. **51**, 597 (1937)] through $L=F_0+F_2$, $K=3F_2$.

following types of potentials:

$$\text{(i) Exponential} \quad V(r)=V_0{}^E e^{-r/r_0},$$

$$\text{(ii) Yukawa} \quad V(r)=V_0{}^Y e^{-r/r_0}(r_0/r), \qquad (12)$$

$$\text{(iii) Gaussian} \quad V(r)=V_0{}^G \exp(-r^2/r_0{}^2),$$

where V_0 is the depth and r_0 the "range" of the potential. The explicit expressions for the integrals I_n for the cases (ii) and (iii) have been given by Talmi,[11] while the corresponding expressions for the case (i) are given in Appendix II.

Concerning the nucleon-nucleon potential (6), in the absence of sufficient knowledge, we shall assume that it is comparable with that between two nucleons unbound in a nucleus. On this assumption, the constants m and n and the depth of the potential V_0 have been obtained from the data on slow neutron scattering at low energies, namely the effective range $=1.72\times10^{-13}$, 2.7×10^{-13} cm, for the triplet and singlet state, respectively.[13] For a ^3S state the interaction (6) simply becomes

$$(m+n)V, \qquad (13)$$

while for the singlet ^1S, it is

$$(m-n)V. \qquad (13a)$$

Only these two combinations enter into the expressions for the energy levels. Applying the method of Wu and Foley[14] to the potentials (10), the values of $(m+n)V$ and $(m-n)V$ for the various types of potentials and "ranges" can be obtained. These are given in Table II.

With these values the Talmi integrals I_l for the various interactions and ranges are calculated, and the energies of the various states (Table I) occurring in the p-p and d-d configurations can be obtained by inserting the appropriate expressions for the integrals F's.

TABLE II. Constants of potential V in (6) and (10).

Type of potential and values of r_0 (cm)	$(m-n)V_0$ (Mev)	$(m+n)V_0$ (Mev)
(i) Exponential		
$r_0=1.0\times10^{-13}$	−57.63	−109.54
$r_0=1.4\times10^{-13}$	−29.28	−57.95
$r_0=2.0\times10^{-13}$	−14.24	−28.62
(ii) Yukawa		
$r_0=1.0\times10^{-13}$	−65.69	−117.20
$r_0=1.4\times10^{-13}$	−32.27	−59.67
$r_0=2.0\times10^{-13}$	−15.34	−29.24
(iii) Gaussian		
$r_0=1.0\times10^{-13}$	−111.89	−138.0
$r_0=1.4\times10^{-13}$	−55.82	−74.8
$r_0=2.0\times10^{-13}$	−26.73	−42.8

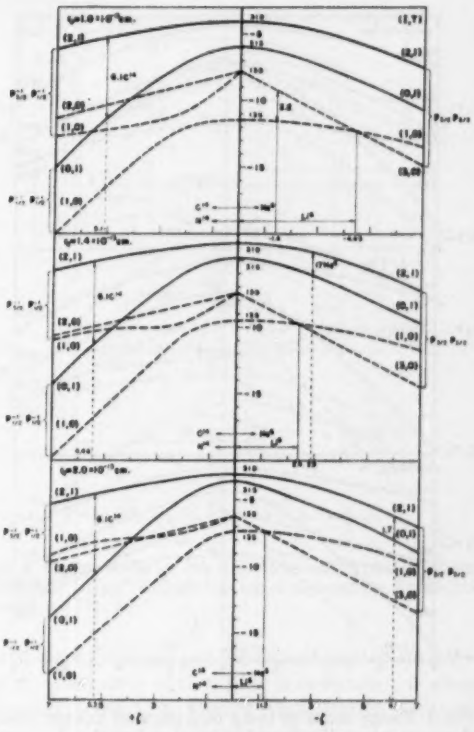

FIG. 1. Energy levels for two p nucleons with exponential potential and various "ranges" indicated on top of each section. Only low-lying energy levels have been included. Curves in full correspond to levels with $T=1$, while dashed curves give levels with $T=0$. Asymptotic behavior is indicated in the margin. Scale: 1 Mev per division for energy levels and spin-orbit interaction. Horizontal arrows indicate range of values of ζ for which the spin of the ground state agrees with the observed spin. The vertical arrows indicate the value of the parameter ζ for which the known excited states are obtained. In all these figures, $31G$ stands for ^{31}G, etc.

IV. ENERGY LEVELS IN INTERMEDIATE COUPLING

To obtain the energies for any intermediate coupling between **LS** and **jj**, the secular equations (given in Appendix I) are solved with the values of the F integrals already obtained, and the energy levels are obtained as a function of the spin-orbit parameter ζ. For three values for the range parameter r_0 in each of the three potentials in (12), the equations have been solved numerically and the energies thus calculated are plotted in Figs. 1–6 as functions of the spin-orbit parameter and the various potentials and ranges considered. In these figures, the curves in dashes represent those states antisymmetric in isotopic spin and hence excluded by the Pauli principle for two identical nucleons.

For a negative value of the spin-orbit parameter ζ one obtains all members of the polyad[15] having two nucleons outside closed shells, while for positive values of ζ the

[13] E. E. Salpeter, Phys. Rev. **82**, 60 (1951).
[14] T.-Y. Wu and H. M. Foley, Phys. Rev. **75**, 1681 (1949).

[15] This expression is due to Inglis[4] and denotes all nuclei having a specified value of A, e.g. Py^6 includes Li^6, He^6, and Be^6 if it existed.

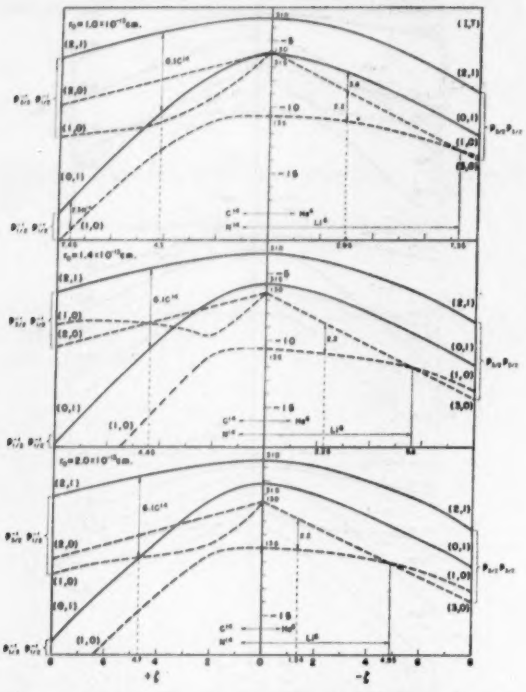

FIG. 2. Energy levels for two p nucleons with Yukawa potential and various "ranges" indicated on top of each section. For notation and scale see Fig. 1.

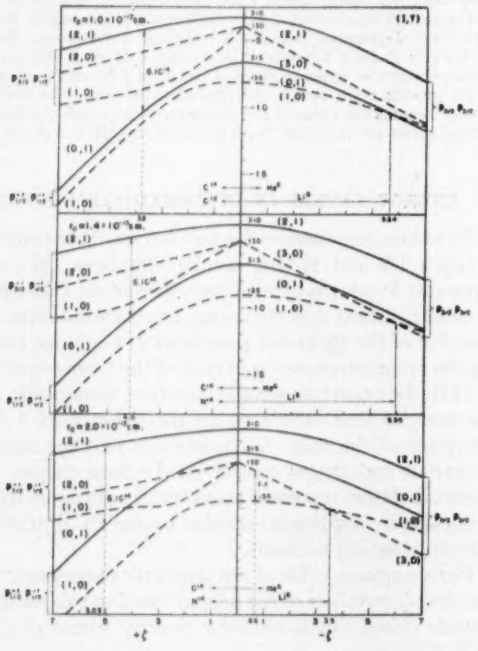

FIG. 3. Energy levels for two p nucleons with Gaussian potential and various "ranges" indicated on top of each section. For notation and scale see Fig. 1.

corresponding polyad with two "holes" is obtained. Thus the curves for $\zeta<0$ in Figs. 1–3 are applicable to He^6, Li^6, and Be^6, having the configuration $(p_N)^2$, p_Np_P, $(p_P)^2$, respectively, while the portions $\zeta>0$ of the curves are applicable to O^{14}, N^{14}, C^{14}, having the configuration $(p_N)^{-2}$, $(p_N)^{-1}(p_P)^{-1}$, $(p_P)^{-2}$, respectively. The range of values of ζ for which the spin of the ground state agrees with the observed spin is indicated by a horizontal line in the figures. Wherever possible the known excited states are also marked in the figures. In nearly all these cases it is possible to find a value for the spin-orbit parameter ζ depending on the potential and "range." For this range the spin of the ground state agrees with

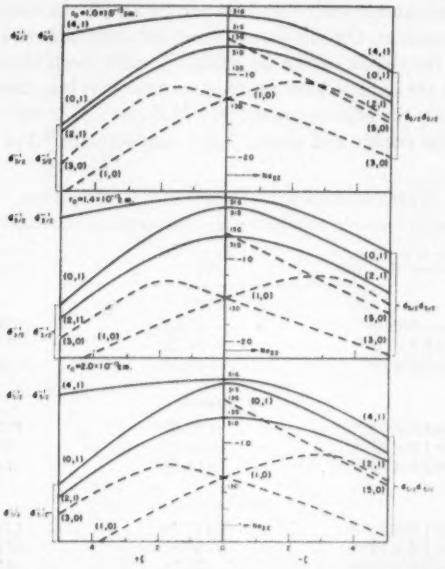

FIG. 4. Energy levels for two d nucleons with exponential potential and various "ranges" indicated on top of each section. Only low-lying energy levels have been included. Curves in full correspond to levels with $T=1$, while dashed curves give levels with $T=0$. Asymptotic behavior is indicated in the margin. Scale: 2 Mev per division for energy levels and 1 Mev per division for spin-orbit interaction. Horizontal arrows indicate range of values of ζ for which the spin of the ground state agrees with the observed spin. The vertical arrows indicate the values of the parameter ζ for which the known excited states are obtained.

that observed. It is interesting to note that in the case of the Yukawa potential (Fig. 2) values of $\zeta=-3$ and $r_0=1.0\times10^{-13}$ cm give both known excited states of Li^6 [3.58 Mev ($I=0$) and 2.2 Mev ($I=3$)[16] above ground][5] as well as the spin of the lowest state. (This is also approximately true with the Gaussian potential with $r_0=2\times10^{-13}$ cm. See Fig. 3.) This may indicate that this interaction and range seem to be favored over the others considered. It is also possible to obtain the

[16] According to the latest experimental results reported at the Second Conference of Medium Energy Nuclear Physics at the University of Pittsburgh, 1953, it seems to be established that the observed value of I for this level is indeed $I=3$ as predicted by the shell model.

energy levels of another member of the Py[6], *viz.*, He[6], but unfortunately not with the same interaction, as seen from Figs. 1 and 2.

In the case of nuclei with two holes in the p shell, namely, N^{14} and C^{14}, the spin of the ground state is correctly given for all values of ζ. For N^{14}, only the Yukawa potential with $r_0=1.0\times10^{-13}$ cm can fit the first excited state at 2.3 Mev with $I=0$ and $T=1$ with a value $\zeta\sim7.45$ Mev. While no great significance should be attached to this matching of one excited state alone, it is nevertheless of interest to note that the same potential also accounts for three states of Li^6 but with a smaller value of $|\zeta|$. That N^{14} corresponds to a larger spin-orbit coupling has already been pointed out by Inglis.[4] Further discussion of the coupling in N^{14} will be given in Sec. V below.

In the case of C^{14}, it has been found not possible to fit the observed level at 4.1 Mev with $I=0$, since with all the potentials and range parameter r_0 considered, the other state $I=0$ of the p^2 configuration always lies more than 4 Mev above the ground state $I=0$.[17] It is possible, however, to account for the level observed at 6.11 Mev if its spin is 2, with a value of about 5 Mev in all the potentials considered.

In Figs. 4–6 the portions $\zeta<0$ of the curves are applicable to $O^{18}(d_N^2)F^{18}(d_Nd_P)Ne^{18}(d_P^2)$, while the $\zeta>0$ portions are applicable to $Ca^{38}(d_N^{-2})$, $K^{38}(d_N^{-1}d_P^{-1})$, $A^{38}(d_P^{-2})$.

It is seen that only for the Yukawa potential with $r_0=1.0\times10^{-13}$ cm and the Gaussian potential with $r_0=1.0$ and 1.4×10^{-13} cm is it possible to obtain a range of values of ζ for which the ground state has spin $I=1$ as is required for F^{18}. It is interesting to note that in these cases the ranges which give the correct spin for I for the ground state for both F^{18} and O^{18} overlap, so that it is possible to account for both these cases by assuming an intermediate coupling with about the same value for ζ. This shows that the observed value $I=0$ for O^{18} does not necessarily have to be taken to suggest an extreme j-j coupling. Moreover, the Gaussian potential with $r_0=1.0\times10^{-13}$ cm seems to be preferred, for it is possible also to match the excited state (1.05 Mev and $I=0$).[18] We have also included Na^{22}, which has a ground state spin $I=3$ and, according to the older picture,[19] the configuration $(1s)^2\cdot(1p)^6(1d)(2s)^2$ for the protons and a similar configuration for the neutrons.[2] In the case of A^{38} it is possible to obtain both the ground-state spin $I=0$ and

[17] It is possible that the low observed position of the level at 4.1 Mev may be due to the result of strong configuration interaction, or may arise from another configuration altogether, since the parity of that state is not definitely known.

[18] The value $I=0$ has been obtained by matching it against the ground state of O^{18} in the figure of reference 5.

[19] This assumption arose from early thoughts regarding F^{19} but is doubtful in view of results concerning O^{17} and Na^{23} [see A. R. Edmonds and B. H. Flowers, Proc. Roy. Soc. (London) **A215**, 128 (1952), who have considered d particles with a Gaussian interaction]. According to present belief the configuration of Na^{22} has three protons and three neutrons in the d shell.

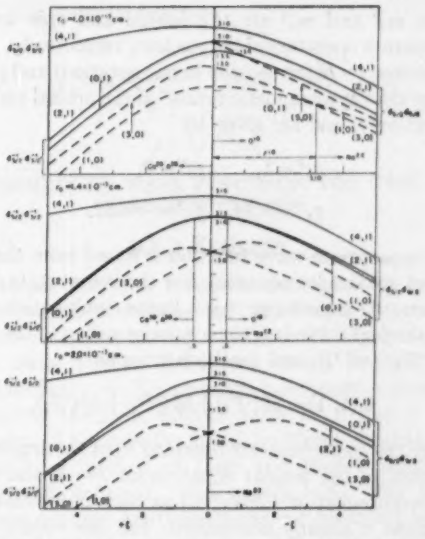

FIG. 5. Energy levels for two d nucleons with Yukawa potential and various "ranges" indicated on top of each section. For notation and scale see Fig. 4.

excited state $I=2$, but not the second excited state $I=3$ (Fig. 6). The parity of that state is not known, however, and would be due to a different configuration if it is odd.

V. MAGNETIC MOMENT OF Li^6, N^{14}

The magnetic moment is defined as the expectation value of the operator

$$\mu=\sum_{i=P,N}(m_i{}^sg_i{}^s+m_i{}^lg_i{}^l)\mu_N, \tag{14}$$

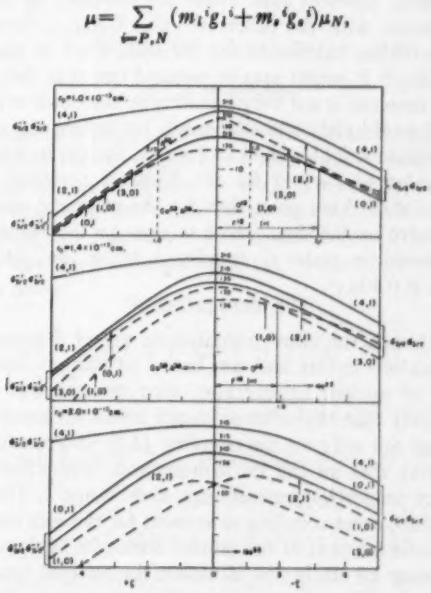

FIG. 6. Energy levels for two d nucleons with Gaussian potential and various "ranges" indicated on top of each section. For notation and scale see Fig. 4.

where m_l^i and m_s^i are the orbital and spin angular momentum operators of the nucleon, respectively, ($i=P$ for proton, $i=N$ for neutron in our notation) and g_l^i and g_s^i are the "gyromagnetic ratios" of the orbital and spin, respectively, and are given by

$$g_l^P=1, \quad g_l^N=0, \qquad g_s^P=5.58, \quad g_s^N=-3.82. \tag{15}$$

The appropriate wave function is found from the solution of the secular equation. For the lowest state of spin 1 from two p nucleons, it is a linear combination of the (zero-order) wave functions corresponding to the states $^3S_1$, $^3D_1$, and $^1P_1$ and can be written as

$$\Psi(1,1)=a\psi(^1P_1)+b\psi(^3D_1)+c\psi(^3S_1), \tag{16}$$

where the coefficients are obtained from the appropriate solution of the secular equation for $J=1$, and satisfy the requirement $a^2+b^2+c^2=1$ as each individual wave function is already normalized. The (zero-order) wave functions are obtained by properly combining the states corresponding to the various values of M_l and M_s into multiplets. The multiplets and wave functions are given in Appendix III.

Applying the operator μ (14) to the wave function, one obtains for the magnetic moment

$$\langle\mu\rangle=(0.5a^2+0.31b^2+0.88c^2)\mu_N. \tag{17}$$

Thus, for Li^6, the value of $\zeta=-3$ for the Yukawa potential with $r_0=1.0\times10^{-13}$ cm (which was used in order to fit both excited levels) gives then for the magnetic moment the value $\mu=0.866\mu_N$, in better agreement with the observed value $0.822\mu_N$ than the value $0.63\mu_N$ calculated for the state $I=1$ in pure jj coupling.[20] It might also be pointed out that the magnetic moment is not very sensitive to the exact value of ζ and would yield a similar result for values of ζ in the immediate neighborhood of $\zeta=-3$. Similarily for N^{14}, the value of $\zeta=7.45$ for the Yukawa potential with $r_0=1.0\times10^{-13}$ cm gives then for the magnetic moment the value $\mu=0.355\mu_N$, which is close to the value 0.37 calculated in pure jj coupling,[5] while the observed value is $0.40\mu_N$[2].

VI. CONCLUSION

Although the above calculations are of a somewhat exploratory nature and are based on various assumptions of nuclear interactions, they nevertheless show definitely that the order of energy levels with various I depend not only on the coupling (LS—intermediate—jj), but also on the nucleon-nucleon interaction (exchange properties, general form, and "range"). Thus, to find the correct coupling to account for the spin and the magnetic moment of the ground state of a nucleus, it is necessary to study the situation for various types of nucleon-nucleon interactions. The present work also seems to suggest that a nucleus having only two nucleons outside closed shells is much closer to LS coupling than to jj coupling. This is definitely demonstrated in the case of Li^6, where the assumption of jj coupling leads to wrong results for the spin of the ground state and gives not as good agreement with the experimental value of the magnetic moment as LS coupling.

At present work is being carried out to investigate nuclei with half-closed shells (such as B^{10}) in order to obtain more information concerning the relation between the coupling scheme and the number of nucleons outside closed shells.

We wish to express our thanks to Miss E. Motard for carrying out the numerical solutions of the secular equations involved. One of us (G.E.T.) also wishes to express his appreciation to the National Research Council of Canada for a postdoctorate fellowship which made this work possible.

APPENDIX I. SECULAR EQUATIONS

(1) Two p Nucleons

(a) States antisymmetric in the space and spin of the two nucleons: $T=1$.

$$I=2: \begin{vmatrix} {}^1D-E & \frac{1}{2}\sqrt{2}\zeta \\ \frac{1}{2}\sqrt{2}\zeta & {}^3P+\frac{1}{2}\zeta-E \end{vmatrix}=0,$$

$$I=1: \quad {}^3P+\tfrac{1}{2}\zeta-E=0,$$

$$I=0: \begin{vmatrix} {}^3P-\zeta-E & -\sqrt{2}\zeta \\ -\sqrt{2}\zeta & {}^1S-E \end{vmatrix}=0.$$

(b) States symmetric in the space and spin of the two nucleons: $T=0$.

$$I=3: \quad {}^3D+\zeta-E=0,$$

$$I=2: \quad {}^3D-\tfrac{1}{2}\zeta-E=0,$$

$$I=1: \begin{vmatrix} {}^3D-\frac{3}{2}\zeta-E & -(5/6)^{\frac{1}{2}}\zeta & 0 \\ -(5/6)^{\frac{1}{2}}\zeta & {}^1P-E & (\frac{3}{2})^{\frac{1}{2}}\zeta \\ 0 & (\frac{3}{2})^{\frac{1}{2}}\zeta & {}^3S-E \end{vmatrix}=0,$$

where ^1D stands for the integral in Table I, etc.

(2) Two d Nucleons

(a) States antisymmetric in the space and spin of the two nucleons: $T=1$.

$$I=4: \begin{vmatrix} {}^1G-E & \zeta \\ \zeta & {}^3F+\frac{3}{2}\zeta-E \end{vmatrix}=0,$$

$$I=3: \quad {}^3F-\tfrac{1}{2}\zeta-E=0,$$

$$I=2: \begin{vmatrix} {}^3F-2\zeta-E & -(12/5)^{\frac{1}{2}}\zeta & 0 \\ -(12/5)^{\frac{1}{2}}\zeta & {}^1D-E & (21/10)^{\frac{1}{2}}\zeta \\ 0 & (21/10)^{\frac{1}{2}}\zeta & {}^3P-\frac{1}{2}\zeta-E \end{vmatrix}=0,$$

[20] I. Talmi, Phys. Rev. 83, 1248 (1951).

$I=1$: $^3P-\frac{1}{2}\zeta-E=0$,

$I=0$: $\begin{vmatrix} ^3P-\zeta-E & -\zeta\sqrt{6} \\ -\zeta\sqrt{6} & ^1S-E \end{vmatrix}=0.$

(b) States symmetric in the space and spin of the two nucleons: $T=0$.

$I=5$: $^3G+2\zeta-E=0$,

$I=4$: $^3G-\frac{1}{2}\zeta-E=0$,

$I=3$: $\begin{vmatrix} ^3G-(5/2)\zeta-E & -(9/7)^{\frac{1}{2}}\zeta & 0 \\ -(9/7)^{\frac{1}{2}}\zeta & ^1F-E & (12/7)^{\frac{1}{2}}\zeta \\ 0 & (12/7)^{\frac{1}{2}}\zeta & ^3D+\zeta-E \end{vmatrix}=0,$

$I=2$: $^3D-\frac{1}{2}\zeta-E=0$,

$I=1$: $\begin{vmatrix} ^3D-\frac{3}{2}\zeta-E & -(7/2)^{\frac{1}{2}}\zeta & 0 \\ -(7/2)^{\frac{1}{2}}\zeta & ^1P-E & \sqrt{2}\zeta \\ 0 & \sqrt{2}\zeta & ^3S-E \end{vmatrix}=0,$

where the ^1G, ^3F, etc., are given in Table I.

APPENDIX II. TALMI INTEGRALS

I for the exponential potential (i) in (10):

$$I_0=2V_0[(1-\phi)(\mu^2+\tfrac{1}{2})\exp(\mu^2)-\mu/\sqrt{\pi}],$$

$$I_1=\frac{4}{3}V_0[(1-\phi)(\mu^4+3\mu^2+\tfrac{3}{4})\exp(\mu^2)-\mu(\mu^2+5/2)/\sqrt{\pi}],$$

$$I_2=\frac{8}{15}V_0\left[(1-\phi)\left(\mu^6+\frac{15}{2}\mu^4+\frac{45}{4}\mu^2+\frac{15}{8}\right)\exp(\mu^2)-\mu\left(\mu^4+7\mu^2+\frac{33}{4}\right)\Big/\sqrt{\pi}\right],$$

$$I_3=\frac{16}{105}V_0\left[(1-\phi)\left(\mu^6+14\mu^6+\frac{105}{2}\mu^4+\frac{105}{2}\mu^2+\frac{105}{16}\right)\times\exp(\mu)^2-\mu\left(\mu^6+\frac{27}{2}\mu^4+\frac{183}{4}\mu^2+\frac{279}{8}\right)\Big/\sqrt{\pi}\right],$$

$$I_4=\frac{32}{945}V_0\left[(1-\phi)\left(\mu^{10}+\frac{45}{2}\mu^8+\frac{315}{2}\mu^6+\frac{1575}{4}\mu^4+\frac{4725}{16}\mu^2+\frac{945}{32}\right)\exp(\mu)^2-\mu\left(\mu^8+22\mu^6+147\mu^4+330\mu^2+\frac{2895}{16}\right)\Big/\sqrt{\pi}\right],$$

where ϕ is the error function

$$\phi(\mu)=\frac{2}{\sqrt{\pi}}\int_0^\mu \exp(-t^2)dt,$$

and

$$\mu=1/2\nu^{\frac{1}{2}}r_0.$$

APPENDIX III. WAVE FUNCTIONS FOR TWO p AND d NUCLEONS

(1) p Nucleons

There are 36 wave functions corresponding to the various values of m_l and m_s which can be grouped together in states having a definite of M_L and M_S. These form various multiplets shown in (4). The corresponding wave functions are linear combinations of the above, having a definite value of L and S and symmetry. They can be found by direct diagonalization or by a method of Gray and Wills[21] using the operators $\mathfrak{L}_\pm=L_x\pm iL_y$ and $\mathfrak{S}_\pm=S_x\pm iS_y$. The wave functions required are those linear combinations which have $J=1$, $M=1$ and occur in (16) and are given below:[22]

$$\psi(^3S_1)=\frac{1}{\sqrt{3}}[(1^+,-1^+)+(-1^+,1^+)-(0^+,0^+)],$$

$$\psi(^1P_1)=\tfrac{1}{2}[(1^+,0^-)-(1^-,0^+)-(0^+,1^-)+(0^-,1^+)],$$

$$\psi(^3D_1)=\frac{1}{\sqrt{10}}\left\{-\frac{\sqrt{3}}{2}[(1^+,0^-)+(0^+,1^-)+(1^-,0^+)+(0^-,1^+)]+\frac{1}{\sqrt{6}}[(1^+,-1^+)+2(0^+,0^+)+(-1^+,1^+)]+\sqrt{6}(1^-,1^-)\right\}.$$

(2) d Nucleons

In this case there are 100 wave functions corresponding to the various values of m_l and m_s. The multiplets formed are those shown in (4a). The corresponding wave functions are again linear combinations of the above and are found by the method indicated. The final wave functions corresponding to $J=3$ and $M=3$ are given below:

$$\psi(^3D_3)=\frac{1}{\sqrt{14}}[2(2^+,0^-)-6(1^+,1^+)+2(0^+,2^+)],$$

$$\psi(^1F_3)=\tfrac{1}{2}[(2^+,1^-)-(2^-,1^+)-(1^+,2^-)+(1^-,2^+)],$$

$$\psi(^3G_3)=\tfrac{1}{6}\{2\sqrt{7}(2^-,2^-)-(\tfrac{1}{2}\sqrt{7})[(2^+,1^-)+(1^+,2^-)+(1^-,2^+)+(2^-,1^+)]+(1/2\sqrt{7})\times[\sqrt{6}(2^+,0^+)+4(1^+,1^+)+\sqrt{6}(0^+,2^+)]\}.$$

[21] N. M. Gray and L. A. Wills, Phys. Rev. 38, 248 (1931).

[22] The usual notation for wave functions is used: The first figure in each set of parentheses indicates the m_l value of the proton, the second that of the neutron; + or − denotes the spin functions for spin values $+\frac{1}{2}$ or $-\frac{1}{2}$, respectively.

On the Matrix Elements of the Spin-Orbit Interaction in the d^3 Configuration

SEIICHI SUEOKA*
Division of Physics, National Research Council, Ottawa, Canada
(Received September 28, 1953)

As a first step in studying the intermediate coupling of the various configurations of d nucleons outside a closed shell, we have calculated the matrix of the spin-orbit interaction in the d^3 configuration, following Jahn's classification of the terms.

IN order to investigate the intermediate coupling of nucleons encountered as a result of nuclear shell structure, one may proceed by obtaining the spin-orbit interaction for various configurations in the LS scheme. In extending the work of Tauber and Wu[1] on nuclei containing two p or d nucleons (or holes) to nuclei containing three d nucleons outside a closed shell, of which we assume F^{19} to be an example, it is necessary to calculate the matrix elements of the spin-orbit interaction in the $(d^2)_N(d)_P$ configuration.[2] Following to the method of Racah,[3] we have obtained all the matrix elements between states of different J and T.

The configuration d^2d corresponds to $T_t=\frac{1}{2}$ and T

TABLE I. The matrix $(d^3TSL\|\Sigma(s_i,l_i)\|d^3T'S'L')$ for $T=\frac{1}{2}$.

	^2S [3](30)	^2P [21](21)	^2P [111](11)	^4P [21](10)	^2D [3](10)	^2D [21](10)	^2D [21](21)	^4D [21](10)	^4D [21](21)	^2F [3](30)
[3](30)^2S	0	$3\sqrt{2}$	0	$-3\sqrt{2}$	0	0	0	0	0	0
[21](21)^2P	$-3\sqrt{2}$	1	$2\sqrt{7}$	1	$\sqrt{6}$	0	0	$-\frac{1}{2}\sqrt{42}$	$\frac{5}{2}\sqrt{2}$	0
[111](11)^2P	0	$2\sqrt{7}$	1	$2\sqrt{7}$	0	$-2\sqrt{6}$	0	$-2\sqrt{6}$	0	0
[21](10)^4P	$-3\sqrt{2}$	-1	$-2\sqrt{7}$	$\sqrt{10}$	$\sqrt{6}$	$\frac{1}{2}\sqrt{42}$	$-\frac{5}{2}\sqrt{2}$	0	0	0
[3](10)^2D	0	$-\sqrt{6}$	0	$\sqrt{6}$	$\sqrt{5}$	$\sqrt{35}$	$\sqrt{15}$	$-\sqrt{35}$	$-\sqrt{15}$	0
[21](10)^2D	0	0	$2\sqrt{6}$	$\frac{1}{2}\sqrt{42}$	$\sqrt{35}$	$\sqrt{5}$	0	$\frac{1}{2}\sqrt{5}$	$-\frac{1}{2}\sqrt{105}$	0
[21](21)^2D	0	0	0	$-\frac{5}{2}\sqrt{2}$	$\sqrt{15}$	0	$\sqrt{5}$	$-\frac{1}{2}\sqrt{105}$	$-\frac{1}{2}\sqrt{5}$	$2\sqrt{10}$
[21](10)^4D	0	$-\frac{1}{2}\sqrt{42}$	$-2\sqrt{6}$	0	$\sqrt{35}$	$-\frac{1}{2}\sqrt{5}$	$\frac{1}{2}\sqrt{105}$	$5\sqrt{2}$	0	0
[21](21)^4D	0	$\frac{5}{2}\sqrt{2}$	0	0	$\sqrt{15}$	$\frac{1}{2}\sqrt{105}$	$\frac{1}{2}\sqrt{5}$	0	$5\sqrt{2}$	$2\sqrt{10}$
[3](30)^2F	0	0	0	0	0	0	$-2\sqrt{10}$	0	$2\sqrt{10}$	$\sqrt{14}$
[21](21)^2F	0	0	0	0	$-2\sqrt{6}$	0	0	$\sqrt{42}$	$\sqrt{2}$	$\frac{1}{2}\sqrt{70}$
[111](11)^2F	0	0	0	0	0	$-\sqrt{21}$	5	$-\sqrt{21}$	5	0
[21](21)^4F	0	0	0	0	$-2\sqrt{6}$	$-\sqrt{42}$	0	0	0	$\frac{1}{2}\sqrt{70}$
[3](30)^2G	0	0	0	0	0	0	0	0	0	0
[21](21)^2G	0	0	0	0	0	0	0	0	0	$-\frac{5}{2}\sqrt{2}$
[21](21)^4G	0	0	0	0	0	0	0	0	0	$\frac{5}{2}\sqrt{2}$
[21](21)^2H	0	0	0	0	0	0	0	0	0	0
[21](21)^4H	0	0	0	0	0	0	0	0	0	0
[3](30)^2I	0	0	0	0	0	0	0	0	0	0

	^2P [21](21)	^2F [111](11)	^4F [21](21)	^2G [3](30)	^2G [21](21)	^4G [21](21)	^2H [21](21)	^4H [21](21)	^2I [3](30)
[3](30)^2S	0	0	0	0	0	0	0	0	0
[21](21)^2P	0	0	0	0	0	0	0	0	0
[111](11)^2P	0	0	0	0	0	0	0	0	0
[21](10)^4P	0	0	0	0	0	0	0	0	0
[3](10)^2D	$2\sqrt{6}$	0	$-2\sqrt{6}$	0	0	0	0	0	0
[21](10)^2D	0	$\sqrt{21}$	$-\sqrt{42}$	0	0	0	0	0	0
[21](21)^2D	0	-5	0	0	0	0	0	0	0
[21](10)^4D	$\sqrt{42}$	$-\sqrt{21}$	0	0	0	0	0	0	0
[21](21)^4D	$\sqrt{2}$	5	0	0	0	0	0	0	0
[3](30)^2F	$\frac{1}{2}\sqrt{70}$	0	$-\frac{1}{2}\sqrt{70}$	0	$\frac{5}{2}\sqrt{2}$	$\frac{5}{2}\sqrt{2}$	0	0	0
[21](21)^2F	$\sqrt{14}$	$-\sqrt{7}$	$-\frac{1}{2}\sqrt{14}$	$\frac{1}{2}\sqrt{22}$	0	$\frac{1}{2}\sqrt{10}$	0	0	0
[111](11)^2F	$-\sqrt{7}$	$\sqrt{14}$	$-\sqrt{7}$	0	$3\sqrt{5}$	$-3\sqrt{5}$	0	0	0
[21](21)^4F	$\frac{1}{2}\sqrt{14}$	$\sqrt{7}$	$2\sqrt{35}$	$\frac{1}{2}\sqrt{22}$	$\frac{1}{2}\sqrt{10}$	0	0	0	0
[3](30)^2G	$-\frac{1}{2}\sqrt{22}$	0	$\frac{1}{2}\sqrt{22}$	$\sqrt{30}$	$\frac{1}{2}\sqrt{66}$	$\frac{1}{2}\sqrt{66}$	$\frac{1}{2}\sqrt{66}$	$\sqrt{6}$	$\sqrt{6}$	0
[21](21)^2G	0	$-3\sqrt{5}$	$\frac{1}{2}\sqrt{10}$	$\frac{1}{2}\sqrt{66}$	$\sqrt{30}$	$\frac{1}{10}\sqrt{30}$	0	$\frac{5}{2}\sqrt{55}$	0	0
[21](21)^4G	$\frac{1}{2}\sqrt{10}$	$-3\sqrt{5}$	0	$-\frac{1}{2}\sqrt{66}$	$-\frac{1}{10}\sqrt{30}$	$10\sqrt{3}$	$-\frac{1}{2}\sqrt{55}$	0	0
[21](21)^2H	0	0	0	$-\sqrt{6}$	0	$-\frac{1}{2}\sqrt{55}$	$\sqrt{55}$	$\frac{1}{2}\sqrt{55}$	$2\sqrt{13}$
[21](21)^4H	0	0	0	$\sqrt{6}$	$\frac{5}{2}\sqrt{55}$	0	$-\frac{5}{2}\sqrt{55}$	$5\sqrt{22}$	$-2\sqrt{13}$
[3](30)^2I	0	0	0	0	0	0	$-2\sqrt{13}$	$-2\sqrt{13}$	$\sqrt{91}$

* National Research Laboratories Postdoctorate Fellow.
[1] G. E. Tauber and Ta-You Wu, Phys. Rev. 93, 295 (1954).
[2] We should like to find the possibility of explaining the ground state of F^{19} on this assumption. However, B. H. Flowers has very kindly communicated the result of a calculation which shows that in the jj limit the configuration of F^{19} is almost certainly s^2s.
[3] G. Racah, Phys. Rev. 62, 438 (1942); 63, 367 (1943).

either $\frac{1}{2}$ or $\frac{3}{2}$. Therefore all the terms in d^3, which has been treated by Jahn[4] in the *LS* limit, have to appear in d^2d, too. Using the fractional parentage coefficients $(d^3TSL\{d^2(T_1S_1L_1), d, TSL)$ obtained by Jahn, we can calculate the matrix elements of the spin-orbit interaction as follows:

$$(d^3TSL, TJM|\sum_{i=1}^{3}(s_i, l_i)|d^3T'S'L', T'JM)$$
$$=(-1)^{S+L'-J}(d^3TSL\|\sum_{i=1}^{3}(s_i, l_i)\|d^3T'S'L')$$
$$\times W(SLS'L'; J1),$$

where

$$(d^3TSL\|\sum_{i=1}^{3}(s_i, l_i)\|d^3T'S'L')$$
$$=3\sum_{T_1S_1L_1}(d^3TSL\{d^2(T_1S_1L_1)d, TSL)$$
$$\times(T_1S_1L_1, d_3, TSL\|(s_3, l_3)\|T_1S_1L_1, d_3, T'S'L')$$
$$\times(d^2(T_1S_1L_1)d, T'S'L'\}d^3T'S'L')$$
$$=(9\sqrt{5})[(2S+1)(2S'+1)(2L+1)(2L'+1)]^{\frac{1}{2}}$$
$$\cdot\sum_{T_1S_1L_1}(-1)^{S_1+L_1-\frac{1}{2}-S'-L'}(d^3TSL\{d^2(T_1S_1L_1)d, TSL)$$
$$\times W(\tfrac{1}{2}S\tfrac{1}{2}S'; S_11)W(2L2L'; L_11)$$
$$\times(d^2(T_1S_1L_1)d, T'S'L'\}d^3T'S'L'),$$

and the final form of this matrix is given in Table I.

The matrix for $T=\frac{3}{2}$ is the same as that obtained by Racah and therefore is omitted. Multiplying it by the function $(-1)^{S+L'-J}W(SLS'L'; J1)$, we easily get the final matrices of spin-orbit interaction for any definite value of J. The results will be reported later with complete numerical results for F^{19}.

The author should like to express his hearty thanks to Dr. T. Y. Wu for his encouragement throughout this work. He is also indebted to Dr. G. E. Tauber for his kind discussion.

[4] H. A. Jahn, Proc. Roy. Soc. (London) **201**, 516 (1950); **205**, 192 (1951).

PHYSICAL REVIEW VOLUME 93, NUMBER 2 JANUARY 15, 1954

Characteristics of a Proposed Double-Mode Cyclotron*

M. J. JAKOBSON AND F. H. SCHMIDT
Department of Physics, University of Washington, Seattle, Washington
(Received July 27, 1953)

It is proposed to accelerate ions in a fixed-frequency cyclotron, either with the dee voltages 180° out-of-phase, or with the dee voltages in-phase. This is possible if the angular extent of the dee electrodes is made less than the customary 180°. Formulas have been derived for the energy gain per turn of ions with various charge-to-mass ratios as a function of the angle of the dees. The threshold dee voltage for acceleration to a given energy is somewhat larger than that for conventional two-dee cyclotrons. For appropriate dee angles it is shown that both protons and deuterons can be accelerated in the nonrelativistic energy region at substantially the same magnetic field and oscillator frequency. Suggested applications to acceleration of ions heavier than alpha particles are discussed.

INTRODUCTION AND SIMPLE THEORY

A CONVENTIONAL two-dee cyclotron accelerates ions with the dee voltages 180° out-of-phase. No use is made of the in-phase mode of oscillation of the dee system. It can be brought about by appropriate minor changes in the coupling of the oscillator to the dee system as, for example, by reversing one of the dee stem coupling loops. The frequency of the two modes of oscillation is approximately the same.[1]

In order to show that ions can be accelerated with the dees resonating in-phase, we consider a two-dee cyclotron as shown in Fig. 1. Each dee subtends an angle θ; the grounded dummy dees simply insure a proper accelerating field. We assume that the peak dee-to-ground potential, V_0, is the same for each dee. The angular frequency of the ions is Ω; the cyclotron oscillator frequency is ω. q is the charge of each ion. ϕ is the phase angle of the ion with respect to the oscillator voltage. It is defined as zero if the ion crosses the center of the dee as the dee voltage is zero and decreasing. The ion energy gain per turn is then given by

$$\Delta W=2qV_0\cos\left(\frac{\omega}{\Omega}\phi\right)\sin\left(\frac{\omega}{\Omega}\frac{\theta}{2}\right)$$
$$\times\left[1+\cos\left(\frac{\omega}{\Omega}\pi+\psi\right)\right], \quad (1)$$

provided ω/Ω is nearly an integer. If ω/Ω were not an integer, the energy gain per turn will vary as $\cos[2m(\omega/\Omega)\pi]$, where m is the number of turns and acceleration would not result. ψ is zero or π corre-

* Partially supported by the U. S. Atomic Energy Commission.
[1] J. Backus, Rev. Sci. Instr. **22**, 84 (1951); F. H. Schmidt and M. J. Jakobson, Rev. Sci. Instr. (to be published).

sponding to the in-phase or out-of-phase mode, respectively.

The term $\sin(\omega\theta/2\Omega)$ expresses the dependence of the energy gain per turn on the angle of the dees. $\cos(\omega\phi/\Omega)$ expresses the dependence on the phase of the ion with respect to the accelerating voltage. ϕ can vary from $-(\Omega/\omega)(\pi/2)$ to $+(\Omega/\omega)(\pi/2)$ and back again. This, as we shall see later, leads to the same total limiting phase variations as in conventional cyclotrons. The first cos term indicates that the ions are more drastically bunched the higher the order of the harmonic, and the number of ion bunches per orbit increases as the order of the harmonic. The term in square brackets expresses the dependence of the energy gain per turn upon the relative phase of the two similar dees. For integral values of ω/Ω the square-bracket term becomes two if the in-phase mode is chosen for ω/Ω even and the out-of-phase mode chosen for ω/Ω odd. The maximum energy gain per turn then becomes

$$\Delta W = 4qV_0\left|\sin\left(\frac{\omega}{\Omega}\frac{\theta}{2}\right)\right|. \tag{2}$$

Hence, those ions for which ω/Ω is odd are accelerated in the out-of-phase mode and those ions for which ω/Ω is even are accelerated in the in-phase mode. Equation (2) shows that all ions for which the ratio of oscillator to ion angular frequency, ω/Ω, is an integer will have an energy gain per turn of $4qV_0$ modulated by $|\sin(\omega\theta/2\Omega)|$.

As an example, consider a double-mode cyclotron with two similar 120° dees. With the dee resonating in phase, ions for which $\omega/\Omega=2, 4, 8, 10, \cdots$ would be accelerated with a maximum energy gain per turn of $2\sqrt{3}qV_0$, as contrasted with $4qV_0$ for a conventional two-dee cyclotron. With the dees resonating 180° out of phase, ions for which $\omega/\Omega=1, 5, 7, 11, \cdots$ would be accelerated with the same energy gain per turn. Ions for which $\omega/\Omega=3, 6, 9, \cdots$ would not be accelerated.

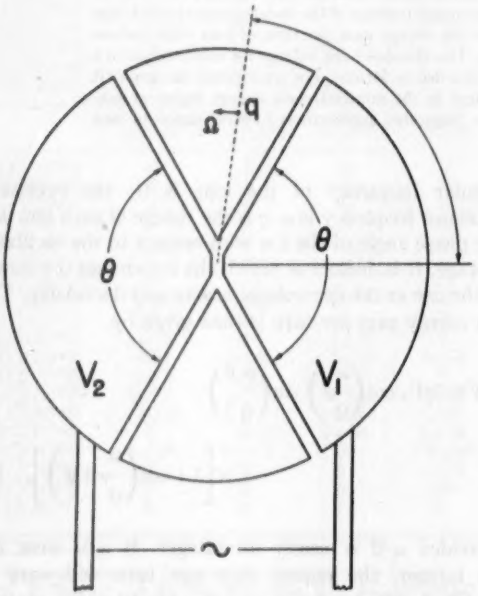

FIG. 1. A schematic of the dee electrodes for a double-mode cyclotron.

If 90° dees were used instead of 120° dees, then ions for which $\omega/\Omega=2, 6, 10, \cdots$ would be accelerated in the in-phase mode with a maximum energy gain per turn of $4qV_0$, and ions for which $\omega/\Omega=1, 3, 5, 7, \cdots$ are accelerated in the out-of-phase mode with a maximum energy gain per turn of $(4/\sqrt{2})qV_0$. In this case, ions for which $\omega/\Omega=4, 8, 12, \cdots$ would not be accelerated. Note that a double-mode cyclotron is unique in that ions for which $\omega/\Omega=1$ or 2, (such as protons and deuterons) can be accelerated in the same machine without changing appreciably the oscillator frequency or magnetic field.

The above calculations have been made assuming a step-function change in potential at the edge of the dees. The fringing electrical field would not change the essential properties of the acceleration. Only the case where both dees have the same angle θ has been considered. If the dees were unequal in angle and less than 180°, electrical forces would make the ion orbits precess and thus tend to produce instability.

COMPARISON WITH A CONVENTIONAL CYCLOTRON

Some of the properties of an accelerator that must be considered from the standpoint of design and operation are (1) starting conditions for the ions, (2) orbit stability, (3) threshold voltage,[2] and (4) exciting power. It is instructive to compare a normal two-dee cyclotron with a double-mode cyclotron with 120° dees. Table I shows a comparison of these properties for the two accelerators.

It is not likely that difficulty would be experienced in starting ions in an accelerator with 120° dees. Starting conditions in the out-of-phase mode are similar to those in a conventional cyclotron. Starting conditions for the in-phase mode could be improved by inserting 60° grounded sectors between the 120° dees. This would provide larger potential gradients for the acceleration of the ions near the ion source.

The requirements for orbit stability are the same for either type accelerator. The magnetic induction must decrease with increasing radius to provide vertical focusing.

The threshold voltage is defined as the lowest dee voltage for which ions will be accelerated to the exit radius of the machine. As shown in Table I the threshold voltage will be slightly increased for a 120°-dee cyclotron accelerating ions *in the same harmonic* as a conventional cyclotron. This is due to the fact that the energy gain per turn is less. For the acceleration of deuterons in a double-mode cyclotron with 90° dees and $\omega=\Omega_{\text{proton}}$, the threshold voltage for corresponding energies is

[2] H. A. Bethe and M. E. Rose, Phys. Rev. 52, 1254 (1937).

twice that of a conventional cyclotron with $\omega = \Omega_{deuteron}$. The energy gain per turn is the same for either accelerator, but the deuterons are accelerated on a second harmonic for the 90°-dee cyclotron. The increase in threshold voltage is partially compensated for by the decrease in power required to excite the smaller angle dees. The exciting power, neglecting ion loading, is proportional to V_0^2/Z_s, where Z_s is the shunt impedance of the resonating dee electrodes. Since Z_s is doubled by decreasing the angular extent of the dees from 180° to 90°, an increase of $\sqrt{2}$ in dee voltage will result for a given power input. This indicates the same power is required to accelerate protons to a given radius in a 90°-dee cyclotron as in a 180°-dee cyclotron. The problem of maintaining higher dee voltages arises with the smaller angle dees since the threshold voltage is higher.

POSSIBLE APPLICATIONS

One of the possible uses of a double-mode cyclotron would be the acceleration of ions heavier than alpha particles. The principal difficulty encountered in producing large beams of such heavy ions is the necessity of stripping inner electrons from the atoms. The present method of obtaining ${}_6C^{12(6+)}$ ion beams relies on a sequence of acceleration that requires harmonic acceleration of large beams of low-energy ions, some of which are stripped and accelerated to higher energies.[3]

[3] J. Miller, Ph.D. thesis, University of California, 1952 (unpublished).

TABLE I. Comparison of normal two-dee cyclotron with 120° dee double-mode cyclotron.

Property	Normal two-dee cyclotron with 180° dees $\omega = \Omega_{proton}$	Double-mode cyclotron with 120° dees $\omega = \Omega_{proton}$ In-phase mode	Out-of-phase mode
Ions accelerated	ω/Ω odd	ω/Ω even except 6, 12, ···	ω/Ω odd except 3, 9, 15, ···
ΔW = energy gain	$4qV_0$	$2\sqrt{3}qV_0$	$2\sqrt{3}qV_0$
Starting conditions	Normal	Probably requires dummy dees	Normal
Orbit stability	Stable	Stable (1-dee cyclotron unstable)	Stable (1-dee cyclotron unstable)
Threshold voltage	V_0	$V_0/0.866$	$V_0/0.866$
Exciting power for threshold voltage	P	(8/9)P	(8/9)P

The principle advantage of a double-mode cyclotron for the purpose of heavy-ion acceleration would be that it permits the harmonic acceleration of a larger variety of ions. As an example, consider the acceleration of ${}_8O^{16}$. A 120° double-mode cyclotron could accelerate ${}_8O^{16(++)}(\omega/\Omega = 8)$. Some of these ions would be stripped and accelerated as ${}_8O^{16(8+)}$. The stripping could possibly be enhanced by a discharge maintained within one of the grounded dummy dees.

Another application would be to a medium-energy cyclotron for the purpose of accelerating protons and deuterons without changing the oscillator frequency or magnetic field. The exciting power required for a 90°-dee double-mode cyclotron would be the same as for a 180°-dee cyclotron of comparable size.

The Tendency for Positive Nuclear Quadrupole Moments*

S. A. Moszkowski† and C. H. Townes
Columbia University, New York, New York

(Received August 31, 1953)

An examination of the signs of nuclear quadrupole moments and of the nuclear states which produce them affords fairly striking evidence that a positive quadrupole moment tends to lower the energy of a nuclear state.

For nuclei containing several particles outside of closed shells the shell model often does not uniquely specify the sign of the quadrupole moment. The ground states of such nuclei are, however, known to have positive quadrupole moments in the great majority of cases. Additional evidence for this tendency is provided by a discussion of:

(a) The ground states of Cu, Ga, As, Br, and Rb.
(b) The exceptions to the single-particle version of the shell model, Na^{23}, Mn^{55}, Se^{79}, Eu^{153}, and Yb^{173}.
(c) The spins of ground states of odd-odd $N=Z$ nuclei.

The favoring of positive quadrupole moments appears to be accounted for by electrostatic and other known forces in conjunction with large core deformations. It may, perhaps, also be influenced by tensor forces.

INTRODUCTION

It has been known for some time that quadrupole moments of odd-A nuclei vary in a more or less regular fashion with the number of odd protons or neutrons.[1,2] Some features of these variations can be accounted for on the basis of the shell model.[1,3] According to the independent-particle j-j coupling shell model, one would expect that quadrupole moments (Q) of nuclei containing one proton outside a closed shell would be negative and that nuclei lacking one from a closed shell would have positive Q. This expectation agrees with experimental observations for all major shells. However, for nuclei containing several particles (or holes) outside closed shells, the sign and magnitude of Q cannot be so uniquely predicted.

The size of some measured quadrupole moments (particularly of rare earth nuclei) is much larger than such a model would predict. Also, a number of odd-neutron nuclei are known to have a quadrupole moment in spite of the absence of electric charge on a neutron. The latter observation can be accounted for on the basis of polarization of the proton distribution by the neutrons.[1] If this type of polarization is allowed to deform the proton distribution including those in closed shells or the nuclear core, qualitative agreement can be obtained with experiment as far as magnitudes are concerned.[4] In fact, simple calculations of this polarization effect tend to overestimate quadrupole moments somewhat. The assumption of a deformable core does not prevent a definite prediction of the sign of Q for nuclei containing one proton outside of, or missing from a closed shell, and it allows prediction of the sign of Q to be made for odd-neutron nuclei.

An examination of the signs of nuclear quadrupole moments and of the nuclear states which produce them affords fairly striking evidence that a positive quadrupole moment tends to lower the energy of a nuclear state.

In Sec. I, evidence for a predominance of positive Q for odd-A nuclei is discussed. Those odd-A nuclei which do not correspond to a closed major shell plus or minus one particle and for which Q has been measured, have a positive quadrupole moment in the large majority of cases. For a number of other nuclei for which the quadrupole moment has not been measured, an interpretation of the measured spins and magnetic moments can be taken as further evidence for a predominance of positive quadrupole moments. In addition, certain exceptions to the expected spins of ground states can be interpreted as due to a favoring of positive Q.

In Sec. II, evidence for the predominance of positive Q in odd-odd $N=Z$ nuclei is discussed. As in the case of odd-A nuclei, support for this tendency comes both from measured Q's and from an interpretation of some spins.

In Sec. III and in the appendix, some theoretical discussion of this tendency for favoring positive Q's is given. It is pointed out that electrostatic and surface forces in conjunction with large core deformations can produce such an effect. Second-order effects of tensor forces might also contribute to it.

I. EVIDENCE FOR FAVORING OF POSITIVE QUADRUPOLE MOMENTS (ODD-A NUCLEI)

Consider a nucleus made up of closed shells of nucleons plus an additional even number of neutrons and an odd number of protons. It is normally expected

* Work partially supported by the U. S. Atomic Energy Commission.

† Now at University of California, Los Angeles 24, California.

[1] Townes, Foley, and Low, Phys. Rev. **76**, 1415 (1949).

[2] W. Gordy, Phys. Rev. **76**, 139 (1949).

[3] M. G. Mayer, Phys. Rev. **75**, 1969 (1949); **78**, 16 (1950); Haxel, Jensen, and Suess, Phys. Rev. **75**, 1766 (1949); Z. Physik **128**, 295 (1950).

[4] J. Rainwater, Phys. Rev. **79**, 432 (1950); A. Bohr, Kgl. Danske Videnskab. Selskab, Mat.-fys. Medd. **26**, No. 14, (1952); R. van Wageningen and J. De Boer, Physica **18**, 369 (1952); D. L. Hill and J. A. Wheeler, Phys. Rev. **89**, 1102 (1953); K. W. Ford, Phys. Rev. **90**, 29 (1953).

that for the ground state of such a nucleus, the neutrons will all be paired[5] and all but the last odd proton will be paired; i.e., the state has seniority 1. If all of these protons are in the same shell and subshell, it can be shown that the nuclear quadrupole moment is a simple linear function of the number of protons, having a maximum negative value when there is only one proton in the subshell, a maximum positive value of equal magnitude when the subshell is complete except for one proton and a value zero when the subshell is half-filled. Hence if this subshell fills regularly as protons are added (or if it fills in a completely random way), there will be an equal number of nuclei with positive and with negative quadrupole moments. A similar argument holds for the signs of the quadrupole moments of odd-neutron nuclei if it is remembered that the neutrons can create an electric quadrupole moment by polarizing the core of the paired protons.

All odd-A nuclei whose quadrupole moments have so far been measured are listed in Table I with the values of their spins.[6–10] Except where noted, the data are taken from Klinkenberg's recent comprehensive table.[6] Klinkenberg's configuration assignments for these nuclei are given in Table I except for some cases discussed below.

A number of nuclei can reliably be considered to have exactly one particle outside of, or missing from, a closed major shell. Such nuclei are labeled by the symbols $+1$ and -1, respectively. For nuclei of this type, the configurations are uniquely specified, and so are the signs of the expected quadrupole moment. In all these cases, the measured signs of the measured quadrupole moments are in agreement with the expected ones. For the other nuclei, the configurations are not necessarily specified uniquely, and in some cases, it is possible to construct reasonable configurations having positive Q and others having negative Q. Table II shows the relative occurrence of positive and negative quadrupole moments. It is seen that positive quadrupole moments clearly predominate, particularly for those nuclei which have several particles outside of, or missing from, a closed shell. It should be noted also that positive quadrupole moments are in general two or three times larger than negative ones, as may be seen from inspection of the plot of quadrupole moments given by Townes, Foley, and Low.[1]

Quadrupole moments for many nuclei may be predicted from the configurations given by Klinkenberg.[6] Of those for which configurations are given and quadrupole moments have not yet been measured, 26 are predicted to be positive and 22 negative. This indicates that for the configurations assigned by Klinkenberg on reasonable bases to those nuclei whose quadrupole moments are unknown, there is no strong preference for positive or negative quadrupole moments. However, there are alternative reasonable configurations for many of these nuclei, and we would expect that measurements will show that there are more positive quadrupole moments in this group of nuclei than are expected from Klinkenberg's assignments.

An examination of Klinkenberg's configuration assignments shows that types of deviations from a simple regular filling of shells and subshells occur to produce a predominance of positive quadrupole moments. There is a pronounced tendency to fill a subshell

TABLE I. Signs of measured quadrupole moments of odd-A nuclei.

Nucleus	Number of odd nucleons	Spin	Configuration of odd nucleons		Sign of Q	Footnotes
B^{11}	5	3/2	$(p_{3/2})^3$		+	
O^{17}	9	5/2	$d_{5/2}$	+1	−	
Na^{23}	11	3/2	$(d_{5/2})^2 s_{1/2}$		+	a
Al^{27}	13	5/2	$(d_{5/2})^5$		+	
S^{33}	17	3/2	$d_{3/2}$		−	
$Cl^{35,37}$	17	3/2	$d_{3/2}$		−	
S^{35}	19	3/2	$(d_{3/2})^3$	−1	+	
Mn^{55}	25	5/2	$(f_{7/2})^5$		+	b
$Cu^{63,65}$	29	3/2	$(p_{3/2})$	+1	−	
$Ga^{69,71}$	31	3/2	$(p_{3/2})^3$		+	
As^{75}	33	3/2	$(p_{3/2})^3(f_{5/2})^3$		+	
$Br^{79,81}$	35	3/2	$(p_{3/2})^3(f_{5/2})^4$		+	
Ge^{73}	41	9/2	$(p_{1/2})^3(g_{9/2})$		−	c
Se^{79}	45	7/2	$(g_{9/2})^7$		+	d
Kr^{83}	47	9/2	$(p_{1/2})^3(g_{9/2})^7$		+	e
$In^{113,115}$	49	9/2	$(p_{1/2})^2(g_{9/2})^9$	−1	+	
Sb^{121}	51	5/2	$d_{5/2}$	+1	−	
Sb^{123}	51	7/2	$g_{7/2}$	+1	−	
I^{127}	53	5/2	$(g_{7/2})^3 d_{5/2}$		−	
I^{129}	53	7/2	$(g_{7/2})^3$		−	
Eu^{151}	63	5/2	$(g_{7/2})^8(d_{5/2})^5$		+	
Eu^{153}	63	5/2	$(g_{7/2})^8(d_{5/2})^6(h_{11/2})^2$		+	f
Lu^{175}	71	7/2	$(g_{7/2})^7$		+	
Ta^{181}	73	7/2	$(g_{7/2})^7$		+	
$Re^{185,187}$	75	5/2	$(d_{5/2})^5$		+	
Xe^{131}	77	3/2	$(d_{3/2})$		−	
$Ir^{191,193}$	77	3/2	$(d_{3/2})^3$		+	g
Bi^{209}	83	9/2	$h_{9/2}$	+1	−	
Yb^{173}	103	5/2	$(f_{7/2})^5$		+	h
Os^{189}	113	3/2	$(p_{3/2})^3$		+	i
Hg^{201}	121	3/2	$(p_{3/2})^3$		+	j

[a] Na^{23}. Q measured by Sagalyn (reference 7). $(d_{5/2})^3$ would give $Q=0$.
[b] Mn^{55}. Q measured by Javan, Silvey, Townes, and Grosse (reference 8).
[c] Ge^{73}. $(g_{9/2})^3$ is an alternative configuration, which also has negative Q.
[d] Se^{79}. Q measured by Hardy, Silvey, and Townes (reference 9). The configuration $(p_{1/2})^3(g_{9/2})^5$ would not be expected to have the large positive quadrupole moment which is observed.
[e] Kr^{83}. $(g_{9/2})^9$ is an alternative configuration which also yields positive Q.
[f] Eu^{153}. This configuration assignment is suggested by both the large deviation of measured μ from the $d_{5/2}$ Schmidt line, and by the large positive measured Q. (In contrast to values of μ and Q for Eu^{151}.)
[g] $Ir^{191,193}$. Q measured by Murakawa and Suwa (reference 10). The assignment[6] $d_{3/2}$ would give $Q<0$.
[h] Yb^{173}. This assignment is suggested by the large deviation of the measured μ from the $f_{5/2}$ Schmidt line and the large positive measured Q. The assignment $(g_{7/2})^5$ would give $Q=0$.
[i] Os^{189}. I and Q measured by Murakawa and Suwa (reference 10).
[j] Hg^{201}. The assignment (reference 6) $p_{3/2}$ would give $Q<0$.

TABLE II. Number of odd-A nuclei having measured positive (or negative) Q.

Type of nucleus	$Q>0$	$Q<0$	Total
Closed shell ±1	3	6	9
Other	22	7	29
Total	25	13	38

[5] M. G. Mayer, Phys. Rev. **78**, 22 (1950).
[6] P. F. A. Klinkenberg, Revs. Modern Phys. **24**, 63 (1952).
[7] P. Sagalyn (to be published).
[8] Javan, Silvey, Townes, and Grosse, Phys. Rev. **91**, 222 (1953).
[9] Hardy, Silvey, and Townes, Phys. Rev. **86**, 608 (1952).
[10] K. Murakawa and S. Suwa, Phys. Rev. **87**, 1048 (1952).

almost, but not quite full. This of course produces positive quadrupole moments. The usual ideas of shell structure and additional stability inherent in a closed shell[5] would lead one to expect a more or less regular filling of a shell, with some tendency to complete the shell. However, experimental results show that some subshells are filled except for the last particle, after which subsequent particles go in pairs into new subshells, hence giving the nucleus a positive quadrupole moment. The tendency to leave shells in an almost filled condition accounts for the large majority of irregularities in the filling of shells.

Consider, for example, the nuclei $_{29}Cu^{63}$, $_{31}Ga^{69}$, $_{33}As^{75}$, $_{35}Br^{79}$, and $_{37}Rb^{85}$—odd-proton nuclei following immediately after a closed major shell of 28 particles. The first particle after 28 occupies a $p_{3/2}$ level, necessarily giving Cu a negative quadrupole moment. In Ga, two more particles have been added to give the filled shell minus one configuration $(p_{3/2})^3$. Pairs of additional particles go into the $f_{5/2}$ shell, so that As and Br also have positive quadrupole moments. Such behavior might possibly be attributed to a large pairing energy in the $f_{5/2}$ state, which requires always an even number of particles in this state, rather than a tendency to leave the $p_{3/2}$ shell almost filled. However, with the addition of two more particles, a configuration $(p_{3/2})^4(f_{5/2})^2$ is obtained in Rb^{85}. Here the $p_{3/2}$ shell has been able to fill in spite of the greater pairing energy in $f_{5/2}$, because the $f_{5/2}$ shell can be left almost filled, thus giving a large positive quadrupole moment. A similar anomaly occurs in the neutron levels at this same number of particles, and in several other subshells.

Another interesting case is the odd-neutron nucleus Hg^{201} for which Klinkenberg[6] gives the reasonable configuration $(f_{5/2})^6(i_{13/2})^{14}(p_{3/2})$. If this configuration were correct, Hg^{201} would have a negative Q instead of the measured positive value.[11] The alternative configuration which gives the proper positive quadrupole moment can be fairly uniquely assigned as $(f_{5/2})^6(i_{13/2})^{12}(p_{3/2})^3$. A similar situation exists for the pair of odd proton nuclei $Ir^{191,193}$, for which Klinkenberg[6] made the assignments $d_{3/2}$. Recently the Q of both nuclei was measured and found to be positive,[10] which requires instead a $(d_{3/2})^3$ assignment. In these three cases, the tendency for positive quadrupole moments appears to dominate over any tendency to complete subshells (e.g., $i_{13/2}$). Measurement of quadrupole moments for some of the other heavy nuclei may reveal other similar cases where Klinkenberg's assignments need modification.

There are five well-known nuclei which represent exceptions to Mayer's[5] scheme for nuclear spins. These are $_{11}Na^{23}$, $_{25}Mn^{55}$, $_{34}Se^{79}$, $_{63}Eu^{153}$, and Yb^{173}.[11] The quadrupole moments of all five of these nuclei have now been measured, and all are large and positive, again indicating that some interaction which tends to lower the energy of nuclei with positive quadrupole moments is strong enough to produce exceptions to the normal nuclear ground states. A more detailed discussion of these five well-established exceptions is given below.

$_{11}Na^{23}$ has recently been found to have a rather large positive quadrupole moment.[7] This is inconsistent with the configuration $(d_{5/2})^3$ which is usually assumed for Na^{23}, since this configuration would give zero quadrupole moment in accordance with Table III. A more likely configuration is $(d_{5/2})^2(s_{1/2})$. With a spin of 3/2 this gives a rather large positive quadrupole moment as observed, and furthermore gives a magnetic moment of 1.77 nuclear magnetons. This is closer to the observed value 2.22 nm than the 2.87 nm to be expected from a $(d_{5/2})^3$ configuration with spin 3/2. There appears to be no good reason why $(d_{5/2})^2(s_{1/2})$ should be less favored energetically as the ground state of Na^{23} than $(d_{5/2})^3$, and it is the only configuration of three protons in $d_{5/2}$ and $s_{1/2}$ orbits which gives the observed positive quadrupole moment.

The alternative configuration $(d_{5/2})^7$ (protons *and* neutrons outside of closed shells), with spin $I=3/2$, "charge" $T_z=-1/2$, isotopic spin $T=1/2$, "seniority" $v=3$, and "reduced isotopic spin" 3/2 which was suggested by Umezawa,[12] gives a theoretical μ of 1.98 nm in good agreement with experiment.[13] It has, in fact, been shown[12] that magnetic moments of light odd-A nuclei calculated by considering both protons *and* neutrons outside of closed shells are in better agreement with observed values than those calculated by considering only the odd nucleons (e.g., the Schmidt lines for only one odd nucleon or hole). However the quadrupole moment of the above configuration was calculated and found to vanish, in disagreement with the experimental result.

In both V^{51} and Mn^{55} with 23 and 25 protons, respectively, all the protons above 20 are believed to go into the $f_{7/2}$ orbit. The only proton assignments consistent with the spins of these nuclei are $(f_{7/2})^3{}_{7/2-}$ for V^{51} and $(f_{7/2})^5{}_{5/2-}$ for Mn^{55}. At present it is not too well understood why these two nuclei have different spins. Two-body velocity-independent interactions between any pair of 7/2 protons would, in first order, give the same level spacing for the configuration $(7/2)^5$ as for the complimentary configuration $(7/2)^3$ provided the radial wave functions are the same.[14]

The quadrupole moments expected for both con. figurations can be calculated by the method of traces. Relative values of quadrupole moments for some configurations of interest are given in Table III. Suppose that for both V^{51} and Mn^{55} there is competition for the

[11] W. G. Holliday and R. G. Sachs have also pointed out in a private communication the necessity for modifying Klinkenberg's assignments for this nucleus and for Yb^{173} (see following).

[12] M. Umezawa, Prog. Theor. Phys. 8, 509 (1952). See also B. H. Flowers, Phil. Mag. 43, 1330 (1952).

[13] Seniority = number of unpaired particles. Reduced isotopic spin = isotopic spin of unpaired particles. Umezawa (reference 12) gives 2.38 nm for this configuration, but our calculations give the above value.

[14] G. Racah, Phys. Rev. 62, 438 (1942); A. M. L. Messiah, Atomic Energy Commission Report NYO-3212 (unpublished).

TABLE III. Relative values of quadrupole moments Q_p for some proton configurations of interest (in terms of the magnitude of quadrupole moment $|Q_{s.p.}|$ produced by a single proton).[a] v = seniority number = number of unpaired particles.

Config. $(j)^n$	Spin I	v	Quadrupole moment of protons Q_p				
			$n=1$				
$(1/2)^n$	1/2	1	0				
			$n=1$	3 (or −1)			
$(3/2)^n$	3/2	1	−1	+1			
			$n=1$	3	5 (or −1)		
$(5/2)^n$	5/2	1	−1	0	+1		
	3/2	3		0			
			$n=1$	3	5 (or −3)	7 (or −1)	
$(7/2)^n$	7/2	1	−1	−0.33	+0.33	+1	
	5/2	3		−0.93	+0.93		
			$n=1$	3	5	7 (or −3)	9 (or −1)
$(9/2)^n$	9/2	1	−1	−0.5	0	+0.5	+1
	7/2	3 or 5		−1.34	degen. $-0.2<Q_p<+0.2$	+1.34	

[a] The quadrupole moment for a single proton in a state of spin j and $m=\pm j$ is

$$Q_{s.p.}=-\frac{2j-1}{2j+2}e\langle\psi_j|r^2|\psi_j\rangle.$$

ground state between the states 7/2− and 5/2−. Then the suggestion that the state of these two which has the largest algebraic (most positive) value of Q is favored energetically would, according to Table III, account for the spins of both V^{51} and Mn^{55}.[15]

The $(g_{9/2})^5$ configuration has two states of spin 7/2. The nuclear quadrupole moment depends on what combination of the two possible states make up the ground state of the nucleus. Hence in Table III the moment is labeled by the word "degenerate," indicating that some, but not much variation is possible. Recently the quadrupole moment of $_{34}Se^{79}$, which has 45 neutrons and a spin of 7/2, has been found to be large and positive.[9] Its magnetic moment[17] has also been found to be consistent with that expected from a configuration of 9/2 neutrons. Hence its state is probably $(g_{9/2})^7$. In any case, this exception to Mayer's rules for nuclear spin has a large positive quadrupole moment.

$_{63}Eu^{153}$ has been assigned the configuration $(g_{7/2})^6(d_{5/2})^5$ by Klinkenberg. However, its magnetic moment does not correspond to the value expected for a $d_{5/2}$ proton. The most reasonable configuration which would give the correct spin and magnetic moment would be $(g_{7/2})^5(d_{5/2})^6(h_{11/2})^2$. In accordance with Table III, a spin of 5/2 in this configuration would give a large positive quadrupole moment as observed.

Yb^{173} has been assigned the configuration $(h_{9/2})^{10}(f_{7/2})^8(f_{5/2})^3$ by Klinkenberg. If this assignment were valid, Yb^{173} would have a zero or very small quadrupole moment instead of the very large positive value which has been measured. Moreover, its magnetic moment does not correspond to the value expected for a $f_{5/2}$ neutron, as pointed out to us by M. G. Mayer. A reasonable configuration which gives both the correct magnetic moment and the observed positive sign of Q is $(h_{9/2})^{10}(f_{5/2})^6(f_{7/2})^5{}_{5/2}$.

II. EVIDENCE FOR FAVORING OF POSITIVE QUADRUPOLE MOMENTS (ODD-ODD NUCLEI WITH $N=Z$)

Quadrupole moments of four odd-odd $N=Z$ nuclei have been measured to date. Three of these (H^2, B^{10}, and N^{14}) are known to be positive. One, Li^6, has a very small value and its sign is not yet determined.

If it is assumed, in addition to j-j coupling, that the shells fill up in known order (*viz.*, $s_{1/2}$, $p_{3/2}$, $p_{1/2}$, $d_{5/2}$, $s_{1/2}$, $d_{3/2}$, $f_{7/2}$, etc.), and if the spin of a given nucleus is also known, the assignment of the nuclear state can often be uniquely determined. From the latter, the expected sign of the quadrupole moment can be predicted.

The ground-state spins of five of these nuclei, H^2, Li^6, B^{10}, N^{14}, and Na^{22}, have been measured.[6] The ground state spins of F^{18}, P^{30}, and K^{38} can be deduced from beta-decay schemes.[18,19] In all the above cases it is likely that $T=0$ and I is odd.[20] However, a recent

[15] The spins of Ca^{43} and Ti^{47} recently measured by C. D. Jeffries (private communication) are 7/2 and 5/2, respectively. This provides another case of the same type of behavior.

[16] The spins of these nuclei may possibly also be accounted for in the following manner. (See the recent paper by A. Bohr and B. R. Mottelson, Kgl. Danske Videnskab. Selskab. Mat.-Fys. Medd. 27, 16, (1952), pp. 34–37). For a nucleus containing three particles or holes in a subshell of spin j, the ground state is expected to have spin j if the interactions between particles are of short range and if other interactions, such as surface effects, are not significant. Such a situation is likely to occur in $_{21}Ca_{22}^{43}$ and $_{23}V_{28}^{51}$, for which the even particles form closed shells. On the other hand, if the nucleus under consideration is strongly deformed, one would expect that surface effects become important and perhaps even dominate over interparticle forces with resulting spin of $j-1$ for the ground state. This may be the case for the nuclei $_{22}Ti_{25}^{47}$ and $_{25}Mn_{30}^{55}$, in which the even particles do not form closed shells.

[17] W. Hardy (private communication).

[18] R. W. King, Ph.D. dissertation, Washington University, St. Louis, Missouri, 1952 (unpublished). See also R. W. King and D. C. Peaslee, Phys. Rev. 90, 1001, 1953.

[19] L. W. Nordheim, Revs. Modern Phys. 23, 322 (1951).

[20] This point is discussed in more detail in a forthcoming paper by D. C. Peaslee and one of the present authors (S. A. M.).

analysis of the Cl^{34} decay scheme suggests an assignment $T=1$, $I=0$ for the ground state of this nucleus.[21]

These data are summarized in Table IV, which also gives j-j coupling configuration assignments, as well as measured and expected signs of quadrupole moments (the latter deduced from Table V, below). In none of the cases listed in Table IV, is a negative Q found experimentally, or expected on the basis of a j-j coupling model with the known spin values. As is seen from Table V, one would expect that a favoring of positive Q would lead to exactly the trend of spins found in Table IV; *viz.*, low spins near the beginning of a subshell and high spins near the end. The analysis of spins of odd-odd $N=Z$ nuclei thus furnishes additional evidence of some mechanism which favors positive quadrupole moments.

TABLE IV. Spins, isotopic spins, configuration assignments, and signs of quadrupole moments for ground states of odd-odd $N=Z$ nuclei.

Nucleus	Spin I	Isotopic spin T	Configuration	Quadrupole moment Measured	Quadrupole moment Expected
H^2	1[a]	0	$(s_{1/2})^2$	+	0
Li^6	1[a]	0	$(p_{3/2})^2$	~0	+
B^{10}	3[a]	0	$(p_{3/2})^{-2}$	+	+
N^{14}	1[a]	0	$(p_{1/2})^2$	+	0
F^{18}	1	0	$(d_{5/2})^2$		+
Na^{22}	3[a]	0	$(d_{5/2})^4$		degen.
P^{30}	1	0	$(s_{1/2})^2$		0
Cl^{34}	0	1	$(d_{3/2})^2$		0
K^{38}	3	0	$(d_{3/2})^{-2}$		+

[a] Denotes measured spin.

TABLE V. Relative values of quadrupole moments calculated for various j-j coupling configurations of isotopic spin 0.

Config. $(j)^n$	Spin I	Quadrupole moment Q_p		
$(1/2)^n$		$n=2$		
	1	0		
$(3/2)^n$		$n=2$	6 (or −2)	
	1	+0.4	−0.4	
	3	−1	+1	
$(5/2)^n$		$n=2$	6	10 (or −2)
	1	+0.32	degen.	−0.32
	3	+0.03	degen.	−0.03
	5	−1	degen.	+1

III. CONCLUSIONS

The regularities pointed out above suggest that in nuclei there is a tendency for states with positive quadrupole moments to be lower in energy than those with negative quadrupole moments. Such a tendency appears to be accounted for by electrostatic and other known forces associated with large core deformations.[4] It may perhaps also be influenced by tensor forces. It is well known that the energy required to deform a spherical nucleus into a spheroid (either disk or cigar-shaped) is proportional to the square of the deformation, in lowest order. However, it can be shown that there is slight favoring of the elongated shape, which increases with the extent of the deformation. A rough estimate of this effect in nuclei (see Appendix) suggests that it is large enough to account for the observed predominance of positive quadrupole moments.

Because of the fact that the positive quadrupole moment of the deuteron can be attributed to tensor forces, it seems reasonable to speculate on whether tensor forces acting between any pair of particles will energetically favor states of positive quadrupole moment also in heavy nuclei. A first-order calculation of the energy matrix of tensor forces shows no such favoring.[22] In fact, it has been shown by several authors[14] that velocity-independent two-body forces which satisfy certain invariance requirements[23] are expected to give the same level spacing for a configuration of particles as for the corresponding configuration of holes, provided the radial wave functions are the same. However, in second order, a favoring of positive quadrupole moment is quite possible due to the distortion of the nucleus by "attractive" tensor forces;[24] [e.g., for a system of nucleons with $L=0$, $S\neq 0$, $V_{12}=S_{12}V(r_{12})$, $V(r_{12})<0$, a positive quadrupole moment results from the deformation of nucleon orbits]. Repulsive tensor forces, $V(r_{12})>0$, would lead to a negative quadrupole moment. Although the known positive quadrupole moment of the H^2 ground state can be accounted for on the basis of an attractive n-p tensor force in the $^3S_1$ state, the character of the p-p tensor forces is not yet known.

Thus it appears that the tendency for positive quadrupole moments in nuclei is consistent with the presently known information about nuclear forces.

ACKNOWLEDGMENTS

We would like to thank Professor J. H. Van Vleck for very helpful suggestions concerning calculation of quadrupole moments, and Dr. Michael Danos for valuable comments on the above work.

APPENDIX. FAVORING OF POSITIVE QUADRUPOLE MOMENTS AS A CONSEQUENCE OF LARGE CORE DEFORMATIONS

Let the nucleus be treated as a system of[4] (1) a core containing the "inner" nucleons in filled shells, the boundary of this core being assumed to change slowly with time compared with the motions of the individual nucleons; (2) "outer" nucleons in unfilled shells.

Let the core be deformed from a sphere of radius R_0 into an axially symmetric shape of radius $\rho(\theta)$ given by

$$\rho(\theta)=R_0[1+a_0+a_2P_2(\theta)+a_4P_4(\theta)+\cdots], \quad (1)$$

[21] W. Arber and P. Stähelin, Helv. Phys. Acta **26**, 433 (1953).

[22] I. Talmi, Phys. Rev. **89**, 1065 (1953).

[23] L. Eisenbud and E. P. Wigner, Proc. Nat. Acad. Sci. **27**, 281 (1941).

[24] G. M. Volkoff, Phys. Rev. **62**, 126 (1942).

where a_2 and a_4 define the sign and magnitude of the deformations, P_2, P_4 are Legendre polynomials, and a_0 is a coefficient whose value is adjusted so as to conserve volume. The magnitude of known quadrupole moments suggests that in many nuclei the core is deformed strongly and that at least a_2 is no more than one order of magnitude smaller than unity.

The change in surface and electrostatic energy of the core, relative to spherical shape, is, for uniform charge and mass density, given by:[25]

$$\Delta E_{S+E}=4\pi R_0^2\Theta[(0.4-0.4x)a_2^2 - (0.03810+0.07619x)a_2^3 + (1-0.3704x)a_4^2-(0.1143+0.3429x)a_2^2a_4 - (0.2171-0.2563x)a_2^4. \quad (2)$$

Here Θ is the surface tension, and $x=3Z^2e^2/40\pi R_0^3\Theta$, which is half the ratio of Coulomb energy to surface energy for a sphere. The first term of ΔE_{S+E} has been considered by many authors.[4] The second term, however, is of interest for large deformations and gives lower energies to positive quadrupole moments ($a_2>0$).

The interaction energy between the outer (identical) particles and the core is taken to be:[26]

$$\Delta E_{INT}=\langle\Psi|\Sigma_i[V(r_i)-V_0(r_i)]|\Psi\rangle, \quad (3)$$

with the potentials assumed to be:

$$V(r)=-D \text{ for } r<\rho, \quad V_0(r)=-D \text{ for } r<R_0,$$
$$=0 \quad \text{for } r>\rho, \qquad =0 \quad \text{for } r>R_0,$$

and where Ψ is the wave function of the outer particles, an antisymmetrized linear combination of products of single-particle wave functions

$$\psi_i=\mathfrak{R}_{nl}(r_i)u_{lj}^{\Omega_i}(\theta_i,\phi_i,\sigma_i), \quad (4)$$

characterized by the quantum numbers Ω_i, the component of angular momentum along the axis of deformation. Then ΔE_{INT} is given approximately by

$$\Delta E_{INT}=-DR_0^3\mathfrak{R}_{nl}^2(R_0)[(a_2+2/7a_2^2)\langle P_2\rangle + (a_4+18/35a_2^2)\langle P_4\rangle], \quad (5)$$

where

$$\langle P_2\rangle=\sum_i \frac{j(j+1)-3\Omega_i^2}{4j(j+1)}$$

and, in general,

$$\langle P_n\rangle=\langle\Psi|\Sigma_i P_n(\theta)|\Psi\rangle.$$

The total energy change of the nucleus is

$$\Delta E_T=\Delta E_{S+E}+\Delta E_{INT}, \quad (6)$$

if direct interactions between the outer particles are not taken into account.

To find the expected ground state for a given number of outer particles, we minimize ΔE_T with respect to a_2 and a_4. Although this minimum energy ΔE_M depends on both $\langle P_2\rangle$ and $\langle P_4\rangle$, the terms in $\langle P_4\rangle$ are ignored here for the sake of simplicity. A more detailed calculation shows that the inclusion of the terms in $\langle P_4\rangle$ leaves the following conclusions essentially unchanged.

The minimum energy to terms up to the third power in $\langle P_2\rangle$ is given by

$$\Delta E_M=-\epsilon_1\langle P_2\rangle^2-\epsilon_2\langle P_2\rangle^3, \quad (7)$$

where

$$\epsilon_1=\frac{[DR_0^3\mathfrak{R}_{nl}^2(R_0)]^2}{16\pi R_0^2\Theta(0.4-0.4x)}$$

and

$$\epsilon_2=\frac{[DR_0^3\mathfrak{R}_{nl}^2(R_0)]^3}{32\pi^2R_0^4\Theta^2(0.4-0.4x)^2}\left[\frac{1}{7}+\frac{0.03810+0.07619x}{4(0.4-0.4x)}\right].$$

The deformation a_{2M} giving lowest energy is

$$a_{2M}=\frac{2\epsilon_1\langle P_2\rangle+2\epsilon_2'\langle P_2\rangle^2}{DR_0^3\mathfrak{R}_{nl}^2(R_0)}, \quad (8)$$

where ϵ_2' is identical with ϵ_2 except for the replacement of the factor 4 by 8/3.

The quadrupole moment of the core[27] is:

$$Q_c=\frac{I}{I+1}\frac{2I-1}{2I+3}\frac{6}{5}ZeR_0^2\left[a_{2M}+\frac{4}{7}a_{2M}^2\right]. \quad (9)$$

The value of ΔE_M depends on the occupation numbers of the various substates in the outer shell and hence on the fraction f to which a shell is filled. For example, for one particle in a state of $j>3/2$, the lowest energy, i.e., the most negative value of ΔE_M, is obtained if $\Omega_i=\pm j$, with P_2, a_{2M}, and Q_c all negative.

To the approximations made in this paper, the lowest state is always one of the following two:[28]

[25] R. D. Present and J. K. Knipp, Phys. Rev. **57**, 751 (1940).

[26] Second-order terms due to nondiagonal contributions of this first-order interaction may well be significant here, as was pointed out by Dr. B. R. Mottelson in a private communication. These terms are probably of at least the same order of magnitude as the other terms in a_2^3 from the first-order interaction. They act in such a way as to lower the energy of the ground state (a general property of all second-order perturbation terms) but do not in general give the same lowering for states of positive and negative quadrupole moments. However, a detailed calculation of their effect on the *relative* energies of states with positive and negative Q for a half-filled shell requires knowledge of the radial wave functions of excited states and has not yet been made.

[27] The quadrupole moment Q of the nucleus is, of course, the sum of the quadrupole moments of the core Q_c and of the outer particles Q_p. The latter was discussed in Secs. I and II. If the core deformation is not negligible; i.e., if $a_{2M}>1/Z$, one would expect that the main contribution to the nuclear quadrupole moment comes from the core. This is likely to be the case for the great majority of nuclei. The factor $[I/(I+1)][(2I-1)/(2I+3)]$ is the ratio of Q_c (for a substate with $M=I$) to the intrinsic quadrupole moment of a symmetric top (with $\Omega=I$), as was pointed out by Aage Bohr, Phys. Rev. **81**, 134 (1951).

[28] The spin values I of the ground state, calculated according to this model, are (see reference 4)

(a) for $Q_c<0$, $I=\Omega=\Sigma_i\Omega_i=N_0-N$ if N is odd; $=0$ if N is even

(b) for $Q_c>0$, $I=\Omega=\Sigma_i\Omega_i=N$ if N is odd; $=0$ if N is even

where j is the spin of each particle. N is the number of nucleons in the subshell.

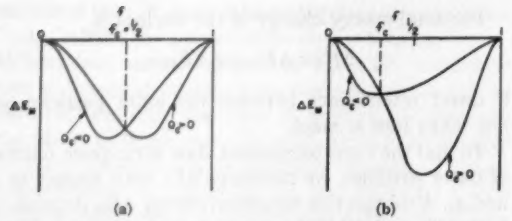

FIG. 1. Expected qualitative behavior of energy lowering as subshell is being filled. j=Fraction of subshell filled. E_M=Minimum energy for states with $Q_e<0$ and for states with $Q_e>0$. In (a) only terms in ϵ_1 are taken into account. In (b) both terms in ϵ_1 and in ϵ_2 are taken into account.

(a) substates filled from j downward

$$\Omega_i=\pm j, \pm j-1, \text{ etc.}, \quad P_2, a_{2M}, Q_e<0.$$

(b) substates filled from 1/2 upward

$$\Omega_i=\pm 1/2, \pm 3/2, \text{ etc.}, \quad P_2, a_{2M}, Q_e>0.$$

Approximate values of $\langle P_2\rangle$ for the fractional filling f of an outer shell of N_0 particles, for large N_0, are given by

$$\langle P_2\rangle_{Q_e<0}\doteq -N_0 f(1-f)(2-f)/4, \tag{10a}$$

$$\langle P_2\rangle_{Q_e>0}\doteq +N_0 f(1-f)(1+f)/4. \tag{10b}$$

In previous discussions,[4] only the term in ϵ_1 [Eq. (7)] has been considered. In this limit, the energy lowering is proportional to $\langle P_2\rangle^2$. As a consequence, for a less than half-filled shell ($f<1/2$), the disk-shaped form is favored, while if the shell is more than half-filled ($f>1/2$), the cigar-shaped form is lowest in energy. However, if the next order term in ϵ_2 is included in minimizing the energy, the "crossover" between these two forms occurs before the shell is half-filled. To the approximations employed here, the fraction f at crossover is given by

$$f_c=0.5-(9N_0\epsilon_2/128\epsilon_1). \tag{11}$$

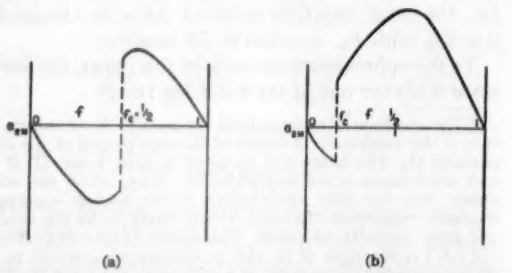

FIG. 2. Expected trend of equilibrium deformations as subshell is being filled. f=Fraction of subshell filled. a_{2M}=Equilibrium deformation. In (a) only terms in ϵ_1 are taken into account. In (b) both terms in ϵ_1 and in ϵ_2 are taken into account.

For a half-filled shell the state of positive quadrupole moment is lower than that of negative quadrupole moment by an energy

$$\Delta E_{M,Q_e<0}-\Delta E_{M,Q_e>0}=(27/16384)N_0^3\epsilon_2. \tag{12}$$

The expected qualitative behavior of energy lowering as function of fraction of subshell filled is sketched in Fig. 1. In Fig. 1(a) only terms in ϵ_1 are taken into account. In Fig. 1(b), both terms in ϵ_1 and in ϵ_2 are considered.

The dependence of energy lowering on the fraction of subshell filled has been calculated [Eqs. (11), (12)] for a special case to estimate the order of magnitude of this effect in a nucleus. The following assumptions were made:[4]

$$j=7/2, \quad Z=70, \quad A=170, \quad 4\pi R_0^3\theta=14A^{2/3}\text{ Mev},$$

$$x=0.60, \quad \text{and} \quad DR_0^3\Re_{nl}^2(R_0)=40\text{ Mev}.$$

Then from Eqs. (7) we have

$$\epsilon_1=5.7\text{ Mev}. \quad \epsilon_2=1.8\text{ Mev}. \tag{13}$$

According to Eq. (11), the calculated crossover between states of negative and positive quadrupole moments occurs when the subshell is about one-third filled ($f_c\sim 0.3$). For a half-filled shell, it follows from Eq. (12) that the lowest state of positive Q is below the state of negative Q_e by 1.5 Mev. The maximum deformation of the core can be fairly large. In the above example, $a_{2M}=0.22$ for a half-filled shell.

It should be kept in mind that this crude calculation may well over-estimate the expected core deformation[4] and therefore the energy lowering. Nevertheless, the surprisingly large result obtained here suggests that the energy lowering of states with positive Q relative to states with negative Q due to large core deformation is enough in many cases to overshadow other effects which might tend to act in the opposite direction, e.g., the known tendency of outer particles to couple to zero spin in pairs.

The qualitative trend of equilibrium deformations a_{2M} which can be deduced from measured quadrupole moments, is plotted as function of shell filling in Fig. 2. The trend of deformations shown in Fig. 2(b) is in qualitative agreement with that deduced from measured quadrupole moments for nuclei in the region $Z=50$ to 82.[1,4] Negative quadrupole moments mainly appear immediately after the closure of major shells. This is presumably connected with the fact that the subshells do not fill strictly one after the other. Thus the dependence of quadrupole moments on filling of subshells tends to be suppressed relative to their dependence on filling of major shells.

The Theory of the Deuteron Stripping Reactions*

N. C. FRANCIS, *Department of Physics, Indiana University, Bloomington, Indiana*

AND

K. M. WATSON, *Department of Physics, University of Wisconsin, Madison, Wisconsin*

(Received October 7, 1953)

The deuteron stripping reactions are analyzed from the point of view of the many-body problem. A rigorous formal solution is given. From this it is shown how assumptions less restricted than Butler's can be employed to reduce the many-body interactions to those of a deuteron moving in a potential well. At this point, the relation to previous theories is readily established. The present theory might be termed "the optical model" of the stripping reactions and represents a considerable generalization of current theories.

I. INTRODUCTION

BUTLER'S analysis[1] of the deuteron stripping reactions at intermediate energies has provided a useful tool for analyzing experiments pertaining to these processes. Alternate methods of calculation[2,3]—that is, the so-called Born-approximation theories—have led to rather similar results. One purpose of the present note is to derive both types of theories from a single model as somewhat limiting cases. It will be seen that the alternate points of view are closely related and that the distinction between them involves questions of nuclear structure as much as of mathematics.

For the sake of being specific, we shall speak of the (d,p) reaction, although the method of analysis applies equally to the (d,n) reaction. Our results are applicable also to the (p,d) and (n,d) processes (the pickup reactions) either directly or by means of the principle of detailed reversibility.

Butler[1] makes three significant assumptions in order to simplify the development of his theory. These are [we are now referring to the (d,p) reaction]:

(1) The proton does not interact at all with the nucleus which is struck.

(2) Once the neutron enters the nucleus, it is captured and does not interact with the proton which was originally in the deuteron.

(3) The incoming deuteron wave function is undistorted by the reaction.

Proceeding from these assumptions, Butler encloses the nucleus within a sphere of radius R_0. Within this sphere the neutron is bound to the nucleus. The outside region contains the incoming deuteron and the outgoing proton. Matching these wave functions and their derivatives on the sphere R_0 determines the cross section.

In the present discussion it will prove convenient to relax somewhat each of the above three assumptions. In so doing we shall cast the theory into a new form which, it is hoped, will add to the understanding of the physical basis of the Butler and "Born-approximation" theories, as well as to provide a more general theoretical basis for analyzing the stripping reactions. Our starting point will be a rigorous formulation of the process as a many-body problem. An exact formal solution will be given. By use of a somewhat modified form of Butler's assumptions, it is then shown how the many-body aspects of the problem can be reduced to those of a deuteron moving in a potential well. By imposing the appropriate conditions on the nature of the potential well, the Butler and "Born-approximation" theories can be obtained directly.

We shall neglect any specific discussion (as have previous analyses) of the role played by the Coulomb field on the stripping reaction. This involves no conceptual difficulties, as we can suppose the (screened) Coulomb interaction to be included in the definitions of the other interactions introduced in the next section. On the other hand, a numerical discussion of effects of the Coulomb forces would be quite involved and presumably would not add greatly to our understanding of the mechanism of the reaction.

II. DEVELOPMENT OF THE BUTLER AND BORN-APPROXIMATION THEORIES

A. General Discussion

We wish to calculate the transition rate for the reaction in which a deuteron strikes a nucleus with emission of a proton, the residual nucleus having "captured" the extra neutron. We suppose that the wave function for the initial nucleus is

$$g_A(\xi),$$

where ξ is a complete set of nuclear coordinates, and that the deuteron is moving with a momentum $\mathbf{K}$ with respect to the nucleus. Then, if $D(r)$ is the deuteron wave function, the initial state is

$$\chi_a=\frac{e^{i\mathbf{K}\cdot\mathbf{z}}}{(2\pi)^{\frac{3}{2}}}D(r)g_A(\xi), \qquad (1)$$

* Supported in part by a grant from the National Science Foundation.

[1] S. T. Butler, Proc. Roy. Soc. (London) **208**, 559 (1951).

[2] Bhatia, Huang, Huby, and Newns, Phil. Mag. **43**, 485 (1952).

[3] P. B. Daitch and J. B. French, Phys. Rev. **87**, 900 (1952).

where $\mathbf{x}=\frac{1}{2}(\mathbf{r}_P+\mathbf{r}_N)$, $\mathbf{r}=\mathbf{r}_P-\mathbf{r}_N$, and $\mathbf{r}_P$ and $\mathbf{r}_N$ are the respective coordinates of the proton and neutron with respect to the center of mass of the nucleus.

The state χ_a is evidently not antisymmetrized in the coordinates of identical particles as required by the Pauli principle, even though we suppose the nuclear states g_A (and g_B) to be so antisymmetrized. The antisymmetrization is most easily effected by first solving the Schrödinger equation with the *unsymmetrized* initial state χ_a and then antisymmetrizing this solution by means of an antisymmetrization operator. In principle this is simple to do, but to avoid complicating the argument, we shall for the moment (apparently) treat the initial neutron and proton as distinguishable from the nucleons in the nucleus (except that the final nuclear state is considered to be properly antisymmetrized). We shall return to this question in Sec. V.

After the reaction is completed, we suppose the system to be in a final state in which the neutron is captured and the proton is moving as a free particle of momentum $\mathbf{p}$ (with spin wave function s_P).

This state we write as

$$\chi_b=\frac{e^{i\mathbf{p}\cdot\mathbf{r}_P}}{(2\pi)^{\frac{3}{2}}}s_P g_B(\xi,\mathbf{r}_N), \tag{2}$$

where g_B is the wave function of the final nucleus including the captured neutron (which may or may not be bound into a stable state).

We next give the explicit Schrödinger equations satisfied by the states χ_a and χ_b. If V is the deuteron binding potential, then

$$(H_0+V)\chi_a=E_a\chi_a, \tag{3}$$

where $H_0(\xi,\mathbf{r}_N,\mathbf{r}_P)$ is the nuclear Hamiltonian plus the kinetic energy operators of the neutron and proton in the deuteron. If further $v(\mathbf{r}_N,\xi)$ represents the interaction of the neutron with the nucleus, then

$$[H_0+v]\chi_b=E_b\chi_b. \tag{4}$$

The final states χ_b ,which are of most interest to us, are those for which energy is conserved, or $E_a=E_b$. We finally suppose that the interaction of the proton with the nucleus is given by the "potential" $u(\mathbf{r}_P,\xi)$. Then the entire process is described by the appropriate solution to the Schrödinger equation

$$[H_0+V+v+u]\Psi=E_a\Psi. \tag{5}$$

B. The Butler Theory

In accordance with Butler's[1] assumptions, we shall in the remainder of the present section set $u=0$. That is, we suppose that the proton does not interact with the nucleus. The solution to Eq. (5) with $u=0$ will be designated by ψ to distinguish it from the exact solution Ψ (which will be given in Sec. III).

The desired solution to Eq. (5) is then easily obtained as[4]

$$\begin{aligned}\psi&=\left[1+\frac{1}{a-V-v}v\right]\chi_a\\&=\chi_a+\frac{1}{a-v}\Lambda\chi_a,\end{aligned} \tag{6}$$

where $a=E_a+i\eta-H_0$ (η is a small positive parameter, such as occurs in the Lippmann-Schwinger[5] formulation of scattering problems). The quantity Λ is

$$\Lambda=v+V\frac{1}{a-V-v}v. \tag{7}$$

The proof of Eq. (6) is trivial. The Schrödinger equation to be satisfied by ψ is

$$[a-V-v]\psi=0.$$

Applying the operator $[a-V-v]$ to the right-hand side of Eq. (6), we have by Eq. (3)

$$-v\chi_a+(a-V-v)\frac{1}{a-V-v}v\chi_a=0.$$

The last step in Eq. (6) is just an algebraic identity.

On introducing a complete set of final states,[6] $g_B^{(-)}\lambda_k$, where

$$\lambda_k=e^{i\mathbf{k}\cdot\mathbf{r}_P}/(2\pi)^{\frac{3}{2}}s_P, \tag{8}$$

Eq. (6) can be expressed as

$$\psi=\chi_a+\sum_{B,k}\frac{1}{a-v}g_B^{(-)}\lambda_k T(B,\mathbf{k}_N;a). \tag{9}$$

Here,

$$T(B,\mathbf{k};a)=(g_B^{(-)}\lambda_k,\ \Lambda\chi_a). \tag{10}$$

Now, because of Eq. (4),

$$\begin{aligned}\frac{1}{a-v}g_B^{(-)}\lambda_k&=\frac{1}{E_a+i\eta-E_b}g_B^{(-)}\lambda_k\\&=\frac{1}{\epsilon_{pB}+i\eta-\epsilon_k}g_B^{(-)}\lambda_k,\end{aligned} \tag{11}$$

where ϵ_{pB} equals the initial kinetic energy of the deuteron plus the difference in binding energies between initial and final nuclear states (or just the energy of the outgoing proton). Also

$$\epsilon_k=k^2/2M, \tag{12}$$

[4] The notation is that introduced by G. F. Chew and M. L. Goldberger, Phys. Rev. 87, 778 (1952).

[5] B. Lippmann and J. Schwinger, Phys. Rev. 79, 469 (1950).

[6] The state $g_B^{(-)}$ is equal to g_B if the state is bound. Otherwise $g_B^{(-)}$ contains *incoming* scattered waves whereas g_B has *outgoing* scattered waves. The necessity for using $g_B^{(-)}$ in Eq. (9) was demonstrated by K. Watson, Phys. Rev. 88, 1163 (1952).

where M is the nucleonic mass. When r_P is large, Eq. (9) becomes[7]

$$\psi=\chi_a+\sum_B(2\pi)^{-4}\int d^3k\frac{e^{i\mathbf{k}\cdot\mathbf{r}_P}}{\epsilon_{pB}+i\eta-\epsilon_k}\times s_P g_B^{(-)}T(B,\mathbf{k};a) \tag{13}$$
$$=\chi_a-\sum_B(2\pi)^{-4}\left\{(2\pi)^2M\frac{e^{ip_Br_P}}{r_P}\times s_P g_B^{(-)}T(B,\mathbf{p}_B;a)\right\},$$

where $p_B^2/2M=\epsilon_{pB}$ and $\mathbf{p}_B=p_B(\mathbf{r}_P/r_P)$.

From Eq. (13) we see that the cross section for stripping is (for a final nuclear state B)

$$\frac{d\sigma}{d\Omega}=(2\pi)^4M^2\frac{2p_B}{K}S|T(B,\mathbf{p}_B;a)|^2, \tag{14}$$

where S is an appropriate sum and average over final and initial spin substates, respectively.

Our next problem is to reduce $T(B,\mathbf{p}_B;a)$ to a more manageable form. Since in Eq. (14) we need $T(B,\mathbf{p}_B;a)$ only on the energy shell, we may suppose $E_b=E_a$ [Eq. (4)] and drop the subscript "B" on p_B. Then from (7) and (10),

$$T(B,\mathbf{p}_B;a)=(g_B^{(-)}\lambda_p,\Lambda\chi_a)$$
$$=\left(g_B^{(-)}\lambda_p,V\left[1+\frac{1}{a-V-v}v\right]\chi_a\right). \tag{15}$$

The last step follows since

$$(g_B^{(-)}\lambda_p,v\chi_a)=(g_B^{(-)}\lambda_p,V\chi_a).$$

[That is, $vg_B^{(-)}\lambda_p=ag_B^{(-)}\lambda_p$ and $V\chi_a=a\chi_a$ are just Eqs. (3) and (4)]. Because of Eq. (6), we may also write Eq. (15) as[8]

$$T(B,\mathbf{p};a)=(g_B^{(-)}\lambda_p,V\psi)=(\chi_b^{(-)},V\psi), \tag{15'}$$

which is a formally exact solution to our problem once ψ is known.

To interpret Eq. (15), we note that

$$V\left[1+\frac{1}{a-V-v}v\right]\chi_a$$

describes the entering of the nucleus by the neutron (as part of the deuteron) and its subsequent interaction with the nucleus. The V on the left means that the last step is a scattering of the neutron and proton. This last scattering leaves the system in the final state χ_b. According to the second of Butler's assumptions mentioned in the Introduction, this final scattering cannot occur when the neutron has entered the nucleus. Thus, according to Butler, the contribution to the stripping reaction occurs from neutron coordinates which lie *outside* the nucleus in Eq. (15). We shall return to this point in a moment.

Instead of Butler's drastic second assumption that the neutron does not interact with the proton once within the nucleus, we shall make the weaker assumption that the neutron does not interact with the proton once it has *excited* the nucleus to a state above its ground state. This seems quite plausible since an interaction which raises the nucleus to an excited state is expected to react violently on the more weakly bound deuteron, breaking it up and separating the neutron and proton of the deuteron. If this happens, we can imagine the chance that the neutron and proton will "find" each other to scatter again via the potential V to be small.

To incorporate this approximation into Eq. (15), we note that ψ contains in general a large number of excited states of the initial nucleus. Our assumption implies that we replace ψ by ψ_e in Eq. (15), where ψ_e is just that part of ψ which describes the nucleus in its ground state.[9] Then ψ_e describes the "elastic scattering" of the deuteron by the nucleus (that is, "elastic" in the sense that the nuclear state is not changed).

It has been shown[9] that such a "wave function" as ψ_e satisfies a Schrödinger equation with an "optical model" potential. If we write ψ_e as $\psi_e=\Omega_{CN}\chi_a$, where Ω_{CN} is the appropriate Møller wave matrix, then Ω_{CN} satisfies the Lippmann-Schwinger integral equation:

$$\Omega_{CN}=1+\frac{1}{a-V}\mathcal{U}_{CN}\Omega_{CN}, \tag{16}$$

where $\mathcal{U}_{CN}$ is the "optical model potential." The important feature of Eq. (16) is that we no longer have to deal with a many-body problem, since $\mathcal{U}_{CN}$ describes the motion of the deuteron in a "potential well" [although $\mathcal{U}_{CN}$ may also depend upon the spins of both the nucleus and the deuteron]. We finally obtain

$$T(B,\mathbf{p};a)=(g_B^{(-)}\lambda_p,V\Omega_{CN}\chi_a). \tag{17}$$

It is quite tempting to relate $\mathcal{U}_{CN}$ to the "optical potential" deduced by Feshbach, Porter, and Weisskopf[10] from Barschall's[11] neutron scattering experiments.

[7] See for instance, P. A. M. Dirac, *Quantum Mechanics* (Oxford University Press, London, 1947), third edition, p. 193.

[8] Equations similar to (15') have recently been derived independently by E. Gerjuoy, Phys. Rev. **91**, 645 (1953), and by M. Gell-Mann and M. Goldberger, Phys. Rev. **91**, 398 (1953) [who considered the pickup process—see Sec. IV]. These authors neglected the many-body aspects of the problem, however, considering the deuteron to interact with a fixed force center only.

[9] N. C. Francis and K. M. Watson, Phys. Rev. **92**, 291 (1953). The replacement of the many-body interaction v by the "potential well," $\mathcal{U}_{CN}$ has been discussed in detail in this reference and here forms the basis of the present model of the stripping reaction.

[10] Feshbach, Porter, and Weisskopf, Phys. Rev. **90**, 166 (1953). We evidently must not take the numerical values of Eq. (18) too literally. For instance, $\mathcal{U}_{CN}$ is expected in general to be energy-dependent.

[11] H. H. Barschall, Phys. Rev. **86**, 431 (1952).

If this were true, we would write

$$\mathcal{V}_{CN}=-(19+i)\text{Mev} \tag{18}$$

within the nucleus and set $\mathcal{V}_{CN}=0$ outside [that is, when the neutron is outside].

In general, we may expect the interaction described by $\mathcal{V}_{CN}$ to polarize the deuteron (that is, distort its wave function). It is this modified wave function on which V operates in Eq. (17). We have, however, made estimates of the importance of this distortion for a potential such as that given by Eq. (18) and found that the effect is small, especially for the innermost parts of the deuteron wave function on which V operates. [The wave function might be distorted more if $\mathcal{V}_{CN}$ contained spin-orbit interactions or a strong absorption coefficient.] For the evaluation of Eq. (17), it is especially convenient to be able to neglect any distortion of the deuteron, since V can then be eliminated from this expression by means of the Schrödinger equation satisfied by the deuteron wave function.

If we suppose that $\mathcal{V}_{CN}$ is such an interaction which does not appreciably excite the deuteron, it is not an unreasonable approximation to set $\Omega_{CN}=1$ in Eq. (17). Then

$$T(B,\mathfrak{p};a)=(g_B{}^{(-)}\lambda_{\mathfrak{p}},V\chi_a) \tag{19}$$

is just the "Born approximation" as proposed by Daitch and French.[3] For a potential $\mathcal{V}_{CN}$ such as that given by Eq. (18), this expression may not be an unsatisfactory approximation.

On the other hand, if one were to suppose that the neutron interacts very strongly with the nucleus so that immediately upon entering it a compound state is formed in which the deuteron is broken up, the effective absorption coefficient[12] in $\mathcal{V}_{CN}$ is expected to be large [this is just the situation supposed by Butler in his assumption (2)]. Then we could expect to write

$$\begin{aligned}\Omega_{CN}\chi_a&=\chi_a \quad \text{when} \quad r_N>R\\ &=0 \quad \text{when} \quad r_N<R,\end{aligned} \tag{20}$$

where R is the radius of the nucleus. Daitch and French have shown that with this modification of the Born approximation one obtains just Butler's result, although they did not present any justification for doing this nor did they give a derivation of their "Born approximation" expression. We thus see that if we make the assumption implied by Eq. (20), which is equivalent to Butler's assumptions (2) and (3), we obtain just Butler's result from our theory, which is formulated quite differently from his.

It is evident that Eqs. (19) and (20) represent somewhat extreme limits on the nature of the physical problem. Equation (19) assumes a weak nuclear interaction with the incoming neutron, whereas Eq. (20) assumes that this interaction is very strong. The analysis of Daitch and French[3] suggests that the deduced cross sections are quite similar for the two models. From this one might hope to conclude that the gross features of the stripping reaction tend to be somewhat insensitive to the exact nature of the potential $\mathcal{V}_{CN}$ and so to that of Ω_{CN}.

III. THE EFFECT OF THE INTERACTION OF THE PROTON WITH THE NUCLEUS

We now no longer set $u=0$. A formally exact solution to Eq. (5) is

$$\Psi=\left[1+\frac{1}{a-V-v-u}u\right]\left[1+\frac{1}{a-V-v}v\right]\chi_a. \tag{21}$$

This differs from Eq. (6) only by the factor on the left. The first factor describes the interaction of the neutron with the nucleus. The second describes the interaction of the proton with the nucleus in a representation which considers the neutron now to be a part of the nucleus [i.e., in which $(a-v)$ is diagonal]. This expression is a little unsymmetrical since the first interaction is just through the potential u while subsequent interactions are through the potential $(u+V)$. Expressed somewhat differently, for the first scattering of the proton, the initial neutron does not contribute. For the subsequent scattering it does, however. Since this neutron is just one of many nuclear particles, its omission for the first scattering is probably[13] not of much importance for our interpretation of the factor on the left in Eq. (21) as a scattering of the proton by the nucleus.

The argument is now similar to that which we used in Sec. II. The proton may or may not excite the final nucleus (containing the extra neutron). If the proton excites the nucleus, we may suppose it to form a compound state from which it may be later emitted. We shall further suppose that this type of process is not of the sort in which we are interested and that it is experimentally distinguishable from the type of stripping reaction considered by Butler.[14] Then, if we consider only the elastic scattering of the proton to contribute, we may make the substitution[9]

$$\left[1+\frac{1}{a-V-v-u}u\right]=\Omega_{CP}, \tag{22}$$

where

$$\Omega_{CP}=1+\frac{1}{a-v}\mathcal{V}_{CP}\Omega_{CP}. \tag{23}$$

[12] It should be noted that the "effective absorption coefficient" for the stripping process is not necessarily identical with that of the potential $\mathcal{V}_{CN}$. The former measures the rate at which the deuteron is completely "broken up," whereas the latter measures the rate at which the deuteron excites the nucleus. A precise definition of the former is not necessary for our purposes, since the problem is specified by the wave function $\Omega_{CN}\chi_a$.

[13] It will become clear in the next paragraph that it is only elastic scattering of the proton which is of interest to us. For elastic scattering there seems to be considerable evidence that one additional nucleon in the nucleus will not be of importance.

[14] For instance, one might construct a wave packet of incident deuterons to measure the lag in time of protons emitted by compound state formation.

$\mathcal{U}_{CP}$ is the "optical model" potential for the elastic scattering of the proton by the nucleus. Defining the elastically scattered proton wave function by f_P, we have

$$f_P = \Omega_{CP}\lambda_P. \tag{24}$$

Following the argument of the previous section, we readily find that Eq. (17) is modified as follows:[8]

$$T(B,\mathbf{p};a) = (g_B^{(-)} f_P^{(-)}, V\Omega_{CN}\chi_a), \tag{25}$$

or that the plane wave λ_P is replaced by the elastically scattered wave $f_P^{(-)}$. $f_P^{(-)}$ contains the "shadow" cast by the nucleus, and as such contains a "bundle" of plane waves centered about the direction $\mathbf{p}$ with an angular spread whose width is that of the diffraction pattern. In a momentum representation, we write $f_P^{(-)} = f_P^{(-)}(k)$, so that Eq. (25) becomes

$$T(B,\mathbf{p};a) = \int d^3k\, f_P^{(-)}(k) T^0(B,\mathbf{k};a), \tag{26}$$

where T^0 is the expression given by Eq. (17). The modification arising from the use of $f_P^{(-)}$ is then seen to be a "smearing" of Butler's angular distribution over angles of the order of the width of the nuclear diffraction pattern. For instance, the zeros in Butler's angular distribution will tend to be filled in somewhat. This correction does not seem to be of much practical importance, since the finite angular resolution of the experimental detecting equipment will also "smear out" the angular distribution. Furthermore, compound nucleus formation, which we neglected when approximation (22) was made, is probably equally important in obscuring the finer details of the angular distribution of Butler. An effect similar to this is the diffraction of the incoming deuteron wave by $\mathcal{U}_{CN}$. The wave function $\Omega_{CN}\chi_a$ includes this automatically, but the effect was neglected, for instance, in Eq. (20).

We conclude from this section, then, that the role played by the proton in the (d,p) reaction can be simply expressed but that it is not of great importance except for the contribution through compound state formation.

IV. THE PICKUP PROCESS

The inverse of the stripping reaction is the deuteron pickup process [i.e., the (p,d) and (n,d) reactions]. The cross section for pickup can be obtained either directly as in the preceding sections or by applying the time reversal operator to Eq. (25). The result is

$$T(a;B,\mathbf{p}) = (\Omega_{CN}^{(-)}\chi_a, V f_P g_B) \tag{27}$$

in the notation of Eq. (25). The matrix $\Omega_{CN}^{(-)}$ is the solution to[9] [see Eq. (16)]:

$$\Omega_{CN}^{(-)} = 1 + \frac{1}{a^\dagger - V}\mathcal{U}_{CN}\Omega_{CN}^{(-)}. \tag{28}$$

Equation (27) describes the reaction in which an incident proton of momentum $\mathbf{p}$ collides with a nucleus and picks up a neutron to emerge as a deuteron with momentum $\mathbf{K}$.

V. FINAL COMMENTS

Except for the need of some additional comment concerning the Pauli principle, a rigorous formulation of the Butler theory has been given by Eqs. (15′) and (21). We may however, antisymmetrize our wave function merely by applying the antisymmetrization operator to it. The antisymmetrization of the proton coordinates will introduce terms corresponding to the exchange of the incident proton with one of those in the nucleus. Because of the fact that rather large impact parameters for the proton seem to be involved,[1] it appears to be consistent with the spirit of the calculation to neglect the proton exchange terms. On the other hand, if we expand the scattered waves in a set of antisymmetrized nuclear states $g_B(\xi,r_N)$—as we have done, for instance, in Eq. (9)—then (except for the incident wave) our wave functions are automatically antisymmetrized in the neutron coordinates. We have thus neglected only the antisymmetrization with respect to the incident proton, and this seems to be a reasonable approximation.

The crucial points in our analysis have been those which replaced the many-body interactions u and v by the "potential well" interactions $\mathcal{U}_{CP}$ and $\mathcal{U}_{CN}$, which do not depend at all upon the nucleon coordinates. These approximations have been explicitly defined mathematically above. Physically, they imply that no large momentum transfers between the proton and the nucleus are permitted.

If the potentials $\mathcal{U}_{CN}$ and $\mathcal{U}_{CP}$ contain spin-orbit interactions, we may expect that in general the spin of the proton will be polarized (this is not expected on the basis of the Butler theory). Such spin-orbit interactions would not be surprising, since it is not unlikely that our $\mathcal{U}_{CN}$ and $\mathcal{U}_{CP}$ are related to the "single particle potential" frequently presupposed in the nuclear shell model. Another mechanism to obtain polarization of the proton in the stripping reaction has been proposed by Newns.[10] In terms of the present theory, his model is equivalent to assuming that $\mathcal{U}_{CP}$ has a large absorption coefficient.

[10] H. C. Newns, Proc. Phys. Soc. (London) **A66**, 477 (1953).

Symmetry Properties of the Wigner 9j Symbol

H. A. JAHN AND J. HOPE
Mathematics Department, The University, Southampton, England

(Received July 9, 1953)

The 72 symmetry relations of the Wigner 9j symbol

$$\begin{Bmatrix} j_1 j_2 j_3 \\ j_4 j_5 j_6 \\ j_7 j_8 j_9 \end{Bmatrix} = \frac{\langle (j_1 j_2) j_3, (j_4 j_5) j_6, j_9 m | (j_1 j_4) j_7, (j_2 j_5) j_8, j_9 m \rangle}{\{(2j_3+1)(2j_6+1)(2j_7+1)(2j_8+1)\}^{\frac{1}{2}}}$$

are given. The group of symmetry may be generated by the following elements: (i) an odd permutation of the rows or columns of the symbol multiplies it by $(-1)^R$, where $R = j_1+j_2+j_3+j_4+j_5+j_6+j_7+j_8+j_9$; (ii) a reflection of the symbol in either of the two diagonals leaves it invariant. These results are conveniently deduced from the Schwinger generating function for the 9j symbol. In an addendum a 12j symbol is defined and some of its properties discussed.

AN important concept in the theory of complex spectra is the Wigner 9j symbol.[1] This is defined (Wigner) by

$$\begin{Bmatrix} j_1 j_2 j_3 \\ j_4 j_5 j_6 \\ j_7 j_8 j_9 \end{Bmatrix} = \frac{\langle (j_1 j_2) j_3, (j_4 j_5) j_6, j_9 m | (j_1 j_4) j_7, (j_2 j_5) j_8, j_9 m \rangle}{\{(2j_3+1)(2j_6+1)(2j_7+1)(2j_8+1)\}^{\frac{1}{2}}}, \quad (1)$$

the relation with the χ function[2] of Hope or the S function[3] of Schwinger being

$$\chi(abcd, ef, gh, k) = \{(2e+1)(2f+1)(2g+1)(2h+1)\}^{\frac{1}{2}} \begin{Bmatrix} a & b & e \\ c & d & f \\ g & h & k \end{Bmatrix}, \quad (1a)$$

$$S(j_1 j_2 j_3 j_4; j_{12} j_{34} j_{13} j_{24}; j) = (-1)^{j_1+j_4-j_{13}-j_{24}} \begin{Bmatrix} j_1 j_2 j_{12} \\ j_4 j_3 j_{34} \\ j_{13} j_{24} j \end{Bmatrix}. \quad (1b)$$

Its numerical evaluation is best carried out from the following expression (Jahn,[4] Hope,[2] Wigner[1]) in terms of Wigner 6j symbols (or Racah W functions):

$$\begin{Bmatrix} j_1 j_2 j_3 \\ j_4 j_5 j_6 \\ j_7 j_8 j_9 \end{Bmatrix} = \sum_x (-1)^{2x} (2x+1) \begin{Bmatrix} j_1 j_4 j_7 \\ j_8 j_9 x \end{Bmatrix} \begin{Bmatrix} j_2 j_5 j_8 \\ j_4 x j_6 \end{Bmatrix} \begin{Bmatrix} j_3 j_6 j_9 \\ x j_1 j_2 \end{Bmatrix}, \quad (2)$$

the relation between the Wigner 6j symbol and the Racah W function being

$$\begin{Bmatrix} j_1 j_2 j_3 \\ j_4 j_5 j_6 \end{Bmatrix} = (-1)^{j_1+j_2+j_4+j_5} W(j_1 j_2 j_5 j_4; j_3 j_6). \quad (3)$$

Related useful formulas,[4] involving Wigner 3j symbols [see (7) below], are:

$$\sum_{\substack{m_1 m_2 m_3 m_4 \\ M_{12} M_{34}}} \langle j_1 m_1 j_2 m_2 | J_{12} M_{12} \rangle \langle j_3 m_3 j_4 m_4 | J_{34} M_{34} \rangle \times \langle J_{13} M_{13} J_{24} M_{24} | JM \rangle \langle j_1 m_1 j_3 m_3 | J_{13} M_{13} \rangle \times \langle j_2 m_2 j_4 m_4 | J_{24} M_{24} \rangle = \langle J_{12} M_{12} J_{34} M_{34} | JM \rangle \times \chi(j_1 j_2 j_3 j_4, J_{12} J_{34}, J_{13} J_{24}, J), \quad (3a)$$

$$\sum_{\substack{m_1 m_2 m_3 m_4 \\ M_{12} M_{34} M_{13} M_{24}}} \langle j_1 m_1 j_2 m_2 | J_{12} M_{12} \rangle \langle j_3 m_3 j_4 m_4 | J_{34} M_{34} \rangle \times \langle J_{12} M_{12} J_{34} M_{34} | JM \rangle \langle j_1 m_1 j_3 m_3 | J_{13} M_{13} \rangle \times \langle j_2 m_2 j_4 m_4 | J_{24} M_{24} \rangle \langle J_{13} M_{13} J_{24} M_{24} | J'M' \rangle = \delta(J, J') \delta(M, M') \chi(j_1 j_2 j_3 j_4, J_{12} J_{34}, J_{13} J_{24}, J). \quad (3b)$$

The 9j symbol, apart from its immediate application to the transformation from one coupling scheme to another, i.e., from ls to jj coupling (see Hope[2]) or to the theory of fractional parentage coefficients (see Elliott[5,6]), has its most important application to the evaluation of the matrix elements of tensor products of tensor operators taken between vector-coupled states. This application is contained in the formula (Hope, Wigner, Schwinger):

$$\langle \gamma j_1 j_2 j \| T^{(k)}(k_1 k_2) \| \gamma' j_1' j_2' j' \rangle = \{(2j+1)(2j'+1)(2k+1)\}^{\frac{1}{2}} \sum_{\gamma''} \langle \gamma j_1 \| T_1^{(k_1)} \| \gamma'' j_1' \rangle \times \langle \gamma'' j_2 \| T_2^{(k_2)} \| \gamma' j_2' \rangle \begin{Bmatrix} j_1 & j_2 & j \\ j_1' & j_2' & j' \\ k_1 & k_2 & k \end{Bmatrix}, \quad (4)$$

for the amplitude matrix of the tensor product

$$T(k_1 k_2 kq) = \sum_{q_1 q_2} \langle k_1 q_1 k_2 q_2 | kq \rangle T_1(k_1 q_1) T_2(k_2 q_2), \quad (5)$$

of tensor operators $T_1(k_1 q_1)$, $T_2(k_2 q_2)$, where the operators T_1 do not act on that part of the system characterized by j_2 and similarly the T_2 operators do not act on the part of the system characterized by j_1 (the variables γ'' enter if the operators act on other parts

[1] E. P. Wigner, "On the matrices which reduce the Kronecker products of representations of simply reducible groups," hectographed paper, Princeton, 1951 (unpublished).
[2] J. Hope, Ph.D. thesis, London University, 1952 (unpublished).
[3] J. Schwinger, "On Angular Momentum," Report NYO-3071, Nuclear Development Associates, Inc., White Plains, New York, 1952 (unpublished).
[4] The senior author (H.A.J.) derived formula (2) and the corresponding expressions (3a), (b) in terms of six Wigner 3j symbols in Birmingham in 1949 in connection with a β-decay problem of Dr. T. H. R. Skyrme. (For an account of the derivation see reference 2, pp. 15–17.)
[5] J. P. Elliott, Ph.D. thesis, London University, 1952 (unpublished).
[6] J. P. Elliott, Proc. Roy. Soc. (London) **A218**, 345 (1953).

of the system). We are using here the tensor amplitude or double-barred matrix elements, as defined by Racah,[7] rather than the slightly different definition of Schwinger (Wigner's definition is identical with that of Racah), *viz.*,

$$\langle \alpha jm | T(k_1k_2kq) | \alpha' j'm' \rangle = (-1)^{2k} \langle j'm'kq | jm \rangle (2j+1)^{-\frac{1}{2}} \langle \alpha j \| T^{(k)}(k_1k_2) \| \alpha' j' \rangle \quad (6)$$

$$= (-1)^{j-m} \begin{pmatrix} j & k & j' \\ -m & q & m' \end{pmatrix} \langle \alpha j \| T^{(k)}(k_1k_2) \| \alpha' j' \rangle, \quad (6a)$$

where the Wigner $3j$ symbol $\begin{pmatrix} j_1 & j_2 & j_3 \\ m_1 & m_2 & m_3 \end{pmatrix}$ is defined (Wigner, Schwinger) by

$$\langle j_1 m_1 j_2 m_2 | jm \rangle \equiv \langle j_1 m_1 j_2 m_2 | j_1 j_2 jm \rangle = (-1)^{j_1 - j_2 + m} (2j+1)^{\frac{1}{2}} \begin{pmatrix} j_1 & j_2 & j \\ m_1 & m_2 & -m \end{pmatrix}, \quad (7)$$

and has the simple symmetry relations described by Wigner and Schwinger [odd permutation of the columns multiplies the symbol by $(-1)^J$, where $J = j_1+j_2+j_3$; a simultaneous change in sign of m_1, m_2, and m_3 has the same effect]. In Hope's notation the above tensor product is denoted by $(T^{k_1}{}_{(1)} \odot_q{}^k T^{k_2}{}_{(2)})$; Talmi[8] uses the notation $[T_1{}^{(k_1)} \times T_2{}^{(k_2)}]_q{}^{(k)}$; the notation used here is that of Schwinger.

Some of the symmetry relations of the $9j$ symbol have been considered by Hope and also by Schwinger. It is the purpose of this note to point out that the complete group of symmetry (consisting of 72 symmetry relations) may be generated by the following elements: (i) An odd permutation of the rows or columns of the symbol multiples it by $(-1)^R$, where $R = \sum_{i=1}^{9} j_i$; i.e., using the abbreviation

$$\begin{Bmatrix} 123 \\ 456 \\ 789 \end{Bmatrix} \equiv \begin{Bmatrix} j_1 j_2 j_3 \\ j_4 j_5 j_6 \\ j_7 j_8 j_9 \end{Bmatrix},$$

we have

$$(-1)^R \begin{Bmatrix} 123 \\ 456 \\ 789 \end{Bmatrix} = \begin{Bmatrix} 213 \\ 546 \\ 879 \end{Bmatrix} = \begin{Bmatrix} 321 \\ 654 \\ 987 \end{Bmatrix} = \begin{Bmatrix} 132 \\ 465 \\ 798 \end{Bmatrix} = \begin{Bmatrix} 456 \\ 123 \\ 789 \end{Bmatrix} = \begin{Bmatrix} 789 \\ 456 \\ 123 \end{Bmatrix} = \begin{Bmatrix} 123 \\ 789 \\ 456 \end{Bmatrix}. \quad (8)$$

(ii) A reflection of the symbol in either of the two diagonals leaves it invariant; i.e.,

$$\begin{Bmatrix} 123 \\ 456 \\ 789 \end{Bmatrix} = \begin{Bmatrix} 147 \\ 258 \\ 369 \end{Bmatrix} = \begin{Bmatrix} 963 \\ 852 \\ 741 \end{Bmatrix}. \quad (9)$$

The full group of permutations (subgroup of the symmetric group S_9), with the elements arranged in classes is as follows, the star on the symbol for the class denoting that the permutations in the starred class multiply the $9j$ symbol by $(-1)^R$. [*Note*: in the following symbols for permutations the decomposition into cycles is indicated by the separate rows of the symbol, i.e., $\binom{1452}{3768}$ means the permutation (1452)(3768) in the usual notation.]

C_1: I,

C_2: $\begin{bmatrix} 15 \\ 38 \\ 67 \end{bmatrix}, \begin{bmatrix} 18 \\ 35 \\ 49 \end{bmatrix}, \begin{bmatrix} 16 \\ 29 \\ 57 \end{bmatrix}, \begin{bmatrix} 27 \\ 34 \\ 59 \end{bmatrix}, \begin{bmatrix} 19 \\ 26 \\ 48 \end{bmatrix}, \begin{bmatrix} 24 \\ 37 \\ 68 \end{bmatrix},$

C_3: $\begin{bmatrix} 12 \\ 48 \\ 57 \\ 69 \end{bmatrix}, \begin{bmatrix} 13 \\ 49 \\ 58 \\ 67 \end{bmatrix}, \begin{bmatrix} 14 \\ 26 \\ 35 \\ 89 \end{bmatrix}, \begin{bmatrix} 15 \\ 24 \\ 36 \\ 78 \end{bmatrix}, \begin{bmatrix} 16 \\ 25 \\ 34 \\ 79 \end{bmatrix}, \begin{bmatrix} 17 \\ 29 \\ 38 \\ 56 \end{bmatrix}, \begin{bmatrix} 18 \\ 27 \\ 39 \\ 45 \end{bmatrix}, \begin{bmatrix} 19 \\ 28 \\ 37 \\ 46 \end{bmatrix}, \begin{bmatrix} 23 \\ 47 \\ 59 \\ 68 \end{bmatrix},$

C_4: $\begin{bmatrix} 123 \\ 456 \\ 789 \end{bmatrix}, \begin{bmatrix} 132 \\ 465 \\ 798 \end{bmatrix}, \begin{bmatrix} 147 \\ 258 \\ 369 \end{bmatrix}, \begin{bmatrix} 174 \\ 285 \\ 396 \end{bmatrix},$

C_5: $\begin{bmatrix} 159 \\ 267 \\ 348 \end{bmatrix}, \begin{bmatrix} 195 \\ 276 \\ 384 \end{bmatrix}, \begin{bmatrix} 168 \\ 249 \\ 357 \end{bmatrix}, \begin{bmatrix} 186 \\ 294 \\ 375 \end{bmatrix},$

C_6: $\begin{pmatrix} 168 \\ 239745 \end{pmatrix}, \begin{pmatrix} 348 \\ 179652 \end{pmatrix}, \begin{pmatrix} 267 \\ 139854 \end{pmatrix}, \begin{pmatrix} 294 \\ 136587 \end{pmatrix}, \begin{pmatrix} 159 \\ 287463 \end{pmatrix}, \begin{pmatrix} 357 \\ 128964 \end{pmatrix}, \begin{pmatrix} 186 \\ 254793 \end{pmatrix}, \begin{pmatrix} 384 \\ 125697 \end{pmatrix}, \begin{pmatrix} 276 \\ 145893 \end{pmatrix}, \begin{pmatrix} 249 \\ 178563 \end{pmatrix}, \begin{pmatrix} 195 \\ 236478 \end{pmatrix}, \begin{pmatrix} 375 \\ 146982 \end{pmatrix},$

C_7*: $\begin{bmatrix} 12 \\ 45 \\ 78 \end{bmatrix}, \begin{bmatrix} 13 \\ 46 \\ 79 \end{bmatrix}, \begin{bmatrix} 23 \\ 56 \\ 89 \end{bmatrix}, \begin{bmatrix} 14 \\ 25 \\ 36 \end{bmatrix}, \begin{bmatrix} 17 \\ 28 \\ 39 \end{bmatrix}, \begin{bmatrix} 47 \\ 58 \\ 69 \end{bmatrix},$

C_8*: $\begin{pmatrix} 123 \\ 486759 \end{pmatrix}, \begin{pmatrix} 456 \\ 183729 \end{pmatrix}, \begin{pmatrix} 789 \\ 153426 \end{pmatrix}, \begin{pmatrix} 147 \\ 268359 \end{pmatrix}, \begin{pmatrix} 258 \\ 167349 \end{pmatrix}, \begin{pmatrix} 369 \\ 157248 \end{pmatrix}, \begin{pmatrix} 132 \\ 495768 \end{pmatrix}, \begin{pmatrix} 465 \\ 192738 \end{pmatrix}, \begin{pmatrix} 798 \\ 162435 \end{pmatrix}, \begin{pmatrix} 174 \\ 295386 \end{pmatrix}, \begin{pmatrix} 285 \\ 194376 \end{pmatrix}, \begin{pmatrix} 396 \\ 184275 \end{pmatrix},$

C_9*: $\begin{pmatrix} 1254 \\ 3867 \end{pmatrix}, \begin{pmatrix} 1364 \\ 2957 \end{pmatrix}, \begin{pmatrix} 1948 \\ 2365 \end{pmatrix}, \begin{pmatrix} 1287 \\ 3594 \end{pmatrix}, \begin{pmatrix} 1397 \\ 2684 \end{pmatrix}, \begin{pmatrix} 1675 \\ 2398 \end{pmatrix}, \begin{pmatrix} 1926 \\ 4785 \end{pmatrix}, \begin{pmatrix} 1835 \\ 4796 \end{pmatrix}, \begin{pmatrix} 2734 \\ 5896 \end{pmatrix},$

C_{10}*: $\begin{pmatrix} 1452 \\ 3768 \end{pmatrix}, \begin{pmatrix} 1463 \\ 2759 \end{pmatrix}, \begin{pmatrix} 1849 \\ 2563 \end{pmatrix}, \begin{pmatrix} 1782 \\ 3495 \end{pmatrix}, \begin{pmatrix} 1793 \\ 2486 \end{pmatrix}, \begin{pmatrix} 1576 \\ 2893 \end{pmatrix}, \begin{pmatrix} 1629 \\ 4587 \end{pmatrix}, \begin{pmatrix} 1538 \\ 4697 \end{pmatrix}, \begin{pmatrix} 2437 \\ 5698 \end{pmatrix}.$

The elements (i), forming the class C_7*, generate a self-conjugate subgroup of 36 elements consisting of

[7] G. Racah, Phys. Rev. **62**, 438 (1942).
[8] I. Talmi, Phys. Rev. **89**, 1065 (1953).

the classes C_1, C_3, C_4, C_5, C_7^*, C_8^*. Addition of either of the elements (ii) in the class C_2 then gives rise to the whole group of 72 elements.

These symmetry relations may be used, as pointed out by Hope and Schwinger, to bring a j from any one place to any other place in the symbol; thus when one of the j's is zero (as in the important application to the matrix elements of the scalar product of two tensor operators of equal rank), we have the relations:

$$\begin{Bmatrix} abe \\ cde \\ ff0 \end{Bmatrix} = \begin{Bmatrix} 0ee \\ fdb \\ fca \end{Bmatrix} = \begin{Bmatrix} e0e \\ cfa \\ dfb \end{Bmatrix} = \begin{Bmatrix} ff0 \\ dce \\ bae \end{Bmatrix} = \begin{Bmatrix} fbd \\ 0ee \\ fac \end{Bmatrix}$$
$$= \begin{Bmatrix} afc \\ e0e \\ bfd \end{Bmatrix} = \begin{Bmatrix} bae \\ ff0 \\ dce \end{Bmatrix} = \begin{Bmatrix} edc \\ eba \\ 0ff \end{Bmatrix} = \begin{Bmatrix} ced \\ aeb \\ f0f \end{Bmatrix}$$
$$= (-1)^{b+c+e+f}\{(2e+1)(2f+1)\}^{-\frac{1}{2}} \begin{Bmatrix} abe \\ dcf \end{Bmatrix}.$$

The simple symmetry relations of the $6j$ symbol given by Wigner [invariance with respect to permutations of the columns and invariance also with respect to simultaneous inversion of any two columns: $\begin{Bmatrix} abe \\ dcf \end{Bmatrix} = \begin{Bmatrix} bae \\ cdf \end{Bmatrix}$, etc., $\begin{Bmatrix} abe \\ dcf \end{Bmatrix} = \begin{Bmatrix} dce \\ abf \end{Bmatrix}$, etc.] may also be deduced from the above relations for the $9j$ symbol.

The above symmetry relations are most simply deduced from the Schwinger generating function for the Wigner $9j$ symbol as described in Schwinger's report. For many applications of this symbol to the evaluation of matrix elements of noncentral forces in nuclei, see Hope's thesis[2] and forthcoming publication.

ADDENDUM: DEFINITION OF THE 12j SYMBOL AND SOME OF ITS PROPERTIES[9]

A natural generalization of the Wigner $9j$ symbol occurs in the direct evaluation of $\langle n|n-2, 2\rangle$ orbital or charge-spin fractional parentage coefficients required in the theory of atomic spectra or nuclear structure. One meets there with the problem of evaluating the effect of the permutation $P_{n-1,n-2}$ of the coordinates of particles $n-1$ and $n-2$ on the following vector-coupled orbital state of n particles:

$$\Phi[\{(j_1^{\alpha} j_2^{\beta} \cdots j_{n-4}^{\gamma})J_\tau, (j_{n-3}^{a} j_{n-2}^{b})J_{ab}\}J'; \times (j_{n-1}^{c} j_n^{d})J_{cd}]J. \quad \text{(A1)}$$

Here the angular momenta j_α, j_β, $\cdots$, j_γ of the first $n-4$ particles are vector-coupled to a resultant J_τ in some definite way uniquely specifying the state of these $n-4$ particles. This resultant J_τ is in turn coupled to the resultant J_{ab} of the respective angular momenta j_a, j_b of particles $n-3$ and $n-2$ to an intermediate resultant J'; this intermediate resultant J' is coupled finally to the resultant J_{cd} of the respective angular momenta j_c, j_d of particles $n-1$ and n to form the total resultant J for the n particle system. The new state obtained by permuting the coordinates of particles $n-1$ and $n-2$ in this state is linearly expressible in terms of states of the same kind (with J_{ac}, J_{bd} replacing, respectively, J_{ab} and J_{cd} and a new intermediate resultant J'' replacing J', but with the same fixed values of J_τ and J). The coefficients of the linear expression, depending on the twelve angular momenta,

$$j_a j_b j_c j_d, \; J_{ab} J_{cd} J_{ac} J_{bd}, \; J' J'', \; J_\tau J,$$

may be used to define a 12j symbol as follows:

$$P_{n-2,n-1}\Phi[\{(j_1^{\alpha} j_2^{\beta} \cdots j_{n-4}^{\gamma})J_\tau, (j_{n-3}^{a} j_{n-2}^{b})J_{ab}\}J'; \times (j_{n-1}^{c} j_n^{d})J_{cd}]J$$
$$= \sum_{J_{ac} J_{bd} J''} \{[J_{ab}][J_{cd}][J_{ac}][J_{bd}][J'][J'']\}^{\frac{1}{2}} \times \begin{Bmatrix} j_a & j_b & J_{ab} J' \\ j_c & j_d & J_{cd} J'' \\ J_{ac} J_{bd} J_\tau & & J \end{Bmatrix} \Phi[\{(j_1^{\alpha} j_2^{\beta} \cdots j_{n-4}^{\gamma})J_\tau, \times (j_{n-3}^{a} j_{n-2}^{c})J_{ac}\}J''; (j_{n-1}^{b} j_n^{d})J_{bd}]J, \quad \text{(A2)}$$

where, following Wigner,[1] we use the abbreviation

$$[J] \equiv 2J+1. \quad \text{(A3)}$$

Defining thus the 12j symbol by

$$\begin{Bmatrix} abep \\ cdfq \\ ghrs \end{Bmatrix} = \{[e][f][g][h][p][q]\}^{-\frac{1}{2}} \times \langle [\{r, (ab)e\}p, (cd)f]sm| \times [\{r, (ac)g\}q, (bd)h]sm\rangle, \quad \text{(A4)}$$

one obtains easily the explicit expression

$$\begin{Bmatrix} abep \\ cdfq \\ ghrs \end{Bmatrix} = (-1)^{e+f+g+h} \sum_x (-1)^{2x}(2x+1) \begin{Bmatrix} abe \\ cdf \\ ghx \end{Bmatrix} \begin{Bmatrix} rep \\ fsx \end{Bmatrix} \begin{Bmatrix} rgq \\ hsx \end{Bmatrix}, \quad \text{(A5)}$$

in terms of Wigner $9j$ and $6j$ symbols. The following symmetry relations also may be simply deduced:

$$\begin{Bmatrix} abep \\ cdfq \\ ghrs \end{Bmatrix} = \begin{Bmatrix} acgq \\ bdhp \\ efrs \end{Bmatrix} = \begin{Bmatrix} dcfp \\ baeq \\ hgsr \end{Bmatrix} = \begin{Bmatrix} dbhq \\ cagp \\ fesr \end{Bmatrix}. \quad \text{(A6)}$$

Important special cases with one argument zero are the following:

$$\begin{Bmatrix} abef \\ cdfh \\ ghr0 \end{Bmatrix} = \begin{Bmatrix} acgh \\ bdhf \\ efr0 \end{Bmatrix} = \begin{Bmatrix} dcff \\ baeh \\ hg0r \end{Bmatrix} = \begin{Bmatrix} dbhh \\ cagf \\ fe0r \end{Bmatrix}$$
$$= \{[f][h]\}^{-\frac{1}{2}} \begin{Bmatrix} abe \\ cdf \\ ghr \end{Bmatrix}. \quad \text{(A7)}$$

[9] The work reported in this Addendum was performed by H. A. Jahn.

The complete set of special values of the $12j$ symbol when any one of its twelve arguments is zero is as follows:

$$\begin{Bmatrix} a0ap \\ cdfq \\ gdrs \end{Bmatrix} = \begin{Bmatrix} dd0a \\ fspg \\ cqar \end{Bmatrix} = \begin{Bmatrix} rpa0 \\ qsdc \\ gfad \end{Bmatrix} = \begin{Bmatrix} acgq \\ 0ddp \\ afrs \end{Bmatrix}$$

$$\begin{Bmatrix} rgqd \\ aa0f \\ pcsd \end{Bmatrix} = \begin{Bmatrix} rqgc \\ psf0 \\ adad \end{Bmatrix} = \begin{Bmatrix} dfcg \\ dsqa \\ 0par \end{Bmatrix} = \begin{Bmatrix} rapf \\ gacd \\ q0sd \end{Bmatrix}$$

$$= \frac{(-1)^{a+2c+d+p+q+r+s}}{\{[a][d]\}^{\frac{1}{2}}} \begin{Bmatrix} pcq \\ dsf \end{Bmatrix} \begin{Bmatrix} pcq \\ gra \end{Bmatrix}, \quad \text{(A8)}$$

together with

$$\begin{Bmatrix} 0bbp \\ cdfq \\ chrs \end{Bmatrix} = \begin{Bmatrix} dcfp \\ b0bq \\ hcsr \end{Bmatrix} = \begin{Bmatrix} rqcc \\ psfb \\ bh0d \end{Bmatrix} = \begin{Bmatrix} sqhb \\ prbc \\ fcd0 \end{Bmatrix}$$

$$= \{[b][c]\}^{-\frac{1}{2}} \begin{Bmatrix} rbp \\ cdf \\ qhs \end{Bmatrix}. \quad \text{(A9)}$$

A group of 16 symmetry relations of the $12j$ symbol, together with a convenient new notation, has been found by R. J. Ord-Smith and will be reported upon shortly.

The $12j$ symbol is being used in Southampton in nuclear structure calculations on light nuclei with interconfigurational mixing.

PHYSICAL REVIEW VOLUME 93, NUMBER 2 JANUARY 15, 1954

The Elastic Scattering of Protons by Alpha Particles*

S. Sack, L. C. Biedenharn, and G. Breit
Yale University, New Haven, Connecticut

(Received October 13, 1953)

The $p_{\frac{1}{2}}$ and $p_{\frac{3}{2}}$ phase shifts determined from analysis of the elastic scattering of protons by alpha particles are treated in terms of a potential interaction between the proton and alpha-particle core, with a spin-orbit interaction of the Thomas type. The results are sensitive to the well shape chosen and favor a Gauss well interaction. The limitations of this type of treatment are discussed.

I. INTRODUCTION

THE elastic scattering of nucleons by alpha particles has been extensively studied by many workers,[1-7] mainly on account of its possible importance for the determination[4,7] of the magnitude of the spin orbit interaction in nuclei. The origin of the latter is still obscure, and none of the work done so far, including that reported here, has any certainty of being more than an attempt to fit the data with formulas having only a slight foundation from a fundamental viewpoint. The possibly large importance of many-body forces in nuclei throws doubt on the applicability of considerations based on interactions between pairs of nucleons. The fact that the spin-orbit interaction is appreciably larger than expected from a simple application of the Thomas term theory or its extensions is an additional deterrent to elaborate calculation with wave functions based on two-body forces and spin-orbit forces which follow from relativistic considerations[8,9] in such cases.

From a purely phenomenological point of view, it is not clear that one-body treatments of nuclear structure are meaningless in such cases as the p-α interaction. There is much evidence that the alpha particle behaves approximately as a unit in nuclei, and the small nuclear radius as well as the large internal tightness of binding of the alpha particle lend plausibility to a view in which this particle produces a general field to which the incident proton is exposed. From this admittedly naive viewpoint it is of interest to determine the magnitude of the p-α interaction in terms of potential well parameters for wells of prescribed shape. The interaction is not taken to be the same for s, $p_{\frac{1}{2}}$, $p_{\frac{3}{2}}$, $\cdots$ terms, but it is supposed below that the potential wells for the $p_{\frac{1}{2}}$ and $p_{\frac{3}{2}}$ states are related to each other as though the difference between them were caused by a Thomas term with an adjustable constant of proportionality. Wells of various shapes are fitted to experimental data, and it is found that the data favor the Gauss potential well shape in preference to the long-tailed exponential well or the short-tailed square well. The wells just referred to are meant to be idealized wells in the absence of the Thomas term. The possibility of distinguishing between wells of different shapes rests on the experimental

* Assisted by the joint program of the U. S. Office of Naval Research and the U. S. Atomic Energy Commission and by the Office of Ordnance Research, U. S. Army.

[1] Freier, Lampi, Sleator, and Williams, Phys. Rev. **75**, 1345 (1949).
[2] C. L. Critchfield and D. C. Dodder, Phys. Rev. **76**, 602 (1949).
[3] M. Heusinkveld and G. Freier, Phys. Rev. **85**, 80 (1952).
[4] R. K. Adair, Phys. Rev. **86**, 155 (1952).
[5] Kreger, Kerman, and Jentschke, Phys. Rev. **86**, 593 (1952).
[6] T. M. Putnam, Phys. Rev. **87**, 932 (1952).
[7] D. C. Dodder and J. L. Gammel, Phys. Rev. **88**, 520 (1952).
[8] G. Breit, Phys. Rev. **51**, 248 (1937).
[9] G. Breit, Phys. Rev. **53**, 153 (1938).

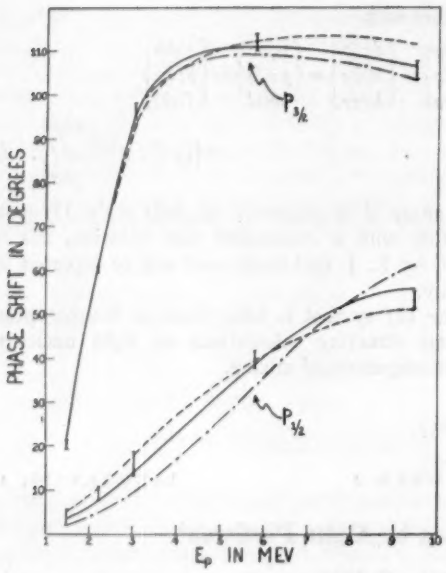

FIG. 1. Phase shifts for p-α scattering as a function of proton energy. The points represent the experimental phase shifts. The curves show the fits to the experimental phases for three well shapes. Legend: —·—·— square well; ——— Gauss well; - - - - - - exponential well.

information regarding the $p_{\frac{1}{2}}$ and $p_{\frac{3}{2}}$ phase shifts at different energies and the influence of well shape on the phase-shift energy dependence.

As in p-p and n-p scattering, the influence of well shape is hard to distinguish from velocity dependence of potential well depth or range. The interpretation of the results presented here is thus subject to reservations regarding the absence of serious effects of such energy dependence. It is possible, therefore, that the significance of the preference of the experimental data for potentials with intermediate-length tails is not direct and that the best effective potentials will be useful primarily as a summary of the data.

Since two-body forces are still one of the most definite ways of dealing with nuclear structure, a discussion is given regarding the approximations needed in order to replace two-body spin-orbit forces by a spin-orbit force corresponding to a central potential. This discussion is explicit only regarding potentials of the Thomas-term type, but requires little modification for more general two-body potentials.

II. EXPERIMENTAL DATA AND PHYSICAL ASSUMPTIONS

The most extensive and quantitatively reliable measurements have been of the p-α differential cross section. Measurements for proton energies of 1 to 3 Mev[1] were analyzed by Critchfield and Dodder[2] giving two sets of phase shifts $(s,p_{\frac{1}{2}},p_{\frac{3}{2}})$ allowed by the data, corresponding to inverted or normal $p_{\frac{1}{2}}-p_{\frac{3}{2}}$ doublets. Measurements of the polarization of the scattered protons[3] showed the correctness of the inverted doublet phase shifts. Measurements at 5.81 Mev[5] and 9.48 Mev[6] were analyzed by Dodder and Gammel,[7] yielding s, $p_{\frac{1}{2}}$, $p_{\frac{3}{2}}$, $d_{\frac{3}{2}}$, $d_{\frac{5}{2}}$ phase shifts, the p and d doublets being inverted. The phase shifts, with errors as estimated in the phase-shift analyses,[2,7] are reproduced in Fig. 1.

The s phase shifts are negative and increase slowly in magnitude with energy, suggesting a repulsive interaction between the proton and alpha particle. The s phase shifts have been fitted qualitatively by Adair[4] and Dodder and Gammel[7] with a hard-sphere interaction having a range of 2.6×10^{-13} cm.

The $p_{\frac{3}{2}}$ and $p_{\frac{1}{2}}$ phase shifts show markedly different energy dependences. The phase shifts are positive, increasing with energy. The $p_{\frac{3}{2}}$ phase shifts increase rapidly with energy, passing through 90° at 2.8-Mev proton energy; the $p_{\frac{1}{2}}$ phase shifts increase more slowly, remaining less than 90° throughout the experimental energy range.

The energy dependence of the p phase shifts suggests a deeper effective attractive potential for $p_{\frac{3}{2}}$ than for $p_{\frac{1}{2}}$. The difference between the $p_{\frac{3}{2}}$ and $p_{\frac{1}{2}}$ potentials can then be interpreted as an effective spin-orbit interaction between nucleon and alpha particle.

Previous discussions of the p states[4,7] have been in terms of resonance models. Adair[4] and Dodder and Gammel[7] have treated the p states in terms of the "reduced width" and "characteristic energy" of the Wigner[10] formalism. These formulations give results similar to treatment in terms of effective potentials for the $p_{\frac{3}{2}}$ and $p_{\frac{1}{2}}$ states, insofar as their applicability depends on the simple energy dependence of the logarithmic derivative of the wave function of relative motion.

However, a description in terms of resonance model parameters has few advantages in the present case, since there are no marked resonance levels. Since the Wigner formalism involves some arbitrariness in the dependence of levels on the choice of the nuclear radius, and since it gives no direct connection between the interactions that apply to the two p states, the more elementary approach of one-body effective potentials was preferred as a temporary expedient. The limitations of this treatment have been mentioned in the introduction and a more precise understanding of such limitations could possibly be obtained by an application of the dispersion theory formalism.

The quantity of interest, for the approach used here as well as the Wigner formalism, is the logarithmic derivative of the wave function of relative motion at moderate internuclear distances. This is readily calculated from the experimental phase shifts and tables of Coulomb functions.[11,12] In the notation of reference 11,

[10] E. P. Wigner and L. Eisenbud, Phys. Rev. **72**, 29 (1947).
[11] Bloch, Hull, Broyles, Bouricius, Freeman, and Breit, Revs. Modern Phys. **23**, 147 (1951).
[12] *Tables of Coulomb Functions I*, National Bureau of Standards Applied Mathematics Series No. 17 (U. S. Government Printing Office, Washington, D. C., 1952).

the homogeneous logarithmic derivative $Y(r)$ is given by

$$Y(r)=rd\mathfrak{F}/\mathfrak{F}dr=(\rho dF/Fd\rho)-1/[(F^2/\rho)\cot K-FG/\rho].$$

The difference in the $p_{\frac{3}{2}}$ and $p_{\frac{1}{2}}$ state interactions is clearly illustrated in the energy dependence of the logarithmic derivatives.[13] The $p_{\frac{3}{2}}$ logarithmic derivative is more negative and decreases more rapidly with energy than that for $p_{\frac{1}{2}}$. These properties are expressed from the standpoint of the Wigner model as follows:[7] (1) the characteristic energy for the $p_{\frac{3}{2}}$ state is higher than that for $p_{\frac{1}{2}}$; (2) the $p_{\frac{3}{2}}$ state has a larger reduced width than the $p_{\frac{1}{2}}$ state. From the standpoint of the present work: (1) the difference in the logarithmic derivatives, $Y_{\frac{3}{2}}<Y_{\frac{1}{2}}$, indicates a deeper potential well for the $p_{\frac{3}{2}}$ state; (2) the different energy dependences, $(dY_{\frac{3}{2}}/dE)<(dY_{\frac{1}{2}}/dE)$, serve to fix qualitatively the dependence on distance of the difference between the $p_{\frac{3}{2}}$ and $p_{\frac{1}{2}}$ state potentials. The values of $Y_{\frac{3}{2}}$ and $Y_{\frac{1}{2}}$ fix the sign and magnitude of the effective spin-orbit interaction while the values of dY_J/dE determine qualitatively its shape.

The effect of the spin-orbit interaction shape may be seen with the aid of a well-known formula relating the change in logarithmic derivative to the change in potential:

$$(Y_{\frac{3}{2}}-Y_{\frac{1}{2}})_{r=a}=(2\mu a/\hbar^2)\left[(1/\mathfrak{F}_{\frac{3}{2}}\mathfrak{F}_{\frac{1}{2}})\int_0^a \mathfrak{F}_{\frac{3}{2}}\mathfrak{F}_{\frac{1}{2}}\Delta V(r)dr\right].$$

Here, Y is the homogeneous logarithmic derivative defined earlier, and $\Delta V(r)$ represents the effective spin-orbit interaction $V_{\frac{3}{2}}-V_{\frac{1}{2}}$. If the spin-orbit interaction has a δ function distance dependence $\delta(r-a)$, $(Y_{\frac{3}{2}}-Y_{\frac{1}{2}})_{r=a}$ is independent of energy. For an inverted doublet spin-orbit interaction at distances $r<a$, the bracketed quantity increases in magnitude with the energy, reproducing qualitatively the behavior of the experimental logarithmic derivatives.

A simple verification of the above conclusions is obtained by fitting experimental data for $p_{\frac{3}{2}}$ and $p_{\frac{1}{2}}$ separately by means of square-well potentials. For $p_{\frac{3}{2}}$ the data require an attractive square well with a range of 3.15×10^{-13} cm. The $p_{\frac{1}{2}}$ phase shifts call for a shallower attractive square well with a range of about 3.6×10^{-13} cm. The effective spin-orbit interaction $V_{\frac{3}{2}}-V_{\frac{1}{2}}$ is seen to be attractive for $r<3.15\times10^{-13}$ cm and repulsive for $r>3.15\times10^{-13}$ cm.

In order to relate the analysis to the customary form of the Thomas term, it was supposed that the Hamiltonian has the form

$$H=T+V+(\alpha\hbar/4M^2c^2)[\mathbf{p}\times\nabla V]\cdot\boldsymbol{\sigma},$$

where T is the kinetic energy, V is a function of r only, $\mathbf{p}$ is the momentum operator, and ∇ in ∇V applies to V only. This Hamiltonian can be written

$$H=T+[1-(\alpha\lambda^2/4)(\mathbf{L}\cdot\boldsymbol{\sigma})d/rdr]V(r), \qquad (1)$$

where $\lambda=\hbar/Mc$ and $\mathbf{L}$ is the orbital angular momentum operator in units $\hbar$. On account of the relatively large difference between the proton mass M and the reduced mass $\mu=4M/5$, there is a question as to whether one should use $\alpha=1$ or $\alpha=25/16$ to reproduce the expectation on the simple scalar equation view. Since the empirical α is appreciably greater than either of these values, this question does not appear to be very significant, there being no possibility of agreement with the scalar equation. In the interests of simplicity, the standardization used here is such as to neglect corrections for reduced mass. There is no reason for supposing such corrections to be simply a matter of changing M to the reduced mass. In fact, in a system composed of several particles, there is a separate Thomas-like term for each particle, so that the contributions of terms referring to the four nucleons in the alpha particle cancel in first approximation.

The employment of Eq. (1) does not strictly correspond to the form which follows from the assumption that Thomas-like terms represent the spin-orbit interactions between pairs of particles, as has been noted by Breit and Stehn.[14] In the approximation of representing the wave function by Slater determinants, the spin-orbit energy for the $p_{\frac{3}{2}}$ state is

$$(\psi,H'\psi)=2(u_2^{\pi}v_1,A_{12}^{\pi}u_2^{\pi}v_1)+2(u_2^{\pi}v_1,A_{12}^{\pi}u_2^{\pi}v_1)-(u_1^{\pi}v_2,(A_{12}^{\pi}+A_{21}^{\pi})u_2^{\pi}v_1), \qquad (2)$$

where the superscripts π,ν refer to proton and neutron wave functions, respectively, and the remainder of the notation is as follows:

u,v = orbital functions for s and p states, respectively; the p function is for magnetic quantum number 1;

$A_{12}^{\pi}=(\hbar/4M^2c^2)[\mathbf{p}_1\times(\nabla_1V(r_{12}))]_z$, with the understanding that $\mathbf{p}_1=(\hbar/i)\nabla_1$ is an operator, while $(\nabla_1V(r_{12}))$ is a number;

$$(U_1V_2,O_{12}X_1Y_2)=\int U^*(\mathbf{r}_1)V^*(\mathbf{r}_2)O_{12}X(\mathbf{r}_1)Y(\mathbf{r}_2)d\mathbf{r}_1d\mathbf{r}_2;$$

where, for brevity, arguments are indicated by subscripts.

The first two terms in Eq. (2) represent direct interactions of the p particle with the s shells of neutrons and protons. The last term arises on account of the identity of the three protons and is an exchange effect. The first two terms can be represented as the effect of an equivalent central field; the last one cannot. It should be pointed out that the scattering problem can be stated in terms of a variational equation for the expectation value of the energy. The radial factors in u and v are varied. On varying v, there results an integro-differential equation for the radial factor of v. The first two terms in Eq. (2) contribute an ordinary potential, while the last contributes a part representable as an

[13] D. C. Dodder and J. L. Gammel, Phys. Rev. 88, 520 (1952), Fig. 1. Note that energy of relative motion is incorrectly given; the values in their Fig. 1 should be multiplied by 5/4.

[14] G. Breit and J. R. Stehn, Phys. Rev. 53, 459 (1938).

integral operator which is not expressible in terms of a local potential.

One finds

$$(u_2v_1,A_{12}^{x}u_2v_1)=-(\alpha\lambda^2/4)$$

$$\times\int R_s^2(2)R_p^2(1)[V'(r_{12})/r_{12}]d\mathbf{r}_1d\mathbf{r}_2/(4\pi)^2, \quad (3)$$

where $R_s(r)$, $R_p(r)$ are the radial s and p functions, respectively, normalized so that

$$\int_0^\infty R_s^2(r)r^2dr=\int_0^\infty R_p^2r^2dr=1.$$

If, on the other hand, use is made of Eq. (1) for a single-particle model, and if V in this model is distinguished as $\mathcal{U}$, one obtains for the spin-orbit energy in the $p_{\frac{1}{2}}$ state:

$$\langle(\mathbf{A}\sigma)\rangle=-(\alpha\lambda^2/16\pi)\int R_p^2(1)[\mathcal{U}'(r_1)/r_1]d\mathbf{r}_1. \quad (4)$$

If one compares this result with Eq. (3), agreement is obtained if one sets

$$\tilde{V}(r_1)=\int V(r_{12})R_s^2(2)d\mathbf{r}_2/(4\pi). \quad (5)$$

This equivalent one body $\tilde{V}$ is just the average potential at $\mathbf{r}_1$ caused by the s particles at $\mathbf{r}_2$. The possibility of interpreting the direct-interaction terms in Eq. (2) as due to an equivalent central potential is thus verified and holds more generally than in the present simple example. Collecting the results for different interactions of a p particle with an s shell for the case of Wigner forces as listed in reference 14, the expectation value is

$$(\psi,H'\psi)=-(\alpha\lambda^2/16\pi^2)\int R_2^2Q_1^2(V'/r_{12})r_1^2d\mathbf{r}_1d\mathbf{r}_2$$

$$-(\alpha\lambda^2/128\pi^2)\int R_1Q_2(V'/r_{12})$$

$$\times\{2(r_2^2-\mathbf{r}_1\cdot\mathbf{r}_2)R_2Q_1+[(R_2Q_1'/r_1)$$

$$-(R_2'Q_1/r_2)]r_1^2r_2^2\sin^2\theta\}d\mathbf{r}_1d\mathbf{r}_2, \quad (6)$$

where $R=R_s$, $R_p=rQ$, and the arguments r_1,r_2 of the radial functions are distinguished by subscripts. The radial functions for s protons and neutrons are assumed to be the same for simplicity although this point is not essential to the argument. If one varies Q, the first integral in Eq. (6) gives rise to a local interaction; the second is not expressible in such simple terms.

The potential energy $V_{12}+V_{23}\cdots$ also gives rise to exchange terms. An improved treatment including exchange effects with two-body forces would thus have to include a modification of the effects of the non-spin-orbit part of the potential. No attempt is made to calculate these effects in the present paper, partly because of the multiplicity of possibilities offered by combinations of exchange effects, and partly because of the unknown magnitude of many-body force contributions. The latter may conceivably result in making the equivalent one-body equation (1) a better approximation than a sum of potentials representing interactions between pairs of particles.

III. COMPARISON WITH EXPERIMENT

Three well shapes, giving a survey of possibilities for the spin-orbit interaction shape, were chosen. For each shape the values of three parameters, well depth, well range, and strength of spin-orbit interaction, were determined by minimizing the mean square deviation of the calculated p phases from experiment. Five experimental energies, $E_p=1.49$, 2.22, 3.04, 5.81, 9.48 Mev, were considered in the fitting procedure. These energies provided an adequate survey of the data without overemphasis of the low-energy data. The three shapes chosen were: (1) square well, giving a δ-function spin-orbit interaction located at the edge of the well, (2) Gauss well, giving a Gauss well with the same range parameter for the spin-orbit interaction, (3) exponential well, giving a Yukawa well shape for the spin-orbit interaction. These well shapes show a regular progression from concentrated potentials with externally located spin-orbit interaction to longer-tailed wells with spin-orbit interaction concentrated at small distances.

In all calculations the repulsive Coulomb field was taken as the field of a uniform volume distribution of charge with a radius of 2.31×10^{-13} cm. The fit for a given well shape does not depend sensitively on the assumed charge distribution. For the Gauss potential, the effect of replacing the uniform volume distribution by a point charge is compensated by increasing the depths of the $p_{\frac{1}{2}}$ and $p_{\frac{3}{2}}$ wells by 0.45 percent, with the range parameter left unchanged. The root-mean-square deviation of calculated phases from experiment is the same in both cases and the maximum difference in the "best fit" phase shifts for the two cases is 0.2°, an amount negligible in comparison with the errors in the experimental phase shifts.

(A) Square Well

The potential arising from a common p state potential, $V_0(r)=-D$, $(r\leq r_0)$, $V_0(r)=0$, $(r>r_0)$, is

$$V(r)=-D-(\beta/r_0)(\sigma\mathbf{L})\delta(r-r_0), \quad (r\leq r_0);$$
$$V(r)=0, \quad (r>r_0),$$

where $\beta=(\alpha/4)(\hbar/Mc)^2$. The spin-orbit interaction produces an energy-independent splitting in the $p_{\frac{1}{2}}$ and $p_{\frac{3}{2}}$ state logarithmic derivatives, as is seen from the relation

$$(Y_{\frac{1}{2}}-Y_{\frac{3}{2}})_{r=r_0+}=-3(2\mu D/\hbar^2)\alpha\lambda^2/4.$$

The parameters for the best fit are

$$r_0=3.21\times10^{-13}\text{ cm},\quad D=19.65\text{ Mev},\quad \alpha=48.8.$$

The root-mean-square deviation of calculated phases from experiment is 4.1°. The best fit is reproduced in Fig. 1. It is apparent that the calculated $p_{\frac{1}{2}}$ phases increase too slowly with energy, while the calculated $p_{\frac{3}{2}}$ phases increase too rapidly.

(B) Gauss Well

The interaction arising from a Gauss well, $V(r)=-A\exp[-(r/a)^2]$, is

$$V_{\frac{1}{2}}=-[1-(4\beta/a^2)]A\exp[-(r/a)^2],$$
$$V_{\frac{3}{2}}=-[1+(2\beta/a^2)]A\exp[-(r/a)^2],$$

where $\beta=(\alpha/4)(\hbar/Mc)^2$. The above set of potentials is equivalent to taking $V_J=-A_J\exp[-(r/a)^2]$, with

$$A_{\frac{1}{2}}=[1-(4\beta/a^2)]A,\quad A_{\frac{3}{2}}=[1+(2\beta/a^2)]A.$$

The parameters for the best fit are:

$$a=2.30\times10^{-13}\text{ cm},\quad A=47.32\text{ Mev},\quad \alpha=29.6,$$

or

$$A_{\frac{1}{2}}=53.17\text{ Mev},\quad A_{\frac{3}{2}}=35.61\text{ Mev}.$$

The phase shifts for the best fit are reproduced in Fig. 1. The root-mean-square deviation of calculated phases from experiment is 1.5°, slightly over $\frac{1}{3}$ the corresponding number for the square well.

For the Gauss potential, the dV/rdr term has the same shape as V. The difference between the $p_{\frac{1}{2}}$ and $p_{\frac{3}{2}}$ potentials is, therefore, the same fraction of V at all r. This fraction has the large value 0.4, supporting the view that the spin-orbit interaction is not a relativistic correction, but a major effect.

(C) Exponential Well

The interaction resulting from a common p state potential, $V_0(r)=-B\exp(-2r/b)$, is

$$V(r)=-B[\exp(-2r/b)+(\sigma\mathbf{L})(4\beta/b^2)\exp(-2r/b)/(r/b)],$$

where $\beta=(\alpha/4)(\hbar/Mc)^2$. The spin-orbit interaction adds a potential having a Yukawa radial dependence, attractive for $p_{\frac{3}{2}}$ and repulsive for $p_{\frac{1}{2}}$. The parameters for the best fits are

$$b=1.924\times10^{-13}\text{ cm},\quad B=155.5\text{ Mev},\quad \alpha=20.0.$$

The spin-orbit splitting is here given by a Yukawa well, $\mathcal{C}\exp(-r/\delta)/(r/\delta)$, with $\mathcal{C}=110$ Mev and $\delta=0.958\times10^{-13}$ cm. The calculated phases are reproduced in Fig. 1. The root-mean-square deviation of calculated phases from experiment is 2.5°. The exponential-well fits show too large a $p_{\frac{3}{2}}$ phase shift and too small a $p_{\frac{1}{2}}$ phase shift at the highest energies, a trend opposite to that shown by the square well fits. This may be attributed to the singular spin-orbit interaction at small distances, which is most effective at high energies for which the centrifugal barrier is least important.

IV. CONCLUSIONS

The best-fit phase shifts calculated for the three well shapes studied are plotted with the experimental p phase shifts in Fig. 1. The graphs indicate that: (1) an exponential well gives a splitting increasing too rapidly with energy; (2) a square well gives a splitting increasing too slowly with energy; (3) a Gauss well gives a good over-all fit to the experimental phase shifts.

The Gauss-well parameters which may be considered as giving a good representation of the p state proton-alpha interaction are

$$V=-[1-\beta(\sigma\mathbf{L})(d/rdr)]A\exp[-(r/a)^2]$$
$$a=2.30\times10^{-13}\text{ cm},\quad A=47.32\text{ Mev},\quad \beta=7.40(\hbar/Mc)^2.$$

These numbers support the general belief that the spin-orbit parameter required by experiment is much larger than the theory of the Thomas term would require, *viz.* $\beta=(1/4)(\hbar/Mc)^2$. The ratio of the spin-orbit interaction needed to account for experiment to that suggested by the Thomas term has the following values:

Square well	Gauss well	Exponential well
49	30	20

The conclusions as to well shape depend sensitively on the values taken for the experimental p phase shifts at the higher energies, as is evident in Fig. 1. The possible presence of small phase shifts for $L>2$, neglected in the phase-shift analysis,[7] might lead to changes in the p phases sufficient to change the preference for the Gauss well. An investigation of this point is outside the scope of the present work; however, the f phase shifts calculated from the same Gauss well that fitted the p phase-shift data are $\approx\frac{1}{2}°$ at 10 Mev, which indicates that the neglect of f phase shifts in the analysis of the experimental data is not unreasonable. On the other hand, there is no compelling reason for taking the potential to be the same in f and in p states, so that it is difficult to exclude f phase shifts of appreciably greater amounts than given by the above estimate. It is also difficult to exclude effects of changes in well shape for large r which can affect f wave phase shifts without producing serious effects on spin-orbit interaction.

For these reasons the phase-shift analysis used here, as well as its consequences as presented in this note, might need modification. In particular, the effect of phase shifts for $L>2$ on the s,p,d phase shifts cannot be claimed to be necessarily negligible in ascertaining effects of well shape on spin-orbit interaction,[1] as has been attempted here.

Meson Production in High-Energy Nucleon-Nucleon Collisions*

WILLIAM L. KRAUSHAAR AND LAWRENCE J. MARKS
Department of Physics and Laboratory for Nuclear Science, Massachusetts Institute of Technology, Cambridge, Massachusetts

(Received August 21, 1953)

A model for meson production in high-energy nucleon-nucleon collisions similar to a model suggested by Takagi is discussed. It is assumed that the primary collisions result in the formation of two highly excited nucleons which decay as free particles. Forward and backward center-of-mass collimation is a natural consequence. Angular momentum is discussed and treated quantitatively by means of thermodynamic arguments similar to those used by Fermi. The model implies a tendency for the mesons to be emitted in a plane. The multiplicities predicted are larger than those predicted from the Fermi model and depend upon an additional parameter related to angular momentum.

I. INTRODUCTION

SOME general characteristics of meson production in very high-energy nucleon-nucleus collisions seem to be established despite the small number of experiments.[1-3] It is by no means certain that these collisions can be correctly interpreted in terms of nucleon-nucleon encounters,[4] but if they are so interpreted, the following general features seem evident: (*a*) the existence, in at least some cases, of two cones of fast particles, one forward and one backward as viewed from the collision center-of-mass system (referred to as frame 1 hereafter); (*b*) a meson multiplicity which is small compared to the maximum multiplicity kinematically possible; and (*c*) a meson multiplicity which probably increases less rapidly than the energy available in the center-of-mass system.

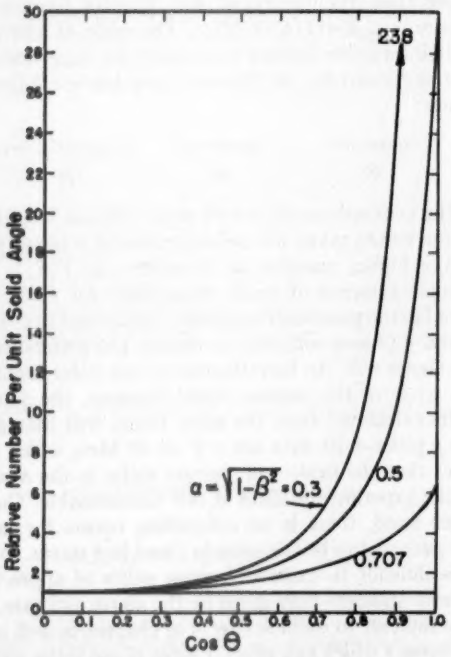

FIG. 1. Collision center-of-mass angular distributions for various values of the parameter $\alpha=(1-\beta^2)^{\frac{1}{2}}$, where βc is the velocity of the excited nucleons in the collision center-of-mass system.

We wish to discuss here a model, certain aspects of which have already been suggested by Takagi.[5] We suppose that the effect of a nucleon-nucleon collision is to excite normal modes of the nucleons, or to change each of the nucleons into greatly excited, heavy isobaric states. Kinematically this amounts to assuming that the nucleons, as viewed from frame 1, exchange a portion of their momentum at the instant of collision, and then travel away from the collision center, each keeping its original total energy but having a *smaller* momentum and hence larger mass than before. We further suppose that these excited nucleons have lifetimes sufficiently long so that by the time they decay into mesons they are free particles. If we neglect for the present any angular momentum considerations, the angular distribution of the emitted mesons is isotropic in the frame of reference (frame 2) in which an excited nucleon is at rest. In other words, we are assuming that there exist high-energy large-multiplicity counterparts of the established heavier-than-nucleon V particles, and that these highly excited nucleons are produced in pairs in very high-energy nucleon-nucleon collisions. The angular distribution of the emitted mesons in frame 1 has then the characteristic two cones of fast particles, one forward and one backward, if the excited nucleons maintain the direction of the incident nucleons.[6] Angular distributions computed according to these assumptions are shown in Fig. 1 for various values of the velocity βc of the excited nucleons relative to frame 1. We have taken here the extreme relativistic limit $\beta_\pi=1$ for the mesons in frame 2. In this approximation the

* This work was supported in part by the joint program of the U. S. Office of Naval Research and the U. S. Atomic Energy Commission.

[1] Lord, Fainberg, and Schein, Phys. Rev. **80**, 970 (1950).
[2] M. F. Kaplan and D. M. Ritson, Phys. Rev. **88**, 386 (1952).
[3] Lal, Pal, Peters, and Swami, Proc. Indian Acad. Sci. **36**, 75 (1952).
[4] F. C. Roesler and C. B. A. McCusker, Phys. Rev. **91**, 690 (1953).
[5] S. Takagi, Progr. Theoret. Phys. (Japan) **1**, 123 (1952).
[6] If the excited nucleons do not maintain the directions of the incident nucleons, the two cones of mesons would no longer be coaxial in the laboratory system.

angular distribution has the simple form given by the equation

$$N(\theta)=\frac{(1-\beta^2)}{8\pi}\left[\frac{1}{(1-\beta\cos\theta)^2}+\frac{1}{(1+\beta\cos\theta)^2}\right], \quad (1)$$

where $N(\theta)$ is the fraction of particles emitted per unit solid angle at the polar angle θ.

It is of interest to apply the above ideas to the "S" star.[1] If we take 20 000 Bev as the energy of the incident nucleon, the observed angular distribution is consistent with the angular distribution which would result from the decay of two excited nucleons traveling in the same direction as the incident nucleons, but with velocities only $0.92c$, as viewed from frame 1. The corresponding value for the rest mass of each of the excited nucleons is about $40M$, where M is the nucleon mass. Upper and lower bounds for the lifetimes of the excited nucleons may be estimated from (a) the fact that the track of the primary colliding particle and the origin of both the wide and diffuse cones of fast particles apparently coincide in the nuclear emulsion, and (b) the fact that, if these excited states do exist, and do live long enough to become free particles, there must have been enough time available for several light-signal traversals of the volume, taken here to be $\sim$ (meson Compton wavelength).[3] These speculative and crude estimates set $10^{-16}>\tau>10^{-21}$ sec.

The inclusion of angular momentum considerations has an interesting consequence. Suppose the total energy in frame 1 is W. Then in the extreme relativistic limit, the angular momentum of the initial state is $W\mathfrak{R}/c$, where $\mathfrak{R}$ is the impact parameter for each of the colliding nucleons. This angular momentum could be carried off entirely via translatory motion, or partly via translatory motion and partly via intrinsic angular momentum of the excited nucleons. It is the latter possibility which we wish to explore further here.

If we characterize the collision by the velocity βc of the excited nucleons in frame 1, the rest mass of the excited nucleons is $U/c^2=\alpha W/2c^2$, where $\alpha=(1-\beta^2)^{\frac{1}{2}}$. Then the angular momentum of the final state is only $W\beta\mathfrak{R}/c$, if the impact parameter of the excited nucleons upon leaving the center of the interaction is the same as that for the initial collision. Angular momentum can then be conserved by assigning a spin-like angular momentum $W\mathfrak{R}(1-\beta)/2c$ to each of the excited nucleons. Conservation of total energy and angular momentum are more conveniently considered in frame 2, in which an excited nucleon is at rest. In this frame the transformed total energy is just U, and the transformed angular momentum is $M_z=U\mathfrak{R}/(1+\beta)c$. Since UR/c, where R is the radius of an excited nucleon, is the maximum angular momentum that can be carried off in the decay process, angular-momentum conservation has the possibility of being a significant restraint. In this case there would be a tendency for the mesons to be emitted in a plane perpendicular to the z direction.

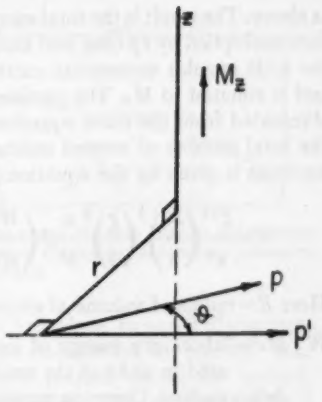

FIG. 2. Coordinate system in the frame of reference in which an excited nucleon is at rest.

If high intrinsic angular-momentum particles are themselves among the decay products, this tendency would be less pronounced.

II. THERMODYNAMIC APPROXIMATION

Some of the above notions can be treated from the standpoint of thermodynamic equilibrium in a manner analogous to Fermi's treatment of high-energy multiple meson production.[7,8] We have already assumed that the excited nucleons are free particles by the time they decay, and have lost all memory of the original collision. Hence there should be sufficient time for the establishment of equilibrium. As the volume of the excited nucleon we take a sphere of radius R. R is taken to be of the order of a meson Compton wavelength. (In the high-energy limit assumed here, the zero-point energy is not an important consideration.) We take cylindrical shells with their axes along z as the volume elements for integration, $4\pi r(R^2-r^2)^{\frac{1}{2}}dr$. Then the number of mesons in a volume element in phase space is given by the equation:

$$dN=\frac{g2\pi p^2 dp d(\cos\vartheta)4\pi r(R^2-r^2)^{\frac{1}{2}}dr}{(2\pi\hbar)^3[\exp(Apc-Bpr\cos\vartheta)-1]}. \quad (2)$$

Here we are assuming Einstein-Bose statistics and π-meson production only with a statistical weight $g=3$. A and B are constants to be determined from energy and angular-momentum conservation. (In the absence of angular momentum considerations, A is essentially the reciprocal temperature.) The angle ϑ is the angle between the meson direction p and the direction p' which the meson would have if it were to carry away the maximum possible angular momentum (see Fig. 2). We integrate Eq. (2) over p from 0 to ∞, over $\cos\vartheta$ from -1 to 1, and over r from 0 to R. The result is the total number of mesons emitted from one of the two excited nucleons, and depends explicitly on A and B. Then we multiply Eq. (2) by pc and integrate over the variables,

[7] E. Fermi, Phys. Rev. **81**, 683 (1951); Progr. Theoret. Phys. (Japan) **5**, 570 (1950).
[8] Hazen, Heineman, and Lennox, Phys. Rev. **86**, 198 (1952).

as above. The result is the total energy U. Equation (2) is then multiplied by $r\dot{\rho}\cos\vartheta$ and integrated. The result is the total angular momentum carried off by the mesons and is equated to M_s. The parameters A and B can be eliminated from the three equations, and the result for the total number of mesons emitted from both excited nucleons is given by the equation:

$$N=\frac{2^{7/8}}{\pi^{\frac{1}{2}}}\left(\frac{R}{\lambda}\right)^{\frac{1}{2}}\left(\frac{g}{3}\right)^{\frac{1}{2}}\frac{a}{b^{\frac{1}{2}}}\alpha^{\frac{1}{2}}\left(\frac{W'}{Mc^2}\right)^{3/8}\frac{F_1(\rho)}{[F_2(\rho)]^{\frac{1}{2}}}. \quad (3)$$

Here R = radius of volume of excited nucleon.

W'/Mc^2 = laboratory energy of incident nucleon measured in units of the nucleon rest energy.

$2\pi\lambda$ = nucleon Compton wavelength. (This appears only because we have measured energy in units of Mc^2.)

$$a=2\sum_{n=1}^{\infty}\frac{1}{n^3}=2.413,$$

$$b=6\sum_{n=1}^{\infty}\frac{1}{n^4}=6.494,$$

$$\alpha=(1-\beta^2)^{\frac{1}{2}},$$

$$F_1(\rho)=\frac{3}{2\rho^2}\left\{\frac{\tan^{-1}[\rho/(1-\rho^2)^{\frac{1}{2}}]}{\rho(1-\rho^2)^{\frac{1}{2}}}-1\right\},$$

$$F_2(\rho)=1+\frac{\rho^2}{1-\rho^2}\left[1+\frac{F_1(\rho)}{3}\right].$$

The parameter ρ affords a measure of the extent to which angular-momentum conservation is an important restraint on the decay process. Its value is given implicitly by the relation:

$$\frac{M_s}{UR/c}=\frac{F_2(\rho)-F_1(\rho)}{\rho F_2(\rho)}\equiv G(\rho). \quad (4)$$

$G(\rho)$ and $F_1(\rho)/[F_2(\rho)]^{\frac{1}{2}}$ are plotted as functions of ρ in Fig. 3.

For comparison, the expression similar to our Eq. (3) from the Fermi model is

$$N=\frac{3}{2^{\frac{1}{2}}\pi^{\frac{1}{2}}}\left(\frac{R}{\lambda}\right)^{\frac{1}{2}}\left(\frac{g}{3}\right)^{\frac{1}{2}}\frac{a}{b^{\frac{1}{2}}}\left(\frac{W'}{Mc^2}\right)^{\frac{1}{2}}K(\mathfrak{R}/R), \quad (5)$$

where the symbols have the same meanings as before, and $K(\mathfrak{R}/R)$ is a function of the impact parameter $\mathfrak{R}$. The similarity of the expressions reflects the thermodynamic treatment used in both models. The difference in the energy dependence arises from the Lorentz contraction of the excited volume assumed only in the Fermi model.

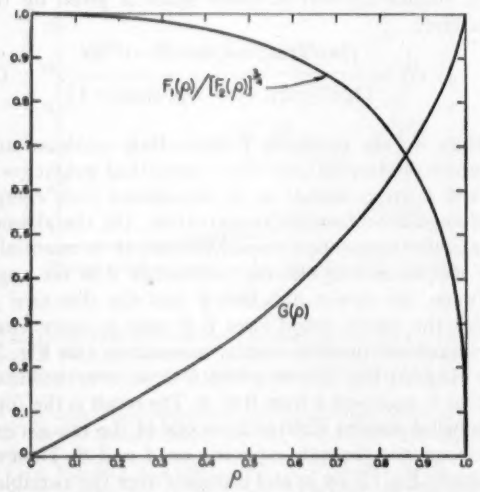

FIG. 3. The functions $G(\rho)$ and $F_1(\rho)/[F_2(\rho)]^{3/4}$ *vs* ρ. $G(\rho)$ serves to define the value of the angular momentum parameter ρ, and $F_1(\rho)/[F_2(\rho)]^{3/4}$ determines the multiplicity.

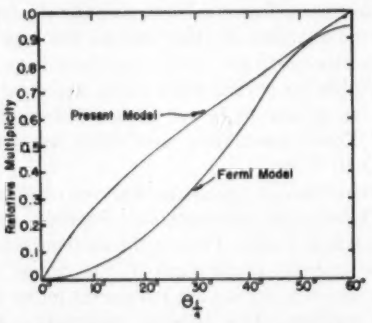

FIG. 4. Relative multiplicity for the present model and for the Fermi model plotted against the collision center-of-mass angle, $\theta_{1/4}$, which contains one-fourth of the emitted particles.

Let us characterize the angular distribution for both models by considering the center-of-mass polar angle $\theta_{\frac{1}{4}}$, which contains one-fourth of the particles. In the Fermi model a small value of $\theta_{\frac{1}{4}}$ means a large angular-momentum-type collision ($\mathfrak{R}/R\sim 1$) with a resultant small multiplicity, as reflected by the behavior of the function $K(\mathfrak{R}/R)$. [$K(\mathfrak{R}/R)$ approaches zero as $\mathfrak{R}/R$ approaches 1, and approaches $2\sqrt{2}/3=0.943$ as $\mathfrak{R}/R$ approaches zero.] In the present model, a small value of $\theta_{\frac{1}{4}}$ means a small momentum transfer between the colliding nucleons, and hence only a small increase in nucleon mass. The excitation energy of the nucleons is therefore small, and few mesons are emitted. In Fig. 4 we have shown $\alpha^{\frac{1}{2}}$ and $K(\mathfrak{R}/R)$ plotted against $\theta_{\frac{1}{4}}$ to show how the angular distribution and meson multiplicity are related in the two models. The numerical factors in the two expressions for N are almost identical, so that, except for the factors $\alpha^{\frac{1}{2}}$ and $K(\mathfrak{R}/R)$ discussed above, the multiplicities from the present model exceed those

from the Fermi model by a factor of $(W'/Mc^2)^{1/8}F_1(\rho)/[F_2(\rho)]^{\frac{1}{2}}$, provided the radius of the excited volume in the present model and the radius of the uncontracted excited volume in the Fermi model are set equal to one another. $[(W'/Mc^2)^{1/8}\approx 3.5$ for $W'=20\,000$ Bev.] The factor $F_1/F_2^{\frac{1}{2}}$ is equal to, or less than 1, and has a value determined by the angular-momentum parameter ρ. This is discussed further in the following paragraphs.

According to Eq. (2), there is predicted an angular distribution of the mesons in frame 2 involving the angle ϑ. This angular distribution is given by the equation

$$F_3(\eta)d(\cos\vartheta) = \left[\frac{2-\eta^2}{2\eta^2(1-\eta^2)}+\frac{\pi}{2\eta^3}-\frac{(\frac{1}{2}\pi+\sin^{-1}\eta)(2-3\eta^2)}{2\eta^3(1-\eta^2)^{\frac{1}{2}}}\right]d(\cos\vartheta), \quad (6)$$

where $\eta=\rho\cos\vartheta$. $F_3(\rho\cos\vartheta)$ is not an observable angular distribution, because ϑ measures the angle between a meson's direction and the direction it would have if it were to carry off its maximum possible amount of angular momentum. It is therefore convenient to consider the angular distribution obtained by projecting the meson directions on a plane passing through the z axis in frame 2. This angular distribution $F_4(\phi)d\phi$, where ϕ is measured from the z axis, is given in terms of the function F_3 by the relation

$$F_4(\phi)=\frac{1}{2\pi}\int_0^\pi\int_0^\pi F_3(\rho\cos\beta(1-\sin^2\gamma\cos^2\phi)^{\frac{1}{2}}) \times\sin\gamma d\beta d\gamma. \quad (7)$$

If the plane in which ϕ is measured is considered to be perpendicular to the direction of flight of the excited nucleon, $F_4(\phi)$ is invariant to a coordinate transformation and so corresponds to the angular distribution in target diagrams such as those given by Kalpon and Ritson.[2] Figure 5 shows $F_4(\phi)$ for various assumed values of the parameter ρ.

As mentioned before, the parameter ρ affords a measure of the extent to which angular momentum is an important restraint on the decay process. In Eq. (4), UR/z is really just the maximum possible angular momentum that can be carried off from an excited nucleon of total energy U and radius R. If M_s is small compared to UR/c, $G(\rho)$ and hence ρ are small. This in turn means that $F_1(\rho)/[F_2(\rho)]^{\frac{1}{2}}$, and hence the meson multiplicity tend towards zero. Such mesons as are emitted tend to be emitted in a plane, and so $F_4(\phi)$ has a strong maxima at 90 and 270 degrees. The details of these considerations depend, of course, upon the thermodynamic approximation that has been used. The more general characteristics are essentially kinematical, and suggest that the low multiplicity limit arising either from low excitation energy or high angular momentum would correspond to the established V_1^0-type particle. This is, of course, not a "prediction" from the model but rather is a return to one of the phenomena which suggested the model in the first place. In part I it was mentioned that the angular distribution for the "S" star was consistent with the present model for excited-nucleon masses of about $40M$. This corresponds to a value of 0.40 for our parameter α and was obtained by taking 20 000 Bev as the incident nucleon energy in the laboratory system and $\theta_1=20°$ in the collision center-of-mass system. The predicted number of charged particles [$\frac{2}{3}$ of N from Eq. (3)] is then $43\,F_1(\rho)/[F_2(\rho)]^{\frac{1}{2}}$, if R is taken as $1/2\pi$ times the meson Compton wavelength. The predicted number from the Fermi model under the same assumptions as above is 4.6, and the observed number was 15.

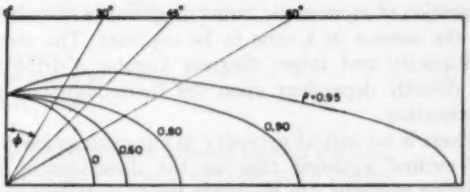

FIG. 5. Polar plot of the target diagram angular distribution, $F_4(\phi)$ *vs* ϕ for various values of the angular momentum parameter ρ. ϕ is measured from the z axis.

A comparison of the group of high-energy interactions observed by Kaplon and Ritson with our predicted charged meson multiplicities shows the same general tendency as shown by the above comparison with the "S" star. That is, if we ignore the factor $F_1(\rho)/[F_2(\rho)]^{\frac{1}{2}}$ by setting it equal to one, some of the predicted multiplicities are in close agreement with those observed, while many of them are a factor of two or more higher. In evaluating this comparison, it should be emphasized that none of these interactions are known to be nucleon-nucleon interactions, and the effects of the other nucleons present in the target nucleus are unknown. In both the Fermi model and in the present model, the radius R is to be considered a free parameter (within reasonable limits). We have ignored the factor $F_1(\rho)/[F_1(\rho)]^{\frac{1}{2}}$ by setting it equal to one, because we have no *a priori* method of evaluating ρ. In pure nucleon-nucleon interactions a study of the target diagram angular distributions would at least permit one to put an approximate upper limit on ρ. This, of course, is a crucial point in evaluating the worth, if any, of the model.

III. CONCLUSIONS

Basic to all the aforementioned considerations are the assumptions that the nucleons in very high-energy nucleon-nucleon collisions are converted into heavy, highly-excited states travelling essentially in the direction of the incident nucleons, and that these states live long enough to become essentially free particles before decaying into mesons or other particles. These assumptions lead to the characteristic center-of-mass forward and backward cones of particles. Essentially independent of the thermodynamic approximation is the

suggestion of asymmetric target diagrams or a tendency for the mesons in a cone to be coplanar. The meson multiplicity and target diagram angular distribution are directly dependent upon the thermodynamic approximation.

There is no logical necessity in our assumption that the excited nucleons take on the directions of the colliding nucleons. On the other hand, excitation energies appropriate to the observed angular distributions result from comparatively small momentum transfers, so that the angles between the colliding and excited nucleons would in general be expected to be small. Similarly, there is no logical necessity in our assumption that (other than on the average) the masses, or excitation energy of the excited nucleons, be equal. That is, while the excited nucleon momenta must be equal and opposite, their excitation energies could be different. This would require energy as well as momentum transfer between the nucleons and would lead to dissimilar center-of-mass forward and backward cones.

Lal, Pal, Peters, and Swami have observed several meson-induced interactions, and remark that most of the mesons seem to be emitted in the backward direction in the center-of-mass system.[8] If the general features of the model are to apply to this type of interaction, it seems necessary to assume either of two alternatives: (a) energy as well as momentum is transferred, and in general the nucleon gets the higher excitation energy; or (b) only momentum is transferred, but the meson and nucleon excited volumes are inherently different, so that the excited nucleon decays into more particles.[9]

[9] If taken seriously, our assumption of momentum transfer without energy transfer would imply that V_1^0 particles, if made in neutron-neutron collisions, would be made in pairs, but that V_1^0 particles made in π^- free-proton collisions would be accompanied by neutral particles of mass 1210 electron masses. Similar reasoning applied to π^- free-proton collisions in which particles of mass 975 electron masses are created, gives a mass of 2060 electron masses to the excited nucleon.

It is a pleasure to acknowledge a helpful discussion of these matters with Professor F. Villars.

APPENDIX

The spherical shape used for the excited volume in the thermodynamic approximation is perhaps the most natural choice. Equation (3) may be written more generally so as to be valid for other volumes. This expression is

$$N=\left(\frac{6\sqrt{2}}{\pi^2}\right)^{\frac{1}{4}}\left(\frac{V^{\frac{1}{3}}}{\lambda}\right)^{\frac{1}{4}}\frac{a}{b^{\frac{1}{4}}}\left(\frac{g}{3}\right)^{\frac{1}{4}}\alpha^{\frac{1}{4}}\left(\frac{W'}{Mc^2}\right)^{3/8}\frac{f_1(\rho)}{[f_2(\rho)]^{\frac{1}{4}}}, \quad (3')$$

where V is the volume assumed. The functions f are given as follows:

$$f_1(\rho)=\frac{1}{V}\int\frac{dV}{(1-\rho^2r^2/R^2)^2},$$

$$f_2(\rho)=\frac{1}{V}\int\frac{(3+\rho^2r^2/R^2)}{(1-\rho^2r^2/R^2)^3}dV,$$

$$f_3(\rho\cos\vartheta)=\frac{1}{V}\int\frac{dV}{[1-\rho(r/R)\cos\vartheta]^3}.$$

Here r is the distance from the z axis to the volume element dV, and R is the maximum radius of the volume. (Symmetry about the z axis has been assumed.)

Quantization of a Nonlinear Field Theory

HERBERT B. ROSENSTOCK*
University of North Carolina, Chapel Hill, North Carolina
(Received September 21, 1953)

A quantization procedure, involving the expansion of the field in a space lattice of classical particles, is suggested for a field theory in which classical particles appear as small regions in which the field is intense. Approximate energy eigenvalues are calculated for certain values of the parameters involved.

INTRODUCTION

IT is known that one can construct classical nonlinear field theories in which all quantities of physical interest are finite.[1] In such theories, the nonlinearity in the field equations is so chosen as to ensure the existence of solutions which have a finite energy-momentum, most of which is concentrated in a finite volume, and which can therefore be interpreted as (classical) particles. The motion of these "particles" is thus fully defined by the field equations, and no separate equations of motion need (in fact, can consistently) be postulated. A simple example of such a field is the one defined by the Lagrangian density:

$$\mathfrak{L}=-\frac{\partial\psi}{\partial x_\lambda}\frac{\partial\psi^*}{\partial x_\lambda}-\sigma^2\psi\psi^*+\tfrac{1}{2}g\psi^2\psi^{*2}, \qquad (1)$$

$$(x_4=ict),$$

which is discussed classically in I.[1] Quantization of any nonlinear theory meets with difficulties of both computation and interpretation[2] (e.g., it may be impossible to find a straightforward method for diagonalizing the Hamiltonian even approximately). In this paper we suggest a quantization procedure which circumvents some of the former difficulties for a theory in which classical particles exist. The procedure consists in expanding the field ψ in a cubic space lattice of lattice constant D of real, classical, static, spherically symmetric, particle-like solutions $\theta(r)$,

$$\psi=\sum_{i,j,k} q_{ijk}\theta[|\mathbf{r}-(\mathbf{i}+\mathbf{j}+\mathbf{k})D|], \qquad (2)$$

and interpreting the expansion coefficients q_{ijk} as operators subject to the usual commutation relations. ($\mathbf{i}$, $\mathbf{j}$, $\mathbf{k}$ are integral multiples of mutually perpendicular unit vectors.) Equation (2) will perhaps appear plausible if we compare it with the well-known "expansion"

$$f(x)=\int f(x')\delta(x-x')dx',$$

and observe that the singular Dirac $\delta(x)$ is the way in which particle-like properties often appear in linear theories. Equation (2) enables us to compute approximate energy eigenvalues for certain values of the parameters σ, g, D. However, we are still faced with the fact that the Hamiltonian does not commute with the quantity that should be interpreted as the momentum of the field. (It should perhaps be noted that similar difficulties arise when the interaction of linear fields is considered.) Furthermore, the original relativistic invariance of the expression (1) is lost in the expansion (2). Finally, the parameter D has been introduced in an *ad hoc* fashion, and a criterion for fixing its value would have to be adopted.

SINGLE CLASSICAL PARTICLE

For simplicity, let us first formally work with one single classical particle, rather than the lattice (2). For that purpose, we recall from I that the field equation obtained from (1) in the spherically symmetric, static case [$\psi=\theta(r)$, θ real] is

$$d^2\theta/dr^2+(2/r)d\theta/dr-\sigma^2\theta=-g\theta^3, \qquad (3)$$

and has a countably infinite number of everywhere analytic, quadratically integrable solutions. Henceforth the symbol θ will refer exclusively to the simplest such solution, which is nodeless, has one finite maximum, and falls off exponentially outside a finite volume. The theory could presumably be extended to include other classical solutions as well.

Assume, then, that we have

$$\psi=q\theta. \qquad (4)$$

The Lagrangian density (1) then becomes

$$\mathfrak{L}=c^{-2}\dot{q}^2\theta^2-q^2\nabla\theta\cdot\nabla\theta-\tfrac{1}{2}gq^4\theta^4. \qquad (5)$$

Let us integrate this over space to get the Lagrangian $L=\int\mathfrak{L}dV$, using the abbreviations, more general than

* Present address: U. S. Naval Research Laboratory, Washington 25, D. C.

[1] N. Rosen, Phys. Rev. **55**, 94 (1939); Finkelstein, LeLevier, and Ruderman, Phys. Rev. **83**, 326 (1951); N. Rosen and H. B. Rosenstock, Phys. Rev. **85**, 257 (1952), henceforth referred to as I. The classical theory discussed by L. I. Schiff [Phys. Rev. **84**, 1 (1951)] differs from I by the sign of the nonlinear term and does not lead to isolated particle-like solutions.

[2] Other approaches to quantization of nonlinear theories have been given by R. J. Finkelstein, Phys. Rev. **75**, 1079 (1949); D. R. Yennie, Phys. Rev. **88**, 527 (1952); and L. I. Schiff, Phys. Rev. **92**, 764 (1953). Schiff utilizes a lattice expansion, although from a viewpoint different from the one here adopted. I wish to thank Professor Schiff for a prepublication copy of his paper.

needed at this point:

$$J_a/\sigma g=\int \theta(r)\theta(|\mathbf{r}-\mathbf{a}D|)dV,$$

$$J_{\nabla a g}/\sigma=\int \nabla\theta(r)\cdot\nabla\theta(|\mathbf{r}-\mathbf{a}D|)dV, \tag{6}$$

$$J_{abc}\sigma/g^2=\int \theta(r)\theta(|\mathbf{r}-\mathbf{a}D|)\theta(|\mathbf{r}-\mathbf{b}D|)\theta(|\mathbf{r}-\mathbf{c}D|)dV.$$

Here a, b, c are numbers and the dimensionless J's are thus presumably known. Using the relation $J_{\nabla a}+J_a=J_{00a}$ which follows from the field equation (3), we get, after a convenient change of scale $(\sigma g)^{-\frac{1}{2}}q\to q$,

$$L=M_0\dot{q}^2-K_{000}q^2+\tfrac{1}{2}\sigma g K_{000}q^4, \tag{7}$$

where we have put $M_a=c^{-2}J_a$ and $K_{abc}=\sigma^2 J_{abc}$. The procedure now is to define the conjugate momentum

$$p=\partial L/\partial\dot{q} \tag{8a}$$

and the Hamiltonian

$$H=p\dot{q}-L, \tag{8b}$$

and to calculate the eigenvalues of the latter with the assumed commutation relations

$$[p,q]=ih. \tag{9}$$

We find

$$H=p^2/4M_0+K_{000}q^2-\tfrac{1}{2}\sigma g K_{000}q^4, \tag{10}$$

representing a harmonic oscillator except for the q^4 term. The energy levels are known if the latter (i.e., its coefficient g) is small enough to be treated as a perturbation.[3] In that case

$$H_N=(h\sigma c/2)[(2N+1)(J_{000}/J_0)^{\frac{1}{2}} -(2N^2+2N+1)3hgc/32J_0]. \tag{11}$$

The number $N=0, 1, 2, \cdots$ may in the usual fashion be interpreted as the number of particles in the field. The values of J_0 and J_{000} are, by a rough numerical integration, found to be about 6.5π and 36π, respectively.

In view of the minus sign in front of the g term in (10), the potential is not strictly binding however small g may be. The number of levels in the potential valley will depend on the value of g. The maximum number of levels with spacing given by the first term in (11) that can get in below the peaks is found to be

$$N\lesssim 10/hgc; \tag{12}$$

the number of levels with small probability of escape by tunneling is, of course, smaller than that. In particular, we get no binding in the "strong-coupling" case of large g.

[3] See, e.g., L. Pauling and E. B. Wilson, *Introduction to Quantum Mechanics* (McGraw-Hill Book Company, Inc., New York, 1935), p. 160.

LATTICE OF CLASSICAL PARTICLES

Now, instead of (4), take

$$\psi=\textstyle\sum_i q_i\theta(r-iD). \tag{13}$$

The field is now expanded in a linear chain of classical particles, each q_i is an operator, and (8) and (9) are to be replaced by

$$p_i=\partial L/\partial\dot{q}_i,\quad H=\textstyle\sum_i p_i\dot{q}_i-L,\quad [p_i,q_j]=ih\delta_{ij}. \tag{14}$$

It should be remarked that although a superposition of solutions of the nonlinear field equation (3) is generally not a solution, (13) is nevertheless acceptable if D is so large that the interaction potential between two adjacent classical particles is proportional to $e^{-\sigma D}/\sigma D$, as will be assumed to be the case. The superposition can then be shown to differ from a solution by a term of the order $(e^{-\sigma D}/\sigma D)^2$.

Proceeding as in the preceding section, we obtain, in place of the one oscillator in (7),

$$L=\sum_{ij} M_{i-j}\dot{q}_i\dot{q}_j-\sum_{ij} K_{00i-j}q_iq_j +\tfrac{1}{2}\sigma g\sum_{ijkl} K_{i-j,\,i-k,\,i-l}q_iq_jq_kq_l, \tag{15}$$

an aggregate of such oscillators (the $i=j=k=l$ terms) coupled to each other (by the $i\neq j$ terms). The magnitude of the last sum is determined by the value of g, that of successive terms in each sum by the value of $e^{-\sigma D}$ (because, as is shown in I, $1/\sigma$ is a measure of the size of a single particle and for reasonably large D, K_{mns} and M_a fall off as $e^{-\sigma\sigma D}/a\sigma D$). For certain values of the dimensionless constants hgc and $e^{-\sigma D}$, certain terms in (15) may therefore be dropped.

Thus, if $e^{-\sigma D}$ is so small that all interaction terms are negligible, we are left with a set of oscillators like (11):

$$H_{\{N_i\}}=(h\sigma c/2)\textstyle\sum_i[(2N_i+1)(J_{000}/J_0)^{\frac{1}{2}} -(2N_i^2+2N_i+1)3hgc/32J_0]. \tag{16}$$

If, in addition, g is negligibly small, this reduces to a set of harmonic oscillators. Extension of (16) to the case where the field is represented by the three-dimensional lattice (2) rather than by (13) is straightforward.

If, on the other hand, hgc is so small that the third sum in (15) may be neglected entirely, but $e^{-\sigma D}$ is large enough to require retention of several terms in the first two sums, i.e.,

$$L=\textstyle\sum_{ij} M_{i-j}\dot{q}_i\dot{q}_j-\sum_{ij} K_{00i-j}q_iq_j, \tag{17}$$

then we must, prior to quantization, bring this into normal form

$$L=\textstyle\sum_r(\dot{Q}_r^2-\omega_r^2Q_r^2), \tag{18}$$

by introducing normal modes, which, for boundary conditions requiring that the 0th and Nth particle be held fast, turn out to be standing waves of the form $\sin(i\pi r/N)$ $(r=1, 2, \cdots, N)$. We find

$$H_{\{N_r\}}=\textstyle\sum_r(2N_r+1)\hbar\omega_r/2, \tag{19}$$

where

$$\omega_r^2=[\sum_l K_{00l}\cos(l\pi r/N)]/[\sum_l M_l(\cos l\pi r/N)]. \quad (20)$$

If $e^{-\sigma D}$ is so small that only nearest neighbors need to be retained, (20) may be written as

$$\omega_r\cong\omega_0\left[1+\tfrac{1}{2}\left(\frac{K_{001}}{K_{000}}-\frac{M_1}{M_0}\right)\cos(\pi r/N)\right], \quad (21)$$

$\omega_0=(K_{000}/M_0)^{\frac{1}{2}}$ being the harmonic oscillator frequency, and each level is seen to be split into N levels by the coupling.

On account of the interaction in all conceivable directions, extension to three dimensions of (19) and (20) is more complicated than previously, but presents no serious difficulties,[4] and there is no need for writing down the corresponding expressions here. In any case, for all σD, the coefficients K and M in each series of (20) or its equivalent fall off exponentially; each series converges for all r.

From the conservation laws,[5] the quantity

$$\mathcal{G}_k=(\partial\mathcal{L}/\partial\dot{\psi})(\partial\psi/\partial x_k)$$

should be interpreted as the k component of the momentum density of the field, and the momentum then becomes, with (1) and (13),

$$G=\sum_{ij} q_i q_j \int\theta(r-iD)\nabla\theta(r-jD)dV.$$

Since it is generally possible simultaneously to diagonalize two quadratic forms (such as the two appearing in the Hamiltonian) but not three, it follows that G will not commute with H.

I wish to thank Professor Nathan Rosen for patiently guiding the preparation of the thesis[4] from which this paper is taken, and for making countless suggestions. I am also grateful to Professor Wayne A. Bowers for discussions.

[4] H. B. Rosenstock, thesis, University of North Carolina, Chapel Hill, North Carolina, 1951 (unpublished).

[5] G. Wentzel, *Quantentheorie der Wellenfelder* (J. W. Edwards, Ann Arbor, 1946), Sec. 2.

PHYSICAL REVIEW VOLUME 93, NUMBER 2 JANUARY 15, 1954

Nucleon Isobars in Intermediate Coupling

FRANCIS H. HARLOW* AND BORIS A. JACOBSOHN
Department of Physics, University of Washington, Seattle, Washington

(Received August 17, 1953)

The energies of excited states of nucleons are calculated for the symmetric pseudoscalar meson theory with a fixed, extended source. A version of the Tomonaga method, which is shown to be approximately correct in the limit of strong coupling, is used. The calculation is carried out for moderate coupling by using trial functions with 0, 1, 2, and 3 mesons. Numerical results are presented for a source of the Yukawa shape. For coupling stronger than a critical strength which varies with state and source size, isobars are found for angular momenta $\frac{1}{2}$, $\frac{3}{2}$ and for isotopic spins $\frac{1}{2}$, $\frac{3}{2}$. The $(\frac{3}{2},\frac{3}{2})$ state always lies lowest in energy. A very large source ($\sim\frac{1}{3}$ the meson Compton wavelength) yields a $(\frac{1}{2},\frac{3}{2})$ isobar at ~350–400 Mev excitation, and a degenerate $(\frac{3}{2},\frac{1}{2})$ and $(\frac{1}{2},\frac{1}{2})$ pair at $\gtrsim$500 Mev. Other isobars lie considerably higher. Smaller sources correspond to higher excitation energies in this range of coupling strength.

I. INTRODUCTION

THE existence of nucleon isobars was first predicted by strong coupling meson theory. Since that time, isobars have been used in phenomenological theories in attempts to explain meson-nucleon[1] and nucleon-nucleon[2,3] scattering, and photomeson production.[4] Until now, the isobars of symmetric pseudoscalar theory have been examined only in the strong coupling limit.[5] The only relevant low-lying isobar predicted in that limit is the one for which $I=\frac{3}{2}$, $J=\frac{3}{2}$. As a result, this excited state is the one which has been considered in scattering problems, although there was no guarantee that at some smaller coupling another state could not lie lower in energy. We have, therefore, calculated the positions of the low-lying isobars using the intermediate-coupling theory of Tomonaga.[6,7]

There is no attempt in this paper to calculate the widths of the isobaric levels. The results should, nonetheless, be useful in predicting the order and approximate spacing of the excited nucleon levels. The motivation is comparable to that of theories of nuclear structure which attempt to predict the same features of the levels of complex nuclei.

One of the results of these calculations is that nucleon isobars do exist for surprisingly low coupling. The

* National Science Foundation Predoctoral Fellow. Present address: The University of California, Los Alamos Scientific Laboratory, Los Alamos, New Mexico.

[1] K. A. Brueckner, Phys. Rev. **86**, 106 (1952).
[2] J. Iwadare, Prog. Theoret. Phys. (Japan) **9**, 94 (1953).
[3] R. B. Raphael and J. Schwinger, Phys. Rev. **90**, 373 (1953).
[4] B. T. Feld, Phys. Rev. **89**, 330 (1953).
[5] W. Pauli and S. M. Dancoff, Phys. Rev. **62**, 85 (1942).
[6] S. Tomonaga, Prog. Theoret. Phys. (Japan) **2**, 6 (1947).
[7] R. Christian and T. D. Lee (to be published).

excitation energies for various source sizes are summarized in Figs. 2 through 5, and a discussion of these results is given in Secs. VI and VII. Some speculations on the relevance of these isobars to meson-nucleon scattering are presented in Sec. VIII.

II. THE TOMONAGA METHOD

We use pseudoscalar symmetric meson theory with a fixed, extended source. Inclusion of the repulsive core term which results from γ_5 coupling has been shown to be equivalent, in an energy calculation, to a change in the source shape and the coupling constant.[8] These changes are considered to have been included here. In particular, we choose a Yukawa source for the *modified* shape

$$\rho_{\text{eff}}(r)=(M^2/4\pi r)\exp(-Mr) \tag{1}$$

[with Fourier transform: $v(k)=M^2/(M^2+k^2)$], where M is the parameter which determines the size of the source.

In this modified problem, only $l=1$ waves interact with the source. Including only these terms, the Hamiltonian is (with $\hbar=c=$ meson mass $=1$)

$$H=\sum_{jak}\omega\bar{a}_j{}^a(k)a_j{}^a(k)+g(12\pi R)^{-\frac{1}{2}} \times\sum_{jak}k^2v(k)\omega^{-\frac{1}{2}}\sigma_j\tau^a[a_j{}^a(k)+\bar{a}_j{}^a(k)], \tag{2}$$

where the superscripts $\alpha=x,y,z$ refer to Cartesian components in charge space, and the subscripts $j=x,y,z$ refer to Cartesian components in ordinary space. $g^2/4\pi$ is the analog of the fine structure constant, R is the radius of the sphere in which the radial functions are quantized, and $\omega=(1+k^2)^{\frac{1}{2}}$. The $l=1$ part of the meson field operators is given by

$$\varphi^a=\sum_{jk}\left(\frac{3}{4\pi\omega R}\right)^{\frac{1}{2}}\frac{x_jF_k(r)}{r^2}[a_j{}^a(k)+\bar{a}_j{}^a(k)],$$

where $F_k(r)=krj_1(kr)$ of Schiff,[9] if the repulsive core is absent.

The Hamiltonian commutes with the operators I^2, I_z, J^2, and J_z where

$$I_z=\tfrac{1}{2}\tau^z-i\sum_{jk}[\bar{a}_j{}^x(k)a_j{}^y(k)-\bar{a}_j{}^y(k)a_j{}^x(k)] \equiv\tfrac{1}{2}\tau^z+T_z, \tag{3}$$

$$J_z=\tfrac{1}{2}\sigma_z-i\sum_{ak}[\bar{a}_x{}^a(k)a_y{}^a(k)-\bar{a}_y{}^a(k)a_x{}^a(k)] \equiv\tfrac{1}{2}\sigma_z+L_z. \tag{4}$$

A transformation which interchanges σ and τ and which simultaneously interchanges upper and lower indices leaves (2) unchanged and interchanges I and J. Thus, all energies and phase shifts will be unchanged by an interchange of I and J.

We now solve the problem $H\Psi=E\Psi$ by means of a variational method in which the trial function is subjected to the following restrictions: (a) It shall be an exact eigenfunction of each of the operators I^2, I_z, J^2, and J_z. (b) All mesons shall be in one mode. This point is further discussed in Appendix A.

The minimization of the energy with a trial function of this type is equivalent to solving exactly the new problem $H_T\Psi=E\Psi$ with

$$H_T=\tilde{\omega}\sum_{j\alpha}[\tilde{A}_j{}^aA_j{}^a+\gamma\tau^a\sigma_j(A_j{}^a+\tilde{A}_j{}^a)]\equiv\tilde{\omega}h_T. \tag{5}$$

Here

$$A_j{}^a\equiv\sum_k f(k)a_j{}^a(k);\quad \sum_k|f(k)|^2=1;$$

and

$$\tilde{\omega}\equiv\sum_k\omega|f(k)|^2;$$
$$\tilde{\omega}\gamma\equiv g(12\pi R)^{-\frac{1}{2}}\sum_k k^2v(k)\omega^{-\frac{1}{2}}f(k).$$

As Christian and Lee[7] have pointed out, the form of $f(k)$ can be determined from the energy minimization

$$f(k)=\frac{N(\lambda)}{R^{\frac{1}{2}}}\frac{k^2v(k)}{\omega^{\frac{1}{2}}(\omega+\lambda)},$$

where λ is a real parameter to be determined by further energy minimization and $N(\lambda)$ is a normalizing constant.

If we set

$$E=\tilde{\omega}(\lambda)U(\gamma^2), \tag{6}$$

then the problem separates into two parts. The first is independent of source, involving only the solution of the eigenvalue equation

$$h_T\Psi=U(\gamma^2)\Psi \tag{7}$$

for various values of the parameter γ. The second part, which does depend on source size and shape, is the minimization of the energy (6) with respect to λ for a fixed value of g. It is this feature of the separability of the problem which facilitates the calculation of results for a large number of source sizes.

III. MINIMIZATION OF THE ENERGY

The eigenvalue equation (7) is discussed in Secs. IV and V; here we develop the results of the energy minimization condition. It is convenient to define

$$L_n(\lambda)\equiv\frac{1}{\pi}\int_0^\infty\frac{k^4v^2(k)dk}{\omega(\omega+\lambda)^n}, \tag{8}$$

from which follows the property $L_n'(\lambda)=-nL_{n+1}(\lambda)$. The expression for $L_1(\lambda)$ is given in Appendix B. We then have

$$\frac{1}{N^2}=L_2,\quad \tilde{\omega}=\frac{L_1}{L_2}-\lambda,\quad \gamma^2=\left(\frac{g^2}{4\pi}\right)\frac{(L_1)^2}{3L_2\tilde{\omega}^2}. \tag{9}$$

From the foregoing it follows that

$$\frac{d\tilde{\omega}}{d\lambda}=\frac{2L_1L_3}{(L_2)^2}-2,\quad \frac{d\gamma^2}{d\lambda}=\frac{\gamma^2}{\tilde{\omega}}\left(\frac{\tilde{\omega}L_2}{L_1}-2\right)\frac{d\tilde{\omega}}{d\lambda}, \tag{10}$$

[8] C. H. Chang and B. A. Jacobsohn (to be published).
[9] L. I. Schiff, *Quantum Mechanics* (McGraw-Hill Book Company, Inc., New York, 1949), p. 77.

so that from (6) the condition of energy minimization becomes

$$\frac{\tilde{\omega}L_2}{L_1}=2-\frac{U(\gamma^2)}{\gamma^2}\frac{d\gamma^2}{dU}. \tag{11}$$

The left side of (11) is plotted as a function of λ in Fig. 1 for several source sizes.

Once (7) has been solved for a particular state, then (11) gives the best value of λ for a given value of γ^2. The corresponding values of E and g^2 are found from (6) and (9).

In the calculation, only those solutions with $\lambda \gtrsim -1$ are considered. This follows from the requirement that the meson field vanish at large distances, so that $f(k)$ must not have a pole on the real k axis. Except in the case of the ground state, this results in a minimum value of γ^2 (at $\lambda=-1$) below which the isobar ceases to exist. This critical value of γ^2 decreases with increasing source size.

IV. THE STRONG COUPLING LIMIT

Before proceeding to the intermediate coupling calculations, we wish to compare the Tomonaga predictions in the limit $\gamma^2 \gg 1$ with those of strong coupling theory.

Part of the Hamiltonian treated by Pauli and Dancoff[5] is similar to that in (5). From their paper we find for the low-lying levels:

$$U=-3\gamma^2+C_1+\frac{C_2}{\gamma^2}+\frac{J(J+1)-\frac{3}{4}}{8\gamma^2}, \quad I=J. \tag{12}$$

C_1 and C_2 are constants independent of I and J. We ignore them since they do not contribute to the excitation energy. They would have to be retained, however, in order to calculate the energy to the point of disappearance of the isobar ($\lambda=-1$) for a very small source.

Inserting (12) into (11) we find

$$\lambda \simeq -\left(\frac{L_1}{L_2}\right)_0 \frac{J(J+1)-\frac{3}{4}}{12\gamma^4}.$$

The leading term in (6) for $\gamma^2 \to \infty$ gives

$$E=-L_1(0)g^2/4\pi$$

and the Yukawa shape for the meson field, in exact agreement with the Pauli-Dancoff result.[6] Disagreement occurs in the excitation energies, where our result must be divided by a source-size dependent factor $K=[L_1L_3/(L_2)^2]_0$ in order to agree with strong-coupling theory. Some typical values of K are $K=1.23$ for $M=0$, $K=1.59$ for $M=2$, $K=1.94$ for $M=7$, and $K=2.47$ for $M=\infty$ (point source). We see, then, that this version of the Tomonaga method, which agrees exactly with the leading term of weak-coupling theory, agrees qualitatively in the limit of strong coupling.

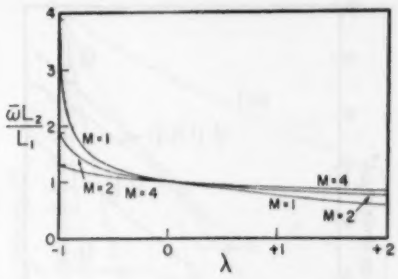

FIG. 1. $\tilde{\omega}L_2/L_1$ plotted as a function of λ for various source sizes [see Eq. (11)].

V. MODERATE COUPLING

We now turn to the problem of solving the eigenvalue problem (7) with $\gamma^2 \lesssim 1$. One should notice particularly that it is not g^2 but γ^2 which determines the coupling strength. They are related by the source-dependent factor of (9). In this region, one may expect to get a good approximation to $U(\gamma^2)$ by using a trial function which contains only a small number of mesons less than or equal to some given number N. The validity of this limitation is discussed in Sec. VI. Since this region probably covers the case of physical interest, it is the only one we have investigated.

The trial function is now of the form

$$\Psi=\sum_{n=0}^{N}\sum_{L=J\pm\frac{1}{2}}\sum_{T=I\pm\frac{1}{2}}\sum_{j}{}^{(n)}{}_jA_L{}^T\,{}^{(n)}{}_j\Psi_{JL}{}^{IT}, \tag{13}$$

where the ${}^{(n)}{}_j\Psi_{JL}{}^{IT}$ are orthonormal eigenfunctions with the indicated quantum numbers, containing just n mesons. The subscript j enumerates the several possible states that may exist with the same quantum numbers and the same n. Table I lists the number of meson states which exist for various n when all mesons are put into one spatial mode. The table was constructed by making use of the properties of the representations of the symmetric group. Only those meson states are included which can be combined with nucleon spins to give I, $J=\frac{1}{2}$ and $\frac{3}{2}$. Since the number of states doubles in going from 3 to 4 mesons, we have cut off the calculation at $N=3$. The wave functions ${}^{(n)}{}_j\Psi_{JL}{}^{IT}$ are formed from the spin and isotopic spin functions of the nucleon combined with the meson functions which are given in Appendix C.

TABLE I. The number of states with given T and L for various values of n (number of mesons).

(T,L)	$n=0$	1	2	3	4	5	6
(0,0)	1		1	1	2	1	3
(0,1) or (1,0)							
(1,1)		1	1	2	2	4	4
(0,2) or (2,0)			1		2	1	3
(1,2) or (2,1)				1	1	2	2
(2,2)			1	1	3	3	7

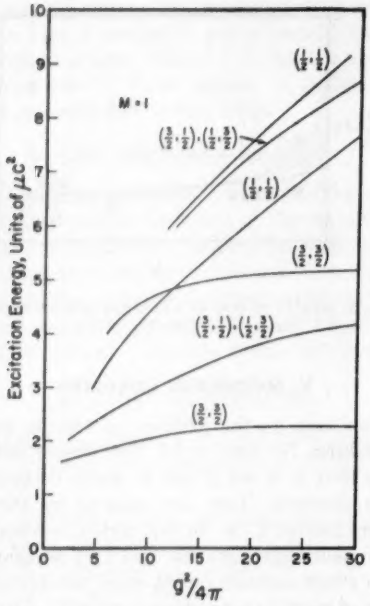

FIG. 2. Excitation energy as a function of coupling for $M=1$.

The calculations from this point on involve many details which are omitted here. A summary of the most important formulas involved in the solution of (7) is given in Appendix D. The solutions for $U(\gamma^2)$ are combined with graphs of the relevant source-dependent quantities appearing in (6), (9), and (11) to give the energy of each state as a function of g^2. Figures 2 through 5 show the results of the calculations of excitation energies for various source sizes. In Fig. 6 we have plotted the absolute energies of the ground state for comparison with the magnitudes of the excitation energies.

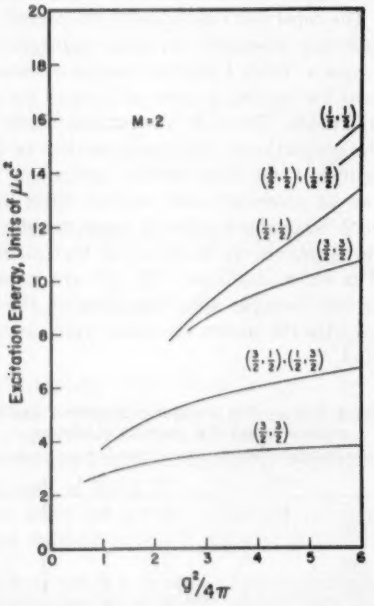

FIG. 3. Excitation energy as a function of coupling for $M=2$.

VI. EFFECT OF NEGLECTING THE FOUR-MESON AMPLITUDES

The errors introduced by cutting off the trial functions at three mesons are here shown to be small in the coupling region of interest. This may be seen from two aspects.

Consider, first, the probabilities P_n for finding n mesons. These are plotted as functions of γ^2 for the ground state in Fig. 7, for the lowest $(\frac{3}{2},\frac{3}{2})$ isobar in Fig. 8, and for the lowest $(\frac{3}{2},\frac{1}{2})$ isobar in Fig. 9. The probabilities do not approach the proper strong coupling limit of zero, since they were calculated from the amplitudes of Appendix D. Nevertheless, it is reasonable to assume that the curves are qualitatively correct in the region for which $P_3(\gamma^2)$ is less than one-half of its asymptotic value. From this, we are led to infer that P_4, which we have neglected, is actually quite small for $\gamma^2 \leqslant \frac{3}{4}$.

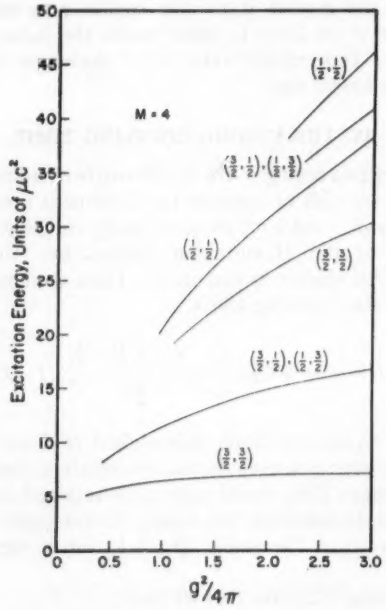

FIG. 4. Excitation energy as a function of coupling for $M=4$.

The association of these probability curves with Figs. 3, 5, and 6 may be accomplished through Table II which gives the relation between γ^2 and $g^2/4\pi$ for several states and source sizes. The first entry in the table for each state is the critical coupling below which the isobar disappears. Table II shows quite clearly the smallness of γ^2 for a large source ($M=2$) and the be-

ginning of the breakdown of the approximation for a small source ($M=7$).

The second justification for the neglect of P_4 is presented in Figs. 10 and 11, which refer only to the case $M=2$. Figure 10 displays the ground-state energy with the trial functions cut off successively at $N=1$, $N=2$, and $N=3$ mesons; Fig. 11 shows the decrease in excitation energy as the calculation is improved one step.[10] The latter figure especially shows the satisfactory empirical convergence of the excitation energy for a large source.

In summary, the above evidence indicates that the excitation energies of the two lowest isobars for large

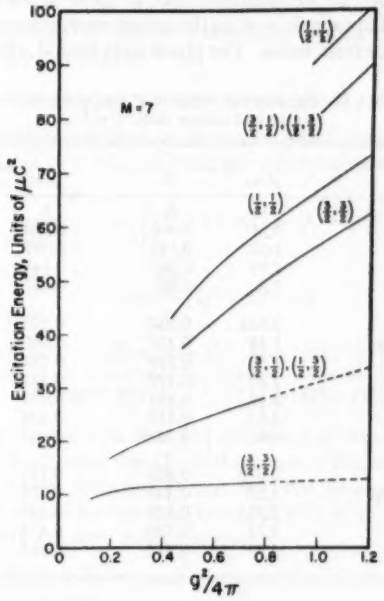

FIG. 5. Excitation energy as a function of coupling for $M=7$.

sources ($M \lesssim 2$) would not be changed significantly by the inclusion of more mesons in the trial function (13). The accuracy of our results decreases for higher isobars with a given source size, or for smaller sources with a given isobar. However, even in a rather extreme case, our results should have at least a rough qualitative significance; for example, for $M=7$ (see Fig. 5) the first $(\frac{1}{2},\frac{1}{2})$ isobar begins at $\gamma^2=1.4$, and the second $(\frac{3}{2},\frac{3}{2})$ begins at $\gamma^2=1.54$.

None of the foregoing remarks should be interpreted as an estimate of the accuracy of the Tomonaga approximation, the justification of which remains solely its agreement with the limits of weak and strong coupling theory.

[10] In each case, the excitation energy was calculated by subtracting the ground-state energy with $N-1$ from the isobar energy with N.

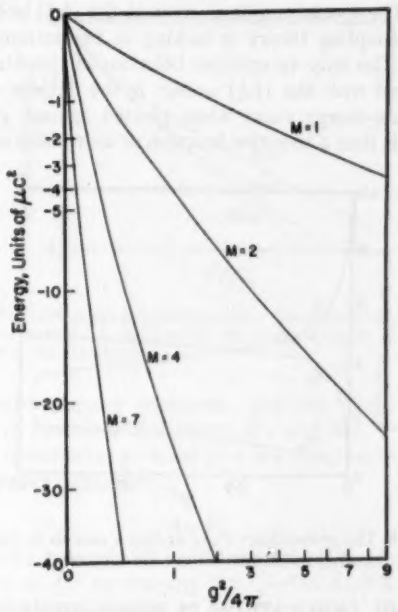

FIG. 6. Energy of the ground state as a function of coupling for various source sizes.

VII. DISCUSSION OF ISOBAR ENERGIES

From the results shown in Figs. 2 through 5, we observe the following features:

(a) No stable isobars ($E_{ex}<1$) exist for this range of coupling and source size.

(b) In all cases, the first excited nucleon state is $(\frac{3}{2},\frac{3}{2})$ and the second is the pair $(\frac{3}{2},\frac{1}{2})$, $(\frac{1}{2},\frac{3}{2})$. The crossing of two higher levels in Fig. 2 illustrates why it was not *a priori* obvious that the two lower levels would never cross.

(c) It is believed that the initial rise in excitation energy with increasing coupling is a real effect (see Sec. VI), although the lowest state must eventually drop.

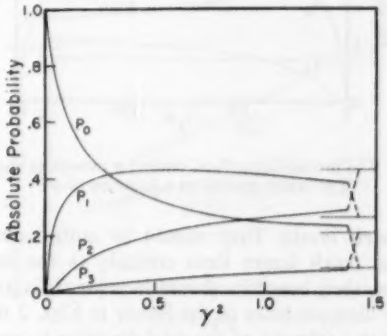

FIG. 7. The probabilities P_n of finding n mesons in the ground state plotted as a function of γ^2.

(d) The special emphasis given to the $(\frac{3}{2},\frac{3}{2})$ isobar by strong coupling theory is lacking in the intermediate region. The only exceptional behavior of this state, as compared with the $(\frac{3}{2},\frac{1}{2})$ isobar, is the flatness of the excitation-energy curve when plotted against g^2. The energy is thus a sensitive function of source size only.

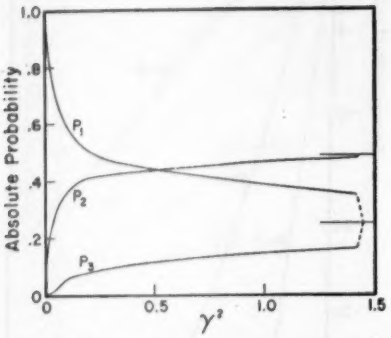

FIG. 8. The probabilities P_n of finding n mesons in the first $(\frac{3}{2},\frac{3}{2})$ isobar plotted as a function of γ^2.

VIII. IMPLICATIONS IN MESON-NUCLEON SCATTERING

Since the concept of isobars is directly related to meson-nucleon scattering, it is of interest to speculate on the consequences of these results when applied qualitatively to a discussion of phase shifts. (A calculation of the effect of the isobaric states on the scattering is under way.)

(a) From the consideration of a simple analogy, the scattering of a particle by a square potential barrier, we extrapolate the following comments on the width of

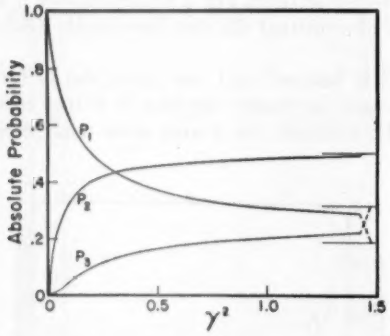

FIG. 9. The probabilities P_n of finding n mesons in the first $(\frac{3}{2},\frac{1}{2})$ isobar plotted as a function of γ^2.

the isobaric levels. They should be quite narrow for couplings much larger than critical; as the coupling decreases, their breadths should increase. It is probable that the disappearance of the isobar in Figs. 2 through 5 marks the attempt of the trial function to represent the disappearance of the true resonance in the scattering as the coupling is decreased. The value of the critical coupling, however, is markedly affected by changes in the trial function (see Fig. 11), moving apparently in the direction of weaker coupling as the trial function is improved.

(b) A resonance in $(\frac{3}{2},\frac{3}{2})$ scattering has been suggested[1] to be at about 300 Mev. Figures 3 and 4 indicate possible agreement with the large source sizes ($M=2$ to 4) indicated by Chew.[11]

(c) For a large source, the $(\frac{3}{2},\frac{1}{2})$ isobar lies at one- to two-hundred Mev above the $(\frac{3}{2},\frac{3}{2})$ level. If the former level is broad, then this is consistent with experiments[12,13] which suggest that the phase shift may change sign at 90 Mev. The low-energy phase shift is predicted by Chew[11] to be negative, but if there is an isobar, $\tan\delta$ will approach $+\infty$ as the meson energy approaches resonance from below. The phase shift should, therefore, change from negative to positive below the resonance energy, although a broad resonance is needed to produce this effect as low as $\sim$100 Mev.

TABLE II. The relation between g^2 and γ^2 for various states and source sizes. $N=3$.

State	$M=2$ $g^2/4\pi$	$M=2$ γ^2	$M=7$ $g^2/4\pi$	$M=7$ γ^2
$(\frac{1}{2},\frac{1}{2})$	0	0	0	0
ground	0.61	0.066	0.039	0.068
	1.53	0.140	0.097	0.138
	4.19	0.297	0.147	0.188
	7.3	0.46	0.267	0.287
$(\frac{3}{2},\frac{3}{2})$	0.644	0.135	0.123	0.396
first isobar	1.18	0.225	0.180	0.470
	1.50	0.270	0.254	0.562
	2.39	0.379	0.337	0.635
	3.11	0.453	0.433	0.750
	3.83	0.519	0.508	0.818
	6.86	0.743	0.843	1.08
$(\frac{3}{2},\frac{1}{2})$	0.975	0.205	0.197	0.617
first isobar	1.55	0.307	0.279	0.728
	2.37	0.427	0.343	0.812
	3.72	0.590	0.453	0.943
	5.99	0.812	0.562	1.06

We would like to thank Dr. John S. Blair for many stimulating and helpful discussions.

APPENDIX A. THE SINGLE MODE RESTRICTION

In his original application of the variational method to charged scalar mesons, Tomonaga[6] introduced two independent non-orthogonal modes, one for positive and one for negative mesons. In this way, he was able to achieve exact agreement in excitation energy with the strong coupling theory. He was able to make this two-mode assumption because his concern was only with charge symmetry. In our case, the requirement that the trial functions possess symmetry properties

[11] G. F. Chew, Phys. Rev. **89**, 591 (1953).
[12] Anderson, Fermi, Martin, and Nagle, Phys. Rev. **91**, 155 (1953).
[13] Bodansky, Sachs, and Steinberger, Phys. Rev. **90**, 997 (1953).

with respect to continuous rotations in charge and ordinary space makes it impossible to put the different kinds of mesons in different modes.

At the expense of considerable extra computational labor, it would be possible to relax the single mode restriction in a way that is illustrated by the following example. A $(\frac{1}{2},\frac{1}{2})$ wave function can always be written

$$\Psi_{\frac{1}{2}}^{\frac{1}{2}}=\Psi_{\frac{1}{2},0}^{\frac{1}{2},0}+\Psi_{\frac{1}{2},1}^{\frac{1}{2},1}+\Psi_{\frac{1}{2},0}^{\frac{1}{2},1}+\Psi_{\frac{1}{2},1}^{\frac{1}{2},0}. \quad \text{(A.1)}$$

One can choose a trial function in which the mesons in the first state are all in one mode, those of the second state are in another non-orthogonal mode, and those in the last two states are in combinations of the two. We have not chosen such trial functions, since their use would be at the sacrifice of the simple splitting of the problem into the source independent part, (7), and source dependent part, (11).

APPENDIX B. THE INTEGRALS L_n

The integrals defined in (8) can be found from the relation $L_n'(\lambda)=-nL_{n+1}(\lambda)$ and the following expression:

$$L_1(\lambda)=\frac{M^4}{\pi(M^2+\lambda^2-1)^2}\Big\{(\lambda^2-1)^{\frac{1}{2}}\ln[\lambda+(\lambda^2-1)^{\frac{1}{2}}]$$
$$-\frac{M^2\lambda(M^2+\lambda^2-1)}{2(M^2-1)}+\frac{M\pi}{4}(M^2+3\lambda^2-3)$$
$$+\frac{M\lambda(2M^2\lambda^2-3M^2-3\lambda^2+3)}{4(M^2-1)^{\frac{1}{2}}}\ln\frac{M-(M^2-1)^{\frac{1}{2}}}{M+(M^2-1)^{\frac{1}{2}}}\Big\}, \quad \text{(B.1)}$$

for $\lambda>1$. In the case that $|\lambda|<1$, the first term in the bracket is replaced by $(1-\lambda^2)^{\frac{1}{2}}\arccos\lambda$. (The value of $\arccos\lambda$ varies between 0 and π.) We have used a Yukawa source for which $v(k)=M^2/(M^2+k^2)$.

At $\lambda=0$, the first three integrals are:

$$L_1(0)=\frac{M^4(M+2)}{4(M+1)^2},$$
$$L_2(0)=\frac{M^4}{2\pi(M^2-1)^2}\Big[M^2+2-\frac{3M}{2(M^2-1)^{\frac{1}{2}}}\times\ln\frac{M+(M^2-1)^{\frac{1}{2}}}{M-(M^2-1)^{\frac{1}{2}}}\Big],$$
$$L_3(0)=\frac{M^4}{4(M+1)^3}. \quad \text{(B.2)}$$

APPENDIX C. WAVE FUNCTIONS

Since the amplitudes ${}^{(n)}{}_ja_L{}^T$ of Eq. (13) are useful in scattering calculations, we will give the expressions from which they may be found in Appendix D; first, it is necessary to give explicitly the phases of the functions that they multiply. We have adhered to the Condon and Shortley[14] conventions for adding nucleon- and meson-angular momenta, and for the relative phases of functions of different M_T and M_L. For each T and L, however, we must give one function to determine phases completely.

[14] E. U. Condon and G. H. Shortley, *The Theory of Atomic Spectra* (The Cambridge University Press, London, 1951), Chap. III.

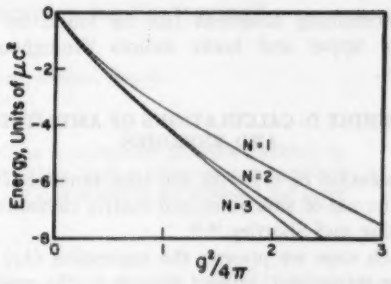

FIG. 10. Subsequent approximations to the ground-state energy for source size $M=2$. N refers to the largest number of mesons included in the calculation.

$n=1$:

The nine operators $\bar{A}_{0,+,-}{}^{0,+,-}$ are determined uniquely in terms of $\bar{A}_j{}^\alpha$ by defining ${}^{(1)}\Phi_{1,M}{}^{1,M'}\equiv\bar{A}_M{}^{M'}\Phi_{\text{vac}}$ and applying the operators $L_{+,-}$, L_z, $T_{+,-}$, and T_z [see (3) and (4)] to the equation ${}^{(1)}\Phi_{1,0}{}^{1,0}\equiv\bar{A}_z{}^z\Phi_{\text{vac}}$.

$n=2$:

$${}^{(2)}\Phi_{0,0}{}^{0,0}=(\sqrt{2}/3)[\bar{A}_+{}^+\bar{A}_-{}^-+\bar{A}_+{}^-\bar{A}_-{}^+-\bar{A}_0{}^+\bar{A}_0{}^-$$
$$-\bar{A}_+{}^0\bar{A}_-{}^0+\tfrac{1}{2}(\bar{A}_0{}^0)^2]\Phi_{\text{vac}},$$
$${}^{(2)}\Phi_{1,1}{}^{1,1}=(1/\sqrt{2})[\bar{A}_+{}^+\bar{A}_0{}^0-\bar{A}_0{}^+\bar{A}_+{}^0]\Phi_{\text{vac}},$$
$${}^{(2)}\Phi_{0,0}{}^{2,2}=6^{-\frac{1}{2}}[2\bar{A}_+{}^+\bar{A}_-{}^+-(\bar{A}_0{}^+)^2]\Phi_{\text{vac}},$$
$${}^{(2)}\Phi_{2,2}{}^{2,2}=(1/\sqrt{2})(\bar{A}_+{}^+)^2\Phi_{\text{vac}}.$$

$n=3$:

$${}^{(3)}\Phi_{0,0}{}^{0,0}=6^{-\frac{1}{2}}\,\text{Det}|\bar{A}_{+,0,-}{}^{+,0,-}|\Phi_{\text{vac}},$$
$$_\alpha{}^{(3)}\Phi_{1,1}{}^{1,1}=3(11)^{-\frac{1}{2}}\bar{A}_+{}^+\,{}^{(2)}\Phi_{0,0}{}^{0,0},$$
$$_\beta{}^{(3)}\Phi_{1,1}{}^{1,1}=(\sqrt{2}/3)\,{}_\alpha{}^{(3)}\Phi_{1,1}{}^{1,1}-[(11)^{\frac{1}{2}}/10][\bar{A}_+{}^+\,{}^{(2)}\Phi_{0,0}{}^{2,0}$$
$$-\sqrt{3}\bar{A}_+{}^0\,{}^{(2)}\Phi_{0,0}{}^{2,1}+6^{\frac{1}{2}}\bar{A}_+{}^-\,{}^{(2)}\Phi_{0,0}{}^{2,2}],$$
$${}^{(3)}\Phi_{1,1}{}^{2,2}=(1/\sqrt{2})\bar{A}_+{}^+\,{}^{(2)}\Phi_{0,0}{}^{2,1}-\bar{A}_+{}^0\,{}^{(2)}\Phi_{0,0}{}^{2,2},$$
$${}^{(3)}\Phi_{2,2}{}^{2,2}=(\sqrt{2}/\sqrt{3})\bar{A}_+{}^+\,{}^{(2)}\Phi_{1,1}{}^{1,1}.$$

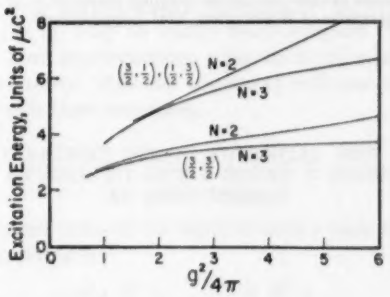

FIG. 11. Subsequent approximations to the excitation energies of the first two isobars for source size $M=2$.

The remaining functions can be found by interchanging upper and lower indices throughout any equation.

APPENDIX D. CALCULATIONS OF AMPLITUDES AND ENERGIES

The solution of (7) with the trial function (13) requires the use of sum rules and matrix elements given by Condon and Shortley.[14,15]

In each case we present the expression $\langle h_T \rangle$ which must be minimized, subject always to the restriction that $\sum|{}^{(n)}{}_\beta a_L{}^T|^2=1$. The result of this minimization is a set of equations for the amplitudes and an eigenvalue equation. In the following, we shall use $X\equiv U-1$, $Y\equiv U-2$, $Z\equiv U-3$.

(a) $I=J=\frac{1}{2}$

$$a={}^{(0)}a_0{}^0,\quad b={}^{(1)}a_1{}^1,\quad c={}^{(2)}a_0{}^0,\quad d={}^{(2)}a_1{}^1,\quad e={}_\alpha{}^{(3)}a_1{}^1,$$
$$f=(83)^{-\frac{1}{2}}[(33)^{\frac{1}{2}}\,{}^{(3)}a_0{}^0+(50)^{\frac{1}{2}}\,{}_\beta{}^{(3)}a_1{}^1]$$
$${}_\beta{}^{(3)}a_1{}^1=(50/33)^{\frac{1}{2}}\,{}^{(3)}a_0{}^0$$
$$\langle h_T\rangle=|b|^2+2[|c|^2+|d|^2]+3[|e|^2+|f|^2]$$
$$+\gamma\{3\bar{b}a+\sqrt{2}[\bar{c}+2\bar{d}]b+(11)^{\frac{1}{2}}\bar{e}c$$
$$+(11)^{-\frac{1}{2}}[4\bar{e}+(83)^{\frac{1}{2}}\bar{f}]d+\text{comp. conj.}\}. \quad \text{(D.1)}$$

The eigenvalue equation is

$$UXY^2Z^2-(20UX+10UZ+9YZ)YZ\gamma^2$$
$$+(83UX+74UZ+180YZ)\gamma^4-747\gamma^6=0. \quad \text{(D.2)}$$

As expected, there is only one root which goes to zero as $\gamma^2\to 0$. This is the ground state for which Eq. (11) possesses solutions for $\lambda\geqslant 0$ with any value of γ^2. The next two roots belong to isobars, for they correspond to solutions of Eq. (11) with $\lambda>-1$ provided γ^2 is large enough. The three highest roots of (D.2) do not correspond to solutions of (11); i.e., the energy in these cases does not possess a minimum when λ is varied.

(b) $I=\frac{3}{2}$, $J=\frac{1}{2}$

$$a={}^{(1)}a_1{}^1,\quad b={}^{(2)}a_1{}^1,\quad c={}^{(2)}a_0{}^2,\quad d={}_\alpha{}^{(3)}a_1{}^1,$$
$$e={}_\beta{}^{(3)}a_1{}^1,\quad f={}^{(3)}a_1{}^2.$$

[14,15] For more details refer to the doctoral thesis by F. H. Harlow at the University of Washington, 1953 (unpublished).

Rotate axes in d, e, f space, introducing three new orthonormal amplitudes g, h, k with

$$g=(88)^{-\frac{1}{2}}[(10)^{\frac{1}{2}}d-(45)^{\frac{1}{2}}e+(33)^{\frac{1}{2}}f],$$
$$h=-\left(\frac{5}{31}\right)^{\frac{1}{2}}\left[\frac{3}{10}\left(\frac{5}{11}\right)^{\frac{1}{2}}d+\frac{7}{4}\left(\frac{10}{11}\right)^{\frac{1}{2}}e+\frac{3}{2}\left(\frac{3}{2}\right)^{\frac{1}{2}}f\right].$$

One then finds $k=0$ and

$$\langle h_T\rangle=|a|^2+2[|b|^2+|c|^2]+3[|g|^2+|h|^2]$$
$$-\gamma\{\bar{a}[(2)^{\frac{1}{2}}b+(5)^{\frac{1}{2}}c]+\tfrac{1}{2}(5)^{\frac{1}{2}}\bar{b}[g-(31/5)^{\frac{1}{2}}h]$$
$$+(8)^{\frac{1}{2}}\bar{c}g+\text{comp. conj.}\}, \quad \text{(D.3)}$$
$$XY^2Z^2-(17X+7Z)YZ\gamma^2+(62X+41Z)\gamma^4=0. \quad \text{(D.4)}$$

The two lowest roots correspond to solutions of (11) for sufficiently large values of γ^2.

(c) $I=J=\frac{3}{2}$

$$a={}^{(1)}a_1{}^1,\quad b={}^{(2)}a_1{}^1,\quad c={}^{(2)}a_2{}^2,\quad d={}_\alpha{}^{(3)}a_1{}^1,$$
$$e={}_\beta{}^{(3)}a_1{}^1,\quad f={}^{(3)}a_2{}^2,\quad \sqrt{2}g={}^{(3)}a_1{}^2={}^{(3)}a_2{}^1.$$

Replace d, e, f, and g by the orthonormal amplitudes h, j, k, and l where

$$h=\left(\frac{2}{27}\right)^{\frac{1}{2}}\left[\frac{1}{(11)^{\frac{1}{2}}}d+\frac{5}{4}\left(\frac{2}{11}\right)^{\frac{1}{2}}e+\frac{5}{2}\left(\frac{3}{2}\right)^{\frac{1}{2}}f+\left(\frac{15}{4}\right)^{\frac{1}{2}}g\right],$$
$$j=-\frac{5}{3(61)^{\frac{1}{2}}}\left[\frac{13}{3}\left(\frac{3}{11}\right)^{\frac{1}{2}}d+\frac{7}{15}\left(\frac{6}{11}\right)^{\frac{1}{2}}e+\frac{7}{2}\sqrt{2}f-\frac{8}{5^{\frac{1}{2}}}g\right].$$

One then finds $k=l=0$, and

$$\langle h_T\rangle=|a|^2+2[|b|^2+|c|^2]+3[|h|^2+|j|^2]$$
$$+\gamma\left\{\bar{a}[b+5c]/\sqrt{2}+(27/2)^{\frac{1}{2}}\bar{b}h\right.$$
$$\left.+\frac{5}{3(6)^{\frac{1}{2}}}\bar{c}h-\frac{2(61)^{\frac{1}{2}}}{3(3)^{\frac{1}{2}}}\bar{c}j+\text{comp. conj.}\right\}, \quad \text{(D.5)}$$
$$XY^2Z^2-(23X+13Z)YZ\gamma^2$$
$$+(122X+161Z)\gamma^4=0. \quad \text{(D.6)}$$

Again the two lowest roots correspond to isobars.

One of Schwinger's Variational Principles for Scattering*

GEOFFREY F. CHEW
Department of Physics, University of Illinois, Urbana, Illinois
(Received October 2, 1953)

An approximation method for scattering calculations, based on a variational principle invented by Schwinger, is discussed. The method is tractable even for interactions, such as the pion-nucleon, which are not diagonal in configuration space. Criteria of validity for the approximation are proposed and made plausible by examples.

SINCE the "potentials" which occur in field theoretical treatments of the pion-nucleon scattering problem are not diagonal in configuration space, one is faced in general with the solution of an integral equation. It is the purpose of this note to discuss an approximate solution of the general scattering integral equation which is based on one of Schwinger's variational principles. This solution is very easy to obtain and is likely to be especially useful in the pion-nucleon case.[1]

It will be assumed that somehow or other, one has found the interaction operator responsible for the scattering.[2] If the kinetic energy of the system is denoted by H_0, and the interaction energy by V, then a possible approach to the scattering problem is to find the solution ψ_a of the following time-independent integral equation:[3]

$$\psi_a=\phi_a+P\frac{1}{E_a-H_0}V\psi_a. \tag{1}$$

ϕ_a is the eigenfunction of H_0, belonging to E_a, which represents either the initial or the final state of the system. The symbol P indicates that the principal value is to be taken of the integral which gives a meaning to the inverse operator. The tangents of the scattering phase shifts are then proportional to the eigenvalues of the reactance matrix[3] K, defined by

$$K_{ba}=(\phi_b, V\psi_a)=(\psi_b, V\phi_a). \tag{2}$$

Now Schwinger[4] has proposed the following general stationary expression for the reactance matrix:

$$K_{ba}=\frac{(\phi_b, V\psi_a)(\psi_b, V\phi_a)}{(\psi_b, V\psi_a)-\left(\psi_b, V\frac{1}{E-H_0}V\psi_a\right)}. \tag{3}$$

Equation (3), when $E_a=E_b=E$, is stationary for variations of ψ_a and ψ_b about the correct solutions of (1). Its importance stems from the fact that it depends on the unknown functions only "within the range" of the interaction V, and even then is independent of the normalization of these functions. If one can find enough symmetry principles to reduce the problem at once to single nonmixing "channels," Eq. (3) is enormously powerful; for ψ_a and ψ_b are then identical and have only one component which depends on only a single variable. If the unknown function has no more than one node within the range of V (i.e., no more than one bound state exists) then almost any simple guess is likely to give a good answer.

Schwinger originally used the zero-energy solutions of (1) as trial functions in (3) to derive the famous and phenomenally accurate effective-range treatment of low-energy nucleon-nucleon scattering. We here wish to explore simpler although energy-dependent trial functions, namely the "unperturbed" functions ϕ_a and ϕ_b. If it is supposed that only a single channel, $a=b=j$, is involved, then from these trial functions one obtains

$$K_{jj}\approx\frac{V_{jj}^2}{V_{jj}-P\sum_k V_{jk}\frac{1}{E_j-E_k}V_{kj}}=\frac{V_{jj}}{1-\Delta_j}, \tag{4}$$

where

$$\Delta_j=\frac{1}{V_{jj}}P\sum_k\frac{|V_{jk}|^2}{E_j-E_k}.$$

The evaluation of the approximation (4) involves exactly the same computations as does the second Born approximation and can easily be seen to yield the second Born approximation when $\Delta_j\ll 1$. However, the expression (4) may be vastly more accurate than the second Born approximation when Δ_j is not small compared to unity. This last statement will now be illustrated with three examples.

(1) ATTRACTIVE STATIC POTENTIAL JUST DEEP ENOUGH TO GIVE A BOUND S STATE AT ZERO ENERGY

The exact value of the depth of such a potential with a square shape is

$$\frac{\pi^2}{8}\left(\frac{\hbar^2}{mr_0^2}\right)=1.234\left(\frac{\hbar^2}{mr_0^2}\right),$$

* This research was supported by the U. S. Office of Naval Research.

[1] An application of the same method to atomic scattering has been made by S. Altshuler, Phys. Rev. **89**, 1278 (1953).

[2] See, for example, K. Brueckner and K. M. Watson, Phys. Rev. **90**, 699 (1953) as well as A. Klein, Phys. Rev. **91**, 1285 (1953).

[3] B. A. Lippmann and J. Schwinger, Phys. Rev. **79**, 469 (1950). In the appendix, the exact relation between the phase shift and the reactance matrix is reproduced from this reference.

[4] J. Schwinger, "Lectures on nuclear physics," Harvard University, 1947 (unpublished). A discussion of the application to the low-energy nuclear force problem may be found in an article by J. Blatt and J. D. Jackson, Phys. Rev. **76**, 18 (1949).

if r_0 is the range and m the (reduced) mass. If we use the approximation (4), on the other hand, and ask for that value of the potential depth which makes $\Delta_j=1$ at $E_j=0$, we find

$$\frac{5}{4}\left(\frac{\hbar^2}{mr_0^2}\right)=1.250\left(\frac{\hbar^2}{mr_0^2}\right),$$

an error of only 1.3 percent. The Born expansion is, of course, completely incapable of handling such resonance scattering. Since our trial function can only improve, relatively speaking, as the energy increases, we see that our approximation will be reasonably accurate at all energies for attractive velocity-independent potentials, at least if they do not produce a very strongly bound state and are not unusually singular.

The approximation becomes less accurate for more singular potentials. With an exponential well the error for the above problem is 10 percent and for a Yukawa well it is 20 percent. We make the conjecture that for the approximation to be valid the ratio of the largest important impact parameter to the smallest must be moderate, say less than 5. A similar statement would hold for the largest and smallest important momenta if one chooses to work in momentum space.

(2) INFINITELY STRONG REPULSIVE POTENTIAL OF RANGE r_0

The exact scattering length at zero energy for such a potential is, of course, just equal to r_0. Using the approximation (4), one finds a scattering length $(5/6)r_0$, or an error of 17 percent. Again the Born expansion is completely useless. Note that this is about the most unfavorable case one can imagine for a purely repulsive ordinary potential.

If one investigates potentials which change sign, e.g., are repulsive at short distances and attractive at large, one finds the approximation inadequate. (The trial function apparently cannot "adjust" its amplitude in a way suitable to both regions.)

(3) A VELOCITY-DEPENDENT POTENTIAL WITH FACTORABLE MATRIX ELEMENTS

We consider finally a potential with momentum matrix elements of the form $(k_2|V_j|k_1)=\lambda g_j(k_2)g_j(k_1)$. The spatial matrix elements of such a potential are also factorable, i.e., $(x_2|V_j|x_1)=\lambda f_j(x_2)f_j(x_1)$, where $f_j(x)$ is the Fourier transform of $g_j(k)$. The index j is written to indicate that the potential may be different in the different channels. It is possible to solve this problem exactly, and one finds

$$K_{jj}=\lambda g_j^2(k_0)\Big/\left[1-P\sum_k\frac{\lambda g_j^2(k)}{E_0-E_k}\right],$$

which a casual inspection shows is identical with the result given by the approximation (4). Thus, our approximation here *always* gives the correct answer, regardless of how strong the potential is and whether it is attractive or repulsive.[5] It is because the pion-nucleon potentials which result from field theory are often "almost" factorable that one feels especially confident that our approximation should handle them accurately. The method has already been used by Chew[6] in discussing a weak-coupling extended-source meson theory.

It is worth pointing out now some important properties of the reaction term Δ_j, as defined in (4).

(1) The sign of Δ_j at low energies is opposite to the sign of V_{jj}. Thus, for a repulsive potential the low-energy effect of the reaction is always to decrease the scattering. For an attractive potential the scattering is enhanced if Δ_j is less than 1; but if Δ_j is greater than 1, the scattering phase shift changes sign.

(2) For an attractive potential, one can generally tell from the magnitude of Δ_j at zero energy whether or not a bound state exists. A study of the factorable potential shows that a bound state exists if $\Delta_j>1$ at zero energy, otherwise not. It is extremely plausible that this criterion holds whenever the approximation (4) is accurate.

(3) For sufficiently high energies Δ_j will pass through zero and change sign. This will happen when the majority of the contribution to the sum comes from below the singularity rather than from above. (Naturally, the situation is more complicated if V_{jj} itself changes sign.)

SUMMARY

An approximate solution of the general one- (or two-) body scattering problem has been discussed, based on a variational principle invented by Schwinger. Examples have been presented which suggest that for short-range forces, the criteria of validity for the approximation are that the potential must

(1) produce no more than one bound state,

(2) be of a single sign, i.e., either purely attractive or purely repulsive,

(3) have a moderate logarithmic range of important Fourier components, i.e., not be excessively singular.

The author wishes to express his gratitude to Professor Francis Low for many useful discussions.

[5] Our earlier observation that the approximation is only reasonable when no more than one bound state exists is not violated by this example. It is easy to show that the factorable potential can have at most one bound state.

[6] G. F. Chew, Phys. Rev. 89, 591 (1953).

APPENDIX

From reference 3 the energy shell eigenvalues and eigenfunctions of K are defined by the equation

$$\sum_a K_{ba}\delta(E_b-E_a)f_a{}^j=K^j f_b{}^j,$$

and the relation between the eigenvalue K^j for the jth channel and the corresponding phase shift δ_j is

$$\tan\delta_j=-\pi K^j.$$

For a one-body problem, the density of states factor is such that $K^j=(k\omega/2\pi^3)K_{jj}$, where k and ω are the momentum and energy ($\hbar=1$) of the scattered particle. Thus,

$$\tan\delta_j=-(k\omega/2\pi)K_{jj}.$$

Letters to the Editor

PUBLICATION of brief reports of important discoveries in physics may be secured by addressing them to this department. The closing date for this department is five weeks prior to the date of issue. No proof will be sent to the authors. The Board of Editors does not hold itself responsible for the opinions expressed by the correspondents. Communications should not exceed 600 words in length and should be submitted in duplicate.

Some Predicted Effects of Temperature Gradients on Diffusion in Crystals

A. D. LECLAIRE
Metallurgy Division, Atomic Energy Research Establishment, Harwell, England
(Received November 10, 1953)

SHOCKLEY has recently proposed[1] that a continuous flow of defects will occur in a crystal in which there exists a temperature gradient, on account of the gradient of defect concentration which exists if the density of defects at any point has the equilibrium value characteristic of the local temperature at that point. Such a flow of defects, he suggests, will produce a mass transport through the lattice towards regions of higher temperature for vacancies and towards regions of lower temperature for interstitials and will be continuous except for limitation imposed by stresses that may be set up by the mass flow. Observations on the direction of such a mass transport, he then proposes, may provide a means of distinguishing between vacancies and interstitials.

It is the purpose of this note to point out that a flow of defects may occur as a direct result of the temperature gradient as well as indirectly through the gradient of local equilibrium concentrations. We shall consider first the more interesting case of vacancies. Figure 1 represents two adjacent lattice planes normal to the direction of the temperature gradient. n and T are, respectively, the numbers of vacancies per unit area and the temperature at plane (1), and $n+\Delta n$ and $T+\Delta T$ are the corresponding quantities for plane (2). In order that a vacancy on plane (1) may move to plane (2), an atom on plane (2) must acquire at temperature $T+\Delta T$ an activation energy Q. The rate of flow of vacancies from plane (1) to (2) is therefore:

$$J_{12}=n\nu\exp[-Q/R(T+\Delta T)],$$

where ν is the vibration frequency of the atoms. Similarly, the rate of flow of vacancies from plane (2) to (1) is:

$$J_{21}=(n+\Delta n)\nu\exp(-Q/RT).$$

The net flow of vacancies from plane (1) to (2) is therefore, for small dT/T,

$$J=J_{12}-J_{21}=\frac{Q(\Delta T)}{RT^2}\nu n\exp(-Q/RT)-\frac{\Delta n}{n}\nu n\exp(-Q/RT).$$

The second term gives the diffusion flow arising from the concentration gradient and is of course proportional to the gradient and directed towards regions of lower concentrations. The first term gives the "thermal diffusion" flow and is directed towards regions of higher temperature.

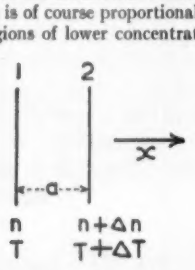

FIG. 1

Now, if we assume with Shockley that the concentration of vacancies is and remains, at each point in the crystal, equal to that which would be found in equilibrium in a crystal at a uniform temperature the same as at that point, then we shall have $\Delta n/n=(U/RT^2)dT$, where U is the energy of formation of a vacancy. Thus n increases in the same direction as does the temperature, and the normal diffusion flow is in a direction opposite to that of the thermal diffusion flow. If $Q=U$, then there will be no flow of vacancies at all. If $Q\neq U$, the net flow of vacancies will be towards the region of higher temperature when $Q>U$ and towards regions of lower temperature when $Q<U$.

In the case of interstitial diffusion, we find by reasoning similar to the above that the net flow of interstitials from plane (1) to (2) is

$$J=-\frac{Q(\Delta T)}{RT^2}\nu n\exp(-Q/RT)-\frac{\Delta n}{n}\nu n\exp(-Q/RT),$$

where Q is the activation energy for the jump of an interstitial, which in this case is to be acquired at the temperature of the plane on which the interstitial is situated. n is the number of interstitials and ν their vibrational frequency.

If again we assume that the concentration of interstitials at any point is that corresponding to thermodynamic equilibrium at the temperature at that point, then n increases in the same direction as does the temperature and the normal diffusion and the thermal diffusion flows are in the same direction, towards regions of lower temperature, and together equal $-\nu\exp(-Q/RT)\times\{(Q+U)/RT^2\}a\cdot dT/dx$, U now being the energy of formation of an interstitial.

We see then that, under the assumptions made, the mass flow accompanying the diffusion of interstitials is always towards the lower temperature regions whereas that accompanying the diffusion of vacancies may be towards either the lower or the higher temperature regions depending on the relative magnitude of Q and U. Observations on the direction of the mass flow will not then necessarily give an unambiguous indication of the type of defect responsible for it.

A detailed analysis of the diffusion of defects in a temperature gradient would have to take account not only of the flux of vacancies but also of the rates at which they are created and annihilated and the variation of these rates with temperature. Two extreme but simple cases can be distinguished. We may suppose that the rates of creation and annihilation of defects are sufficiently rapid to maintain at each point a concentration corresponding to isothermal equilibrium at the local temperature. A continuous flow of defects will then occur as here described. On the other hand, we may consider the case where the rates of creation and annihilation of defects are very slow compared to the diffusion flux. (This might be true for a time for regions well inside a single crystal if defects were generated only at the crystal surfaces.) The total number of defects present at the moment the temperature gradient was imposed would then diffuse until a quasi-stationary state was established where the normal diffusion flow exactly balances the thermal diffusion flow. The concentration of defects at any point would then remain constant but change with distance so that $d\log n/dx=(Q/RT^2)(dT/dx)$ for vacancies and $d\log n/dx=-(Q/RT^2)(dT/dx)$ for interstitials; i.e., the concentration of defects increases towards higher temperature for vacancies but towards lower temperature for interstitials. Such a creation of a concentration gradient by the action of a temperature gradient is, of course, an example of the Soret effect, and these same results may be obtained by the methods of irreversible thermodynamics if we put for the "heat of transport"[2] the activation energy Q for the motion of defects; the difference in sign arises because the transport of heat is in the same direction as the movement of interstitials but in the opposite direction to the movement of vacancies.

[1] W. Shockley, Phys. Rev. 91, 1563 (1953).
[2] K. G. Denbigh, *Thermodynamics of the Steady State* (Methuen, London, 1951).

The Effect of Temperature Gradients on Diffusion in Crystals

J. A. BRINKMAN
Atomic Energy Research Department, North American Aviation, Downey, California
(Received December 3, 1953)

IT has been proposed by Shockley[1] that it may be possible to distinguish experimentally between the vacancy and interstitial diffusion mechanisms by observing mass transfer as the result of a temperature gradient. In particular, it was stated that the temperature gradient should give rise to a diffusion current of defects under steady state conditions and that this current should produce mass transport toward high temperature for vacancies and toward low temperature for interstitial atoms. It is the purpose of the present note to show that this is true only for vacancies in case the formation energy of vacancies, E_f, exceeds the activation energy for their migration, E_m, whereas if the reverse is true, the direction of mass flow should be reversed. Thus, the experiments proposed by Shockley may prove of value in determining which energy, E_m or E_f, is the larger for materials in which the diffusion mechanism is known to be vacancy migration, rather than in determining whether an interstitial or vacancy migration mechanism is responsible for diffusion.

Consider two parallel neighboring planes of atoms perpendicular to the temperature gradient in the material, the first at a temperature T, and the second at $T+\Delta T$, as in Fig. 1. The flow of

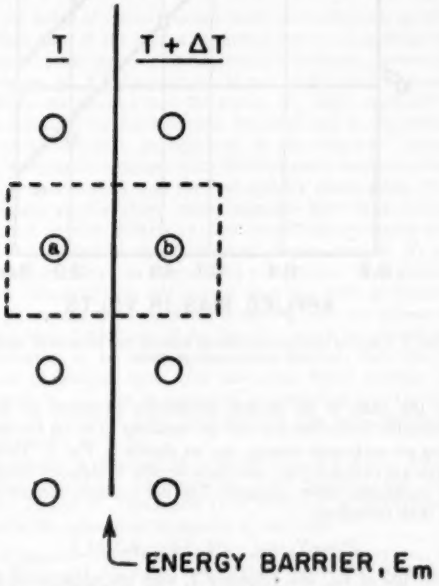

FIG. 1. Two neighboring planes of atoms in a crystal, each perpendicular to the temperature gradient.

vacancies across a representative pair of atom sites, a and b, will be calculated. In order for a vacancy to flow toward higher temperature via this pair, (1) a must first be vacant and (2) the atom on b must jump the energy barrier, E_m, representing the activation energy for vacancy migration. The probability of (1) can be written:

$$Ae^{-E_f/kT},$$

assuming that the thermal equilibrium concentration is maintained in each plane, and the probability of (2):

$$Be^{-E_m/k(T+\Delta T)},$$

where both the entropy factor, A, and the frequency factor, B, are temperature independent. Thus, the vacancy flow to the right is:

$$ABe^{-E_f/kT}e^{-E_m/k(T+\Delta T)}.$$

Similarly, the vacancy flow to the left is:

$$ABe^{-E_f/k(T+\Delta T)}e^{-E_m/kT}.$$

The net flow of vacancies to the right is:

$$ABe^{-(E_m+E_f)/kT}[\exp(E_m\Delta T/kT^2)-\exp(E_f\Delta T/kT^2)],$$

if all terms higher than first order in $\Delta T/T$ are neglected. Thus, the net flow of vacancies is toward higher vacancy concentrations if $E_m>E_f$ and toward lower concentrations if $E_m<E_f$, whereas there should be no net flow if $E_m=E_f$. Recent work[2] indicates that $E_m>E_f$ for face-centered cubic metals, implying that the mass flow should be opposite in direction to that assumed by Shockley.

The geometry associated with interstitial migration is more complex, and the conditions under which mass transfer should be toward lower or higher temperatures cannot be calculated easily in an analogous manner.

[1] W. Shockley, Phys. Rev. 91, 1563 (1953).
[2] A. D. LeClaire, Acta Metallurgica 1, 438 (1953).

Some Predicted Effects of Temperature Gradients on Diffusion in Crystals

W. SHOCKLEY
Bell Telephone Laboratories, Murray Hill, New Jersey
(Received November 27, 1953)

THE writer is entirely in agreement with the conclusion reached by LeClaire[1] and Brinkman[2] that one of the major mechanisms was unwarrantably disregarded in his first publication.[3]

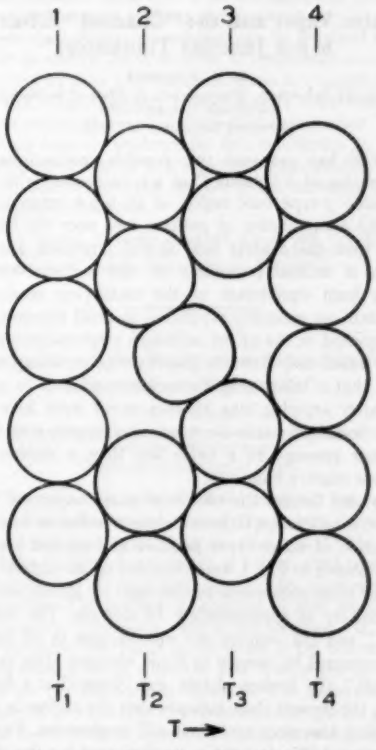

FIG. 1. Schematic representation of how the activation energy for jumping is furnished in part by neighbors of a jumping atom.

On the other hand, it appears to the writer that both LeClaire and Brinkman have rather oversimplified the problem with the result that they have overestimated the effect of jump activation energy. This may be illustrated for the case of vacancy diffusion in a two-dimensional hexagonal lattice as shown in Fig. 1. This figure represents a vacancy midway between planes 2 and 3, a situation produced by an atom that has jumped halfway from one plane into a vacancy on the other.

Evidently some of the energy Q for jumping will be stored in the interactions between the neighbors and next neighbors of the jumping atom. This energy would appear to be furnished thermally from a source at temperature of $T_{2.5}$, about midway between that on planes 2 and 3, regardless of the jump direction. Only a fraction of the activation energy Q will be furnished by the jumping atom itself.

This reasoning suggests that driving force for thermal diffusion will be smaller than that estimated from Q and, hence, that the domination of mass transport by the concentration gradient, as originally predicted by the writer, will be greater than LeClaire and Brinkman conclude. The effects they discuss will play an important role, but it is difficult to see how a quantitative theory can be developed.

In the case of germanium, it may be remarked, there appears to be a good possibility[4] of measuring both the energy of formation of centers U and jump energy Q. If Q turns out to be less than U, a unique determination of the nature of the heat centers may be possible.

[1] A. D. LeClaire, this issue [Phys. Rev. 93, 344 (1954)].
[2] J. A. Brinkman, preceding Letter [Phys. Rev. 93, 345 (1954)].
[3] W. Shockley, Phys. Rev. 91, 1563 (1953).
[4] R. A. Logan, Phys. Rev. 91, 757–758 (1953).

Water Vapor and the "Channel" Effect in *n-p-n* Junction Transistors*

R. H. KINGSTON
Lincoln Laboratory, Massachusetts Institute of Technology, Cambridge, Massachusetts
(Received November 13, 1953)

BROWN[1] has proposed two possible mechanisms for the formation of a "channel" or n-type conductivity layer on the normally p-type base region of an n-p-n transistor. These are (1) the accumulation of positive ions over the base region resulting from the electric field at the junctions, and (2) the ionization of neutral impurities on the surface due to the departure from equilibrium of the underlying semiconductor. These effects are generally attributed to small amounts of water vapor deposited on the surface although other contaminants have not been ruled out. Brown's observations on encapsuled units indicated that it takes several minutes to an hour to establish a channel after applying bias whereas recent work here indicates that this conditioning time decreases continuously with increasing water-vapor pressure to a value less than a millisecond near 100 percent relative humidity.

To examine further the effects of water vapor on "channel" formation, conductance, G, from emitter to collector was measured as a function of water-vapor pressure and applied reverse bias. The data shown in Fig. 1 were obtained on an etched[2] n-p-n bar having the same dimensions as that used by Brown and a p-type base resistivity of approximately 10 ohm-cm. The temperature was 25°C, and the ambient gas was nitrogen in all cases. Since Brown immersed his sample in liquid nitrogen after establishing a "channel," the surface charge was "frozen" at a fixed value; however, the present data indicate that the charge is increasing with applied bias since no "pinch-off" is observed. Furthermore, the apparent $1/V$ relationship (as indicated by the solid lines) points to the following explanation of the effect.

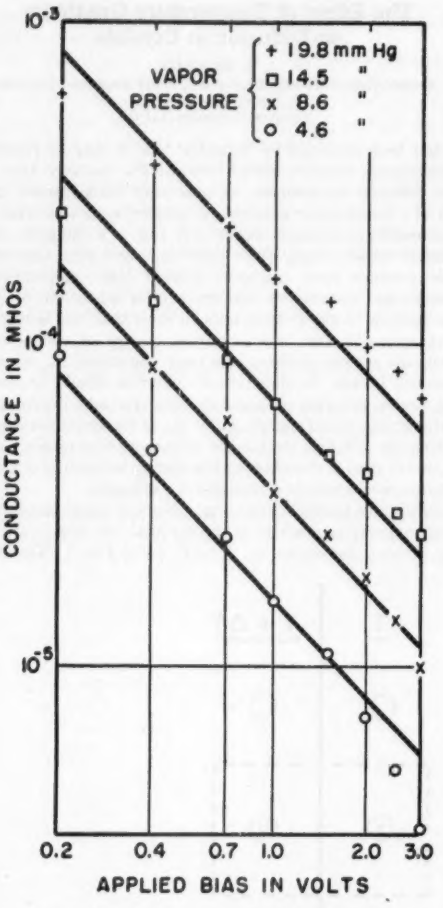

FIG. 1. Channel conductance *versus* applied bias at several values of water-vapor pressure.

On the basis of the second mechanism proposed by Brown, N_s ionizable impurities per cm² are assumed to be on the surface, having an excitation energy, ψ_D, as shown in Fig. 2. These impurities are of donor type, and their density is assumed to increase with increasing vapor pressure. The net positive surface charge may then be written

$$Q_s = qN_s \exp[-q(\psi_s+\psi_D-\phi_n)/kT]; \quad (1)$$

and by use of Eq. (6), reference 1, with the notation of Fig. 2, the conductance is found to be

$$G \propto \left\{V_A - 2\psi_p + \frac{kT}{q}\left[\exp\left(\frac{q(\psi_s-\psi_p-\phi_n)}{kT}\right)-1\right]\right\}^{\frac{1}{2}} - (V_A-2\psi_p)^{\frac{1}{2}}, \quad (2)$$

since G is proportional to the number of conduction electrons, which is, in turn, proportional to the difference between the total field at the surface and that due to the acceptor ions alone. For most of the data considered, V_A is much greater than any of the other terms under the radicals in Eq. (2); therefore,

$$Q_s \propto \sqrt{V_A}, \quad (3)$$

since the first term in Eq. (2) represents the total field at the surface. Furthermore, the exponential in Eq. (2) is much greater than unity and is inversely proportional to Q_s/N_s from Eq. (1).

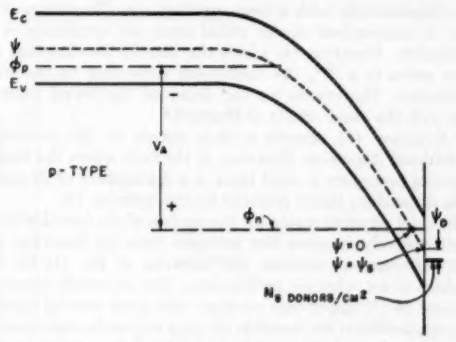

FIG. 2. Energy diagram at surface of p-type material.

Therefore,

$$G = k_1\left\{\left(V_A - 2\psi_p + \frac{k_2 N_s}{\sqrt{V_A}}\right)^{\frac{1}{2}} - (V_A - 2\psi_p)^{\frac{1}{2}}\right\} \approx \frac{k_1 k_2 N_s}{2V_A}, \quad (4)$$

where k_1 and k_2 are constants directly calculable from the theory. The more detailed theory, which avoids the above approximations, gives:

$$10^{10} < N_s \exp(-q\psi_D/kT) < 10^{12} \text{ cm}^{-2} \quad (5)$$

over the range of vapor pressure used. If the electron mobility is less than that of the bulk and surface states are included in the calculation, the shape of the curves is unchanged; however, the magnitude of N_s given above is not completely accurate. It should be emphasized that the states, N_s, differ markedly from those discussed by Bardeen and Brattain[2] and by Brown[1] since their ionization time, as evidenced by the "channel" formation time, is much too long and since they are also a function of water-vapor pressure contrary to the first authors' observation. Further speculation on the above model suggests that these impurities might act as hole generators, thus producing increased reverse currents in junction transistors and diodes, and, if N_s has a random fluctuation, an excess noise component. Hole generation is quite conceivable in this picture since the fields at the surface are high enough to cause direct tunneling from the valence band to the ionized impurities. If the impurity levels are considered to be embedded in an oxide layer on the surface, then the rapid decrease of buildup time with increasing vapor pressure (and, consequently, N_s) can be explained by assuming that the rate of transfer of electrons from impurities to the semiconductor increases rapidly with N_s.

The author is indebted to J. A. Morton and K. D. Smith of the Bell Telephone Laboratories, who supplied the sample crystals, and to M. Green and G. I. Hitchcox of this laboratory for aid in the experimental aspects of the work.

* The research in this document was supported jointly by the U. S. Army, Navy, and Air Force under contract with the Massachusetts Institute of Technology.

[1] W. L. Brown, Phys. Rev. 91, 518 (1953).
[2] The treatment is the same as that described on page 8 of J. Bardeen and W. L. Brattain, Bell System Tech. J. 32, 1 (1953).

Radiation from CdS Crystals Generated by DC Electric Fields

R. W. SMITH
RCA Laboratories Division, Radio Corporation of America, Princeton, New Jersey
(Received October 19, 1953)

BÖER and Kummel[1] report radiation from CdS crystals immersed in liquid air and subjected to dc fields $\sim 10^3$ volts/cm. At these fields the current is observed to rise abruptly (but reversibly) and radiation (red and green) is observed at currents just under those that normally cause the crystal to break down thermally. Böer and Kummel interpret the rapid rise current to collision ionization by conduction electrons that have been accelerated to several volts energy by the applied field. The radiation is described as "luminescence" caused by the energetic electrons.

The purpose of this letter is to describe work in this laboratory on CdS crystals that indicates at least two types of radiation can be generated electrically, and that the fields may be an order of magnitude or more lower than reported by Böer and Kummel.

The emission from a crystal depends on its conductivity and past history. One type of radiation, observed in the more conducting crystals, is best described as incandescence. It is red or straw-colored emission and has been obtained at dc electric fields $\lesssim 150$ volts/cm when the current is of the order of tens of milliamperes. The crystals are operating near thermal breakdown. The emission is independent of the electrode configuration and material, and is observed at room temperature.

Another type of electrically-excited radiation is green emission (often unaccompanied by red) from more insulating crystals at dc electric fields $\sim 10^3$ volts/cm. Green emission has been obtained from CdS crystals several mm long with In electrodes. The emission is most intense around the positive electrode and tapers off in intensity over an appreciable fraction of the spacing between electrodes, often appearing to flow and ripple. The current is usually low and of the order of several hundred μa.

Recently[2,3] we have reported space-charge-limited currents drawn through thin insulating CdS crystals using ohmic contacts of In or Ga. These currents increase as a high-power function of the voltage even at low fields (10^2–10^3 volts/cm). The fact that the current increased more rapidly with voltage than theory predicted was ascribed to the presence of traps. These insulating crystals have been subjected to fields $\sim 10^3$ volts/cm and green (and red) emission observed. This configuration most nearly approximates that used by Böer and Kummel.

It is seen then that green emission can be obtained from CdS crystals at dc electric fields an order of magnitude or more lower than reported by Böer and Kummel. There is a question whether fields of this magnitude can impart several volts energy to an electron as would be required for collision ionization. Although there is little concrete evidence for hole conduction in CdS, it is possible that there is some hole injection at the positive electrode. This could account for the intense green emission emanating from the positive electrode.

[1] K. W. Böer and U. Kummel, Z. physik. Chem. 200, 190 (1952).
[2] R. W. Smith and A. Rose, Phys. Rev. 92, 857 (1953).
[3] A. Rose and R. W. Smith, Phys. Rev. 92, 857 (1953).

Solution of the Boltzmann Equation for Maxwellian Molecules*

E. P. GROSS
Laboratory for Insulation Research, Massachusetts Institute of Technology, Cambridge, Massachusetts
(Received November 23, 1953)

THE Boltzmann integrodifferential equation for monatomic gases has been studied extensively in two limiting cases. When the mean free path is small compared to the relevant lengths of the problem (wavelength of sound, thickness of shock front, dimensions of container, etc.), the Enskog-Chapman method applies.[1] The method is defective in that general microscopic boundary conditions cannot be satisfied. It becomes unwieldy for mean free paths of the order of the relevant length and breaks down entirely when the flow is sensitive to boundary conditions on the distribution function. For mean free paths large compared to a container dimension, Jaffé[2] gave a procedure for solving the Bolzmann equation by successive approximations and satisfying general boundary conditions. This method breaks down at higher pressures. In view of the present active interest in

processes occurring in rarefied gases, it is desirable to have a method of solution which deals with the entire range of pressures in a unified manner and which can satisfy general microscopic boundary conditions. The present communication sketches such a method for the special case of Maxwellian molecules, which repel each other with an inverse fifth-power law of force.

The Boltzmann equation governing the distribution function $f(\mathbf{v},\mathbf{x},t)$, in the absence of external forces, is

$$\frac{\partial f}{\partial t}+\mathbf{v}\cdot\nabla_x f=\int f(\mathbf{v}',\mathbf{x},t)\,f(\mathbf{v}_1',\mathbf{x},t)\,dA\,d\mathbf{v}_1 - f(\mathbf{v},\mathbf{x},t)\int f(\mathbf{v}_1,\mathbf{x},t)\,dA\,d\mathbf{v}_1, \quad (1)$$

where dA contains the geometrical variables specifying a collision and is independent of velocity; $\mathbf{v}'$ and $\mathbf{v}_1'$ are velocities after collision and are expressed in terms of $\mathbf{v},\mathbf{v}_1$ and the geometrical variables.

We introduce a cutoff in the form of a maximum impact parameter so that the integrals converge separately. We give the names "emission term" and "absorption term" to the first and second terms, respectively, on the right-hand side of (1). Our procedure is then the following: at each step the absorption term is left intact. For the first step we insert a locally Maxwellian distribution f_0 in the emission term. Here,

$$f_0=\rho(\mathbf{x},t)\left(\frac{m}{2\pi kT(\mathbf{x},t)}\right)^{\frac{3}{2}}\exp\left\{-\frac{m}{2kT}[\mathbf{v}-\mathbf{q}(\mathbf{x},t)]^2\right\}, \quad (2a)$$

with

$$\rho(\mathbf{x},t)=\int f d\mathbf{v}, \quad (2b)$$

$$\mathbf{q}(\mathbf{x},t)=\frac{1}{\rho}\int \mathbf{v} f d\mathbf{v}, \quad (2c)$$

$$\frac{3kT(\mathbf{x},t)}{m}=\frac{1}{\rho}\int\{\mathbf{v}-\mathbf{q}(\mathbf{x},t)\}^2 f d\mathbf{v}, \quad (2d)$$

where k is Boltzmann's constant and m is the mass of the molecule. Using the conservation laws $v^2+v_1^2=v'^2+v_1'^2$ and $\mathbf{v}+\mathbf{v}_1=\mathbf{v}'+\mathbf{v}_1'$, we obtain

$$\frac{\partial f}{\partial t}+\mathbf{v}\cdot\nabla_x f=(f_0-f)\frac{\rho(\mathbf{x},t)}{\sigma}, \quad (3)$$

where σ is a constant depending on the cutoff; to insure consistency of the procedure it has a definite value for a given force constant. In the second step we insert the solution f_1 of (3) into the emission term. The equation satisfied at the nth step is

$$\frac{\partial f_n}{\partial t}+\mathbf{v}\cdot\nabla_x f_n+\frac{f_n\rho_n}{\sigma}=\int f_{n-1}(\mathbf{v}_1',\mathbf{x},t)\,f_{n-1}(\mathbf{v}',\mathbf{x},t)\,dA\,d\mathbf{v}_1. \quad (4)$$

Equation (3) is the kinetic equation proposed by Bhatnagar, Gross, and Krook[3] as a model for collision processes. It has the feature that particle number, momentum, and energy are instantaneously conserved by collisions. While (3) is a nonlinear integro-differential equation, it is of a simpler mathematical nature than the Boltzmann equation since only the first few moments of the distribution function occur in the collision terms. Indeed, for small-amplitude sound oscillations (translational dispersion of sound) the exact solution can be exhibited as a contour integral[3] and investigated as a function of mean free path and boundary conditions. While (3) leads to sensible physical results for a wide variety of situations, the solutions are not quantitatively exact. The sequence (4) is proposed as a systematic improvement. A general study of the convergence of (4) to the solution of the Boltzmann equation can be made using the methods of Wild.[4] We discuss here the results of (3) for three different types of problem and indicate the improvement brought about by (4).

a. A calculation of transport properties using (3) yields a ratio of heat conductivity to viscosity, which is $\frac{2}{3}$ the correct value. Equation (4) gives the series $\frac{2}{3}[1+\frac{1}{2}+\cdots+(\frac{1}{2})^{n-1}]$, which converges rapidly to unity.

b. According to (3), a spatially homogeneous velocity distribution which is non-Maxwellian initially, decays to Maxwellian form exponentially with a time constant σ/ρ. The nature of the decay is independent of the initial form and amplitude of the distribution. Equation (4) yields the distribution function as a power series in $e^{-t\rho/\sigma}$, the coefficients depending on the initial distribution. The results for the decay of the lowest moments agree with the exact results of Maxwell.[5]

c. Equation (3) permits a clear survey of the problem of translational dispersion. However, in the limit where the Enskog-Chapman procedure is valid there is a discrepancy of 20 percent in the dispersion; this is removed by the iteration (4).

The chief physical reason for the success of the iteration is that we successively improve the emission term by inserting more exact distribution functions; the behavior of Eq. (1) for most problems is not sensitive to this term. The physically reasonable solutions of (3) imply that we start with good over-all behavior. For some problems the iteration (4) may not be the most practical procedure. Nevertheless, methods involving a successive set of kinetic equations which are solved exactly appear promising for cases where the expansion of the distribution function in some orthogonal set does not lead to definite results.

A more extensive treatment, together with applications, will be published later.

The author would like to thank Dr. M. Krook for helpful discussions.

* Sponsored by the U. S. Office of Naval Research, the Army Signal Corps, and the Air Force.

[1] S. Chapman and T. G. Cowling, *The Mathematical Theory of Non-Uniform Gases* (Cambridge University Press, London, 1952). Another method of the same type is given by H. Grad, Comm. Pure Appl. Math. 2, 331 (1949).

[2] H. Jaffé, Ann. Physik 6, 195 (1930).

[3] Bhatnagar, Gross, and Krook, Technical Report 69, Laboratory for Insulation Research, Massachusetts Institute of Technology (unpublished); Technical Report 11, Solar Project, Harvard University (unpublished); Phys. Rev. (to be published).

[4] E. Wild, Proc. Cambridge Phil. Soc. 47, 602 (1951).

[5] J. C. Maxwell, *Scientific Papers* (Dover Press, New York, 1952), Vol. 2.

Further Correlation between Magnetoresistance Variations and the de Haas-van Alphen Effect

TED G. BERLINCOURT AND JOHN K. LOGAN
U. S. Naval Research Laboratory, Washington, D. C.
(Received November 12, 1953)

MAGNETORESISTANCE anomalies have been observed in a single crystal of natural graphite at low temperatures, further verifying and extending the correlation already illustrated in bismuth[1,2] between the magnetoresistance variations and the de Haas-van Alphen effect (oscillatory dependence of magnetic susceptibility upon magnetic field). Furthermore, application of the same type of analysis used in bismuth and graphite to the zinc magnetoresistance data of Nachimovich[3] and the de Haas-van Alphen data of Marcus[4] and Mackinnon[5] reveals the existence of a like correlation. The existence of such a correlation in zinc, which is a relatively good conductor, implies that the electrons causing the susceptibility oscillations, i.e., the de Haas-van Alphen electrons (while as few as 10^{-6} per atom) may play a greater role in determining the electronic properties of metal single crystals than was heretofore believed. Indeed, such magneto-oscillatory behavior must be expected in still other electronic properties measured at low temperatures. Because de Haas-van Alphen effect investigations yield relatively precise values for electronic effective masses and chemical potentials, they should prove valuable in interpreting such behavior.

The magnetoresistance measurements on graphite were carried out at 4.22°K on a sample cleaved from a large single crystal of natural graphite (Catalog No. 48789, Essex County, New York) kindly loaned by Dr. George Switzer of the Smithsonian Institution. The magnetic field was parallel to the hexagonal or c axis, and the direction of the measuring current was along a binary or a axis. Electrical contact was obtained by copper plating the ends of the crystal which were then clamped to an insulating member with small copper bars to which current and potential

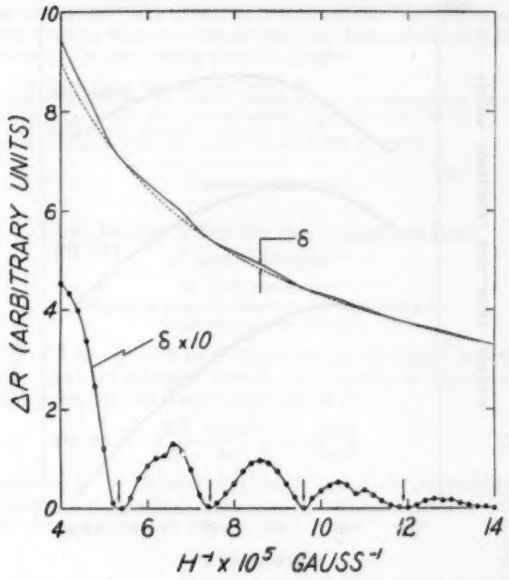

FIG. 1. Change in resistance ΔR in a graphite single crystal as a function of H^{-1} at 4.22°K (solid line). δ is the difference between the experimental values and the dashed curve.

leads were soldered. Since an unknown amount of contact resistance is present in such a configuration, the change in resistance (rather than the usual ratio of change in resistance to zero field resistance) is reported. In Fig. 1, the change of resistance ΔR of the sample in a magnetic field H is plotted as a function of H^{-1}. Since the probable error was estimated as less than the thickness of the plotted curve, the experimental points could not be indicated. Consequently, in order to illustrate the nature of the anomalies better, the differences δ (as read from a larger graph) between the experimental points and the dashed curve (which is accurately represented by $\Delta R \propto H^{0.811}$ between 12 and 25 kilogauss) are plotted on an expanded scale at the bottom of Fig. 1. Values of H^{-1} for which δ exhibits minima are indicated by arrows in Fig. 1 and are plotted against integers in Fig. 2 (solid line). For comparison, Shoenberg's de Haas-van Alphen data[6] on graphite were extrapolated to the same orientation (H parallel to the hexagonal axis), and values of H^{-1} for which graphite exhibits susceptibility minima are also plotted on Fig. 2 (dashed line). Since these lines are parallel, a one-to-one correspondence in period $\beta/E_0 = 2.2\times10^{-5}$ gauss^{-1} is indicated.[7] This point should be emphasized in view of the fact that the more complicated nature of the electronic constant energy surfaces for bismuth had made it impossible to state unambiguously from the experimental evidence alone whether the period of the magnetoresistance oscillations was one half that of the long-period susceptibility oscillations or was just equal to the period of the short-period susceptibility oscillations. (The one-to-one correspondence in period is further borne out by the zinc data.) Although the separation between the lines in Fig. 2 indicates a phase difference of approximately $\pi/2$ between the resistance variations along a binary axis and the susceptibility oscillations along the hexagonal axis in graphite, no great accuracy is claimed for this parameter since the susceptibility and resistance measurements were not carried out on the same crystal. Furthermore, the analysis is complicated somewhat by the fact that δ is not a simple monatonically modulated sinusoid (see Fig. 1). However, this is to be expected in view of the existence of a subordinate term in the susceptibility[6] having a period $\frac{1}{2}$ that of the dominant term.

More detailed investigations of the correlative effects are in progress and will be reported at a later date.

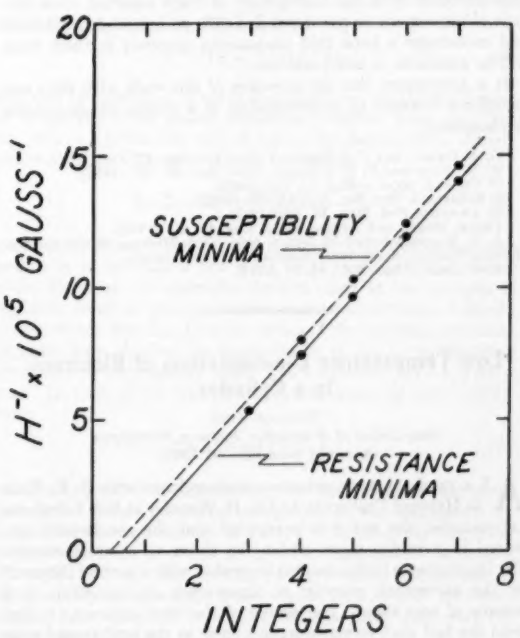

FIG. 2. Values of H^{-1} for which magnetoresistance and susceptibility oscillations in graphite exhibit minima are plotted against integers. The susceptibility data are those of Shoenberg (reference 6).

[1] P. B. Alers and R. T. Webber, Phys. Rev. **91**, 1060 (1953).
[2] Ted G. Berlincourt, Phys. Rev. **91**, 1277 (1953).
[3] N. M. Nachimovich, J. Phys. (U.S.S.R.) **6**, 111 (1942).
[4] Jules A. Marcus, Phys. Rev. **76**, 621 (1949).
[5] L. Mackinnon, Proc. Phys. Soc. (London) **B62**, 170 (1949).
[6] D. Shoenberg, Trans. Roy. Soc. (London) **245**, 1 (1952).
[7] β is a double effective Bohr magneton involving the effective mass, and E_0 is the chemical potential of the pertinent electrons.

Electroluminescence in Thin Films of ZnS:Mn

R. E. HALSTED AND L. R. KOLLER
General Electric Research Laboratory, Schenectady, New York
(Received November 10, 1953)

TRANSPARENT films of sulfide phosphors of the order of 10 microns in thickness have been prepared by the vapor reaction method of Cusano and Studer.[1] Such films offer a crystalline form of these materials particularly suitable for study under high voltage gradients. Preliminary data on films of ZnS:Mn (approximately 0.5 percent Mn) reveal some interesting variations from previously reported electroluminescent behavior.

Samples were prepared in the form of condensers with one transparent conducting electrode on a glass substrate, a transparent phosphor dielectric, and a second electrode of evaporated metal. ZnS:Mn films so prepared respond with a Mn emission peaked at 5900A to either cathode-ray or electroluminescent excitation. They have a specific resistance in the dark of the order of 10^{13} ohm cm measured at an average gradient of 10^4 volts/cm. Thermoluminescent measurements between −196° and +200°C yield one "glow peak" corresponding to a 0.3-ev trap (frequency factor of 10^8/sec assumed). This trap is observed also in ZnS films with no Mn.

Except for a transient flash on application and removal of dc fields, no dc luminescence is produced by fields below breakdown (approximately 5×10^5 volts/cm). Two light pulses per cycle are observed on application of an ac potential. As can be seen in Fig. 1, these light pulses are very closely in phase with the applied

voltage and are of unequal amplitude. The larger pulse occurs when the metal electrode is negative. The light output produced by a pulsed wave form, also given in Fig. 1, confirms that the light is associated with voltage changes in the film.

The average brightness of the films varies approximately as the seventh power of the applied voltage through 5 decades in brightness. A small difference is observed in this dependence for the alternate light pulses, but a strong power relationship gives a good approximation for each. The electroluminescent emission color of the samples is not altered by variations of either frequency or voltage of excitation. For a fixed voltage the average brightness increases with the frequency from 20 to approximately 5000 cps. The specific brightness *versus* frequency relationship is influenced by several factors: (1) The decay time constant of the electroluminescent Mn emission is 1.3 milliseconds. (2) Above approximately 2000 cps the resistance of the transparent conducting substrate competes with the dielectric impedance for the applied voltage. (3) The electroluminescent emission is temperature-dependent. The dependence of average brightness on temperature for three different frequencies of excitation is shown for one sample in Fig. 2. The position and sharpness of the maxima vary

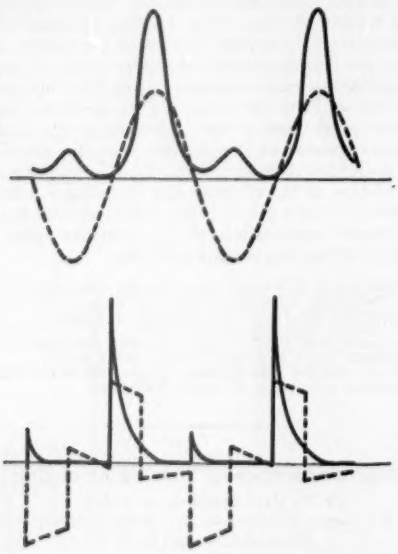

FIG. 1. Light output and voltage *versus* time for sinusoidal and pulsed excitation of ZnS:Mn films. Broken line indicates 60 cps voltage wave form.

appreciably for different samples and are dependent in a given sample on its history of exposure to temperatures of the order of 200°C. However, the general feature of a single, frequency-dependent maximum in brightness has always been observed in this temperature range.

No contradiction with the qualitative impact excitation mechanism proposed by Piper and Williams[2] and Curie[3] is apparent in the information noted above. The absence of dc luminescence can be correlated with the high resistivity of the ZnS:Mn. Variations in the phase relation between light pulses and applied sinusoidal voltages could be explained by variations in the donor level distribution. For example, the "in-phase" ac light production of ZnS:Mn might be the result of a reduction in the number of shallow donors postulated[3] in ZnS:Cu to produce the space charge for "out-of-phase" luminescence.

The voltage dependence of electroluminescent brightness in ZnS:Mn films is stronger than previously reported.[4-6] The near linearity of brightness *versus* frequency of excitation at low frequencies and room temperature is in agreement with previous

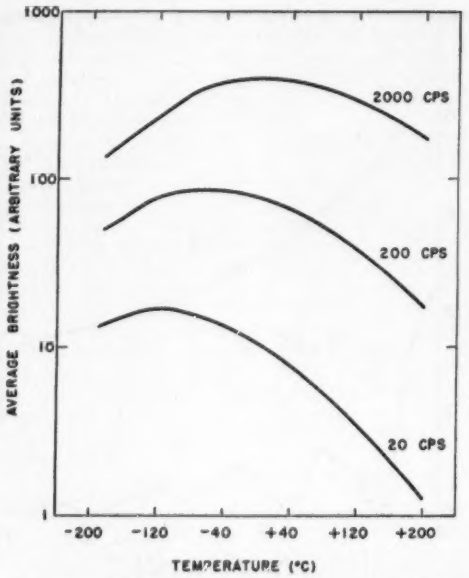

FIG. 2. Average brightness of electroluminescence of ZnS:Mn film *versus* temperature for three frequencies of excitation. Data for the three frequencies were taken on the same temperature run with the sample in vacuum.

results, in particular the demonstration by Waymouth that the integrated electroluminescent light output is independent of the rise time of a single voltage pulse.[7] The structure of thin film cells permits an examination of the temperature dependence of their electroluminescence over a somewhat greater range than has been reported for powder cells.[4,5] The single 0.3-ev electron trap contrasts with the multiplicity of traps reported from this type of experiment on powdered ZnS:Mn phosphors (e.g., Bube[8]) and encourages a hope that phenomena observed in these films will be amenable to interpretation.

It is anticipated that an extension of this work with films can contribute towards an understanding of a variety of phenomena in phosphors.

[1] D. A. Cusano and F. J. Studer, J. Opt. Soc. Am. **42**, 878 (1952).
[2] W. W. Piper and F. E. Williams, Phys. Rev. **87**, 151 (1952).
[3] D. Curie, J. phys. radium **13**, 317 (1952).
[4] S. Roberts, J. Opt. Soc. Am. **42**, 850 (1952).
[5] G. Destriau, Phil. Mag. **38**, 700 (1947).
[6] Payne, Mager, and Jerome, Illum. Eng. **45**, 688 (1950).
[7] J. F. Waymouth and F. Bitter, New York Meeting of the Electrochemical Society, April, 1953, Abstract 27 (unpublished).
[8] R. H. Bube, Phys. Rev. **90**, 70 (1953).

Low Temperature Diamagnetism of Electrons in a Cylinder

WILLIAM BAND
State College of Washington, Pullman, Washington
(Received November 30, 1953)

AS a result of some private correspondence with S. F. Ham at Harvard University and G. H. Wannier at Bell Telephone Laboratories, the writer is persuaded that the conclusions presented in a recent paper under the above title[1] are incorrect. The leading term in the result is in conflict with a general theorem[2] on the asymptotic number of eigenvalues corresponding to a volume of any shape. The source of the error appears to stem from the fact that terms to second order in the field should have been retained in the general expression for the wave functions, Eqs. (8) and (9), to yield a consistent theory of the susceptibility.

If this is done, one arrives at a problem that was solved ten years ago by Wannier,[3] and the resulting theory of susceptibility is essentially that already given by Dingle.[4]

[1] W. Band, Phys. Rev. **91**, 249 (1953).
[2] R. Courant and D. Hilbert, *Methoden der Mathematischen Physik* (J. Springer, Berlin, 1931), second edition, Vol. I, Chap. 6, Sec. 4.
[3] G. H. Wannier, Phys. Rev. **64**, 358 (1943).
[4] R. B. Dingle, Proc. Roy. Soc. (London) **A212**, 47 (1952).

The Density Effect for the Ionization Loss at Low Energies*

R. M. STERNHEIMER
Brookhaven National Laboratory, Upton, New York
(Received November 18, 1953)

THE density effect for the ionization loss of charged particles has been evaluated recently for a number of substances.[1] At low energies, the density effect is given by[1]

$$\Delta\frac{dE}{dx}=\frac{2\pi n_0 e^4}{mv^2}\sum_j f_j \ln\left(\frac{l_j^2}{\nu_j^2}\right), \tag{1}$$

where n_0 is the electronic density, f_j and ν_j are the oscillator strength and the atomic frequency [in units $\nu_p=(n_0e^2/\pi m)^{\frac{1}{2}}$] for the jth transition; l_j is given by

$$l_j=(\nu_j^2+f_j)^{\frac{1}{2}}. \tag{2}$$

In the experiment of Bakker and Segrè[2] on the stopping power for 340-Mev protons, this density effect was included, so that this experiment measures the ionization potential,[3]

$$I_{BS}=h\nu_p\prod_j l_j^{f_j}, \tag{3}$$

rather than the ionization potential for the isolated atom, $I=h\nu_p\Pi_j\,\nu_j^{f_j}$. When the values of I_{BS} are used to calculate the ionization loss, the density effect correction is given by

$$\delta=\sum_j f_j\ln\left(\frac{l_j^2+l^2}{\nu_j^2}\right)-l^2(1-\beta^2)-\sum_j f_j\ln\frac{l_j^2}{\nu_j^2}, \tag{4}$$

where l is determined by the equation:

$$\beta^{-2}-1=\sum_j f_j/(\nu_j^2+l^2). \tag{5}$$

The first two terms of (4) give the correction which would have to be applied if the atomic ionization potential were used [see Eq. (46) of A]. The last term is due to the density effect already included in I_{BS}. Equation (4) can be written

$$\delta=\sum_j f_j\ln\left(\frac{l_j^2+l^2}{l_j^2}\right)-l^2(1-\beta^2), \tag{6}$$

where the l_j are such that Eq. (3) is satisfied. This procedure was used in A to calculate δ and gives exact results for the case of solids. However, for gases the density effect at low energies is negligibly small so that the atomic ionization potential I should be used rather than I_{BS}. In A the values of the ionization potential for gases were obtained by interpolation of I_{BS} for neighboring substances in the periodic table. The correction $I_{BS}-I$ is very small. In view of (1) and (2), I/I_{BS} is given by $\exp(-D/2)$, where

$$D=\sum_j f_j\ln\left(1+\frac{f_j}{\nu_j^2}\right), \tag{7}$$

and $(2\pi n_0e^4/mv^2)D$ is the amount by which dE/dx for gases exceeds the value calculated using I_{BS}. D was calculated for some of the substances listed in Table I of A, using the ionization potentials and the f_j which are given in this table. The results are: $D(\mathrm{Li})=0.34$, $D(\mathrm{C})=0.22$, $D(\mathrm{Al})=0.056$, $D(\mathrm{Fe})=0.14$, $D(\mathrm{Cu})=0.13$, $D(\mathrm{Ag})=0.09$, $D(\mathrm{Sn})=0.05$, $D(\mathrm{W})=0.07$. By interpolation one finds: $D(\mathrm{N_2})=0.20$, $D(\mathrm{O_2})=0.17$, $D(\mathrm{Ne})=0.13$, $D(\mathrm{A})=0.09$, $D(\mathrm{Kr})=0.11$, $D(\mathrm{Xe})=0.05$.

It should be emphasized that these values of D are considerably uncertain because of the sensitivity of D to the distribution of the low frequencies ν_j which correspond to excitation of the outer electron shells. An alternative method of obtaining D is to deduce the effective ionization potential I_j of the outermost electron shell for the gas from the observed index of refraction n in the optical region,[4] which is given by:

$$n=1+\frac{f_j}{2[I_j/(h\nu_p)_{\mathrm{gas}}]^2}, \tag{8}$$

where $f_j=N_j/Z$ and N_j is the number of valence electrons which was taken as the number of electrons with the highest principal quantum number. Thus, for[4] Kr, $n=1.00043$, $f_j=8/36$, and $h\nu_p=0.085$ ry lead to $I_j=1.37$ ry. The density effect which would be measured for this dispersion oscillator in a solid is given by:

$$D=f_j\ln\left\{1+\frac{f_j}{[I_j/(h\nu_p)_{\mathrm{solid}}]^2}\right\}, \tag{9}$$

where $(h\nu_p)_{\mathrm{solid}}$ is the average of $h\nu_p$ for the neighboring solids measured by Bakker and Segrè.[2] Equation (9) gives: $D(\mathrm{N_2})=0.53$, $D(\mathrm{O_2})=0.48$, $D(\mathrm{Ne})=0.24$, $D(\mathrm{Kr})=0.26$, $D(\mathrm{Xe})=0.17$. A comparison of these values with those obtained above indicates the uncertainty in D. However, it should be noted that even with the larger values obtained from the index of refraction the correction is quite small. D may be compared with the square bracket of Eq. (11) of A for dE/dx which is $\sim$20. Thus, $D=0.5$ corresponds to $a\sim2.5$ percent increase of dE/dx. This correction is hardly outside the limits of error owing to the uncertainty of the experimental values[2,5] of I.

In view of the smallness of D and the uncertainty about its value, it seems questionable whether this correction should be applied at present to the ionization loss for gases.[6] For high energies ($p/\mu c\gtrsim100$) when the density effect for the gas is important, D is smaller than Eq. (7) and becomes zero when the ionization loss has attained saturation (dE/dx independent of I).

I would like to thank Dr. A. O. Hanson and Dr. G. N. Whyte for pointing out the existence of the correction for the ionization potential of gases.

* Work done under the auspices of the U. S. Atomic Energy Commission.
[1] R. M. Sternheimer, Phys. Rev. **88**, 851 (1952). Unless otherwise indicated, we use here the same notation as in that paper, which will be referred to as A.
[2] C. J. Bakker and E. Segrè, Phys. Rev. **81**, 489 (1951).
[3] Goldwasser, Mills, and Hanson, Phys. Rev. **88**, 1137 (1952).
[4] H. H. Landolt and R. Bornstein, *Physikalisch-Chemische Tabellen* (Julius Springer, Berlin, 1923), fifth edition, Vol. 2, p. 961.
[5] R. Mather and E. Segrè, Phys. Rev. **84**, 191 (1951); D. C. Sachs and J. R. Richardson, Phys. Rev. **89**, 1163 (1953).
[6] We note that the Lorentz term and the damping effect (see reference 1) introduce additional corrections which may be of the same order as D.

Coulomb Excitation of Heavy and Medium Heavy Nuclei by Alpha Particles*

G. M. TEMMER AND N. P. HEYDENBURG
Department of Terrestrial Magnetism, Carnegie Institution of Washington, Washington, D. C.
(Received December 2, 1953)

WE wish to report some preliminary results concerning the Coulomb excitation of some 35 nuclei between $Z=20$ and $Z=90$ by both alpha particles and protons with energies up to 3.8 Mev. Recent work on this process induced by protons in tantalum, tungsten, and a few other heavy elements[1,2] has pointed up the great usefulness of this method in studying transition probabilities between low-lying nuclear energy levels. It seemed desirable to extend the scope of these investigations, especially since such very definite predictions are made concerning the properties of many of these excited states by the collective model of the nucleus.[3,4]

Because of their higher charge and lower velocity for a given energy, alpha particles are eminently suited for the electric excitation of nuclei of lower atomic number since the condition for the simplified classical treatment of the process,[5,6] $2Z_1Z_2e^2/h\nu$

$\gg 1$ (Z_1 and Z_2 are the charges of projectile and target, v is their relative velocity), is well satisfied down to the lower end of the periodic table. A further advantage in the use of helium ions lies in the fact that they turn out to be relatively much less effective in exciting the troublesome characteristic K x-radiation as compared with the nuclear gamma radiation in the targets; for instance, at 3 Mev the relative yields of K x-rays and 137-kev

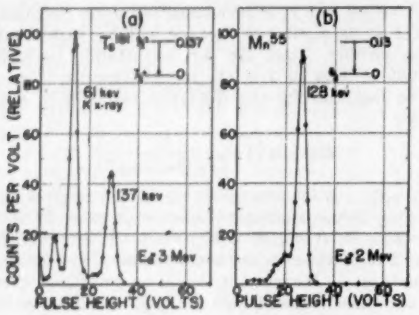

FIG. 1. (a) Pulse-height distribution of 137-kev gamma radiation and 61-kev K x-radiation from Ta^{181} bombarded by 3-Mev alphas. No absorber. (b) Pulse-height distribution of 128-kev gamma radiation from Mn^{55} bombarded by 2-Mev alphas. For previous level information, see reference 8.

gamma rays from tantalum are 2.27 for alpha particles and 14.8 for protons. Background problems are reduced by several orders of magnitude compared with proton excitation,[7] permitting us to operate with solid angles approaching 2π.

Our experimental set-up is very simple. The beam from our electrostatic generator strikes the target which is thick to the incident particles but thin to the emerging radiation. Either a 1-in. or 2-in. thick NaI(Tl) crystal (depending on the energy of the gamma radiation under study), separated from the target by about 0.040 in. aluminum and mounted on a Dumont 6292 photomultiplier tube, serves as the gamma-ray detector. This entire assembly is surrounded by a 1-in. layer of lead. The output is fed through a conventional linear amplifier to a single-channel pulse-height analyzer. A one-volt channel width is used throughout. The known gamma-ray lines of ionium (Th^{230}) at 68 kev and 142 kev, In^{114} at 190 kev, Cd^{111} at 170 kev and 247 kev, Na^{22} at 0.511 Mev (annihilation) and 1.28 Mev, and Cs^{137} at 662 kev are used for energy calibration of the system. We are able satisfactorily to detect radiation down to about 10 kev. Figure 1(a) shows the pulse-height distribution we obtain with a 5-mil tantalum target bombarded with 3-Mev alphas, exhibiting the K x-ray line at about 61 kev and the 137-kev gamma ray. Figure 1(b) gives a similar plot for a metallic 35-mil manganese target showing a line at 128 kev.[8] Space does not permit our including the spectra for all the targets we have examined; we shall do so in our more complete publication.

TABLE I. Survey of levels below 500 kev observed by Coulomb excitation with 3-Mev alphas. Approximate intensity relative to Ta^{181} (*uncorrected* for relative abundance and internal conversion).

Element[a]	Abundance %	E_γ(observed) kev	Approx. int.	E_γ(known)[b] kev
$_3Li^{7,e}$	92.5	478	···	478
$_9F^{19,e}$	100	108, 196	···	110, 190
		1280	···	1280
$_{11}Na^{23,e}$	100	430	···	440
$_{21}Sc^{45}$	100	388	0.1	450
$_{22}Ti^{47}$	7.8	155, 433	0.5, 0.08	185
$_{23}V^{51}$	99.8	320	0.24	320
$_{25}Mn^{55}$	100	128	10	130
$_{26}Fe^{57}$	2.2	122	0.14	14, 117, 131
$_{30}Zn^{67}$	4.1	93, 182	0.02, 0.06	92, 182
$_{32}Ge^{73}$	7.7	68	0.23	54
$_{33}As^{75}$	100	68, 199, 283	0.02, 0.4, 0.3	67, 202, 281
$_{34}Se^{77}$	7.6	(155), 237, 440	0.15, 0.2	160, 237
$_{37}Rb^{85,87}$	72, 28	150	0.05	150, 410
$_{38}Sr^{g}$	···	362	0.07	[f]
$_{40}Zr^{d}$	1.5[d]	90[d]	0.1[d]	89, 93[d]
(+$_{72}$Hf[176,180])				
$_{42}Mo^{93}$	15.7	198	0.05	200
$_{45}Rh^{103}$	100	305, 370	0.1, 0.04	40
$_{46}Pd^{105}$	22.6	68?	0.02	63
$_{48}Cd^{111}$	12.8	300?	0.01	247, 340
$_{49}In^{115,e}$	95.8	500	···[e]	500[e]
$_{51}Sb^{123}$	42.8	~160	0.02	153
$_{55}Cs^{133}$	100	85	0.6	81
$_{59}Pr^{141}$	100	~150	0.01	145
$_{62}Sm^{149}$	26.6	119	2.5	122
$_{70}Yb^{170}$	3.0	82	0.6	84
$_{73}Ta^{181}$	100	137	*1.00*	137
$_{74}W^{180,184,186}$	85.4	~120	1.3	102, 113, 124[f]
$_{81}Tl^{205}$	29.5	220?	0.003	279
$_{90}Th^{232}$	100	50	0.20	50

[a] The following elements did not show lines below 500 kev with alphas: Mg, Al, Si, P, S, Cl, K, Ca, Cr, Co, Ni, Cu, Ga, Nb, Ag, Te, Pt, Au, Pb, Bi.
[b] See reference 9.
[e] Via compound nucleus. For $Z<20$ see text.
[d] All entries refer to Hf impurity (3%).
[e] With protons only.
[f] T. Huus and J. H. Bjerregaard, Phys. Rev. 92, 1579 (1953).

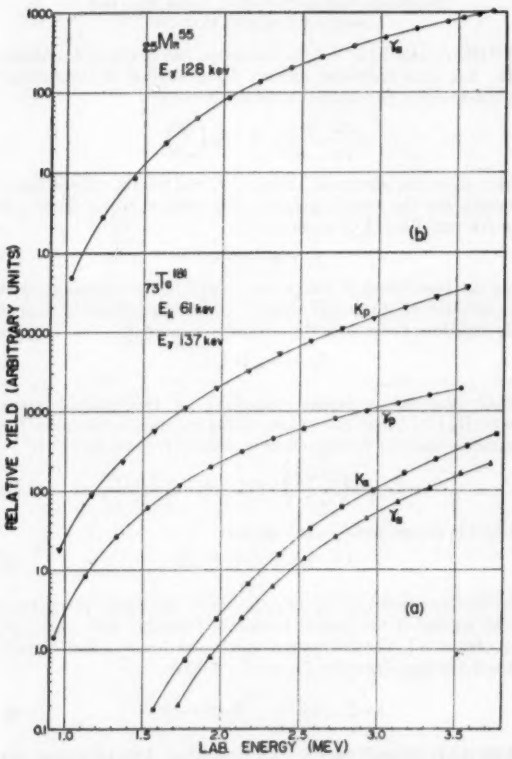

FIG. 2. (a) Excitation functions for K x-rays and gamma rays from $_{73}Ta^{181}$. $K_p = K$ x-ray yield (protons); γ_p = 137-kev gamma-ray yield (protons); $K_\alpha = K$ x-ray yield (alphas); γ_α = 137-kev gamma-ray yield (alphas). γ_p and γ_α curves are *theoretical* thick target yield curves, normalized at the highest energy points. (b) Coulomb excitation of the 128-kev gamma ray from $_{25}Mn^{55}$ by alpha particles. Solid curve is *theoretical* thick target yield curve, normalized at the highest energy. One-half the excitation energy has been subtracted before plotting experimental points in both (a) and (b).

The relative yields of K x-rays and gamma rays from tantalum under both proton and alpha-particle bombardment are shown in Fig. 2(a), illustrating the point mentioned above. The alpha-particle excitation function for one of the lighter nuclei ($_{25}Mn^{55}$) is shown in Fig. 2(b). Note that the curves for gamma excitation by protons and alphas in tantalum and by alphas in manganese are *theoretical* thick-target curves, calculated by numerically integrating the theoretical cross sections[6] over the particle ranges and normalized at the experimental points of highest energy. The agreement is indeed gratifying, completely confirming the

nature of the excitation process down to at least $Z=25$ for alphas and up to 3.6 Mev for protons on tantalum ($Z=73$). We postpone a detailed discussion of the results on the various nuclei we have investigated and restrict ourselves to a tabular presentation of the salient features in Table I. We list, in turn, the target nucleus, mass number, and relative abundance of the isotope believed responsible for the radiation, gamma-ray energy observed and energy levels known from other sources,[9] and a qualitative estimate of the relative yield of the observed radiation under 3-Mev alpha bombardment, *uncorrected* for internal conversion. The highest line excited was at 500 kev (In^{115}).

Elements with $Z<20$ are included here mainly for the purpose of demonstrating the main sources of radiation from possible light-element impurities. Li, F, and Na are found to be the only light elements yielding gamma rays below 500 kev under alpha bombardment. The excitations of the 478-kev state in Li^7 and the first two excited states in F^{19} at 108 kev and 196 kev (mainly by ordinary interlastic scattering of alphas involving compound nucleus formation with sharp resonances) have been studied and will be the subject of another publication.[10] In this connection, we have found striking evidence for Coulomb excitation of the 196-kev level in fluorine (second excited state) by alphas below 2.2 Mev before the onset of the resonances. This phenomenon is not observable with protons because of the complicated resonance structure which then extends down to very low energies.

We are extending our measurements into the rare-earth region where many nuclei have low-lying excited states. Our final results will include determinations of absolute yields and hence values of the reduced transition probabilities $B_\epsilon(2)$,[6] as well as a comparison of the experimental facts with the rotational interpretation[3,4] of these levels.

* A preliminary account of this work will be presented at the New York meeting of the American Physical Society, January 28–30, 1954.

[1] T. Huus and C. Zupančič, Kgl. Danske Videnskab. Selskab, Mat.-fys. Medd. **28**, No. 1 (1953).

[2] C. McClelland and C. Goodman, Phys. Rev. **91**, 760 (1953).

[3] A. Bohr and B. R. Mottelson, Kgl. Danske Videnskab. Selskab, Mat.-fys. Medd. **27**, No. 16 (1953).

[4] D. Hill and J. A. Wheeler, Phys. Rev. **89**, 1102 (1953).

[5] K. A. Ter-Martirosyan, J. Exptl. Theor. Phys. (U.S.S.R.) **22**, 284 (1952).

[6] K. Alder and A. Winther, Phys. Rev. **91**, 1578 (1953).

[7] We observe (capture) gamma radiation with energies greater than 4 Mev from most medium-heavy nuclei under proton bombardment.

[8] This level is known only from $Mn^{55}(p,p')Mn^{55m}$; see Hausman, Allen, Arthur, Bender, and McDole, Phys. Rev. **88**, 1296 (1951).

[9] Mostly as collected in Way, Fano, Scott, and Thew, *Nuclear Data*, National Bureau of Standards Circular 499 (U. S. Government Printing Office, Washington, D. C., 1950) and supplements; and Hollander, Perlman, and Seaborg, Revs. Modern Phys. **25**, 469 (1953).

[10] N. P. Heydenburg and G. M. Temmer, Phys. Rev. (to be published); a preliminary account will be presented at the New York meeting of the American Physical Society, January 28–30, 1954.

The Specific Ionization and Energy Loss of a Fast Charged Particle

J. R. Allen*
H. H. Wills Physical Laboratory, Bristol, England
(Received October 19, 1953)

It may be shown that the primary ionization and excitation density j_P (i.e., the average number of electrons excited or ejected per unit volume either directly or by absorption of Čerenkov radiation), because of the passage of a fast charged particle through a medium, is, at distances greater than ρ_0, the minimum impact parameter, given by

$$j_P=\frac{c}{\hbar}\int\tau\frac{\mathfrak{E}^*\cdot\mathfrak{E}}{\omega}d\omega. \tag{1}$$

In this equation, the particle's field is treated as a perturbation in a semiclassical approximation; $\tau(\omega)$ is the photoelectric absorption coefficient; $\mathfrak{E}(\omega,\rho)$ is the Fourier time transform of the effective electric field.

If $\mathfrak{E}$ is calculated by the phenomenological approximation due to Fermi,[1] Eq. (1) and the similarly derived equation for the energy absorption density may be integrated over all impact parameters greater than ρ_0. We obtain for the total primary ionization and excitation ($\rho>\rho_0$)

$$P(\rho_0)=\int\Phi dE,\quad \tau\neq0;\quad P=0,\quad \tau=0 \tag{2}$$

and for the total energy absorption ($\rho>\rho_0$)

$$\Gamma_T(\rho_0)=W_0\int\Phi E dE,\quad \tau\neq0;\quad \Gamma_T=0,\quad \tau=0, \tag{3}$$

where

$$\Phi=\frac{\alpha^2Z^2}{\pi a_0\beta^2}\frac{g}{\kappa^2\kappa}\,\mathrm{Im}[\kappa\zeta^2K_0^*(\zeta)K_1(\zeta)];$$

$\kappa=\epsilon'+i\epsilon''$ is the complex dielectric constant; $g=(\eta^2+\xi^2)^{\frac{1}{2}}$; $\eta=1-\beta^2\epsilon'$, $\xi=\beta^2\epsilon''$; $\zeta=[\alpha\rho_0E/2\sqrt{2}a_0\beta][\sqrt{(g+\eta)}-i\sqrt{(g-\eta)}]$; W_0 is the Rydberg energy; a_0 is the Bohr radius; and E, the energy of the field components, is in rydbergs. Equation (3) is equivalent to Fermi's formula (22)[1] when $\tau\neq0$.

The absorption coefficient τ and the dielectric constant ϵ' were obtained for silver bromide by the methods described below and Eqs. (2) and (3) were integrated numerically for all transfers less than 5000 ev. The results relative to the plateau values are shown in Fig. 1 plotted against the kinetic energy of the particle

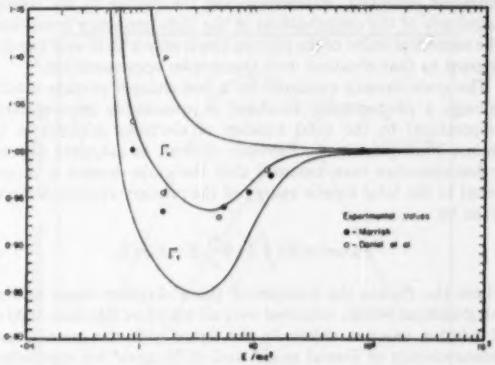

Fig. 1. P, the primary ionization and excitation; Γ_T, the energy absorption; and Γ_K, the kinetic energy of the primary electrons: computed for a singly charged particle (transfers <5000 ev, distances $>2a_0$) and shown relative to the plateau values $P(\beta=1)=50\,690$/cm, $\Gamma_T(\beta=1)=3.31$ Mev/cm, $\Gamma_K(\beta=1)=1.21$ Mev/cm as functions of E/mc^2 (E = kinetic energy). Experimental values of relative grain density are due to Daniel *et al.* (reference 8) (marked ○) and Morrish (reference 9) (marked ●).

in units of mc^2. A discussion of the absorption resulting from the valence band of silver bromide has already been published,[2] and it was shown that the large polarizability of this salt results in a considerable modification in the shape of the absorption bands. Also, partly because of the large polarizability and partly because of the effect of the exclusion principle, there is a shift in the oscillator strengths towards the lower frequency bands. These considerations have been extended to the calculation of the absorption from the next few bands lying below the valence levels. The shape of the absorption curves being assumed to be in accordance with these calculations, their magnitudes were checked by a comparison of the computed with the empirically observed dispersion in the visible and ultraviolet. The oscillator strengths and absorption coefficients for the far x-ray region were taken from experimental values,[3,4] whereas for intermediate frequencies the absorption was calculated by the methods of Stobbe[5] using appropriate screening constants and a correction for the polarization effect near the absorption edge. The values of the absorption edges (in Rydberg units) and the total oscillator strengths for the various bands are shown in Table I. The dielectric constant was computed from the absorption coefficient.

These detailed expressions for τ and ϵ' change considerably the conclusions obtained when a simple line absorption model is used, and the oscillator strengths are assumed proportional to the

TABLE I. Absorption edges (ry) and oscillator strengths for AgBr.

Band	Ag E (ry)	Ag f	Br E (ry)	Br f
$K(1s)$[1]	1880	1.13	993	1.2
$L(2s)$[1]	280.9	1.3	130.5	1.4
$(2p)$[1]	260.2	1.5	117.8	1.5
$(2p)$[2]	247.5	2.5	114.3	2.5
$M(3s)$[1]	53.5	1.4	19.48	1.5
$(3p)$[1]	45.0	2.4	13.60	2.5
$(3p)$[2]	42.7	2.7	13.21	2.8
$(3d)$[4]	28.1	9.0	5.27	9.6
$(3d)$[5]	27.7		5.13	
$N(4s)$[1]	7.67	1.8	1.76	2.3
$(4p)$[3]	4.80	6.5	0.42	12.1
$(4d)$[10]	0.85	14.4		

number of electrons. The Čerenkov radiation may be shown to contribute a very small proportion of the energy loss and to lie entirely in the visible, ultraviolet, and soft x-ray regions. Because of the shift of the oscillator strengths and the breadth of the absorption regions, the total energy loss saturates very rapidly as may be seen from the figure. The relative rise is much greater than that obtained by previous authors[6,7] who calculated the ionization loss by assuming low damping and introducing a mean ionization potential, underestimating the change in the relative magnitude of the contributions of the high-frequency transitions. The numerical value of the plateau loss is only a little over one-half as great as that obtained with the simpler approximation.[7]

The grain density produced by a fast charged particle moving through a photographic emulsion is presumably approximately proportional to the total number of electrons released in the grains. This quantity is, however, difficult to calculate directly. It has therefore been assumed that the grain density is proportional to the total kinetic energy of the primary ejected electrons, given by

$$\Gamma_K(\rho_0) = W_0 \int \Sigma_i \Phi \frac{\gamma_i}{\gamma}(E-E_i)dE, \qquad (4)$$

where the E_i are the energies of the absorption edges and the integral is, as before, extended over all transfers less than 5000 ev. It relative value is shown in the figure with the grain density measurements of Daniel *et al.*[8] and of Morrish[9] for comparison. The curve predicts a slightly more rapid rate of rise and a somewhat smaller percentage rise from the minimum to the plateau value than is shown by the measurements. This discrepancy could result from an overestimate of the shift in the oscillator strengths.

A detailed account of this work will be published elsewhere.

* Now at Department of Physics, Queen's University, Kingston, Canada.
[1] E. Fermi, Phys. Rev. **57**, 485 (1940).
[2] J. R. Allen, Can. J. Phys. **31**, 218 (1953).
[3] A. H. Compton and S. K. Allison, *X-Rays in Theory and Experiment* (D. Van Nostrand Co., Inc., New York, 1935), second edition.
[4] H. H. Landolt and R. Börnstein, *Zahlenwerte und Funktionen aus Physik, Chemie, Astronomie* (J. Springer, Berlin, 1950), Vol. I.
[5] M. Stobbe, Ann. Physik **7**, 661 (1930).
[6] O. Halpern and H. Hall, Phys. Rev. **73**, 477 (1948).
[7] M. Huybrechts and M. Schönberg, Nuovo cimento **9**, 764 (1952).
[8] Daniel, Davies, Mulvey, and Perkins, Phil. Mag. **43**, 753 (1952).
[9] A. H. Morrish, Phys. Rev. **91**, 423 (1953).

μ-Meson Decay, β Radioactivity, and Universal Fermi Interaction

L. MICHEL, *Institute for Advanced Study, Princeton, New Jersey*
AND
A. WIGHTMAN, *Princeton University, Princeton, New Jersey*

RECENT experimental data on the μ-meson mass and the μ-meson decay spectrum suggest a reconsideration of the hypothesis of a universal Fermi interaction. The purpose of this letter is to show that the data on μ decay and β radioactivity can be reconciled with a universal Fermi interaction but that the most often proposed interactions are excluded.

The new data to which we refer are: *the μ-meson mass*[1]: $m_\mu = 207.0\times 0.4 m_e$ or $207.1\pm 1.1 m_e$, for which we adopt:

$$m_\mu = 207.0\pm 1.0 m_e \text{ (standard error)}$$

and *the shape of the energy spectrum of secondary electrons* from decay at rest of μ mesons. If the decay is governed by a Fermi interaction, the shape of the decay spectrum can be characterized by m_μ and a single parameter ρ. If the two neutrinos emitted in μ-meson decay are distinguishable ($\nu\neq$), $0\leq\rho\leq 1$. If the two emitted neutrinos are identical ($\nu=$), then $0\leq\rho\leq\frac{3}{4}$.[2] A statistical analysis of the shape of the μ-meson spectrum gives a relation between ρ and m_μ. (The various published values of ρ have then to be adjusted to the new m_μ value.) We adopt here the most recent determination of Vilain and Williams[3]:

$$\rho = 0.50\pm 0.12 \text{ (standard error)}.$$

For the sake of simplicity, we shall apply these new data only to the discussion of the most often proposed linear combinations of the five interactions of β radioactivity, i.e., $\pm S+T\pm P$ or $\pm S+T\mp P$ (the usual notations of β radioactivity are used). These four chosen interactions seem not to be excluded by the β-radioactivity data to date (except that the relative sign of T and P could be determined from the radium E spectrum if the assumptions of Petschek and Marshak[4] are correct).

To compare μ decay and β radioactivity, we have to choose a one-to-one correspondence between the two sets of particles n, p, e, ν, and μ, ϵ, ν, ν. The 4! possible correspondences fall into three essentially different classes of which the following are samples: (a) $pn\epsilon\nu \to \nu\mu\epsilon\nu$; (b) $pn\epsilon\nu$, $\mu\nu\epsilon\nu$; (c) $pn\epsilon\nu$, $\mu\epsilon\nu\nu$. The examples of (a) and (b) are the correspondences suggested by the triangle of Fermi interactions between the three pairs np, $e\nu$, $\mu\nu$. Such $\pm S+T\pm P$ or $\pm S+T\mp P$ interactions have been proposed by Caianiello,[5,6] and in previous papers cited in that paper:

	$\pm S+T\pm P$
Pursey[7]:	$-S+T-P$
Peaslee[8]:	$-S+T-P$
Konopinski and Mahmoud[9]:	$\pm S+T+P$
Finkelstein and Kaus[10]:	$-S+T-P$

all with $\nu=$ and correspondence (b). These four chosen β-radioactivity interactions predict values[11] of ρ and τ_μ which have to be compared with experiment. These results are given in Table I

TABLE I. Values of the shape parameter ρ of μ decay and of the ratio λ of the ft values of μ decay and β radioactivity for various universal Fermi interactions.

	$\nu\neq$ (a) ρ	(a) λ	(b) ρ	(b) λ	(c) ρ	(c) λ	$\nu=$ (a) ρ	(a) λ	(b) ρ	(b) λ	(c) ρ	(c) λ
$S+T+P$	0	4/3	3/4	4/3	3/4	4/3	0	4/3	0	1/3	0	1/3
$-S+T-P$	3/4	4/3	0	4/3	3/4	4/3	0	1/3	0	4/3	0	1/3
$\pm S+T\mp P$	3/8	4/3	3/8	4/3	3/4	4/3	0.14	0.92	0.14	0.92	0	1/3

but instead of τ_μ, we shall use the parameter λ proposed by Michel,[12] which is essentially the ratio of ft values for μ and β decays.

We adopt here[13] $B=2650\pm 10$ percent for the rate constant of β radioactivity. Using the μ-meson lifetime $\tau_\mu = (2.22\pm 0.02)\times 10^{-6}$ sec,[14] we obtain: $\lambda = 1.16\pm 0.12$. Table I shows that the closest to a fit is $\rho = 3/8$, $\lambda = 4/3$. These values are not in very good agreement with experiment. However, they cannot be safely excluded, because systematic errors in the theoretical evaluation of nuclear matrix elements of β radioactivity are possible. Nevertheless, it is clear that *the interactions proposed by the authors listed above are excluded.*

By considering more general interactions, one can obtain a very good fit for ρ and λ. For example, interactions of the type $\pm S+T+pP$ give essentially two possibilities: one with $\nu\neq$, $|p|<\frac{1}{2}$, (a) or (b), e.g., $_{b+}{}^{a-}S+T$, $\rho=0.54$, $\lambda=1.17$; the other with $\nu=$, $|p|\sim 3.5$, (a) or (b), e.g., $_{b-}{}^{a+}S+T\mp 3.5P$, $\rho=0.58$, $\lambda=1.10$.

Apart from these possibilities and the above-mentioned borderline case [$\nu\neq$, $\pm S+T\mp pP$ with $p\sim 1$, (a) or (b)], no new

domains of solutions appear when one considers the general interaction $sS+vV+T+aA+pP$ with $|s|<1.2$, $|v|<0.4$, $|a|<0.2$.

Although the simple connection between Fermi interactions adopted here includes most of the usual choices, it should be emphasized that there exists other possibilities no more and no less arbitrary (see, e.g., Caianiello, Finkelstein and Kaus). A complete discussion is found in the thesis of the first-named author.[5]

[1] Smith, Birnbaum, and Barkas, Phys. Rev. **91**, 765 (1953).
[2] L. Michel, Nature **163**, 959 (1949).
[3] J. Vilain and R. W. Williams, Phys. Rev. **92**, 1586 (1953).
[4] A. Petschek and R. Marshak, Phys. Rev. **85**, 698 (1952).
[5] E. Caianiello, Nuovo cimento **10**, 43 (1953).
[6] Caianiello's hypotheses are different from ours. In his case the λ values given in Table I must be multiplied by 2, to be compared with experiment.
[7] D. Pursey, Physica **18**, 1017 (1952).
[8] D. C. Peaslee, Phys. Rev. **91**, 1447 (1953).
[9] E. J. Konopinski and H. M. Mahmoud, Phys. Rev. **92**, 1045 (1953). In fact, in their discussion, these authors compare ρ with experiment for an interaction of the type $sS+T+pP$, (a), $\nu=$, with $0.55<|s|<1$.
[10] R. Finkelstein and P. Kaus, Phys. Rev. **92**, 1316 (1953).
[11] L. Michel, thesis, Sorbonne, 1953 (unpublished).
[12] L. Michel, *Progress in Cosmic Ray Physics* (North Holland Publ. Company, Amsterdam, 1952), Chapter 3, Eq. (43).
[13] See A. Winther and O. Kofoed-Hansen, Kgl. Danske Vidensk. Selskab, Mat.-fys. Medd. **27**, No. 14 (1953) for the definition and the determination of B. Their value agrees within the given error with an as yet unpublished value of Feenberg (private communication).
[14] W. E. Bell and E. P. Hincks, Phys. Rev. **84**, 1243 (1951).

Coulomb Corrections in Stripping*

S. T. Butler† and N. Austern
Laboratory of Nuclear Studies, Cornell University, Ithaca, New York
(Received November 20, 1953)

We wish to report some preliminary results from our investigation of the influences of Coulomb forces on the deuteron stripping cross section. It is, in general, still not obvious what new effects should be anticipated, but we can describe one case for which we used numerical methods to carry through a calculation of reliable accuracy. Although some preliminary ideas had suggested that in this case the Coulomb effects might be large, the angular distribution actually is found to agree surprisingly well with the non-Coulomb result.

Our method differs from the now-familiar approach of Butler[1] only in that the various wave functions are replaced by their Coulomb analogs. The Coulomb analog of a plane wave beam of deuterons must be treated approximately, as its exact derivation would require the solution of a three-body dynamical problem. We replace this wave function by $\chi(r)C(\mathbf{K},\mathbf{R})$, where $\chi(r)$ is the undistorted internal deuteron function, and $C(\mathbf{K},\mathbf{R})$ is the Coulomb wave function for a particle of deuteron mass and charge and incident wave vector $\mathbf{K}$. We have also been able to carry through a fairly good calculation of the stripping effects which this approximation omits—those resulting from the distortion of the deuteron by the Coulomb field. For the usual sorts of targets and bombarding energies these "polarization" effects are found small enough to be ignored safely.

Accepting the above approximation for the wave function of the incident deuteron, the only difficult step in the derivation is the computation of the "stripping transform." This is the transform which expresses the incident wave function as expanded into states in which the outgoing particle has definite linear momentum at large distances, and in which the captured particle has definite angular momentum. For example, for (d,p) reactions the stripping transform is

$$\int d\Omega_N d\mathbf{r}_p \chi(|\mathbf{r}_p-\mathbf{r}_N|)C\left(\mathbf{K},\frac{\mathbf{r}_p+\mathbf{r}_N}{2}\right)Y_{L,M}^*(\theta_N,\phi_N)C(-\mathbf{k}_p,\mathbf{r}_p). \quad (1)$$

We have not succeeded in finding any approximations to this integral which are both simple and also sufficiently accurate for the problem. Various approximate evaluations led us to believe that the Coulomb effects might very much change the stripping angular distribution, in contradiction to the familiar good fit between experiment and the non-Coulomb theory. It seemed desirable to check the approximations in one case by making a more accurate calculation, necessarily largely numerical, and quite lengthy.

The method of the more accurate calculation can only be employed for a (d,n) reaction, where $C(-\mathbf{k}_p,\mathbf{r}_p)$ in (1) is replaced by $\exp[-i(\mathbf{k}_N\cdot\mathbf{r}_N)]$. We first consider the integration over $\mathbf{r}_N$:

$$\int d\mathbf{r}_N \chi(r)C(\mathbf{K},\mathbf{R})\exp[-i(\mathbf{k}_N\cdot\mathbf{r}_N)]. \quad (2)$$

In this integral we go over to $\mathbf{r}=\mathbf{r}_p-\mathbf{r}_N$ as the variable of integration, and replace C by the usual form of an exponential times a hypergeometric function. Then the hypergeometric function is written in integral representation. Thus C appears in the form

$$C(\mathbf{K},\mathbf{r}_p-\mathbf{r}/2)=\frac{e^{-\pi n/2}}{\Gamma(-in)}\int_0^1 du\, u^{-1-in}(1-u)^{in} \times\exp\{i(1-u)[\mathbf{K}\cdot(\mathbf{r}_p-\mathbf{r}/2)]\}\exp(iuK|\mathbf{r}_p-\mathbf{r}/2|). \quad (3)$$

Here $n=2Ze^2M/\hbar^2K$, the usual Coulomb parameter. Now we expand $|\mathbf{r}_p-\mathbf{r}/2|$ in (3), and carry only the first two terms, $r_p-(\mathbf{r}\cdot\mathbf{r}_p)/2r_p$. Having made only this quite reliable approximation it is possible to integrate over $\mathbf{r}$ in (2), leaving to be performed only the one-dimensional integral over u. Both this integral and the spherical harmonic expansion are now done numerically, it being possible to put the analytic expressions into a suitably convenient form for the numerical work.

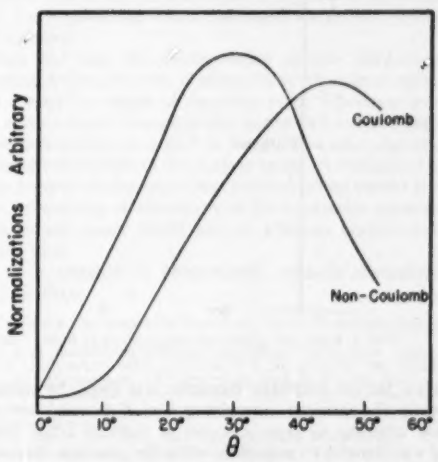

FIG. 1. Angular distributions computed for a (d,n) reaction on a nucleus of $Z\approx15$. Angular momentum transfer, $l=2$. Incident energy, $E_d=8$ Mev. Outgoing energy, $E_n=12$ Mev. Coulomb parameter, $n_d=1.2$.

The particular case that we have worked through involves the capture of $l=2$ protons, an 8-Mev deuteron beam being incident on a nucleus of $Z\approx15$, with the outgoing particles having 12 Mev, approximately corresponding to the $P^{31}(d,p)P^{32}$ reactions of Parkinson *et al.*[2] Figure 1 shows the resulting angular distribution, also including the non-Coulomb curve of the old theory. The peak of the Coulomb curve is somewhat displaced towards larger angles, but otherwise gives an angular distribution which is essentially the same as the non-Coulomb result, and in a region where large Coulomb changes were anticipated ($n=1.2$).

We are very grateful to Professor H. A. Bethe for his generous help and encouragement, and to Max Goldstein of the Los Alamos staff for performing the numerical calculations.

* Supported by the joint program of the U. S. Office of Naval Research and the U. S. Atomic Energy Commission.
† Now at Australian National University, Canberra, Australia.
[1] S. T. Butler, Proc. Roy. Soc. (London) **208**, 559 (1951).
[2] Parkinson, Beach, and King, Phys. Rev. **87**, 387 (1952); J. S. King and W. C. Parkinson, Phys. Rev. **88**, 141 (1952); E. H. Beach and J. S. King, Phys. Rev. **90**, 381 (1953).

Spins and Parities of Energy Levels in Pb^{208}

L. G. Elliott, R. L. Graham, J. Walker, and J. L. Wolfson
Physics Division, Atomic Energy of Canada Limited, Chalk River, Ontario, Canada
(Received November 19, 1953)

MEASUREMENTS of the K internal conversion coefficients α_K of the 2.62, 0.583, 0.860, and 0.511 Mev γ-ray transitions in Pb^{208} following the decay of Tl^{208} (3.1 min) together with a determination of the angular correlations between selected pairs of these γ rays have recently been made at this laboratory. The results lead unambiguously to the spin and parity assignments shown in Fig. 1 with the sole assumption of zero spin and even parity for the ground state of Pb^{208}.

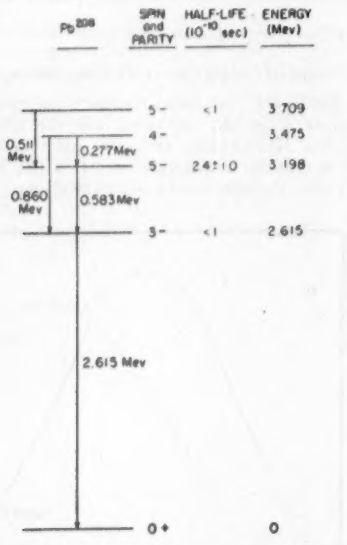

FIG. 1. Spins and parities of energy levels in Pb^{208}.

The α_K for the 2.62-Mev transition was found by measuring separately the quantum intensity q, and K internal conversion electron intensity ϵ_K from a source of thorium active deposit. The q was found by comparison with the quantum intensity of the 2.76-Mev γ radiation from a standardized source of Na^{24} using a NaI(Tl) scintillation spectrometer. The ϵ_K was determined by measurement of the "X" line intensity in a magnetic β-ray spectrometer having an accurately measured transmission. The α_K for the 0.583-Mev transition was found in a similar manner. The values obtained were $(1.78\pm0.12)\times10^{-3}$ and $(1.52\pm0.11)\times10^{-2}$ for the 2.62-Mev and 0.583-Mev transitions, respectively. The former is in good agreement with the theoretical value[1] of 1.86×10^{-3} for $E3$ radiation and the latter with the theoretical value[1] of 1.61×10^{-2} for $E2$ radiation. Both measured values are in agreement with those reported by Martin and Richardson.[2]

The angular correlation experiment was performed using a source of thorium active deposit in a 1N nitric acid solution with a small amount of $Pb(NO_3)_2$ added as carrier. The detectors were NaI(Tl) crystals and 6292 Dumont or 5819 RCA photomultipliers. Each channel of the coincidence circuit incorporated a single-channel pulse-height analyzer. By appropriate pulse-height selection coincidences between the 0.511-Mev γ ray and the 2.62-Mev γ ray were avoided entirely. Except for a 3 percent contribution caused by the Compton effect from the 0.860-Mev transition the true coincidences recorded were due entirely to those of the 0.583-Mev and 2.62-Mev cascade.

Coincidences were recorded at seven angles and the rates, corrected for (1) chance coincidences, (2) the contribution owing to the 0.860-Mev transition, and (3) the decay of the sample, are shown in Fig. 2. The experimental data are plotted as points, normalized to the value at 90°. The curves are the theoretical functions (corrected for the finite angular resolution) for the 0–3–5 assignment and the previously proposed assignments[2,3] 0–2–4 and 0–1–3. The experimental results are consistent only with the assignment 0–3–5.

Similar but less detailed measurements of α_K for the 0.86-Mev and 0.511-Mev γ rays and of the angular correlations of these γ rays with respect to the 2.62-Mev γ ray indicate: (1) an assignment of 4− for the 3.48-Mev level with an intensity ratio of $E2/M1=(6.5\pm6.5)\times10^{-4}$ and 180° phase difference for the 0.86-Mev γ ray, and (2) an assignment of 5− for the 3.71-Mev level with $E2/M1=1.7\pm0.3$ and 0° phase difference for the 0.511-Mev γ ray.

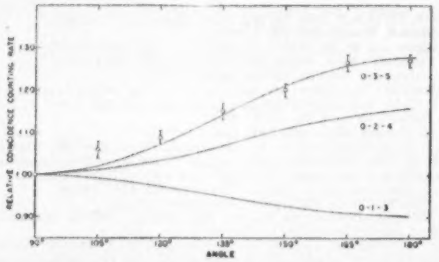

FIG. 2. Angular correlation between the 0.583-Mev and 2.615-Mev γ rays. The experimental data are plotted as points normalized to the value at 90°. The vertical bars represent the standard deviations. The curves are the theoretical functions corrected for the finite angular resolution for the assignments 0–3–5, 0–2–4, and 0–1–3.

Coincidences were observed in a double magnetic β-ray spectrometer between the β-ray continuum and the 0.583-Mev K internal conversion line, and indicate that the 0.583-Mev transition is delayed with a half-life of $(2.4\pm1.0)\times10^{-10}$ sec. Observed coincidences between the 0.583-Mev γ ray and the 2.62-Mev γ ray indicate a half-life of less than 1×10^{-10} sec. An upper limit of 1×10^{-10} sec for the half-life of the 0.511-Mev transition has also been obtained. These data are incorporated in Fig. 1.

A detailed investigation of the decay of Tl^{208} is being carried out and a complete report will be submitted for publication in the *Canadian Journal of Physics*.

The authors wish to thank Mr. J. S. Geiger for aid in making the conversion coefficient measurements, Mr. R. C. Hawkings and Mr. W. F. Merritt for standardization of Na^{24} sources, and Dr. B. B. Kinsey for interesting discussions of this problem.

[1] Rose, Goertzel, and Perry, Oak Ridge National Laboratory Report ORNL-1023, 1951 (unpublished).
[2] D. G. E. Martin and H. O. W. Richardson, Proc. Phys. Soc. (London) **A63**, 223 (1950).
[3] H. E. Petch and M. W. Johns, Phys. Rev. **80**, 478 (1950).

Elastic Scattering of Intermediate-Energy Alpha Particles by Gold*

George W. Farwell and Harvey E. Wegner†
Department of Physics, University of Washington, Seattle, Washington
(Received November 24, 1953)

THE elastic scattering by Au of alpha particles of energies 14 to 42 Mev has recently been observed in this laboratory. The variation of cross section with alpha-particle energy has been studied for scattering angles of 60° and 95° (lab system). At low bombarding energies, the cross section is given by the Rutherford formula for Coulomb scattering; at higher energies, the decrease in cross section with increasing alpha-particle energy is much more rapid.

The distance of closest approach of alpha particle and scattering nucleus, or apsidal distance, can be calculated for the classical

trajectory of an alpha particle of a given energy scattered through a particular angle. For the energy E_α^0 (hereinafter called the critical energy) at which the deviation from Coulomb scattering is first observed, the apsidal distance is found to be $(12.5\pm0.2)\times10^{-13}$ cm for the 60° case. This distance is significantly larger than a reasonable estimate $(9-10\times10^{-13}$ cm) of the sum of the radii of the Au nucleus and the alpha particle.[1] A similar value, $(12.9\pm0.3)\times10^{-13}$ cm, is found for the apsidal distance at the critical energy in the 95° case.

Departures from Coulomb's law were observed by Bieler,[2] who studied the angular distribution of alphas scattered by Mg and Al, and by Rutherford and Chadwick,[3] who measured the dependence of elastic-scattering cross section upon alpha energy for Al. Data in the non-Coulomb region were very meager because of the limited range of alpha energy available, and interest in the elastic scattering of alphas by intermediate and heavy nuclei seems to have lapsed after these experiments.

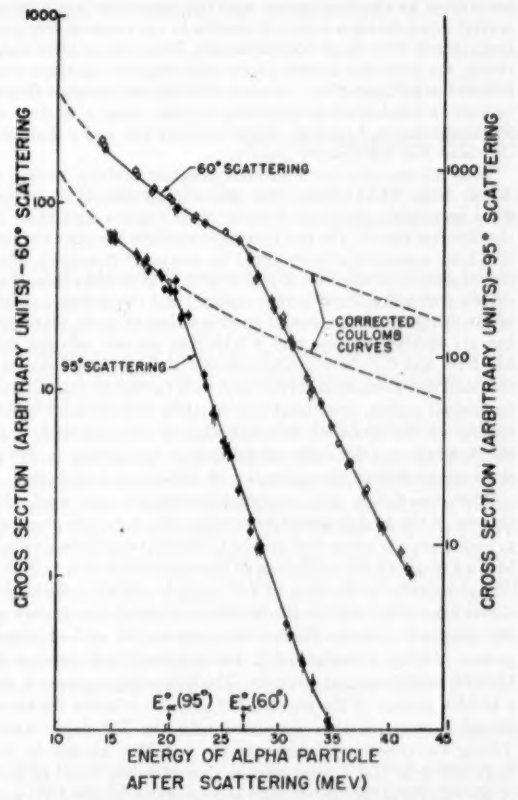

FIG. 1. Elastic scattering of alpha particles by gold. Cross section (relative) is plotted against alpha-particle energy for 60° scattering and for 95° scattering. The low-energy part of each curve is normalized to a corrected Coulomb curve (see text). The critical energy E_α^0 corresponds to the intercept of the straight line portion of the experimental curve with the corrected Coulomb curve.

The deflected alpha-particle beam of the University of Washington 60-in. cyclotron was used in the present experiments. A remotely controlled absorber was installed which could reduce the incident alpha-particle energy from 42 Mev to zero in steps of about 1 Mev. Scattered alpha particles were observed by means of a differential-range coincidence proportional-counter telescope. At each value of the incident alpha-particle energy, the number of elastically scattered alpha particles observed was normalized to the integrated beam current.

Results are shown in Fig. 1. For each scattering angle, relative elastic-scattering cross section is plotted against alpha-particle energy after scattering. Each curve is normalized to a "corrected Coulomb curve," i.e., a curve in which the energy dependence predicted by the Rutherford formula is modified very slightly to take into account a small variation in scattering angle with energy. (This variation is due to the fringing magnetic field of the cyclotron.)

At low energies, the cross section at 60° is seen to follow the Coulomb dependence closely. At an energy of about 27 Mev, however, the cross section begins to drop very rapidly as the alpha-particle energy E_α is increased. The energy dependence in the range 27–40 Mev is very well represented by the simple empirical formula:

$$\sigma(E_\alpha)=\sigma(E_\alpha^0)\exp\{-K(E_\alpha-E_\alpha^0)\},$$

where $\sigma(E_\alpha)$ = cross section at energy E_α (Mev), E_α^0 = critical energy = 27.0 ± 0.3 Mev, and K = constant = 0.28 Mev^{-1}.

The curve for scattering through 90° is similar in form, the critical energy E_α^0 being lower (20.25 ± 0.4 Mev) and K being higher (0.40 Mev^{-1}).

Studies are in progress using other heavy elements. Preliminary results are very similar to those for Au. The critical energy E_α^0 increases with Z but the parameter K appears to be independent of Z (for a particular scattering angle) within the experimental uncertainties.

Since E_α^0 and the corresponding apsidal distance can be measured quite precisely, it seems likely that these experiments offer a sensitive means of detecting small differences in nuclear size, and we expect to explore this aspect. It is evident that strong absorption occurs when nuclear forces come into play at apsidal distances comparable to the nuclear radius. A theoretical analysis of the present results and others to be obtained should give more exact information on the nature of the interaction between alpha particles and heavy nuclei and on effective nuclear and alpha particle radii.

It is a pleasure to acknowledge valuable discussions with Dr. J. S. Blair.

* This work was supported in part by the U. S. Atomic Energy Commission.

† Now at Brookhaven National Laboratory, Upton, New York.

[1] Use of $R_0=r_0A^{\frac{1}{3}}$, with $r_0=1.4\times10^{-13}$ cm, gives for the radius of the Au nucleus the value $R_{Au}=8.1\times10^{-13}$ cm. Following J. M. Blatt and V. F. Weisskopf, *Theoretical Nuclear Physics* (John Wiley and Sons, Inc., New York, 1952), a value $R_\alpha=1.2\times10^{-13}$ cm is assumed here for the effective alpha-particle radius.

[2] E. S. Bieler, Proc. Roy. Soc. (London) **A105**, 434 (1924).

[3] E. Rutherford and J. Chadwick, Phil. Mag. **50**, 889 (1925).

Proton Distribution in Heavy Nuclei*

M. H. JOHNSON AND E. TELLER
Radiation Laboratory, University of California, Livermore, California
(Received November 23, 1953)

THE Coulomb repulsion tends to force protons as far apart as possible, thereby lowering the proton density at the center of a nucleus. One might conclude that such an expansion would cause a proton excess on the nuclear surface. It is easy to see that the stability against β decay brings about the opposite result, a neutron excess on the surface.

The top part of Fig. 1 gives a qualitative picture of the average potential acting on neutrons and protons. It is assumed that the proton potential and the neutron potential are the same except for the electrostatic energy. The dashed line indicates the highest filled energy state in the Fermi distribution for both protons and neutrons. Beta stability requires that the highest filled proton state have the same energy as the highest filled neutron state (actually the proton should have 0.79 Mev more energy, a difference that may be neglected compared to the Coulomb potential in heavy nuclei). If the nuclear potential at the surface has a finite slope, the dashed line intercepts the potential at a somewhat smaller radius for protons. Consequently, the proton

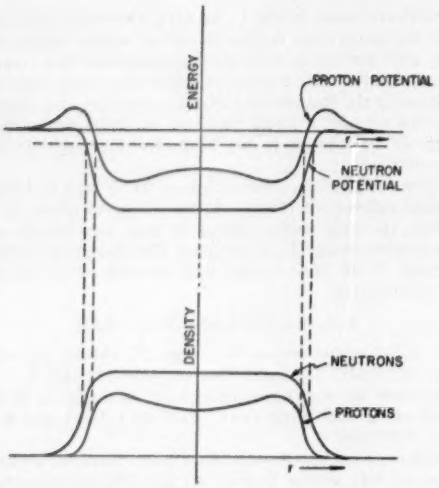

FIG. 1. Potentials and densities for protons and neutrons inside the nucleus.

distribution lies inside the neutron distribution. For the heaviest elements the difference in radii could easily be ½ to ¾ the thickness of the sloping part of the nuclear potential; the latter is likely to be of the order of the meson Compton wavelength. Thus the radius of the proton distribution may turn out smaller than the neutron radius by about 10^{-13} cm.

A more detailed examination of the nucleon orbits gives qualitatively the same result. The intercept of the energy level with the radial potential determines a point of inflection for the wave function; beyond this point the wave function is always convex to the axis. This point will be different for different angular momenta but will lie at systematically smaller radii for protons. In addition, the higher potential barrier for protons outside this point causes proton wave functions to vanish more rapidly than neutron wave functions. The lower part of Fig. 1 gives a qualitative picture of the proton and neutron densities within the nucleus.

In experiments with nucleons and π mesons which interact strongly with nuclear matter, one may find the surface of the nucleus at radii where practically no protons are present and the neutron density is well below its plateau value. In experiments with electrons and μ mesons which interact only with the electrostatic field, one may find the smaller radii characteristic of the proton distribution.

* Work supported by the U. S. Atomic Energy Commission.

A New Titanium Nuclide: Ti^{44}†

R. A. SHARP AND R. M. DIAMOND
Department of Chemistry, Harvard University, Cambridge, Massachusetts
(Received November 30, 1953)

A LONG-LIVED titanium activity has been produced by the irradiation of scandium oxide with 30–45-Mev protons. Spectroscopic analysis showed that the scandium oxide available[1] contained about 1 percent each of zirconium and calcium and about ½ percent each of thorium and combined rare earths; initial studies indicated that these impurities caused too much radioactive contamination to observe any long-lived titanium activity. The necessary scandium purification was accomplished by the development of a solvent extraction method using thenoyltrifluoroacetone (TTA).[2] Samples of approximately 70 mg of the purified oxide were wrapped in aluminum foil and bombarded for ~1 microampere hour in the internal beam of the Harvard 95-inch synchrocyclotron, yielding ~100 dis/sec of the new activity.

After the 3.1-hour Ti^{45} and the 3.9-hour Sc^{43} and Sc^{44} activities had been allowed to decay, the target material and 10 mg of titanium metal as carrier were dissolved in boiling 6*N* HCl. Hydrogen peroxide was added to insure that all the titanium was in the (IV) state and was then destroyed by further boiling. The titanium fraction was isolated by repeated cupferron precipitation from chilled 6*N* HCl solution and subsequent extraction into chloroform.[2]

By a similar procedure the scandium daughter could be separated from its titanium parent, and this separation was effected several times during a period of months to the titanium fractions from targets from three bombardments. Immediately after separation, the activities of both parent and daughter fractions were followed in an argon-filled, chlorine-quenched, end-window Geiger counter, a windowless proportional counter using a mixture of 95 percent argon, 5 percent CO_2 as counting gas, and a thallium-activated NaI scintillation counter.

With all counters the scandium daughter activity showed a 4-hour decay which turned over into a small amount of a long-lived component, probably because of incomplete separation of the titanium parent. The fact that approximately the same amount of 4-hour scandium activity could be separated repeatedly from the titanium fraction over a period of several months shows the presence of a long-lived parent nuclide, and the 4-hour half-life of the daughter indicates mass number either 43 or 44. Since Sc^{44} has a 1.46-Mev positron and a 1.16-Mev gamma, whereas Sc^{43} has 1.18- and 0.77-Mev positron groups and a 375-kev gamma,[3] an aluminum absorption curve taken with the Geiger counter and an integral gamma pulse-height curve taken with the scintillation counter on the scandium daughter showed unambiguously that the daughter was Sc^{44}. This assignment of the activity to Ti^{44} is to be expected from a consideration of beta-decay systematics.

When the Geiger and proportional counters were used, the activity of the freshly separated titanium fractions was observed to grow from just above background to the final equilibrium values with a 4-hour half-life, indicating no particulate radiation (<5 percent abundance) in the decay of Ti^{44}. Integral gamma pulse-height curves taken with the scintillation counter during the growth of the daughter activity showed the presence of an ~1.2-Mev gamma activity growing with a 4-hour half-life and another of 160±60 kev of constant intensity. The high-energy gamma is the 1.16-Mev gamma of the growing Sc^{44} activity, whereas the lower energy gamma must be associated with the Ti^{44} decay itself. Taking the counting efficiency of the 1.16-Mev gamma in the large well-type NaI crystal used as approximately equal to that of the experimentally determined average value for the 1.17- and 1.33-Mev gammas of Co^{60} and assuming that the counting effici-

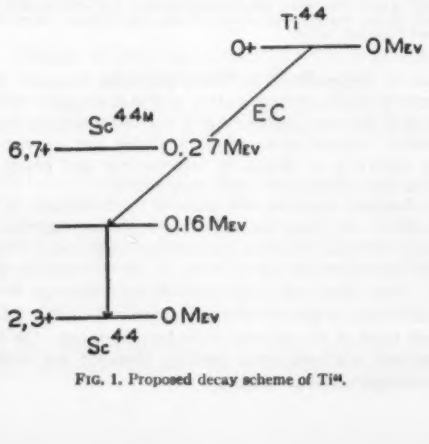

FIG. 1. Proposed decay scheme of Ti^{44}.

ency for the low-energy gamma is 80 percent (or higher), we obtain a 1:1 correspondence in the number of the low- and high-energy gammas at radioactive equilibrium between the parent and daughter. Because of the assumptions made and the complicating presence of annihilation radiation from the Sc^{44} positron, this ratio could possibly be as large as $\frac{4}{3}$ or as small as $\frac{2}{3}$; but certainly the association of a low-energy gamma with every Ti^{44} disintegration is suggested. Consideration of a possible decay scheme, Fig. 1, confirms this view. Decay of Ti^{44} to the 3+ or 2+ ground state of Sc^{44} would be at least second-forbidden with a log(ft) value of 13–14.[4] Decay measurements made over a period of one half-year indicate, by a least-squares analysis, a half-life of 2.7 years with a rather large estimated error of ±0.7 year because of the small amount of titanium activity available. Such a value for the half-life would require an impossibly large decay energy to yield a log(ft) value of 13–14. No decay to the 2.4-day Sc^{44m} would be expected because of the high-spin change involved, and none is observed. Thus a less forbidden transition to an excited state of Sc^{44} followed by gamma emission to the 4-hour ground state is to be expected.

† This work was supported by the U. S. Atomic Energy Commission.
[1] This scandium oxide was generously given by Professor G. Wilkinson. It had been prepared from thortveitite ore by the late Professor G. P. Baxter.
[2] Details to be published elsewhere.
[3] Hollander, Perlman, and Seaborg, Revs. Modern Phys. **25**, 469 (1953).
[4] L. W. Nordheim, Revs. Modern Phys. **23**, 322 (1951).

PHYSICAL REVIEW VOLUME 93, NUMBER 2 JANUARY 15, 1954

Proceedings of the American Physical Society

Minutes of the 1953 Autumn Meeting of the New York State Section at Poughkeepsie, October 16 and 17, 1953

THE thirtieth meeting of the New York State Section convened at Poughkeepsie, New York, on October 16 and 17 with just under 100 registrants. The meeting was sponsored jointly by Vassar College and International Business Machines Corporation.

Following tours through the IBM laboratories on Friday morning, registrants attended an invitation luncheon at which Dr. A. L. Samuel spoke on "Functions of the IBM Research Laboratory." The Friday afternoon session, held in the Physics Laboratory at Vassar College, was devoted to three invited papers. The Section met with faculty and students of Vassar College on Friday evening for a lecture by Dr. George B. Collins of Brookhaven National Laboratory on "Particle Physics."

A group of three invited papers followed the business meeting of the Section on Saturday morning. The major item on the agenda for the business meeting was discussion of two proposed amendments to the constitution—one having to do with the definition of specific procedures for amending the constitution, the other with removal of a phrase in the article on "membership" which defines the geographical limits of the Section as "exclusive, in general, of the Metropolitan area of New York City." Vote on the amendments will be taken at the next meeting of the Section.

A list of the invited papers is appended.

L. W. Phillips, *Secretary*
New York State Section
The University of Buffalo
Buffalo 14, New York

Invited Papers

The 701 Calculator. C. Frizzell, *International Business Machines.*
Transistor Physics. L. P. Hunter, *International Business Machines.*
Dielectric Constant Measurements of Barium Titanate. D. R. Young, *International Business Machines.*
The Use of Radioactive Iodine in the Study of Thyroid Function. Rosalyn Yalow, *Bronx Veterans Administration Hospital.*
A Simple Bent-Crystal X-Ray Spectrograph for a Senior Experiment. John Weymouth, *Vassar College.*
Some New Applications of X-Ray Diffraction. Isador Fankuchen, *Brooklyn Polytechnic Institute.*

Minutes of the 1953 Autumn Meeting of the Ohio Section of the American Physical Society at General Electric Light Institute, Nela Park, Cleveland, Ohio, October 23 and 24, 1953

THE regular fall meeting of the Ohio Section of the American Physical Society was held at the General Electric Light Institute, Nela Park, Cleveland, Ohio, on Friday and Saturday, October 23–24, 1953. No program, save a trip through the Light Institute, was prepared for Friday morning, but this trip was of sufficient interest that 80 persons appeared for it. Invited papers began at 1:00 P.M. on Friday with more than 150 in attendance. The following invited papers on the general theme of the electric lamp development were presented:

Physics and Physicists in an Ohio Industry—Electric Lamps. R. N. Thayer, *Lamp Development Laboratory, Nela Park.*

Physical Processes in Fluorescent Lamps. B. T. Barnes, *Lamp Development Laboratory, Nela Park.*

Physical Characteristics of Phosphors for Fluorescent Lamps. SHANNON JONES, *Chemical Products Works, G.E. Lamp Division.*

Critical Effects of Electric Fields in Fluorescent Lamp Starting and Their Use in New Lamp Design. W. J. KARASH, *Lamp Development Laboratory.*

Spectroscopy in the Manufacture of Tungsten. A. PORITSKY, *Cleveland Wire Works, G.E. Lamp Division.*

Opportunities for Physics Graduates in General Electric. D. E. BEENINGA, *G.E. Physics Program, Schenectady.*

Is Electroluminescence a Practical Light Source? J. ELLIOTT, *Lamp Development Laboratory.*

Some Problems in Evaluating Radiant Energy from Light Sources. E. S. STEEB, *Testing Section, Nela Park.*

Physics Problems in High-Pressure Mercury-Vapor Light Sources. E. B. NOEL, *Lamp Development Laboratory.*

After dinner the Cleveland Physics Society joined us and our numbers rose to over 200 as we listened to a more extensive invited paper—"Solid-State Luminescence" by Dr. Ferd Williams of the General Electric Research Laboratory, Schenectady, New York.

The Section reconvened at 9:00 A.M. on Saturday with three additional invited papers:

Glass Absorption Factors in Light Bulbs. R. E. SMITH, *Glass Technology Laboratory.*

Prismatic Light Control. KURT FRANCK, *Holophane Company, Newark, Ohio.*

The G.E.-Case Fellowship Program for High-School Physics Teachers. L. O. OLSEN, *Case Institute of Technology.*

The Science Day Program for High-School Students in Ohio. R. E. MCKAY, *Bowling Green State University.*

Then followed nineteen contributed papers, which were presented in two sections so that adjournment could be accomplished at mid-day. The Ohio Section adjourned at 12:30 P.M. The abstracts of the contributed papers follow.

LEON E. SMITH, *Secretary*
The Ohio Section
American Physical Society
Granville, Ohio

1. Nuclear Quadrupole Transition in a Single Crystal of Sodium Chlorate. EDWARD MANRING, YU TING, AND DUDLEY WILLIAMS, *The Ohio State University.**—Powdered samples of sodium chlorate have been found to exhibit an extremely narrow absorption line near 30 Mc/sec due to nuclear quadrupole transitions involving Cl^{35}. The present work has been concerned with a study of single crystals of sodium chlorate. In the experimental work a single crystal was mounted in the coil of an oscillating detector, and an external magnetic field was employed to produce Zeeman splitting. The observed Zeeman pattern is dependent upon the orientation of the crystal in the external magnetic field. The patterns to be expected can be calculated. The patterns for five orientations will be compared in detail with theoretical predictions. From the observed patterns it is possible to calculate the nuclear magnetic moment of Cl^{35}. The preliminary value of 0.820 $\pm$0.001 nuclear magnetons compares favorably with the value 0.8210 nuclear magnetons obtained in nuclear magnetic resonance studies of liquid samples and serves as a check on the validity of theory.

* Supported by a contract between Wright Air Development Center, Air Research and Development Command, and The Ohio State University Research Foundation.

2. The Microwave Spectrum of Ozone. PETER N. WOLFE AND DUDLEY WILLIAMS, *The Ohio State University.**—The absorption spectrum of O_3^{16} has been investigated in the microwave region between 20 and 30.3 kMc/sec. Accurate determinations of line frequencies were made between 20 and 26 kMc/sec and approximate measurements were made with a calibrated resonant cavity at frequencies above 26 kMc/sec. The lines observed in this region are in excellent agreement with those observed by Hughes but some improvements in frequency determinations seem to have been achieved. The observed spectrum is readily interpreted in terms of the obtuse-angled isosceles triangular model proposed by Hughes. Splitting of the ground vibrational state due to intramolecular inversions in such a triangular model is found to be negligible within the limits of the frequency discrepancies between observed and predicted lines. If such inversion occurs, its frequency is extremely low.

* Supported by a contract between Office of Scientific Research, Air Research and Development Command, and The Ohio State University Research Foundation.

3. Proton Line Shapes in the Magnetic Resonance Spectra of Ammonium Salts. ROBERT CARPENTER AND DUDLEY WILLIAMS, *The Ohio State University.**—Proton magnetic resonance line shapes have been observed in the ammonium halides, ammonium sulfate, and ammonium nitrate at room temperature. Measurements were made with an unquenched radio-frequency oscillating detector in a field of approximately 7800 gauss. Frequency measurements were made with a radio receiver and a 10-kc/sec crystal-controlled multivibrator. The line widths in ammonium halides showed a monotonic decrease with increasing atomic number of the halide. The proton resonance line in ammonium fluoride was the widest observed in this study. Ammonium sulfate and ammonium nitrate both showed comparatively narrow proton absorption lines, the ammonium nitrate line showing the narrowest width of any of the salts studied. The second moments of the proton line for the different salts were computed from the observed line shapes and were found to be smaller than would be expected for a rigid lattice structure.

* Supported by a contract between the Wright Air Development Center and The Ohio State University Research Foundation.

4. A Study of Pressure Broadening in the Near Infrared. HENRY H. BLAU, JR., JOHN H. SHAW, AND DUDLEY WILLIAMS, *The Ohio State University.**—This study has been concerned with the total absorption by the $P(6)$ and $P(8)$ lines of the fundamental band of CO. The observed total absorption is a function of the pressure of CO and the pressure of foreign gases in the absorption cell. The effects of self-broadening and pressure broadening by A, N_2, and NH_3 have been studied over a pressure range extending from a few millimeters of Hg to atmospheric pressure. The experimental arrangement and the results obtained will be described. From the observed total absorption, an "equivalent line width" can be obtained. The equivalent line width is found to be approximately proportional to the square root of the total pressure in the case of broadening by foreign gases. From the equivalent line widths, the ratios of collision cross sections $A:N_2$, $A:NH_3$, and $N_2:NH_3$ can be obtained. Preliminary values for these ratios compare favorably with similar ratios obtained in microwave studies and with ratios obtained from kinetic theory.

* Supported by a contract between Air Force Cambridge Research Center and The Ohio State University Research Foundation.

5. A New Vacuum Near-Infrared Spectrometer. T. J. COBURN, H. H. NIELSEN, AND DUDLEY WILLIAMS, *The Ohio State University.**—A high-dispersion infrared spectrometer designed by Nielsen has been completed and placed in operation. The spectrometer is a Pfund-type instrument. The size of the

optical components is such that the system is $f/4$. The optical system of the spectrometer may be enclosed in a vacuum tank approximately 6 feet long by 3 feet wide by 1.5 feet high. The tank is constructed of 1-inch steel plate. The vacuum attainable within the tank is less than 10 microns. This is entirely adequate for eliminating interference due to the atmospheric bands. The spectrometer has been used with both lead-sulfide and thermocouple detectors. The wavelengths of the spectral lines are determined by readings taken from a 12-inch grating circle which was marked by the National Bureau of Standards. Slits, fore-prism, and the grating are driven by selsyns. A Model 81 Perkin-Elmer amplifier and a Leeds and Northrup recorder are used. Results of measurements of the 1.4μ H_2O water-vapor absorption band will be shown to give an illustration of the operation of the spectrometer.

* Supported by a contract between the Office of Ordnance Research and The Ohio State University Research Foundation.

6. The Infrared Emission Spectrum of CO in the 2.4μ Region. F. W. DALBY, F. P. DICKEY, AND DUDLEY WILLIAMS, *The Ohio State University.**—The new high-dispersion, vacuum spectrometer described in an earlier paper on this program has been used to study the emission spectrum of carbon monoxide. The sources employed were oxy-acetylene and oxy-carbon-monoxide flames. The emission spectra of these flames were observed in the 2.4μ region with gratings having 7500 lines/inch and 15 000 lines/inch; a PbS detector was employed. Several vibration-rotation bands were observed. Clearly developed band heads were observed for bands corresponding to the $2-0$, $3-1$, and $4-2$ vibrational transitions; lines from the $5-3$ band were also observed. The spectrum observed in the present work will be compared with the earlier work of Plyler *et al.*[1]

* Supported by a contract between U. S. Office of Ordnance Research and The Ohio State University Research Foundation.
[1] Plyler, Benedict, and Silverman, J. Chem. Phys. **20**, 175 (1952).

7. Total Emission of HCl and CO in the Region of Their Fundamentals. ROBERT D. SMITH* AND DUDLEY WILLIAMS, *The Ohio State University.*†—The total infrared emission of hot gases is a subject of considerable importance to an understanding of the heat balance in the earth's atmosphere as well as to various other systems involving radiative energy transfers. The present report deals with preliminary results of a study of emission from heated HCl and CO. In the experimental work a sample cell with transparent windows was placed inside an open-ended cylindrical furnace. Radiation from the gas in the cell was focused on the entrance slit of a prism spectrograph, care being taken to prevent direct radiation from the furnace walls from reaching the spectrograph. The observed band area was taken as a measure of integrated emission $\int E_\lambda d_\lambda$ for the band under study, since effective slit width was nearly constant across the band. The observed total emission was then compared with the net flow of energy in the same spectral interval from a black body at the same temperature as the sample gas. Curves showing this comparison for sample temperatures between 420°K and 580°K with the receiver temperature 300°K will be presented.

* Now with the General Electric Company.
† Supported by a contract between the U. S. Office of Ordnance Research and The Ohio State University Research Foundation.

8. Atomic Spectra in the Infrared and an Electrodeless Discharge Source. F. P. DICKEY, R. V. ZUMSTEIN, AND DUDLEY WILLIAMS, *The Ohio State University.**—An electrodeless discharge source has been constructed to be used in the study of emission spectra in the infrared. The source consists of a medium power push-pull self-excited oscillator operating at a frequency of about 8 megacycles. Inside the tank circuit of the oscillator is located a quartz tube which contains the gas to be investigated. The pressure of the gas may be controlled by means of a needle valve and a vacuum pump. The tube is continuously pumped and the gas is admitted to it through a needle valve. Preliminary measurements have been made of the spectra of a number of atoms and molecules in the gaseous state. Measurements of the spectrum of argon in the region from about 1.00μ to 2.60μ will be presented.

* Supported by a contract between the U. S. Office of Ordnance Research and The Ohio State University Research Foundation.

9. Formation of Dislocation Rings by Vacancy Migration.* R. D. DANIELS AND R. W. HOFFMAN, *Case Institute of Technology.*—The macrotension of evaporated nickel films has been measured as a function of both substrate deposition temperature and annealing temperature. Films were deposited at five temperatures from 75°C to 250°C and pulse annealed in 25 degree intervals to 350°C. The intrinsic stress, measured at room temperature, decreased with increasing temperature up to 250°C and then increased at higher temperatures. For a sample deposited at 75°C, the stress changed from 6.4 at 75°C to 1.9 at 250°C and rose to 2.8 at 350°C, in units of 10^9 dynes/cm^2. With increasing deposition temperature, the stress decreased linearly from 6.4 at 75°C to 0.3 at 250°C. Electrical resistance values also decreased rapidly in the region of 250°C. These results are consistent with the mechanism of vacancies coalescing into aggregates and then collapsing to form dislocation rings.[1]

* Supported by the U. S. Office of Naval Research.
[1] Hoffman, Anders, and Crittenden, J. Appl. Phys. **24**, 231 (1953).

10. A Thin Lens Beta-Ray Spectrometer. G. R. GROVE AND L. N. RUSSELL, *Mound Laboratory.*—The general design of the thin lens beta-ray spectrometer was based on the discussion of Deutsch, Elliott, and Evans[1] and incorporates some of the features of the spectrometers described by others.[2,3] The vacuum chamber was fabricated from a selected aluminum tube and has an inside diameter of eight inches and an axial length of about one meter. The focusing coil consists of four concentric subcoils each of which has about 400 turns of No. 12 equivalent rectangular wire. The subcoils are separated from each other by a single layer of $\frac{1}{4}$-in. copper tubing which provides internal water cooling for the coil. A set of six rectangular coils surrounding the spectrometer provides an extended region around the axis of the spectrometer in which the earth's magnetic field is very nearly neutralized. The figures of merit for this spectrometer compare favorably with those compiled by Persico and Geoffrion[4] for similar spectrometers.

[1] Deutsch, Elliott, and Evans, Rev. Sci. Instr. **15**, 178 (1944).
[2] Jensen, Laslett, and Pratt, Phys. Rev. **75**, 458 (1949).
[3] Broyles, Thomas, and Haynes, Phys. Rev. **89**, 715 (1953).
[4] E. Persico and C. Geoffrion, Rev. Sci. Instr. **21**, 945 (1950).

11. The Specific Heat of 96 Percent Liquid He^3 between 1.3°K and 2.3°K.* G. DE VRIES AND J. G. DAUNT, *The Ohio State University.*—Calorimetric determinations have been made of the specific heat of liquid He^3 in the region 1.3 to 2.3°K. The helium used was 8-cc gas (NTP) of 96 percent He^3 (4 percent He^4) kindly supplied by the U. S. Atomic Energy Commission. The results are preliminary and, due to the small quantity of He^3 involved, are subject to about ± 10 percent error. The specific heat was found to increase monotonically from 1.6 cal/mole-deg at 1.3°K to 3.6 cal/mole-deg at 2.3°K. It was, within experimental accuracy, in approximate agreement with the formula

$$C_v = 0.68T + 0.2T^3 \text{ cal/mole-deg}$$

previously proposed by one of us.[1] At the lowest temperature, C_v may be somewhat larger than expected from this formula, but the measurements are not yet sufficiently extensive to

decide whether this indicates an anomaly. Measurements are being made at lower temperatures.

* Assisted by a contract between the U. S. Atomic Energy Commission and The Ohio State University Research Foundation.
[1] J. G. Daunt, Advances in Physics 1, 209 (1952).

12. Operational Data for a Magnetic Refrigerator for Maintaining Temperatures below 1°K.* C. V. HEER, C. B. BARNES, AND J. G. DAUNT, *The Ohio State University.*—In 1949 two of us (J.G.D. and C.V.H.)[1] proposed a technique for the realization of continuous refrigeration at temperatures well below 1°K. This proposal considered a heat engine in which the working substance was a paramagnetic salt and in which the heat "valves" were constructed of superconducting metallic links. Preliminary results regarding the operation of the magnetic refrigerator have been published.[2] In more recent experiments heat extraction rates as high as 100 ergs/second from a reservoir at 0.3°K have been obtained. The technique has been extended to a more compact design for the experimental chamber and the manual switching operations changed to automatic operation. This latter design of the magnetic refrigerator makes available a cooling unit for experimental work between 0.3°K and 0.9°K.

* Assisted by a contract between the U. S. Atomic Energy Commission and The Ohio State University Research Foundation.
[1] J. G. Daunt and C. V. Heer, Phys. Rev. 76, 985 (1949).
[2] Heer, Barnes, and Daunt, Phys. Rev. 91, 412 (1953).

13. Low-Temperature Coefficient Ceramics. D. A. BERLINCOURT, *Brush Laboratories Company.*—The properties of barium titanate ceramics containing up to 25 weight percent calcium titanate are reviewed with emphasis on application in tuned devices. The addition of calcium titanate greatly decreases the temperature dependence of resonant frequency, and mechanical Q factors well over 1000 are obtained. The transverse and longitudinal piezoelectric coupling factors for such compositions are lower than for plain barium titanate, but the hydrostatic coupling factor is raised due to an increase in the ratio k_{33}/k_{31} for these compositions. The piezoelectric, dielectric, and elastic coefficients for the various compositions are given, and curves of resonant frequency *vs* temperature are shown. The effect of aging on the elastic coefficient s_{11}^E is also given.

14. Mechanical Properties of Ceramic Barium Titanate. HELMUT KRUEGER, *Brush Laboratories Company.*—Ferroelectric barium titanate has interesting mechanical properties not usually associated with ceramic materials. It exhibits reversible creep under high loads. The creep is not present for samples whose Curie point is below room temperature or for samples that are highly conducting. These facts hint at a strong interdependence of these time-dependent mechanical phenomena and the ferroelectric properties of barium titanate.

15. The Angular Distribution of Compton Scattered Gamma Rays.* W. H. VOELKER, *Case Institute of Technology.*—The angular distribution of the Compton scattered gamma rays was determined for an incident gamma-ray energy of 15 Mev. The Case betatron was used as the gamma-ray source with the incident gamma energy being selected by detecting the scattered gamma and electron in coincidence (resolving time 5×10^{-9} sec) at known angles with the incident beam. The incident energy acceptance band had a width of 2 Mev. The experimental distribution agreed with the Klein-Nishina prediction within the experimental error.

* This work was supported by the U. S. Atomic Energy Commission.

16. Energy Loss and Scattering of 0.624-Mev Electrons.* J. W. ROBSON, R. L. STEARNS, AND ARTHUR LINDENER, *Case Institute of Technology.*—The most probable energy loss of 0.624-Mev electrons in passing through thin foils of various Z has been measured using a 60° magnetic spectrometer. Monoenergetic interval conversion electrons from C_s^{137} were used. The electron beam was collimated so as to provide good geometry, since it was found that with poor geometry, scattering in the foil led to significant deviations in energy loss measurements. It was also found that electrons scattered out of the beam suffered an energy loss commensurate with their increased path length in the foil. With good geometry, agreement with the Landau theory for the most probable energy loss was obtained within the experimental uncertainty of ±5 percent. Using somewhat poorer geometry, the most probable angle of scattering was measured for several thicknesses of aluminum and good agreement was obtained with both the diffusion theory of Bethe, Rose, and Smith[1] and the cloud-chamber observations of Slawsky and Crane.[2]

* This work supported by the U. S. Atomic Energy Commission.
[1] Bethe, Rose, and Smith, Proc. Am. Phil. Soc. 78, 573 (1938).
[2] M. M. Slawsky and H. R. Crane, Phys. Rev. 56, 1203 (1939).

17. The Branching Ratio of the $Be^9(\alpha,n)C^{12*}$ Reaction.† D. E. DILLER AND M. F. CROUCH, *Case Institute of Technology.*—The gamma and neutron emission produced by Po α's on a thin Be target has been investigated. Using a NaI(Tl) detector, a single gamma energy of 4.4 Mev is observed, in agreement with other published results. A gamma-neutron delayed coincidence circuit was next used with a differential pulse-height analyzer to measure the coincidence rate *versus* gamma detector pulse height. The resulting coincidence gamma spectrum has a single peak believed due to the 4.4-Mev gamma ray. This spectrum confirms the evidence that only a single excited level of C^{12} is involved for $E_\alpha \leq 5.3$ Mev. With this assumption, measured rates and efficiencies yield the branching ratio b, i.e., the fraction of cases in which the reaction proceeds to the excited level of C^{12}. The value of b obtained is 0.60 ± 0.06.[1] Some additional systematic error may exist because of variation of neutron detector efficiency with energy.

† Supported by the U. S. Atomic Energy Commission.
[1] D. E. Diller, thesis, Case Institute of Technology, 1953.

18. Resonances in the $Li^7(\gamma,p)He^6$ Cross Section and the High-Energy Limit of Bremsstrahlung Spectra.* B. L. TUCKER AND E. C. GREGG, *Case Institute of Technology.*—Beta-active He^6 provides a means of detecting the $Li^7(\gamma,p)He^6$ reaction with a scintillation counter operating during the dead times of the betatron. The resulting activation curve shows at least two pronounced steps about 0.1 Mev wide. Four factors are involved in these sharp increases in activity. They are: (1) resonances in the (γ,p) cross section; (2) the shape of the intrinsic bremsstrahlung curve; (3) the effect of the betatron target thickness; and (4) electron beam expansion errors. The data indicates that the resonances are sharp with widths of approximately 0.06 Mev, the high-energy limit of the intrinsic bremsstrahlung spectrum has the form of a step function, and the apparent target thickness is much less than its physical thickness. The two resonances in the $Li^7(\gamma,p)He^6$ cross section occur at 15.0 and 15.4 Mev. Other resonances are probable but unresolved in the data. It is believed that these cross-section resonances indicate energy levels in the Li^7 nucleus at 15.0 and 15.4 Mev.

* This work was supported by the U. S. Atomic Energy Commission.

19. A Study of Alpha-Particle Pulse Heights from Organic Scintillators.* D. G. PROCTOR AND T. A. ROMANOWSKI, *Case Institute of Technology.*—Alpha particles from 2–5.3 Mev have been used to study the scintillation photon yield of stilbene as a function of α-particle energy. A 1-cm^2×1-mm thick stilbene crystal mounted directly on the window of an RCA 5819 photomultiplier served as a particle detector. The number of photoelectrons emitted from the photocathode is computed from the mean output pulse height and the measured gain of

the RCA 5819. The mean pulse height was determined by photographing a synchroscope display of the photomultiplier output pulses, and the gain of the RCA 5819 was calculated from the pulse-height distribution due to thermal electrons. The number of photoelectrons emitted was then plotted against the energy of the incident particles. Over the 2–5.3-Mev region, the curve can be approximated by a straight line not passing through the origin. For 5.3-Mev α particles, about 50 photoelectrons were collected; reasonable values of phosphor efficiency (5 percent) and light collection (50 percent) give a photon yield of 2×10^3 photons. The value of dN/dE is about 600 photons per Mev where N is the number of photons and E is the energy of the α particle. A liquid scintillator using various concentrations of terphenyl in phenylcyclohexane showed a maximum photon yield at 8 g/l.

* Work supported by the U. S. Atomic Energy Commission.

MINUTES OF THE 1953 AUTUMN MEETING OF THE NEW ENGLAND SECTION AT STORRS, CONNECTICUT, NOVEMBER 7, 1953

THE New England Section of the American Physical Society held its 1953 autumn meeting on Saturday, November 7, 1953 in the Student Union building of the University of Connecticut at Storrs, Connecticut. The Section was welcomed by the Provost of the University, Dr. A. E. Waugh. There followed four invited papers:

The Decay of Elementary Particles. RAYMOND V. ADAMS, *Mt. Holyoke.*

Are We Achieving Our Aims in General Education. GERALD HOLTON, *Harvard.*

High Frequency Performance of Junction Tetrode Transistors. ROBERT WALLACE, *Bell Telephone Laboratories.*

Meson-Nucleon Interaction Experiments at the Brookhaven Cosmotron. LUKE C. L YUAN, *Brookhaven National Laboratory.*

In the afternoon, the retiring Chairman, F. Woodbridge Constant of Trinity College delivered an address entitled, "The Role of Analogy in Physics." This was followed by nine contributed papers; the abstracts are appended.

At the Annual Business Meeting, the following officers were elected for one-year terms:

Chairman:	V. E. Eaton, *Wesleyan*
Vice-Chairman:	T. Soller, *Amherst*
Secretary-Treasurer:	W. M. Preston, *Harvard*
Member of the Council:	G. Holton, *Harvard*
Member of the Council:	R. V. Adams, *Mt. Holyoke*

W. M. PRESTON, *Secretary*
New England Section
Harvard University
Cambridge, Massachusetts

Contributed Papers

1. A Time-of-Flight Mass Spectrometer.* HENRY S. KATZENSTEIN AND STEPHEN S. FRIEDLAND, *University of Connecticut.*—A time-of-flight mass spectrometer based on principles previously described[1] has been constructed with two major modifications to facilitate appearance potential measurements. These modifications are (1) an axial electron beam is pulsed through an ionization chamber utilizing techniques of Fox *et al.*[2] and (2) a gated ion detector is employed to allow for integration of the resolved ion current from successive cycles. The instrument has been constructed of stainless steel to allow for measurements on chemically active gases. Theoretical resolution, limited by thermal energies of the ions, appears to be well over mass 200. Preliminary experimental work has verified this up to the region of mass 100.

* Work sponsored by the U. S. Atomic Energy Commission.
[1] M. M. Wolf and W. E. Stephens, Rev. Sci. Instr. 24, 616 (1953).
[2] Fox, Hickam, Kjeldaas, and Grove, Phys. Rev. 84, 859 (1951).

2. Mass Spectrometry of Low Vapor-Pressure Molecules.* GEORGE H. LANE, HENRY S. KATZENSTEIN, AND STEPHEN S. FRIEDLAND, *University of Connecticut.*—A program has been undertaken to determine if a mass spectrometer can be utilized to identify and study structural properties of low vapor-pressure molecules such as the steroids. It has been determined that characteristic spectra may be obtained from the dissociation products of the molecule which has undergone pyrolysis external to the mass spectrometer. These spectra are similar in nature to those obtained by vaporizing the material in the mass-spectrometer tube which is operated at elevated temperatures.

* Work sponsored by the American Cancer Society.

3. Improved Chronotron for Time-of-Flight Measurements.* HOWARD OGUSHWITZ AND STEPHEN S. FRIEDLAND, *University of Connecticut.*—Modifying a chronotron timing circuit[1] by inverting the polarity of one of the pulses and detecting the resulting null instead of the previously described technique of detecting a maximum has enabled the measurement of two pulses from a mercury relay pulser[2] to be resolved when they are separated in time by 3×10^{-10} sec. The circuit is to be used for a neutron time-of-flight spectrometer in the range of 3 to 10 Mev.

* Work supported by the U. S. Atomic Energy Commission.
[1] J. W. Keuffel, Rev. Sci. Instr. 20, 197 (1949).
[2] R. L. Garwin, Rev. Sci. Instr. 21, 903 (1950).

4. The "Closed" Fountain Effect in Liquid Helium II.* CHARLES A. REYNOLDS, *University of Connecticut.*—A heat current is sent through a fritted glass disk and packed rouge in a tube filled with liquid helium. The tube is sealed at the bottom with a metal seal for good thermal contact at the bottom with the surrounding liquid-helium bath. The level above the fritted disk is observed as a function of temperature and power input. The temperature difference between the liquid above the frit and the bath has also been measured. The liquid level rises and the temperature difference increases with increasing power until the temperature of the liquid above the frit exceeds the lambda point, at which time the liquid above the frit bubbles and a geyser effect takes place. It is found that the height of the liquid level is proportional to the temperature difference. This is analogous to the formerly measured open "fountain effect." However, the rise in the level here is much less than in the usual case and, more important, it is not the pressure head which is proportional to the temperature difference, but more nearly the volume of liquid helium above the frit. Also the level rise increases with decreasing temperature in the range investigated here (2.1°

to 1.6°K). The results may be qualitatively understood by considering that the normal fountain effect contributes an (upward) pressure and that the lifting of the liquid gives rise to a (downward) tension.

* Sponsored in part by the Research Corporation, National Science Foundation, and U. S. Office of Naval Research.

5. An Improved Radiotracer Technique for the Study of Gaseous Adsorption on Metals. JOHN A. DILLON, JR.,* AND H. E. FARNSWORTH, *Brown University.*†—Radiotracer methods for studying gaseous adsorption on metal surfaces usually require either the removal of the sample from the vacuum system in order to measure its activity or the use of the sample itself as part of the counter mechanism. Exposure of the sample to the atmosphere or to counter gases introduces the possibility of surface poisoning which may alter the results. An improved technique, applicable to the study of adsorption on single-crystal faces, has been developed. By constructing a thin window counter inside the adsorption chamber, the exposure of the sample to extraneous gases between runs has been eliminated. Details of counter construction and operation are discussed. The adsorption chamber is designed so that the sample can be moved either to the counting position opposite the counter window or to the outgassing position where it can be heated by electron bombardment. A movable shield is used to prevent evaporation products from depositing on the counter window during outgassing. This method has been used in the study of the adsorption of $C^{14}O_2$ on the (110) and (100) faces of a nickel single crystal.

* Now at the Geophysics Research Directorate, Air Force Cambridge Research Center.
† Assisted in part by the U. S. Office of Naval Research.

6. Physical Factors Involved in Sonic Irradiation of Liquids.* S. A. ELDER, J. KOLB, AND W. L. NYBORG, *Brown University.*—Though a tremendous literature exists on various physical, chemical, and biological phenomena due to sounds of high amplitude, in only rare cases are the mechanisms well understood. If the physical principles involved in these irradiations are to be learned, it is necessary that the fields be described in much more detail than is the usual practice. Not only must distributions of first-order quantities, such as the pressure amplitude, be known, but also second-order quantities, such as those governing turbulent motions, must be determined. In this paper is described the first-order sound field in a typical cylindrical irradiation chamber; theory is compared with experiment for the pressure distribution in a well-known unit provided by the Raytheon Manufacturing Company. Also, various elementary situations are described in which the sound field generates steady vortex motions. These motions appear to be profoundly dependent on prevailing configurations of gas bubbles. There is evidence that these motions (for which adequate theory does not yet exist) are very important in certain applications of high-amplitude sound.

* Supported in part by Air Force Contract, Aeromedical Laboratory, Wright-Patterson Air Force Base, Ohio.

7. Impedance Concept in Nuclear Scattering. D. L. FALKOFF, *Brandeis University and M.I.T.*—The description of the scattering of incident particles by complex nuclei has much in common with the methods used in describing the scattering of electromagnetic waves by obstacles or the effect of discontinuities in wave-guide and transmission line junctions. Many of the general features of both kinds of scattering, e.g., reciprocity conditions, conservation laws, resonant frequencies, and associated resonance formulas may be established within the framework of a common formalism. In particular, the familiar impedance concept of electrical network theory has its counterpart in the "logarithmic derivative of the wave function" which is the crucial function for the quantum-mechanical description of nuclear scattering. Hence all the well-known properties of the impedance as a function of frequency have immediate application to the energy dependence of nuclear cross section. As further examples of the parallelism, the counterparts of the Breit-Wigner resonance formula and the Campbell-Foster theorem will be given.

8. On Deriving Schrödinger's Equation. SAUL T. EPSTEIN, *Cambridge, Massachusetts.*—Most classroom derivations of the Schrödinger equation follow the path used by Schrödinger himself—treating the passage from classical mechanics to quantum mechanics as analogous to the passage from geometrical optics to wave optics. However, this method has the disadvantage that even when one has arrived at the equation, the significance of the wave function is not clear, and the instructor usually simply states the probability interpretation and shows that it is consistent with the equation and with various *Gedanken* experiments. Since at this point the student is likely to feel that the consistency of the probability interpretation is somewhat fortuitous, it would seem useful to supplement this first discussion by a second in which one approaches the problem from just the other end—starting with the interpretation and finishing with the Schrödinger equation. We shall attempt to give such a discussion starting from (a) the results of the *Gedanken* experiments as expressed in the uncertainty relations and (b) the correspondence principle.

9. European and American Productivity in Basic Science. J. B. BLIZARD, *University of Connecticut, Stamford Center.*—This paper discusses the scientific contributions from the United States and European countries during the half-century preceding World War II. Two indexes of scientific activity are used: (1) scientific discoveries and inventions,[1] and (2) Nobel prize awards in the physical sciences. Population is considered; the United States totals nearly the populations of England, France, and Germany combined. In order of decreasing contributions per million of population were: The Netherlands, Germany, Switzerland, England, France, Sweden, and the United States, with the Netherlands contributing close to three times the U. S. total. The 113 Nobel prize winners in physics and chemistry (1901–1952) by country in order of decreasing numbers per million of population: Switzerland, Sweden, The Netherlands, England, Germany, France, and the United States, and Switzerland totaling five times the U. S. proportion of Nobel scientists. The relative scientific productivities are in sharp contrast to the extent of higher education. The American enrollment in higher-educational institutions has continuously averaged six times the proportionate enrollment in the above European countries. Thus in 1952, 1.76 percent of the U. S. population and an average of 0.28 percent of the European countries were enrolled.[2] *Per college graduate,* the cited European countries contributed approximately fifteen scientific discoveries and inventions for each American contribution.
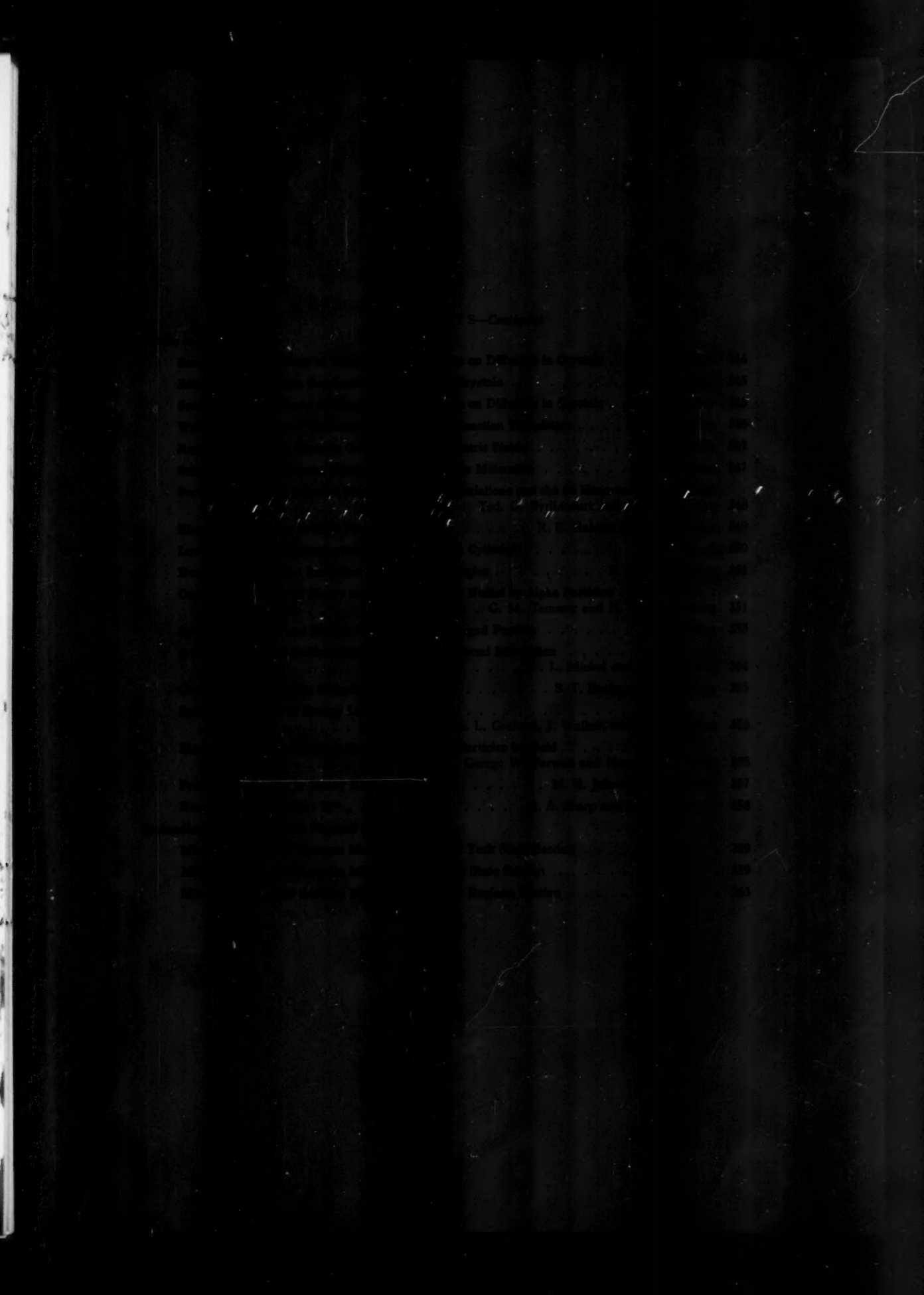
[1] Thorner, Am. J. Sociology **58**, 25 (1952).
[2] *Statistical Yearbook of the United Nations* (Columbia University Press, New York, 1952).